

# **Mechanistic investigation of catalytic organometallic reactions using ESI MS**

by

Jingwei Luo

M.Sc., Queen's University, 2009

M.Sc., Minzu University of China, 2007

B.Sc., Minzu University of China, 2004

A Dissertation Submitted in Partial Fulfillment  
of the Requirements for the Degree of

**DOCTOR OF PHILOSOPHY**

in the Department of Chemistry

© Jingwei Luo, 2014  
University of Victoria

All rights reserved. This dissertation may not be reproduced in whole or in part, by photocopy or other means, without the permission of the author.

## **Supervisory Committee**

**Mechanistic investigation of catalytic organometallic reactions using ESI MS**

by

Jingwei Luo

M.Sc., Queen's University, 2009

M.Sc., Minzu University of China, 2007

B.Sc., Minzu University of China, 2004

### **Supervisory Committee**

Dr. J. Scott McIndoe, Department of Chemistry

**Supervisor**

Dr. Lisa Rosenberg, Department of Chemistry

**Departmental Member**

Dr. Frank van Veggel, Department of Chemistry

**Department Member**

Dr. Laurence Coogan, Department of Earth and Ocean Science

**Outside Member**

## Abstract

### Supervisory Committee

Dr. J. Scott McIndoe, Department of Chemistry  
**Supervisor**

Dr. Lisa Rosenberg, Department of Chemistry  
**Departmental Member**

Dr. Frank van Veggel, Department of Chemistry  
**Department Member**

Dr. Laurence Coogan, Department of Earth and Ocean Science  
**Outside Member**

Electrospray ionization mass spectrometry (ESI-MS) has been applied to the real time study of air-sensitive homogenous organometallic catalytic reactions due to its soft ionization properties. Therefore, fragile molecules and complexes in these reactions were characterized. The kinetic studies of these reactions have also been done by following the relative abundance of different species including starting material(s), products, by-product(s) as well as intermediates. Based on the results, reaction pathways and mechanisms were proposed and numerical models were built to accurately mimic the reactions under specific condition.

In order to make the reactions detectable by ESI-MS, many charged ESI-MS friendly substrates were synthesized as tracking tags, including 1-allyl-1-(prop-2-yn-1-yl)piperidin-1-ium hexafluorophosphate(V), 1-allyl-1-(prop-2-yn-1-yl)pyrrolidin-1-ium hexafluorophosphate(V), (4-ethynylbenzyl)triphenylphosphonium hexafluorophosphate(V), hex-5-yn-1-yltriphenylphosphonium hexafluorophosphate(V) etc. The method for continuously monitoring water- and oxygen-sensitive reactions in real time named pressurized sample infusion (PSI) was developed, optimized and applied throughout all the projects in the thesis.

These techniques were applied to detailed studies of the intramolecular Pauson-Khand reaction (PKR) with  $\text{Co}_2\text{CO}_8$  under different temperatures. The kinetic study results gave the entropy and

enthalpy of the reaction and evidence suggested that the ligand dissociation step was the rate-determining step of the reaction.

Hydrogenation of alkynes with Wilkinson's catalyst and Weller's catalyst were also studied using PSI. The behaviour of starting materials and products were tracked, then various reactions were carried out by using different temperatures and concentrations. Furthermore, competition reaction and kinetic isotope effect study, mechanisms were proposed based on experimental results, numerical models were built, and rate constants for each step were estimated.

Different Si-H activation reactions were studied including hydrolysis of silanes, hydrosilation, dehydrocoupling of silanes, alcoholysis of silane and silane redistribution by using (3-(methylsilyl)propyl)triphenylphosphonium hexafluorophosphate(V). A variety of collaborative projects were also carried out including hydroacylation, fast-activating Pd catalyst precursor, catalyst analysis for Cu-mediated fluorination, CdSe - NiDHLA analysis, Ru catalyzed propargylic amination reaction, Zn catalyzed lactide polymerization, and Fe<sub>4</sub>S<sub>4</sub> clusters.



## Table of Contents

|  |       |
|--|-------|
| Supervisory Committee .....  | ii    |
| Abstract .....   | iii   |
| Table of Contents .....  | v     |
| List of Tables .....   | vii   |
| List of Schemes .....  | viii  |
| List of Figures .....  | ix    |
| List of Abbreviations .....  | xvi   |
| List of Structures .....   | xviii |
| Acknowledgments .....  | xxii  |
| Dedication .....   | xxiii |
| 1. Literature Review .....   | 1     |
| 1.1 Organometallic catalysis .....   | 1     |
| 1.2 Traditional methods for analysis of organometallic reactions .....       | 4     |
| 1.2.1 NMR Spectroscopy .....   | 5     |
| 1.2.2 UV/Vis Spectroscopy .....  | 11    |
| 1.2.3 IR Spectroscopy .....  | 13    |
| 1.2.4 Mass Spectrometry .....  | 16    |
| 2. Techniques and methodologies .....  | 25    |
| 2.1 Introduction .....   | 25    |
| 2.2 Electrospray Ionization Mass Spectrometry .....                          | 26    |
| 2.3 Quadrupole –Time of Flight (Q-TOF) .....                                 | 29    |
| 2.4 Continuous reaction monitoring with ESI-MS .....                         | 33    |
| 3. Methodological innovations .....  | 37    |
| 3.1 Numerical modeling .....   | 37    |
| 3.2 Powersim model design .....  | 41    |
| 3.3 Handling air and moisture sensitive reactions .....                      | 46    |
| 3.4 PSI-ESI-MS optimization .....  | 48    |
| 3.4.1 PSI-ESI-MS filter .....  | 48    |
| 3.4.2 PSI-ESI-MS dilution system .....                                       | 50    |
| 3.4.3 PSI glassware .....  | 51    |
| 4. The Pauson-Khand Reaction .....   | 54    |
| 4.1 Introduction .....   | 54    |
| 4.2 Selected studies .....   | 56    |
| 4.3 Challenges of ESI-MS for Pauson-Khand studies .....                      | 57    |
| 4.4 Advantages of ESI-MS for the Pauson-Khand Reaction studies .....         | 58    |
| 4.5 Results and Discussion .....   | 59    |
| 4.5.1 Design of charged substrate .....                                      | 59    |
| 4.5.2 Synthesis of cobalt complexes .....                                    | 60    |
| 4.5.3 Previous gas phase reaction .....                                      | 62    |
| 4.5.4 Intramolecular Pauson-Khand reaction .....                             | 63    |
| 4.6 Conclusion .....   | 68    |
| 4.7 Experimental .....   | 68    |
| 5. Detailed kinetic analysis of rhodium-catalyzed alkyne hydrogenation ..... | 75    |
| 5.1 Hydrogenation of olefins by Rh (PPh <sub>3</sub> ) <sub>3</sub> Cl ..... | 75    |

|       |   |     |
|-------|---|-----|
| 5.1.1 | Introduction.....   | 75  |
| 5.1.2 | Previous investigation with ESI-MS.....   | 78  |
| 5.1.3 | Results and Discussion .....  | 80  |
| 5.1.4 | Conclusion .....  | 92  |
| 5.2   | Hydrogenation of olefins by Weller's catalyst .....   | 93  |
| 5.2.1 | Introduction.....   | 93  |
| 5.2.2 | Results and Discussion .....  | 94  |
| 5.2.3 | Conclusion .....  | 109 |
| 5.3   | Experimental.....   | 109 |
| 6.    | The use of charged substrates to investigate Si-H activation by ESI MS.....   | 113 |
| 6.1   | Current research in the area of Si-H activation.....  | 113 |
| 6.1.1 | Dehydrocoupling of silane.....  | 113 |
| 6.1.2 | Hydrolysis of silanes.....  | 118 |
| 6.1.3 | Hydrosilation.....  | 120 |
| 6.2   | Results and Discussion .....  | 122 |
| 6.3   | Future work.....  | 132 |
| 6.4   | Experimental.....   | 133 |
| 7.    | Collaborative studies.....  | 135 |
| 7.1   | CdSe-DHLA for H <sub>2</sub> production .....   | 135 |
| 7.2   | Fe <sub>4</sub> S <sub>4</sub> clusters .....   | 137 |
| 7.3   | Lactide polymerization by cationic zinc complexes.....  | 140 |
| 7.4   | Copper-Mediated Fluorination of Arylboronate Esters. Identification of a Copper(III) Fluoride Complex .....                   | 142 |
| 7.5   | Ti, Hf and Zr complexes .....   | 143 |
| 7.6   | Unusually Effective Catalyst Precursor for Suzuki–Miyaura Cross-Coupling Reactions .....                                      | 145 |
| 7.7   | Rhodium complexes catalyzed hydroacylation reaction.....  | 148 |
| 7.8   | CryoSpray MS (CSI-MS) .....   | 152 |
| 8.    | Conclusion .....  | 155 |
|       | References.....   | 157 |
|       | Appendix A: Intermediate data for Pauson-Khand reaction.....  | 165 |
|       | Appendix B: Numerical modeling, rate constants and ESI-MS data for hydrogenation reactions .....                              | 166 |
|       | Appendix C: Crystal data and structure refinement for PPh <sub>3</sub> P(CH <sub>2</sub> ) <sub>4</sub> CCH.....              | 170 |
|       | Appendix D: Crystal data and structure refinement for PPh <sub>3</sub> P(CH <sub>2</sub> ) <sub>5</sub> CH <sub>3</sub> ..... | 178 |
|       | Appendix E: Crystal data and structure refinement for (4-ethynylbenzyl)triphenylphosphonium hexafluorophosphate(V). .....     | 188 |
|       | Appendix F: Supporting data for Weller's hydrogenation .....  | 205 |
|       | Appendix G: Crystal data and structure refinement for PPh <sub>3</sub> P(CH <sub>2</sub> ) <sub>5</sub> CH <sub>3</sub> ..... | 209 |
|       | Appendix H: Data for collaboration projects.....  | 217 |

## List of Tables

|  |     |
|--|-----|
| Table 1: Ferrocenyl polyphosphanes structures and decoupled proton $^{31}\text{P}$ NMR data <sup>19</sup> . Reprinted with permission from “Congested Ferrocenyl Polyphosphanes Bearing Electron-Donating or Electron-Withdrawing Phosphanyl Groups: Assessment of Metallocene Conformation from NMR Spin Couplings and Use in Palladium-Catalyzed Chloroarenes Activation” S. Mom, M. Beaupérin, D. Roy, S. Royer, R. Amardeil, H. Cattey, H. Doucet and J. C. Hierso, <i>Inorganic Chemistry</i> , 2011, 50, 11592-11603. Copyright © 2011 American Chemical Society ..... | 8   |
| Table 2: Filter performance table.....   | 50  |
| Table 3: Aggregates and species in the reaction solution: .....  | 72  |
| Table 4: Rate constants for the numerically modelled reaction at 23°C.....   | 90  |
| Table 5: Estimated rate constants by different COPASI methods. First order rate constants are in units of $\text{min}^{-1}$ and second order rate constants in units of $\text{min}^{-1} \text{mmol}^{-1} \text{L}$ . .....  | 106 |
| Table 6: Samples for CdSe-DHLA for $\text{H}_2$ production.....  | 137 |
| Table 7: Samples with Ni and DHLA only.....  | 137 |
| Table 8 Assignment of peaks in the spectrum .....  | 224 |

## List of Schemes

|  |     |
|--|-----|
| Scheme 1: Chauvin's mechanism for alkene metathesis .....  | 2   |
| Scheme 2: Proposed catalytic cycle for the intermolecular Pauson-Khand reaction.....   | 55  |
| Scheme 3: Five different ways of ionizing neutral metal complexes. ....  | 57  |
| Scheme 4: Synthetic strategy applied to the charged acetylene substrates.....  | 60  |
| Scheme 5: Synthetic strategy for ionizing neutral metal complexes. ....  | 60  |
| Scheme 6: Mechanism of alkene hydrogenation using Wilkinson's catalyst, adapted from Halpern. <sup>156</sup> .....   | 77  |
| Scheme 7 Mechanism of alkene hydrogenation using Wilkinson's catalyst with dimerization and off-cycle processes. Reprinted with permission from "Mono-alkylated bisphosphines as dopants for ESI-MS analysis of catalytic reactions" D. M. Chisholm, A. G. Oliver and J. S. McIndoe, <i>Dalton Transactions</i> , 2010, 39, 364-373. Copyright © 2010 Royal Society of Chemistry ..... | 78  |
| Scheme 8: Synthesis route of (5-2).....  | 81  |
| Scheme 9: Synthesize route of (5-3).....   | 82  |
| Scheme 10: Synthesis route of (5-4).....   | 83  |
| Scheme 11: Hydrogenation of alkyne to alkene and then to alkane. ....  | 85  |
| Scheme 12: Exclusive terminal hydrosilation product. ....  | 120 |
| Scheme 13 Oxidative addition of Si-H into metal center occurs with retention of configuration at Si. ....  | 121 |
| Scheme 14: Attempted routes for making charged silane substrates.....  | 123 |
| Scheme 15: Silane alcoholysis between 6-5 and MeOD. ....   | 130 |
| Scheme 16: Copper-Mediated Fluorination of Arylboronate Esters. Reprinted with permission from "Copper-Mediated Fluorination of Arylboronate Esters. Identification of a Copper(III) Fluoride Complex" P. S. Fier, J. Luo and J. F. Hartwig, <i>Journal of the American Chemical Society</i> , 2013, 135, 2552-2559. Copyright © 2013 American Chemical Society .....                  | 142 |
| Scheme 17: Widely accepted Suzuki reaction catalytic cycle. ....   | 146 |
| Scheme 18: Rhodium complexes catalyzed hydroacylation reaction.....  | 149 |
| Scheme 19: Hydroacylation reactions by different Rh catalysts. ....  | 150 |

## List of Figures

|  |    |
|--|----|
| Figure 1: (1) First asymmetric Schrock catalyst; (2) 1st Generation Grubbs' Catalyst; (3) 2nd Generation Grubbs' Catalyst .....  | 3  |
| Figure 2: Catalytic cycle for Heck reaction .....  | 3  |
| Figure 3: Catalytic cycle for Negishi reaction (E = ZnX) and Suzuki reaction (E = B(OR) <sub>2</sub> ). .....  | 4  |
| Figure 4: Para-hydrogen enhanced NMR is used to detect signals of H on different species in the reaction, detected H is in red color. <sup>17</sup> Reprinted with permission from “An NMR study of cobalt-catalyzed hydroformylation using para-hydrogen induced polarisation” C. Godard, S. B. Duckett, S. Polas, R. Tooze and A. C. Whitwood, <i>Dalton Transactions</i> , 2009, 2496-2509. Copyright © 2009 The Royal Society of Chemistry .....   | 6  |
| Figure 5: <sup>1</sup> H NOESY spectrum of oxidative degradation product of [Cp*Ir(bzpy)(NO <sub>3</sub> )] <sup>18</sup> Reprinted with permission from “An NMR Study of the Oxidative Degradation of Cp*Ir Catalysts for Water Oxidation: Evidence for a Preliminary Attack on the Quaternary Carbon Atom of the –C–CH <sub>3</sub> Moiety” C. Zuccaccia, G. Bellachioma, S. Bolaño, L. Rocchigiani, A. Savini and A. Macchioni, <i>European Journal of Inorganic Chemistry</i> , 2012, 2012, 1462-1468. Copyright © 2012 Wiley-VCH Verlag GmbH & Co. KGaA, Weinheim .....   | 7  |
| Figure 6: <sup>1</sup> H- <sup>31</sup> P HMQC spectrum indicates the existence of a key intermediate during the reaction. <sup>20</sup> Reprinted with permission from “A parahydrogen based NMR study of Pt catalysed alkyne hydrogenation” M. Boutain, S. B. Duckett, J. P. Dunne, C. Godard, J. M. Hernandez, A. J. Holmes, I. G. Khazal and J. Lopez-Serrano, <i>Dalton Transactions</i> , 2010, 39, 3495-3500. © The Royal Society of Chemistry 2010 .....   | 9  |
| Figure 7: <sup>1</sup> H NMR spectra show a new formate hydrogen signal and a methyl hydrogen atoms signal which are related with <i>trans</i> -Ru(dmpc) <sub>2</sub> (Me)(O <sub>2</sub> CH). And the integration of these peaks changes over time. <sup>21</sup> Reprinted with permission from “Kinetic and Thermodynamic Investigations of CO <sub>2</sub> Insertion Reactions into Ru–Me and Ru–H Bonds – An Experimental and Computational Study” D. J. Darensbourg, S. J. Kyran, A. D. Yeung and A. A. Bengali, <i>European Journal of Inorganic Chemistry</i> , 2013, 2013, 4024-4031. Copyright © 2013 WILEY-VCH Verlag GmbH & Co. KGaA, Weinheim ..... | 10 |
| Figure 8: Synthesis of allylic silanes and boronates by using Pd catalysts reaction was monitored by <sup>1</sup> H NMR over 12 hours. Different species were tracked. <sup>23</sup> The concentration of each species correspond to the NMR signal integration. Reprinted with permission from “Mechanistic Investigation of the Palladium-Catalyzed Synthesis of Allylic Silanes and Boronates from Allylic Alcohols” J. M. Larsson and K. J. Szabó, <i>Journal of the American Chemical Society</i> , 2012, 135, 443-455. Copyright © 2012 American Chemical Society .....  | 11 |
| Figure 9: Generation of the solvate complex [Rh(Me-DuPHOS)(MeOH) <sub>2</sub> ]BF <sub>4</sub> . cod= cyclooctadiene; coe = cyclooctene <sup>25</sup> .....  | 12 |
| Figure 10: Reaction data for the stoichiometric hydrogenation of 0.01 mmol [Rh(Me-DuPHOS)(cod)]BF <sub>4</sub> in 15 mL MeOH at 25 °C and 1 bar overall pressure (cycle time 3 min, layer thickness 0.5 cm). <sup>25</sup> Reprinted with permission from “Kinetic and mechanistic investigations in homogeneous catalysis using operando UV/vis spectroscopy” C. Fischer, T. Beweries, A. Preetz, H.-J. Drexler, W. Baumann, S. Peitz, U. Rosenthal and D. Heller, <i>Catalysis Today</i> , 2010, 155, 282-288. Copyright © 2009 Elsevier B.V. ....   | 12 |
| Figure 11: Extinction diagram (left) and comparison of spectroscopic values (points) and values fitted as pseudo-first order (solid line) for several wavelengths. <sup>25</sup> Reprinted with permission from  |    |

|  |    |
|--|----|
| “Kinetic and mechanistic investigations in homogeneous catalysis using operando UV/vis spectroscopy” C. Fischer, T. Beweries, A. Preetz, H.-J. Drexler, W. Baumann, S. Peitz, U. Rosenthal and D. Heller, <i>Catalysis Today</i> , 2010, 155, 282-288. Copyright © 2009 Elsevier B.V.  | 12 |
| Figure 12: Attenuated Total Reflectance (ATR).   | 14 |
| Figure 13: Latest version of React-IR, the ReactIR™ 45m. <sup>36</sup>   | 14 |
| Figure 14: ReactIR spectrum of lithiation of <i>N</i> -Boc pyrrolidine compound. <sup>37</sup> Reprinted with permission from “Enantioselective, Palladium-Catalyzed $\alpha$ -Arylation of <i>N</i> -Boc Pyrrolidine: In Situ React IR Spectroscopic Monitoring, Scope, and Synthetic Applications” G. Barker, J. L. McGrath, A. Klapars, D. Stead, G. Zhou, K. R. Campos and P. O’Brien, <i>The Journal of Organic Chemistry</i> , 2011, 76, 5936-5953. Copyright © 2011 American Chemical Society | 15 |
| Figure 15: Overlay of different spectra including starting reagents, product and putative imine intermediate. <sup>38</sup> Reprinted with permission from “Mannich-like three-component synthesis of $\alpha$ -branched amines involving organozinc compounds: ReactIR monitoring and mechanistic aspects” E. Le Gall, S. Sengmany, C. Hauréna, E. Léonel and T. Martens, <i>Journal of Organometallic Chemistry</i> , 2013, 736, 27-35. Copyright © 2013 Elsevier B.V.                             | 16 |
| Figure 16: MALDI (left) and ESI sources. <sup>41, 42</sup> Reprinted with permission from “Electrospray and MALDI Mass Spectrometry: Fundamentals, Instrumentation, Practicalities, and Biological Applications, Second Edition” R. B. Cole, <i>Electrospray and MALDI Mass Spectrometry: Fundamentals, Instrumentation, Practicalities, and Biological Applications</i> , John Wiley & Sons, 2009. Copyright © 2010 John Wiley & Sons, Inc.   | 17 |
| Figure 17: ESI-MS study of the mechanism of a Baylis-Hillman reaction catalyzed by DABCO. <sup>58</sup>  | 18 |
| Figure 18: Charged intermediates were detected during the DKR of amines reaction, each intermediate can be represented by a characteristic peak. <sup>60</sup> Reprinted with permission from “Shvo's catalyst in chemoenzymatic dynamic kinetic resolution of amines – inner or outer sphere mechanism?” B. G. Vaz, C. D. F. Milagre, M. N. Eberlin and H. M. S. Milagre, <i>Organic &amp; Biomolecular Chemistry</i> , 2013, 11, 6695-6698. Copyright © The Royal Society of Chemistry 2013.       | 19 |
| Figure 19: Shvo’s catalyst catalysed amine racemization mechanism revealed by ESI-MS. <sup>60</sup> Reprinted with permission from “Shvo's catalyst in chemoenzymatic dynamic kinetic resolution of amines – inner or outer sphere mechanism?” B. G. Vaz, C. D. F. Milagre, M. N. Eberlin and H. M. S. Milagre, <i>Organic &amp; Biomolecular Chemistry</i> , 2013, 11, 6695-6698. Copyright © The Royal Society of Chemistry 2013.  | 20 |
| Figure 20: Collision-induced fragmentation of cationic species. <sup>61</sup> Reprinted with permission from “C–H Activation at a Ruthenium(II) Complex – The Key Step for a Base-Free Catalytic Transfer Hydrogenation?” L. Taghizadeh Ghoochany, C. Kerner, S. Farsadpour, F. Menges, Y. Sun, G. Niedner-Schatteburg and W. R. Thiel, <i>European Journal of Inorganic Chemistry</i> , 2013, 2013, 4305-4317. Copyright © 2013 WILEY-VCH Verlag GmbH & Co. KGaA, Weinheim....                      | 21 |
| Figure 21: ESI-MS of dba-free arylpalladium species. <sup>62</sup> Reprinted with permission from ““Dba-free” palladium intermediates of the Heck–Matsuda reaction. A. H. L. Machado, H. M. S. Milagre, L. S. Eberlin, A. A. Sabino, C. R. D. Correia and M. N. Eberlin, <i>Organic &amp; Biomolecular Chemistry</i> , 2013, 11, 3277-3281. Copyright © The Royal Society of Chemistry.  | 22 |
| Figure 22: MS/MS of MAO anion <i>m/z</i> 1881. <sup>63</sup> Ten losses of 72 Da from the parent ion are indicated by red arrows with a second series of fragment ions occurring at –16 Da, between <i>m/z</i> 1075 and 1507, depicted by blue arrows. Reprinted with permission from “Mass Spectrometric  |    |

|   |    |
|---|----|
| Characterization of Methylaluminumoxane” T. K. Trefz, M. A. Henderson, M. Y. Wang, S. Collins and J. S. McIndoe, <i>Organometallics</i> , 2013, 32, 3149-3152. Copyright © 2013 American Chemical Society .....   | 23 |
| Figure 23: CID (collision induced dissociation) mass spectrum of the ion at $m/z=1000.3$ , a Rh(I) intermediate. <sup>64</sup> Reprinted with permission from “Direct Detection of Key Intermediates in Rhodium(I)-Catalyzed [2+2+2] Cycloadditions of Alkynes by ESI-MS” M. Parera, A. Dachs, M. Solà, A. Pla-Quintana and A. Roglans, <i>Chemistry – A European Journal</i> , 2012, 18, 13097-13107. Copyright © 2012 WILEY-VCH Verlag GmbH & Co. KGaA, Weinheim.....   | 24 |
| Figure 24: The desolvation process in electrospray ionization. Modified with permission of the author from Henderson, W., McIndoe J. S., <i>Mass Spectrometry of Inorganic and Organometallic Compounds</i> . John Wiley & Sons, Ltd. West Sussex: 2005, p. 92. ....  | 27 |
| Figure 25: (a) IEM: Small ion ejection from a charged nanodroplet. (b) CRM: Release of a globular protein into the gas phase. <sup>86</sup> Reprinted with permission from “Unraveling the Mechanism of Electrospray Ionization” L. Konermann, E. Ahadi, A. D. Rodriguez and S. Vahidi, <i>Analytical Chemistry</i> , 2012, 85, 2-9. Copyright © 2012 American Chemical Society ...   | 28 |
| Figure 26: Electrospray source with QTOF-Micro scheme. <sup>87</sup> Reprinted with permission from “Micromass Q-TOF micro Mass Spectrometer Operator’s Guide” Copyright © 2012 Waters Corporation .....  | 29 |
| Figure 27: The Ion Optical System of the Q-TOF micro. <sup>87</sup> Reprinted with permission from “Micromass Q-TOF micro Mass Spectrometer Operator’s Guide” Copyright © 2012 Waters Corporation .....   | 30 |
| Figure 28: The Prefilter and Main Analyzer of the Q-TOF <i>micro</i> <sup>87</sup> Reprinted with permission from “Micromass Q-TOF micro Mass Spectrometer Operator’s Guide” Copyright © 2012 Waters Corporation.....   | 31 |
| Figure 29 Positive-ion energy-dependent ESI-MS of a representative example.X axis is the $m/z$ , Y axis is collision energy in voltage, the red and blue dots are the detected signal of a certain species at the applied voltage. <sup>88</sup> Reprinted with permission from “Synthesis and characterization of a new class of anti-angiogenic agents based on ruthenium clusters” A. A. Nazarov, M. Baquie, P. Nowak-Sliwinska, O. Zava, J. R. van Beijnum, M. Groessl, D. M. Chisholm, Z. Ahmadi, J. S. McIndoe, A. W. Griffioen, H. van den Bergh and P. J. Dyson, <i>Sci. Rep.</i> , 2013, 3. Copyright © 2013 Macmillan Publishers Limited..... | 32 |
| Figure 30 Time of Flight analyzer <sup>87</sup> Reprinted with permission from “Micromass Q-TOF micro Mass Spectrometer Operator’s Guide” Copyright © 2012 Waters Corporation .....   | 33 |
| Figure 31 Pressurized sample infusion system setup.....   | 35 |
| Figure 32: Normalized intensity vs. time trace for a charged silane ( $m/z$ 349) and appearance of the product of redistribution ( $m/z$ 425). <sup>72</sup> .....  | 36 |
| Figure 33: Proposed mechanism for hydrogenation of alkyne by Wilkinson’s catalyst. <sup>95</sup> .....  | 37 |
| Figure 34: Powersim Numerical model <sup>95</sup> , this figure represents a Wilkinson’s hydrogenation reaction.....  | 38 |
| Figure 35: COPASI interface.....  | 39 |
| Figure 36: COPASI model for reversible reaction .....   | 40 |
| Figure 37: simulation method of COPASI.....   | 41 |
| Figure 38: Powersim model for irreversible first order reaction. ....   | 41 |
| Figure 39: Reductive elimination.....   | 42 |
| Figure 40: Dimer splits into two monomers .....   | 43 |
| Figure 41: Oxidative addition .....   | 44 |

|   |    |
|---|----|
| Figure 42: Reversible reductive elimination.....  | 45 |
| Figure 43: Powersim model for second order reversible reaction.....   | 46 |
| Figure 44: Glovebox next to MS .....  | 47 |
| Figure 45: Online monitoring with blocked PEEK tubing .....   | 48 |
| Figure 46: Eight generations of filter.....   | 49 |
| Figure 47: The new online dilution system.....  | 51 |
| Figure 48: Photo of online dilution system.....   | 51 |
| Figure 49: PSI NMR tube .....   | 52 |
| Figure 50: PSI sample vial. In a glovebox, small amounts of solid sample can be introduced into a vial capped with a septum, then taken out of the glovebox and solvent injected into it. Two PEEK tubes pierce through a septum into the vial. The yellow PEEK tube is connected to a pressure supply (e.g. Ar or N <sub>2</sub> ), and the red PEEK tube is dipped into the solution and the other end is connected to the ESI-MS. If the sample is not soluble enough, a filter must be installed on the red PEEK tube and the septum fitted before the vial is capped.....                        | 53 |
| Figure 51: Energetics of the PK reaction. Reprinted with permission from “Density Functional Studies on the Pauson–Khand Reaction” M. Yamanaka and E. Nakamura, <i>Journal of the American Chemical Society</i> , 2001, 123, 1703-1708. Copyright © 2001 American Chemical Society.....   | 56 |
| Figure 52: Functionalized pyrrolidinium and piperidinium salts. X <sup>-</sup> = Br <sup>-</sup> , PF <sub>6</sub> <sup>-</sup> , BPh <sub>4</sub> <sup>-</sup> , Tf <sub>2</sub> N <sup>-</sup> ..   | 59 |
| Figure 53: Positive-ion ESI-MS in dichloromethane [Co <sub>2</sub> (CO) <sub>6</sub> (4-3)][PF <sub>6</sub> ] (top) and [Co <sub>2</sub> (CO) <sub>6</sub> (4-1)][PF <sub>6</sub> ] (bottom). In both cases, the single peak corresponds to the intact cation. 61   |    |
| Figure 54: Single crystal X-ray structure of the cationic part of [Co <sub>2</sub> (CO) <sub>6</sub> (4-1)] <sup>+</sup> [BPh <sub>4</sub> ] <sup>-</sup> . The tetraphenylborate anion is not shown for the sake of clarity. Key bond lengths: Co1-Co2 2.461 Å; C7-C8 1.334 Å; C8-C9 1.488 Å; 1.311 ± 0.01 Å; Co-C 1.96 ± 0.01 Å; C-O 1.13 ± 0.01 Å; Co-CO 1.81 ± 0.02 Å; C-N 1.52 ± 0.02 Å. Key bond angles: C6-C7-C8 146.2°; Co-Co-C 51 ± 1°, Co-C-Co 77.5 ± 0.3°. .....   | 62 |
| Figure 55: Gas phase reactions of [Co <sub>2</sub> (CO) <sub>6</sub> (4-1)] <sup>+</sup> with three different alkenes at a cone voltage of 20 V. In each case, one CO ligand is removed and the alkene adds to [Co <sub>2</sub> (CO) <sub>5</sub> (1)] <sup>+</sup> . The alkene does <i>not</i> add to the fully saturated ion.....  | 62 |
| Figure 56: Abundance vs. time data for [4-3] <sup>+</sup> (starting material), [Co <sub>2</sub> (CO) <sub>6</sub> (4-3)] <sup>+</sup> (intermediate) and [4-3 + CO] <sup>+</sup> (product). Data collected using positive ion PSI-ESI-MS in chlorobenzene, online dilution with acetone, Schlenk flask saturated and pressurized with CO. Data has been normalized to the total ion current. Scan time of 10 seconds per spectrum. Approximately 20% of the total ion current at the end of the reaction consisted of numerous low abundance by-products, none of which exceeded 5% of the total..... | 65 |
| Figure 57: During the PSI-ESI-MS, the collision voltage was set to 2 V. The breakdown graph shows [Co <sub>2</sub> (CO) <sub>6</sub> (4-3)] <sup>+</sup> is a stable species at this voltage and it can only be fragmented when the collision voltage reaches 8 V. ....   | 66 |
| Figure 58: Intensity vs. time data for [Co <sub>2</sub> (CO) <sub>6</sub> (4-3)] <sup>+</sup> (starting material) and [4-3 + CO] <sup>+</sup> (product), collected at three different temperatures. Inset: Eyring plot for the three different temperatures.....  | 67 |
| Figure 59: Positive ions of ionized Wilkinson’s catalyst, where 5-1 <sup>+</sup> is [Ph <sub>2</sub> P(CH <sub>2</sub> ) <sub>4</sub> PPh <sub>2</sub> Bn] <sup>+</sup> . Reprinted with permission from “Mono-alkylated bisphosphines as dopants for ESI-MS analysis of catalytic reactions” D. M. Chisholm, A. G. Oliver and J. S. McIndoe, <i>Dalton Transactions</i> , 2010, 39, 364-373. Copyright © 2010 Royal Society of Chemistry .....   | 79 |



|  |     |
|--|-----|
| Figure 60: X-ray crystal structure of $[\text{Ph}_3\text{P}(\text{CH}_2)_4\text{C}_2\text{H}]^+ \Gamma$ . Key structural parameters: C5-C6 1.118 Å; C4-C5-C6 177.51°.  | 82  |
| Figure 61: X-ray crystal structure of $[\text{Ph}_3\text{P}(\text{CH}_2)_4\text{C}_2\text{H}]^+ \Gamma$ (the precursor to 5-4). Key structural parameters: C5-C6 1.118 Å; C4-C5-C6 177.51°.  | 84  |
| Figure 62: Positive-ion ESI-MS in fluorobenzene, $[\text{PPh}_3\text{P}(\text{CH}_2)_4\text{CCH}]\text{PF}_6$ (bottom) is the starting material. $[\text{PPh}_3\text{P}(\text{CH}_2)_5\text{CH}_3]\text{PF}_6$ (top) is the final product.   | 86  |
| Figure 63 Relative intensity vs time traces for alkyne (5-4), alkene (5-5) and alkane (5-6).   | 86  |
| Figure 64: Traces for disappearance of alkyne (top), appearance and disappearance of alkene (middle), and appearance of alkane (bottom) at temperatures of 0°C, 23°C and 58°C.   | 88  |
| Figure 65: Catalytic cycle for hydrogenation of alkyne to alkane, where the two hydrogenations compete with one another.   | 89  |
| Figure 66: Match between simulated and experimental reaction progress curves. The thin black lines are the experimental curves; the thick transparent lines are the calculated curves.   | 90  |
| Figure 67: Experimental traces for hydrogenation of 5-4 using Wilkinson's catalyst (5 mol%) at 91°C in the presence of (a) no added $\text{PPh}_3$ , (b) one equivalent of $\text{PPh}_3$ , and (c) two equivalents of $\text{PPh}_3$ . The right-hand column shows the corresponding traces calculated by the numerical model, wherein only the starting concentration of $\text{PPh}_3$ has been altered.                          | 92  |
| Figure 68: Alkane hydrogenation product. Key bond lengths and angles: C5-C6 1.500 Å; C4-C5-C6 113.83°.   | 95  |
| Figure 69: Hydrogenation of $[\text{Ph}_3\text{P}(\text{CH}_2)_4\text{CH}=\text{CH}_2][\text{PF}_6]$ under 3 psi of $\text{H}_2$ , with 13.3% of $[\text{Rh}(\text{PR}_3)_2(\text{FPh})]^+[\text{BAr}^{\text{F}}_4]^-$ as catalyst at room temperature with FPh as solvent. Inset: relative intensity vs time plot exhibiting behavior of $[\text{Rh}(\text{PR}_3)_2(\text{FPh})]^+$ (5-7) and $[\text{Rh}(\text{PR}_3)_2]^+$ (5-8). | 96  |
| Figure 70: Top: disappearance of alkyne 5-4 at 0, 23, 38 and 49°C (fast at all temperatures). Middle: appearance and consumption of alkene 3. Bottom: appearance of alkane 5-6.  | 97  |
| Figure 71: Reaction rate as a function of catalyst loading, illustrating that the reaction is first order in the concentration of $[\text{RhP}_2(\text{FPh})]^+[\text{BAr}^{\text{F}}_4]^-$ used.  | 98  |
| Figure 72: Selective hydrogenation of the charge-tagged alkyne in the presence of 1.1 equivalents of $\text{H}_2$ . Inset: $\ln[x]$ vs time plot exhibiting 1st order behavior.  | 98  |
| Figure 73: Comparison of hydrogenation with excess hydrogen and one equivalent of hydrogen.  | 99  |
| Figure 74: Reaction profiles for the reduction of alkyne to alkane using $\text{H}_2$ (blue/yellow) vs. $\text{D}_2$ (green/red).  | 99  |
| Figure 75: Precatalyst signal before hydrogenation started: mostly $[\text{RhP}_2(\text{PhF})]^+$ .  | 100 |
| Figure 76: Precatalyst signal after hydrogenation started: a mix of $[\text{RhP}_2]^+$ and $[\text{RhP}_2(\text{PhF})]^+$ .  | 101 |
| Figure 77: Mass spectrum of $[\text{Rh}(\text{PR}_3)_2(\text{octyne})_n]^+$ ( $n = 1$ , left, and $n = 2$ , right). Experimental data shown by line, calculated isotope pattern shown by columns.  | 101 |
| Figure 78: Pathways for alkene hydrogenation, after Schrock and Osborn.  | 102 |
| Figure 79: The effect of $\text{NEt}_3$ on the rate and selectivity of hydrogenation.  | 103 |
| Figure 80: Addition of $\text{NEt}_3$ leads to the disappearance of $[\text{RhP}_2]^+$ and the appearance of $[\text{HNEt}_3]^+$ .   | 104 |
| Figure 81: The mechanism of alkyne/alkene hydrogenation. $\text{P} = \text{P}(\text{cyclopropyl})_3$ .   | 105 |
| Figure 82: Direct comparison between simulated (coloured lines) and experimental results (black). The simulation is for the genetic algorithm, but similarly good matches were obtained for the other methods.   | 107 |
| Figure 83: Competition reaction: reduction of alkyne vs. alkene. Note that the alkenes remain essentially untouched until the alkyne is completely consumed. Reduction of the two alkenes  |     |

|   |     |
|---|-----|
| proceed at similar pace, though the hydrogenation of $[\text{Ph}_3\text{P}(\text{CH}_2)_3\text{CH}=\text{CH}_2]^+$ was slightly faster than that of $[\text{Ph}_3\text{P}(\text{CH}_2)_4\text{CH}=\text{CH}_2]^+$ .....   | 108 |
| Figure 84: Dehydrocoupling of silanes for early transition metal complexes, following the $\sigma$ bond metathesis mechanism. ....  | 114 |
| Figure 85: Dehydrocoupling of silanes for late transition metal complexes, following the oxidative addition/reductive elimination mechanism. ....   | 115 |
| Figure 86: 1,2 silyl migration (or silylene insertion) mechanism for dehydrocoupling of silanes by late transition metal complexes.....   | 115 |
| Figure 87: Proposed dehydrocoupling of silane mechanism based on observation. ....  | 116 |
| Figure 88: Charged phosphine ligand benzyl(4-(diphenylphosphino)butyl)diphenylphosphonium hexafluorophosphate(V). ....  | 117 |
| Figure 89: Red species should be visible in ESI-MS by using a charged silane substrate. ....  | 117 |
| Figure 90: Hydrolysis of dichlorosilane .....   | 118 |
| Figure 91: Hydrolysis and condensation of hydrosilanes. ....  | 118 |
| Figure 92: Cationic oxorhenium catalyst for hydrolysis of silane.....   | 119 |
| Figure 93: A ruthenium complex catalyzed hydrolysis of silane mechanism proposed by Lee et al. <sup>215</sup> .....   | 119 |
| Figure 94: Fe complex for hydrosilation .....   | 120 |
| Figure 95: The Chalk-Harrod mechanism. ....   | 121 |
| Figure 96: Proposed Ru–silylene-based catalytic cycle.....  | 122 |
| Figure 97: X-ray crystal structure of compound 6-5. ....  | 123 |
| Figure 98: Dehydrocoupling of silanes catalyzed by Wilkinson’s catalyst, $\text{RhCl}(\text{PPh}_3)_3$ .....  | 124 |
| Figure 99: Hydrolysis of silanes catalyzed by Wilkinson’s catalyst, $\text{RhCl}(\text{PPh}_3)_3$ . ....  | 124 |
| Figure 100: PSI-ESI-MS online monitoring result of hydrolysis of silane. Left: whole reaction process over 130 minutes. Reaction started when $\text{RhCl}(\text{PPh}_3)_3$ was introduced into reaction system around the 8th minute. Right: enlarged graph of converting part. The whole reaction finished in 3 minutes. .... | 125 |
| Figure 101: PSI-ESI-MS online monitoring result of hydrolysis of silane. Whole reaction process was over 210 minutes. Reaction started when $\text{RhCl}(\text{PPh}_3)_3$ was introduced into reaction system around the 10th minute. ....  | 126 |
| Figure 102: Hydrolysis of silanes, even longer oligomer products were detected. ....  | 127 |
| Figure 103: PSI-ESI-MS online monitor of hydrolysis of silane by $[\text{Cp}^*\text{Ru}(\text{MeCN})_3][\text{PF}_6]$ . The data quality is poor because the PEEK tubing was partially blocked by large molecular weight oligomer products. Target product %P485 is stable with water, no hydrolysis of silane.....             | 128 |
| Figure 104: Silane alcoholysis between 6-5 and MeOH under 51 °C.....  | 129 |
| Figure 105: Silane alcoholysis between 6-5 and MeOD under 51 °C. ....   | 130 |
| Figure 106: Relative intensity vs time for Wilkinson’s catalyst fragment $[\text{Rh}(\text{PPh}_3)_3]^+$ at $m/z=889.7$ . ....  | 131 |
| Figure 107: A potential intermediate of alcoholysis of silane by Wilkinson’s catalyst. ....   | 131 |
| Figure 108: Mixture of potential intermediates, mixture of two potential intermediate with formular $[(\text{PPh}_3)_2\text{RhCl}+\text{MeSi}(\text{CH}_2)_3\text{PPh}_3+\text{H}]^+$ (blue peaks) and $[(\text{PPh}_3)_2\text{RhCl}+\text{MeSi}(\text{CH}_2)_3\text{PPh}_3+\text{D}]^+$ (gray peaks) at ratio 1:2. ....        | 132 |
| Figure 109: CdSe-DHLA for $\text{H}_2$ production.....  | 136 |
| Figure 110: Difference between adding and not adding Ni in the hydrogen production system. ....   | 136 |
| Figure 111: FeS cluster samples .....   | 138 |

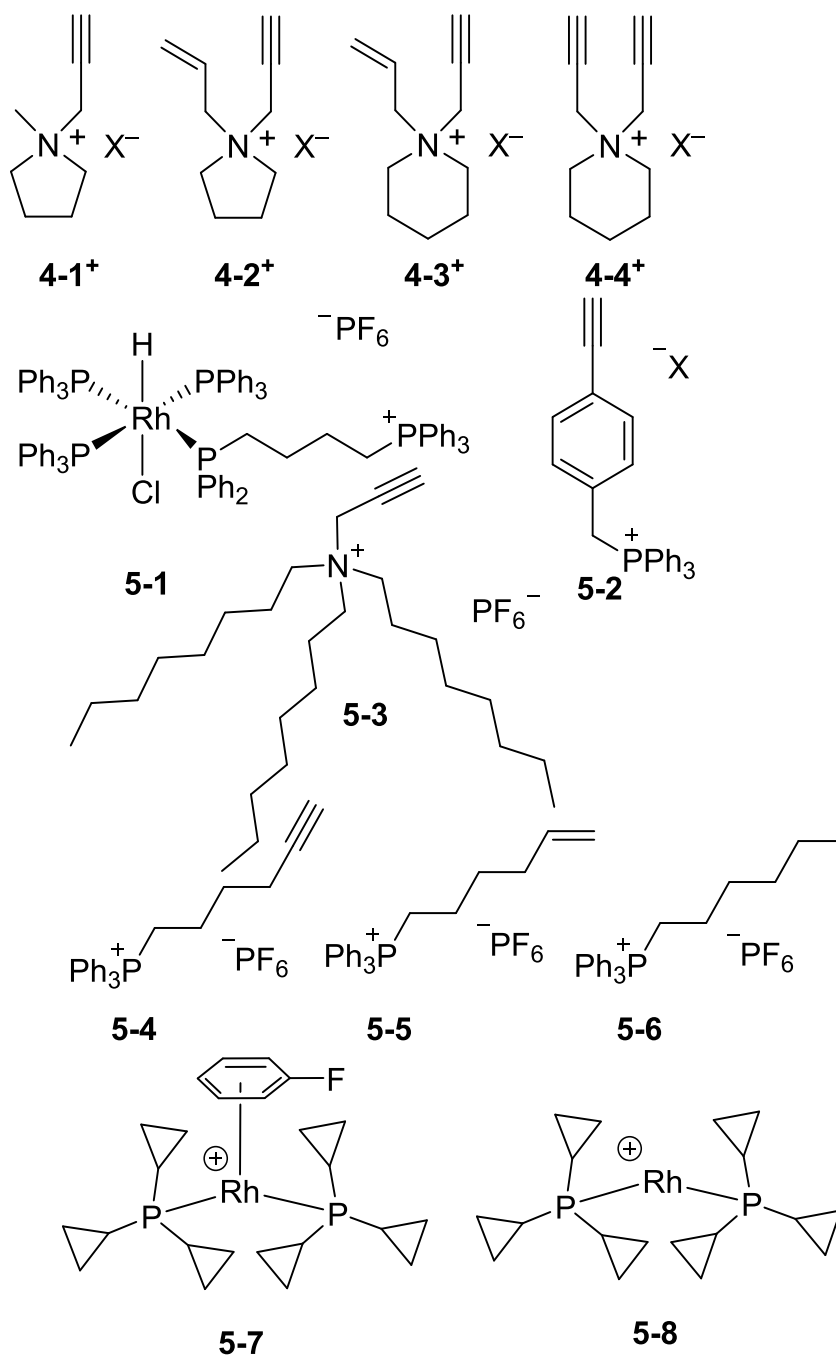
|  |     |
|--|-----|
| Figure 112: MS of the $\text{Fe}_4\text{S}_4(\text{Cy}_3)_4$ cluster, the blue bar is the calculated isotope pattern, the line is the experimental data. ....  | 138 |
| Figure 113: MS/MS of the 7.2-1. We can see many fragments of the mother ion-1472.9, the daughter ions: 1192.6, 912.0, 631.9 and 351.7 are due to lose of $\text{PCy}_3$ . ....   | 139 |
| Figure 114: MS/MS of the 7.2-2, 623.7 is $[\text{7.2-2} + \text{Et}_4\text{N}]^+$ , 493.5 is 7.2-2, 458.5 is $[\text{7.2-2} - \text{Cl}]^+$ . ....   | 139 |
| Figure 115: MS/MS of 7.2-3, 838.0 is $[\text{7.2-2} + \text{Et}_4\text{N}]^+$ , 618.8 is $[\text{7.2-2} - \text{SBu}]^+$ , 383.6 is $[\text{7.2-2} - 3*\text{SBu}]^+$ .....  | 140 |
| Figure 116: Structure of the cationic zinc complex. ....   | 141 |
| Figure 117: MS data of the Zn complex and the calculated isotope pattern (blue bars). ....   | 141 |
| Figure 118: MS of intermediate in copper-mediated fluorination Reprinted with permission from “Copper-Mediated Fluorination of Arylboronate Esters. Identification of a Copper(III) Fluoride Complex” P. S. Fier, J. Luo and J. F. Hartwig, <i>Journal of the American Chemical Society</i> , 2013, 135, 2552-2559. Copyright © 2013 American Chemical Society ..... | 143 |
| Figure 119: Ti, Hf and Zr complexes.....   | 144 |
| Figure 120: MS experimental data shows as $[\text{M}+\text{Na}-\text{H}]^+$ of 7-5-1, calculated isotope pattern of $[\text{M}+\text{Na}-\text{H}]^+$ .....  | 145 |
| Figure 121: Ligands for $\text{Pd}(\eta^3\text{-1-PhC}_3\text{H}_4)(\eta^5\text{-C}_5\text{H}_5)$ activation.....  | 146 |
| Figure 122: Negative mode, ESI-MS. Addition of $\text{Pd}(\eta^3\text{-1-Ph-C}_3\text{H}_4)(\eta^5\text{-C}_5\text{H}_5)$ to charged ligand 7-7-1 makes ligand disappear over the course of about 20 minutes. ....   | 147 |
| Figure 123: $(\text{7.7.1})_2\text{Pd}$ species is the main Pd containing peak in the reaction, however the calculated isotope pattern (blue bars) shows a extra H is present.....   | 147 |
| Figure 124: In positive mode of ESI-MS. Reaction with 7-7-2 as ligand. The blue species is $[\text{PhC}_3\text{H}_4+7.7.2]^+$ , the red species is $[\eta^3\text{-1-PhC}_3\text{H}_4+\text{Pd}+7-7-2]^+$ .....   | 148 |
| Figure 125: Proposed mechanism for hydroacylation by rhodium complexes.....  | 149 |
| Figure 126: Hydroacylation catalytic cycle with reaction online monitoring results. ....   | 151 |
| Figure 127: Weak bonding supramolecular complexes characterized by CSI. ....   | 153 |
| Figure 128: Experiment data of 7-8-1 (2+) and calculated isotope pattern (blue bars).....  | 153 |
| Figure 129: Experimental data of 7-8-2 (4+) and calculated isotope pattern (blue bars).....  | 154 |

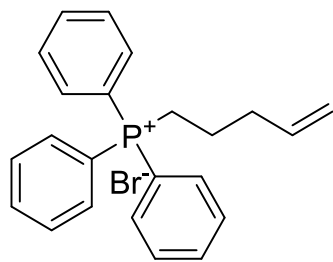
## List of Abbreviations

|                     |   |
|---------------------|---|
| [X] <sup>-</sup>    | anion   |
| [X] <sup>+</sup>    | cation  |
| Ar                  | aryl  |
| b.p                 | boiling point   |
| Boc                 | <i>tert</i> -Butyl carbamates   |
| bpy                 | 2,2'-bipyridyl  |
| <sup>t</sup> bucope | (C <sub>8</sub> H <sub>14</sub> )PC <sub>6</sub> H <sub>4</sub> CH <sub>2</sub> P(tBu) <sub>2</sub> |
| cat                 | catalyst  |
| CI                  | chemical ionization   |
| CID                 | collision induced dissociation  |
| COD                 | cyclooctadiene  |
| Col V               | collision voltage   |
| CSI                 | CryoSpray Ionization  |
| Cp                  | cyclopentadienyl ligand   |
| Cp*                 | pentamethylcyclopentadienyl ligand  |
| CV                  | cone voltage  |
| Da                  | Dalton  |
| DABCO               | 1,4-diazabicyclo[2.2.2]octane   |
| DFT                 | density functional theory   |
| DHLA                | Dihydrolipoic acid  |
| dppp                | 1,3-Bis(diphenylphosphino)propane   |
| EDESI               | energy-dependent electrospray ionization  |
| EDG                 | electron donating group   |
| EI                  | electron impact   |
| EPR                 | electron paramagnetic resonance   |
| ESI                 | electrospray ionization   |
| ESI(-)-MS           | negative-ion electrospray ionization mass spectrometry  |
| ESI(+)-MS           | positive-ion electrospray ionization mass spectrometry  |
| FT-ICR              | Fourier transform ion cyclotron resonance   |
| GC                  | gas chromatography  |
| GPC                 | gel permeation chromatography   |
| Hex                 | hexyl group   |
| HPLC                | high performance liquid chromatography  |
| ID                  | inner diameter  |
| <i>iPr</i>          | isopropyl   |
| IR                  | infrared  |
| IS                  | internal standard   |
| KE                  | kinetic energy  |
| KIE                 | kinetic isotope effect  |
| L                   | ligand  |

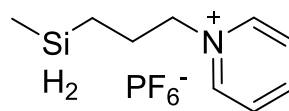
|                                 |  |
|---------------------------------|--|
| m                               | meta   |
| m.p.                            | melting point  |
| m/z                             | mass-to-charge ratio                                   |
| MALDI                           | matrix-assisted laser desorption<br>ionization         |
| MAO                             | methylaluminoxane                                      |
| MCP                             | microchannel plate                                     |
| Me                              | methyl   |
| MS                              | mass spectrometry/ mass spectrometer/<br>mass spectrum |
| MS/MS                           | tandem mass spectrometry                               |
| NMR                             | nuclear magnetic resonance                             |
| OA                              | oxidative addition                                     |
| OAc                             | acetate  |
| OTf                             | trifluoromethanesulfonate                              |
| p                               | para   |
| P <sup>c</sup> Pr <sub>3</sub>  | tricyclopropylphosphane                                |
| PCy <sub>3</sub>                | Tricyclohexylphosphine                                 |
| PEEK                            | polyetheretherketone                                   |
| [PF <sub>6</sub> ] <sup>-</sup> | hexafluorophosphate                                    |
| Ph                              | phenyl   |
| ppm                             | parts per million                                      |
| PSI                             | pressurized sample infusion                            |
| Q-TOF                           | quadrupole-time-of-flight                              |
| RE                              | reductive elimination                                  |
| RF                              | radio frequency  |
| RSD                             | relative standard deviation                            |
| SBU                             | -S-[(CH <sub>2</sub> ) <sub>3</sub> CH <sub>3</sub> ]  |
| SPS                             | Solvent Purification System                            |
| <i>t</i> Bu                     | tertiary butyl   |
| THF                             | tetrahydrofuran  |
| TIC                             | total ion current                                      |
| TOF                             | time-of-flight   |
| UV                              | ultraviolet  |
| UV/Vis                          | ultraviolet/visible                                    |

## List of Structures

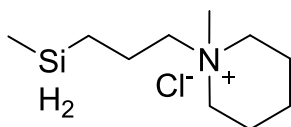




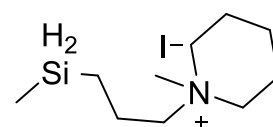
5-9



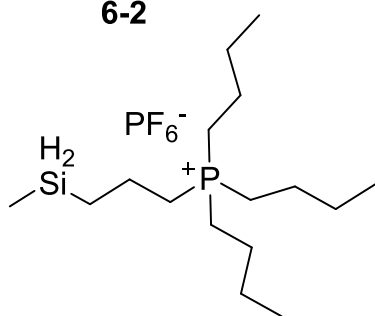
6-1



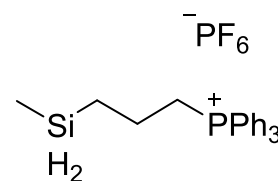
6-2



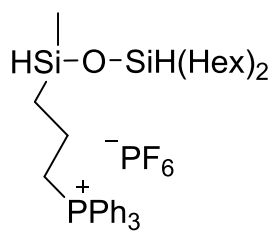
6-3



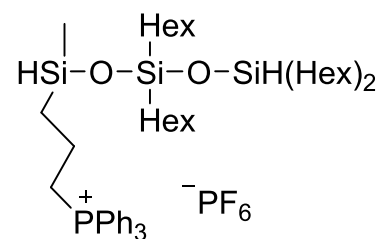
6-4



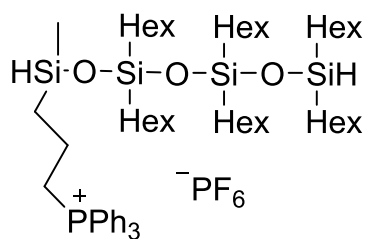
6-5



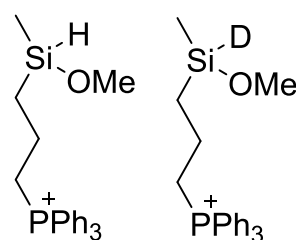
6.7



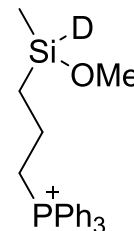
6.8



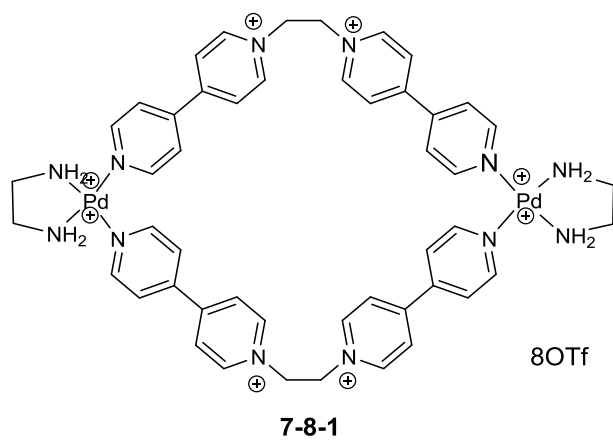
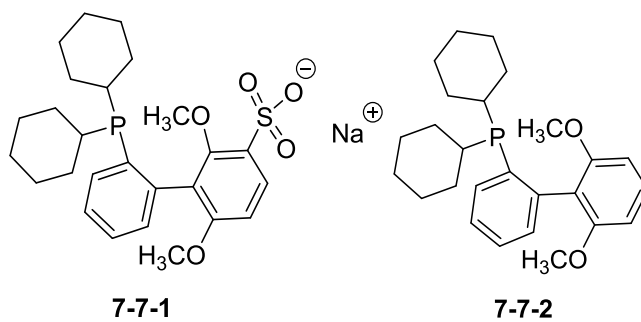
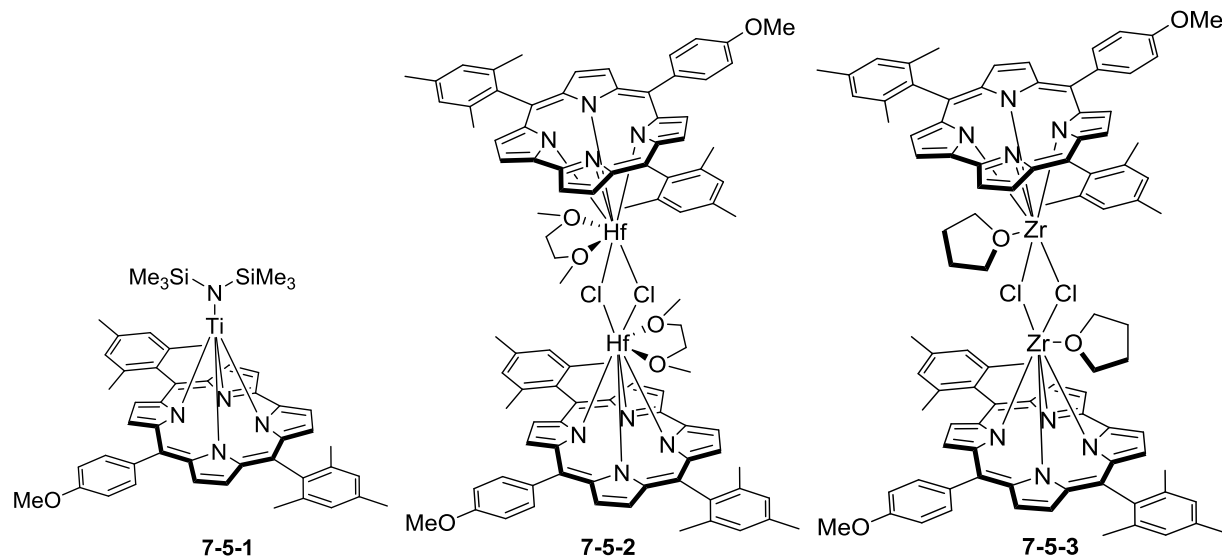
6.9



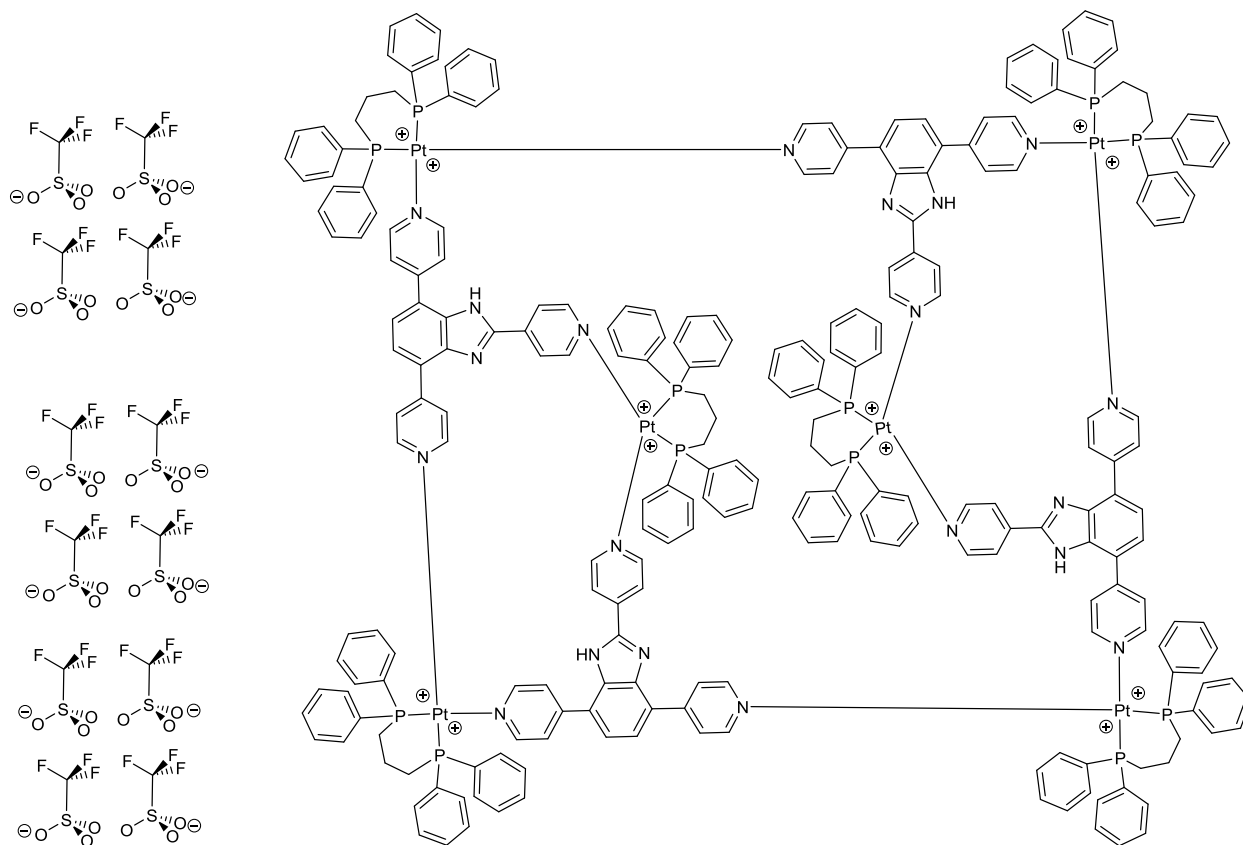
silane-H



silane-D







7-8-2

## Acknowledgments

Firstly I would like to thank my supervisor Professor Scott McIndoe for his teaching, supporting, encouraging and inspiring in my five years' Ph.D study. My thanks to him for teaching me how to manage my time instead of hurrying me up when I was slow on research. I feel so lucky to be in such a great research team.

Thank you to all past and present members of the McIndoe group (Ali, Matt, Danielle, Mike, Jenny, Tyler, Krista, Cara, Miles, Jessamyn, Lars, Eric, Rhonda and Zohrab) and my fellow past and present graduate students across the department of University of Victoria and University of Montreal, for sharing your help and great stories to make every day enjoyable. Especial thanks to Dr. Zohrab Ahmadi for working together with me and sharing knowledge and experience with me for four years, and Rhonda Stoddard for helping me and understand me. Especial thanks to Peter Lee as a labmate and roommate who shared his chemistry knowledge, optimistic attitude and same house with me for two and half years..

I also really appreciate Professor Lisa Rosenberg and Professor Garry Hanan for their help on my research. I want to thank UVic faculty and staff for all their technical support and expertise. I am also most grateful to Dr. Ori Granot for helping me with all MS instrument issues, Dr. Allen Oliver for providing the X-ray crystallography and Christopher Barr for NMR services.

The bottom of this appreciation letter is also from the bottom of my heart, I will never make these achievements without the love and selfless support of my mom Xiaohua Wang and my dad Shimin Luo. They are great parents who sacrifice their life to raise me and support me, whenever I fall down; they help me to stand up. They both did not have a chance to go to university, but they deserve to have their name printed in a doctor's thesis. I love you forever.

## **Dedication**

To Mom and Dad

# 1. Literature Review

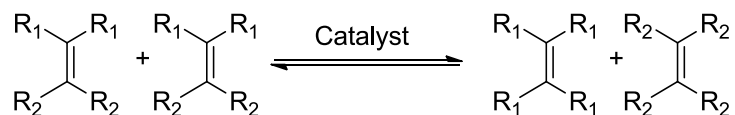
## 1.1 Organometallic catalysis

Synthetic chemicals are an essential part of our daily life. Countless chemicals are synthesized efficiently by optimising the production process to reduce reaction time, waste and expense. This cannot happen without catalysis. The function of a catalyst is to make the reaction faster and/or more selective for the target molecule, and theoretically catalysts can be recycled 100 percent as they are not consumed in the reaction. Ideally, they allow atom-economical reactions (which avoid protecting groups and minimize waste). Traditional stoichiometric strategies are gradually being replaced by this new “greener” chemistry and this is an inevitable trend for the future of chemistry.<sup>1</sup>

Catalysts do not appear in the overall reaction equation nor do they influence the thermodynamics of a reaction, however they change the reaction *pathway* and lower the activation energy, and can also boost the selectivity of one product over another (especially important in enantioselective reactions). Organometallic catalysis involves the activation of organic molecules and their transformation by metals from the main group, transition metals, lanthanides and actinides.<sup>2, 3</sup> Transition metal catalysts especially have been applied in many industrial applications due to their ability to achieve sufficient yields of pure target products, in which some of these products cannot be synthesized without using catalysts (e.g. olefin metathesis, crosscoupling, hydrogen fuel cells). One of the major differences between transition metal and main group elements is the presence of *d* electrons in the valence shell.<sup>4</sup> This property gives transition metals great potential for catalytic reactions: (1) the transition metal can have different coordination numbers, so the binding geometry is variable; (2) they can easily gain or lose electrons in redox processes, during which their oxidation state will also change accordingly; (3) transition metals can form both  $\sigma$  bonds and  $\pi$  bonds with other molecules; (4) transition metals can form chemical bonds with a variety of different ligands, and the presence of ligands can help the metal with steric targeting and can influence the electron distribution at the metal center.<sup>5</sup>

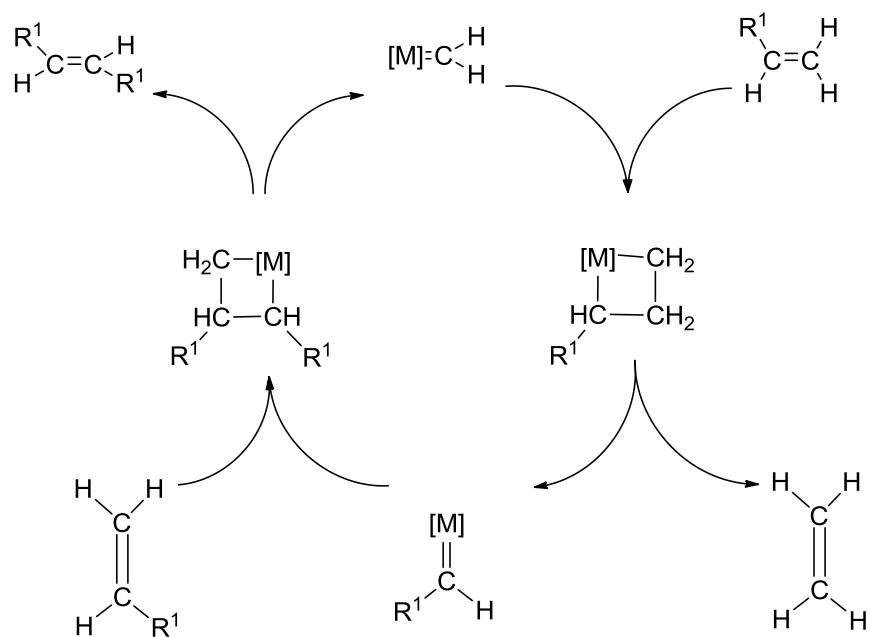
Catalysts can also be classified as homogeneous and heterogeneous based on their physical state. Most industrial catalysts are heterogeneous (i.e. they are in the solid state whereas the reactants are in the gas or sometimes solution phase), but in this thesis, we mainly focus on homogeneous catalysis reactions (in which all components are in solution). Homogeneous reactions are inherently easier to study, and the mechanistic insights so gained are often transferable to heterogeneous systems.

Some notable examples of modern organometallic chemistry are contained in the 2005 and 2010 Nobel Prizes in Chemistry. In 2005, Yves Chauvin, Robert H. Grubbs and Richard R. Schrock won the prize “for the development of the metathesis method in organic synthesis”.<sup>6</sup>



**Equation 1:** Metathesis of alkenes

However, catalyzed metathesis was discovered a long time before the catalyst's role in the reaction was understood. In 1970, Yves Chauvin published a paper proposing the catalyst is a metal alkylidene, and later he used experimental results to explain the mechanism,<sup>7</sup> and now this mechanism is well accepted.



**Scheme 1:** Chauvin's mechanism for alkene metathesis

Grubbs and Schrock did a lot of the mechanistic work proving Chauvin's theory, especially Grubbs. They developed independent and highly complementary catalytic systems, and nowadays, they are extremely useful in the synthesis of pharmaceuticals, agrochemicals, materials etc.<sup>8</sup> Grubbs' catalysts are based on ruthenium whereas Schrock's on molybdenum (Figure 1).

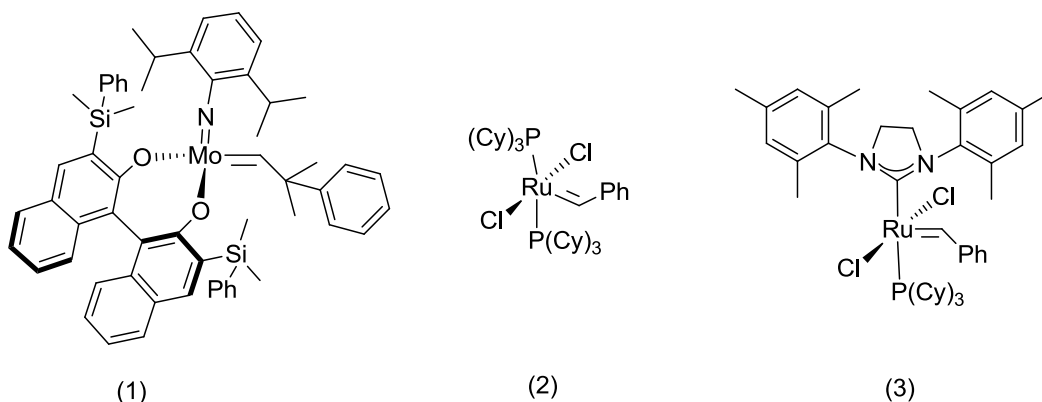


**Figure 1:** (1) First asymmetric Schrock catalyst; (2) 1st Generation Grubbs' Catalyst; (3) 2nd Generation Grubbs' Catalyst

In 2010, Richard F. Heck, Ei-ichi Negishi and Akira Suzuki won the Nobel prize for “palladium-catalyzed cross couplings in organic synthesis”. These catalysts are efficient for activating various organic compounds and catalyzing the formation of new carbon-carbon bonds, and have become an essential methodology for total synthesis of new drugs and materials.<sup>9</sup>

The Heck reaction is between an organohalide compound and an alkene to form a substituted alkene (Figure 2).<sup>10-12</sup>

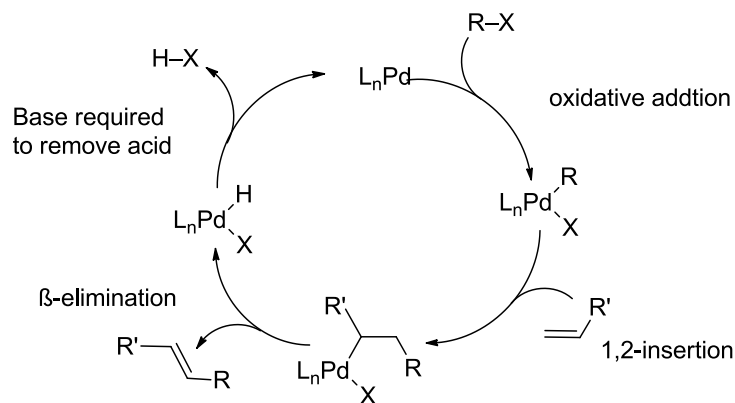


**Figure 2:** Catalytic cycle for Heck reaction

Similar to the Heck reaction, the Negishi reaction is a reaction between R-X (R = aryl, sometimes vinyl; X = halide) with  $RZnX$ ,<sup>13</sup> while the Suzuki reaction is between R-X and  $R'B(OH)_2$ .<sup>14</sup> They have similar catalytic cycles, differing only in substituting a transmetalation step for the insertion reaction as shown in Figure 3.<sup>14</sup>

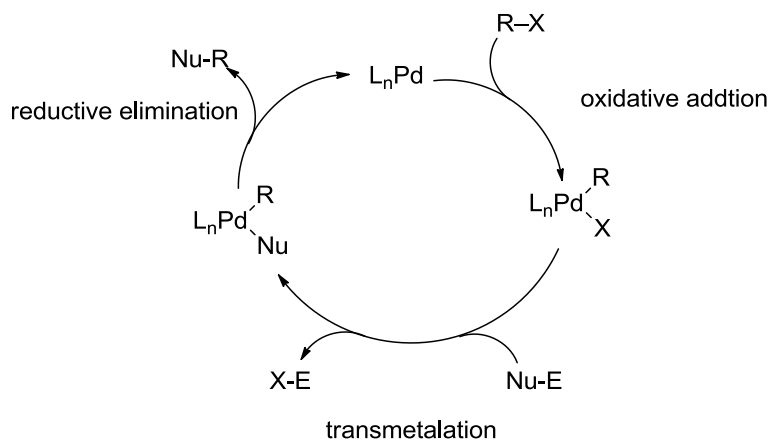


**Figure 3:** Catalytic cycle for Negishi reaction (E = ZnX) and Suzuki reaction (E = B(OR)<sub>2</sub>).

## 1.2 Traditional methods for analysis of organometallic reactions

The strategies for understanding organometallic reactions can be classified into two categories: (1) investigation of overall behaviour of reagents and products, in this way, the catalysis cycle is untouched and predicted by the overall behaviour of the reaction; (2) the direct investigation of the catalytic cycle, where much more effort will be put on the detection, isolation of intermediates in the catalytic cycle and the study of the kinetic profiles of intermediates. The second methodology is perhaps the most powerful method for solving mechanistic problems, however, it is more complicated.

In organometallic catalytic reactions, there are some issues for the investigation of reaction pathways and intermediates. The species are usually present in low concentration, and they are relatively unstable under reaction conditions, which mean they are very hard to detect and characterize. The presence of air, water, impurities, by-products, inactive species, decomposition products and cross-contaminants are all problems for the investigation.

With these issues in mind, and considering current techniques and methodologies, this chapter will discuss some of the many techniques that are currently used in this research field.

### 1.2.1 NMR Spectroscopy

Nuclear magnetic resonance (NMR) spectroscopy provides detailed information about the physical and chemical properties of molecules.<sup>15</sup> It is the most important method for the structural determination of molecules. Based on coupling constants, chemical shift, relaxation times, exchange lifetimes and intensities, the chemical environment of a certain atom ( $^1\text{H}$ ,  $^{13}\text{C}$ ,  $^{19}\text{F}$ ,  $^{31}\text{P}$  etc.) can be well explained. Furthermore, a variety of two dimensional and three dimensional NMR experiments can provide data of through-bond and through-space interactions. This is especially useful for metal elements in the organometallic compounds. For example, the Rosenberg group investigated the mechanism of dehydrocoupling of silanes catalyzed by Wilkinson's catalyst. A number of NMR experiments were carried out, including  $^1\text{H}$ ,  $^{31}\text{P}$ . Different intermediates can be identified including the oxidative addition intermediate  $\text{Rh}(\text{PPh}_3)_2(\text{Cl})(\text{H})(\text{Si}\{n\text{Hex}\}_2\text{-H})$ , hydrido complexes  $\text{HRh}(\text{PPh}_3)_3$ ,  $\text{H}_2\text{Rh}(\text{PPh}_3)_3\text{Cl}$  and  $\text{HRh}(\text{PR}_3)_4$ .<sup>16</sup>

A series of  $\text{Co}(\eta^3\text{-C}_3\text{H}_5)(\text{CO})_2(\text{PR}_2\text{R}')$  complexes were synthesized by Godard *et al.* and used in hydroformylation reactions.<sup>17</sup> A para-hydrogen induced polarisation (PHIP) NMR technique was utilized to study the reaction, and many of the key intermediates including  $\text{Co}(\text{COCH}_2\text{CH}_2\text{CH}_3)(\text{CO})_3(\text{PR}_2\text{R}')$  and branched  $\text{Co}(\text{COCH}_2\text{CH}_2\text{CH}_3)(\text{CO})_3(\text{PR}_2\text{R}')$  were detected and a reaction mechanism was proposed (Figure 4).



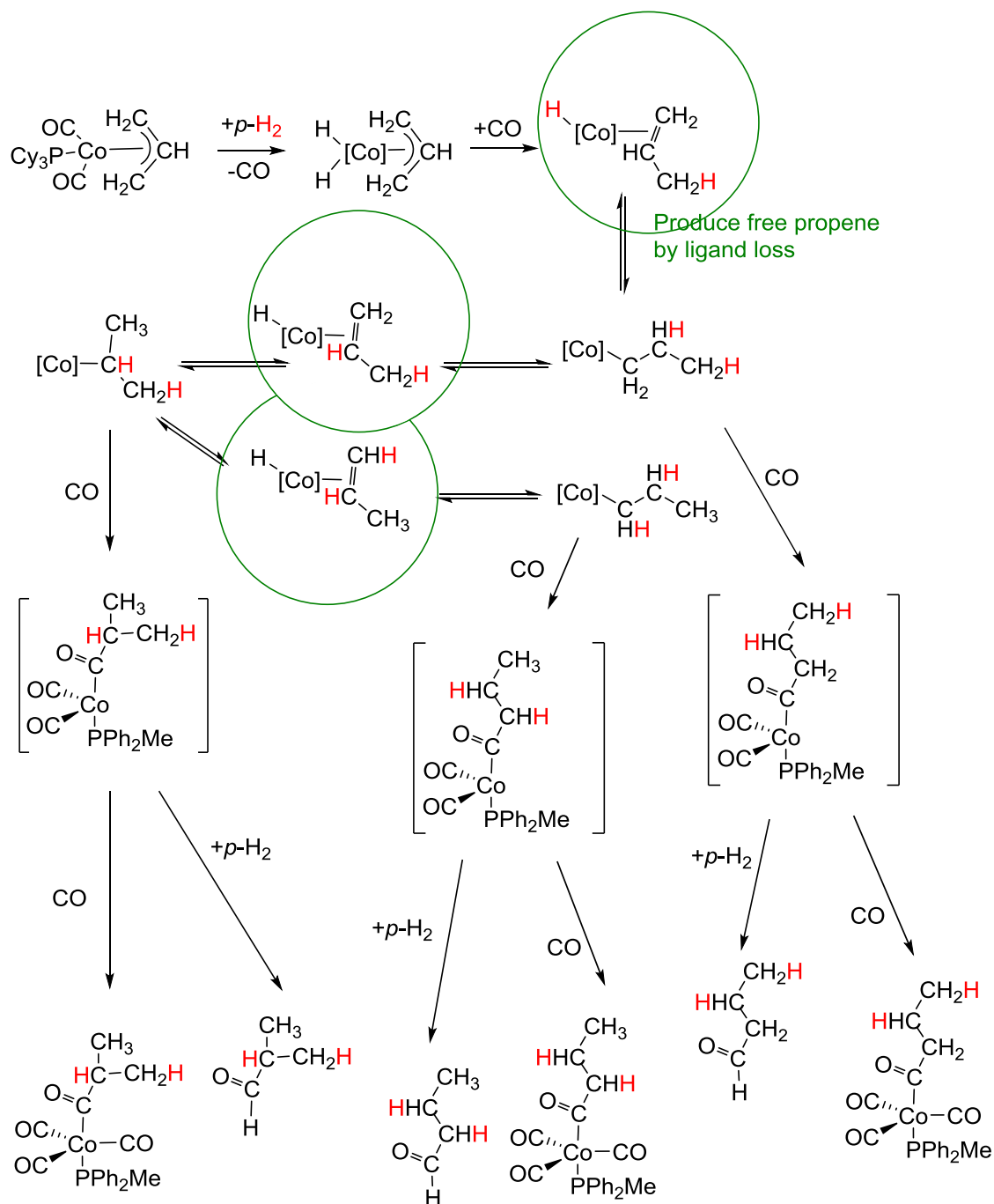


**Figure 4:** Para-hydrogen enhanced NMR is used to detect signals of H on different species in the reaction, detected H is in red color.<sup>17</sup> Reprinted with permission from “An NMR study of cobalt-catalyzed hydroformylation using para-hydrogen induced polarisation” C. Godard, S. B. Duckett, S. Polas, R. Toozé and A. C. Whitwood, *Dalton Transactions*, 2009, 2496-2509. Copyright © 2009 The Royal Society of Chemistry

Multidimensional NMR is a powerful technique for characterizing chemical structures. Zuccaccia *et al.* investigated the degradation process of two Ir oxidation catalysts,<sup>18</sup>  $[\text{Cp}^*\text{Ir}(\text{H}_2\text{O})_3][\text{NO}_3]_2$  ( $\text{Cp}^*$  = pentamethylcyclopentadienyl) and  $[\text{Cp}^*\text{Ir}(\text{bzpy})(\text{NO}_3)]$  ( $\text{bzpy}$  = 2-benzoylpyridine). Their goal was to determine whether or not the degradation is initiated by functionalization of Carbon atom (C-attack) or by hydrogen abstraction (H-attack) by using NMR. Using a series of 2D  $^1\text{H}$  NMR experiments, the functionalization of the  $\text{Cp}^*$  ligand could be assigned (Figure 5). The two resulting intermediates were found to degrade via the C-attack pathway.

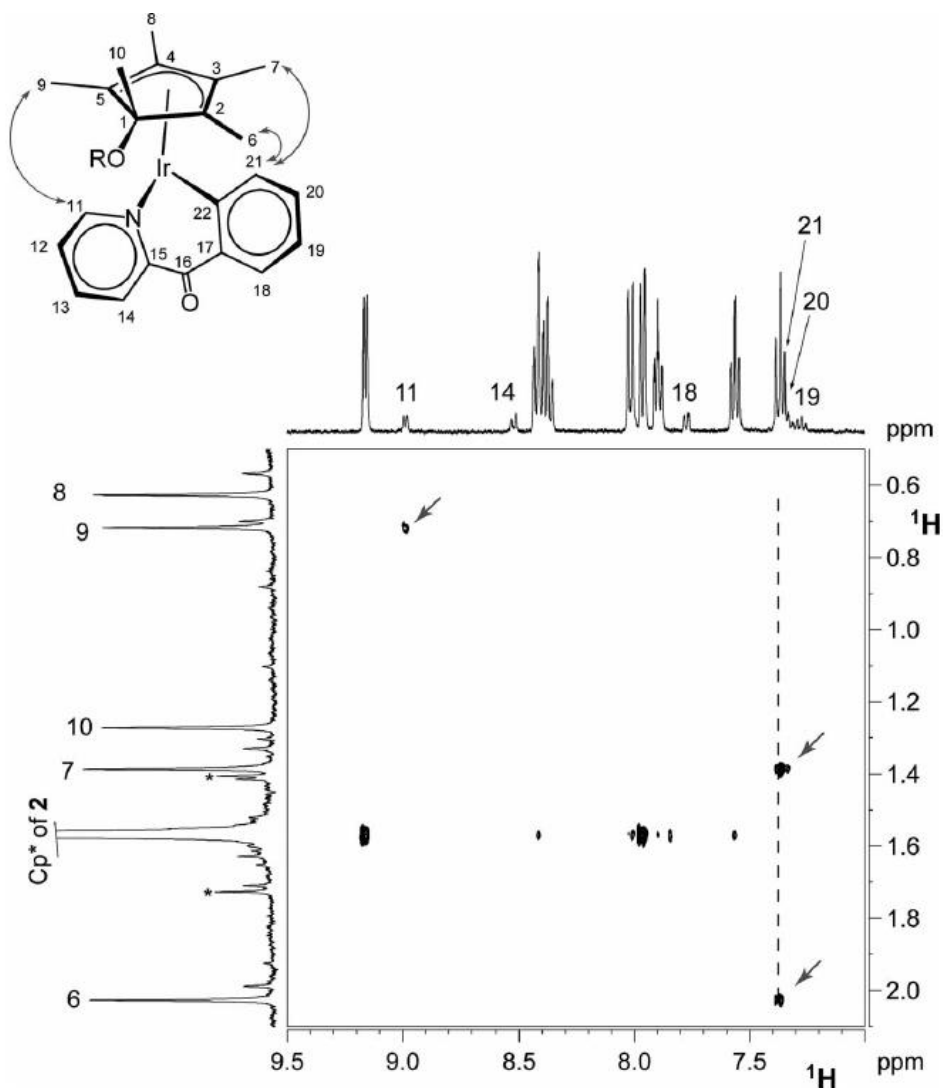


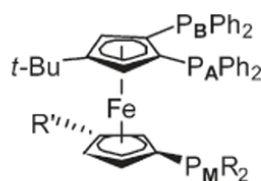
**Figure 5:**  $^1\text{H}$  NOESY spectrum of oxidative degradation product of  $[\text{Cp}^*\text{Ir}(\text{bzpy})(\text{NO}_3)]$ <sup>18</sup> Reprinted with permission from “An NMR Study of the Oxidative Degradation of  $\text{Cp}^*\text{Ir}$  Catalysts for Water Oxidation: Evidence for a Preliminary Attack on the Quaternary Carbon Atom of the  $-\text{C}-\text{CH}_3$  Moiety” C. Zuccaccia,

G. Bellachioma, S. Bolaño, L. Rocchigiani, A. Savini and A. Macchioni, *European Journal of Inorganic Chemistry*, 2012, 2012, 1462-1468. Copyright © 2012 Wiley-VCH Verlag GmbH & Co. KGaA, Weinheim

Mom *et al.* reported a series of ferrocenyl polyphosphane molecules,<sup>19</sup> the structures of which were studied by NMR and X-ray crystallography. <sup>31</sup>P NMR was heavily used in the research, with coupling constants of interactions among long distance P atoms being used to give strong support for the final confirmation of structures of these molecules in solution phase as shown in Table 1.

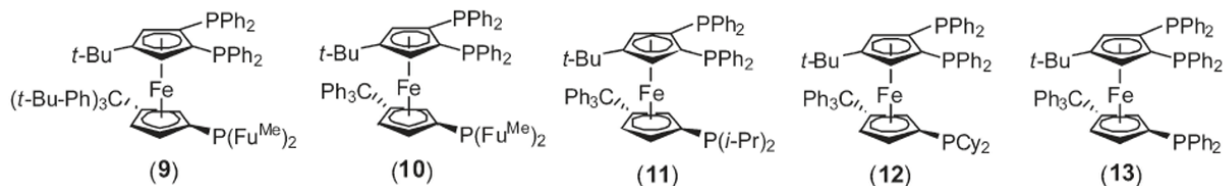
**Table 1:** Ferrocenyl polyphosphanes structures and decoupled proton <sup>31</sup>P NMR data<sup>19</sup>. Reprinted with permission from "Congested Ferrocenyl Polyphosphanes Bearing Electron-Donating or Electron-Withdrawing Phosphanyl Groups: Assessment of Metallocene Conformation from NMR Spin Couplings and Use in Palladium-Catalyzed Chloroarenes Activation" S. Mom, M. Beaupérin, D. Roy, S. Royer, R. Amardeil, H. Cattey, H. Doucet and J. C. Hierso, *Inorganic Chemistry*, 2011, 50, 11592-11603. Copyright

© 2011 American Chemical Society



| triphosphane | $\delta P_A$ |        | $\delta P_B$ |        | $\delta P_M$ |        | $J_{P_A P_B}$ (Hz) | $J_{P_A P_M}$ (Hz) | $J_{P_B P_M}$ (Hz) |
|--------------|--------------|--------|--------------|--------|--------------|--------|--------------------|--------------------|--------------------|
|              | (ppm)        | signal | (ppm)        | signal | (ppm)        | signal |                    |                    |                    |
| (9)          | -16.8        | dd     | -23.6        | dd     | -69.3        | p-t    | 56                 | 17                 | 17                 |
| (10)         | -19.3        | dd     | -24.3        | dd     | -68.9        | p-t    | 72                 | 23                 | 23                 |
| (11)         | -24.0        | dd     | -21.4        | d      | -3.7         | d      | 59                 | 6                  | <i>a</i>           |
| (12)         | -24.0        | dd     | -21.9        | dd     | -13.0        | dd     | 63                 | 22                 | 6                  |
| (13)         | -18.8        | dd     | -24.9        | dd     | -21.7        | p-t    | 41                 | 12                 | 11                 |

<sup>a</sup> Not detected (below 0.5 Hz).



Boutain *et al.*<sup>20</sup> reported a parahydrogen based NMR study of an alkyne hydrogenation reaction catalyzed by platinum(II) bis-phosphine triflate complexes. Key intermediates  $[\text{Pt}(\text{}^t\text{bucope})(\text{CHPhCH}_2\text{Ph})][\text{OTf}]$  where  $\text{}^t\text{bucope}$  is  $(\text{C}_8\text{H}_{14})\text{PC}_6\text{H}_4\text{CH}_2\text{P}(\text{tBu})_2$ ,  $[\text{Pt}(\text{dppp})(\text{CHPhCH}_2\text{Ph})][\text{OTf}]$  (where dppp is 1,3-Bis(diphenylphosphino)propane) and

[Pt(dppp)(CHPhCH-(OMe)Ph)][OTf] were observed based on a variety of 2D NMR experiments including  $^1\text{H}$ - $^{31}\text{P}$  (Figure 6),  $^1\text{H}$ - $^{195}\text{Pt}$ ,  $^1\text{H}$ - $^{13}\text{C}$  as well as deuterium labelling reactions. A hydrogenation mechanism was also proposed.

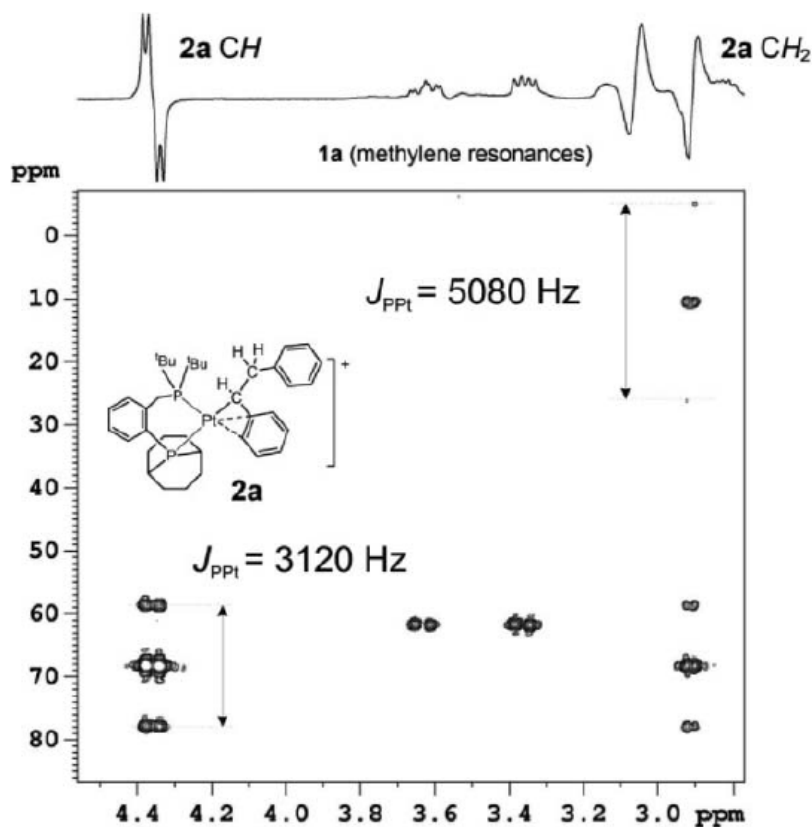


**Figure 6:**  $^1\text{H}$ - $^{31}\text{P}$  HMQC spectrum indicates the existence of a key intermediate during the reaction.<sup>20</sup> Reprinted with permission from “A parahydrogen based NMR study of Pt catalysed alkyne hydrogenation” M. Boutain, S. B. Duckett, J. P. Dunne, C. Godard, J. M. Hernandez, A. J. Holmes, I. G. Khazal and J. Lopez-Serrano, *Dalton Transactions*, 2010, 39, 3495-3500. © The Royal Society of Chemistry 2010

Darensbourg *et al.*<sup>21</sup> reported a kinetic study of a  $\text{CO}_2$  insertion reaction into Ru-Me and Ru-H bonds of trans-Ru(dmpe) $_2$ (Me)H and trans-Ru(dmpe) $_2$ (Me) $_2$  by  $^1\text{H}$  NMR (Figure 7) and IR experiments. Their results showed that the insertion of  $\text{CO}_2$  into Ru-H required less activation energy than into the Ru-Me bond.

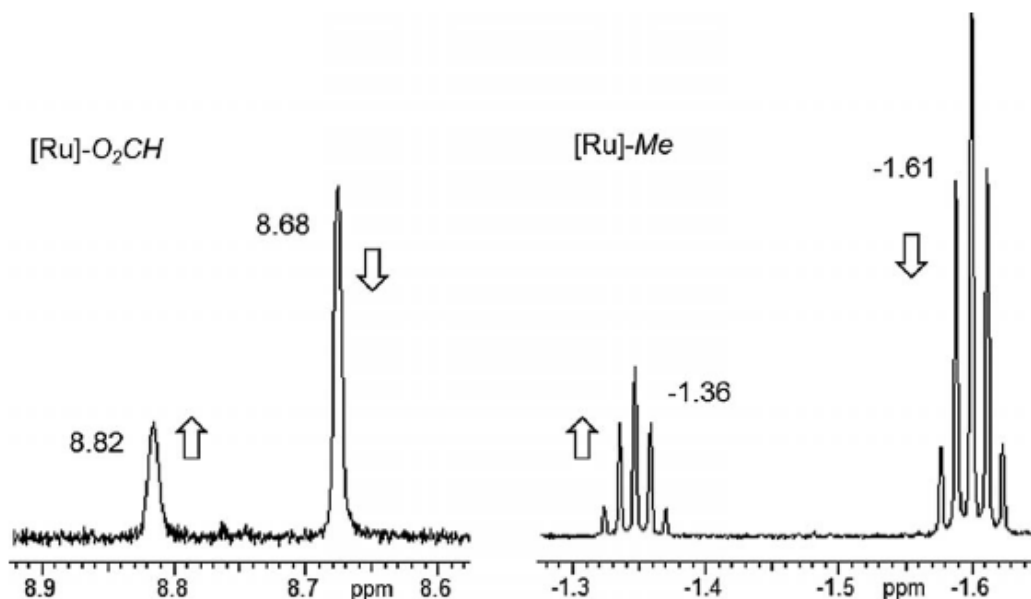


**Figure 7:**  $^1\text{H}$  NMR spectra show a new formate hydrogen signal and a methyl hydrogen atoms signal which are related with *trans*-Ru(dmpc) $_2$ (Me)(O $_2$ CH). And the integration of these peaks changes over time.<sup>21</sup> Reprinted with permission from "Kinetic and Thermodynamic Investigations of CO $_2$  Insertion Reactions into Ru–Me and Ru–H Bonds – An Experimental and Computational Study" D. J. Darensbourg, S. J. Kyran, A. D. Yeung and A. A. Bengali, *European Journal of Inorganic Chemistry*, 2013, 2013, 4024-4031. Copyright © 2013 WILEY-VCH Verlag GmbH & Co. KGaA, Weinheim

Pernik *et al.*<sup>22</sup> investigated into a Rh catalyzed intermolecular hydroacylation. During the study of the mechanism, NMR was used for detection of the key acyl hydride intermediates. Due to the fast turnover rate of the reaction NMR tests were carried out at low temperature (-80 to -60 °C). Larsson *et al.*<sup>23</sup> reported the synthesis of allylic silanes and boronates by using Pd catalysts, and they identified the key intermediate ( $\eta^3$ -allyl)palladium using multinuclear NMR analysis with  $^1\text{H}$ ,  $^{29}\text{Si}$ ,  $^{19}\text{F}$  and  $^{11}\text{B}$  NMR. The kinetic study (Figure 8) of the catalytic reaction was also monitored by  $^1\text{H}$  NMR over time. Transmetalation was believed to be the turnover limiting step.

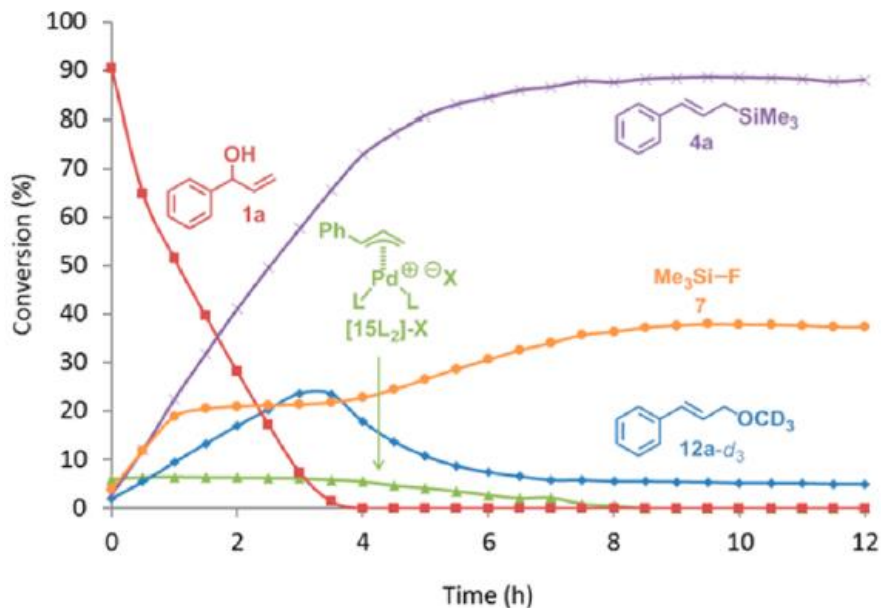


**Figure 8:** Synthesis of allylic silanes and boronates by using Pd catalysts reaction was monitored by  $^1\text{H}$  NMR over 12 hours. The concentration of each species correspond to the NMR signal integration.<sup>23</sup> Reprinted with permission from “Mechanistic Investigation of the Palladium-Catalyzed Synthesis of Allylic Silanes and Boronates from Allylic Alcohols” J. M. Larsson and K. J. Szabó, *Journal of the American Chemical Society*, 2012, 135, 443-455. Copyright © 2012 American Chemical Society

### 1.2.2 UV/Vis Spectroscopy

When UV/visible light passes through a sample (liquid, gas or solid), molecules will absorb electromagnetic radiation and electrons will transit from the ground state to an excited state.<sup>24</sup> Absorption is directly related with the concentration of the molecule, according to Beer’s Law. Based on this, a UV/Vis spectrophotometer can be used to obtain dynamic concentration information on species with appropriate chromophores.

For organometallic catalytic reactions, UV/Vis can be used for characterization of compounds as well as for kinetic studies. For example, Fischer et al. investigated the stoichiometric hydrogenation of diolefin by  $[\text{Rh}(\text{Me-DuPHOS})(\text{cyclooctadiene})][\text{BF}_4]$  in MeOH (Figure 9). In the hydrogenation reaction, the UV/Vis-derived pseudo-rate constants are influenced by experimental factors including diphosphine ligand, diolefin, solvent, temperature and hydrogen pressure, the UV/Vis spectra were recorded every three minutes (Figure 10, Figure 11).<sup>25</sup>

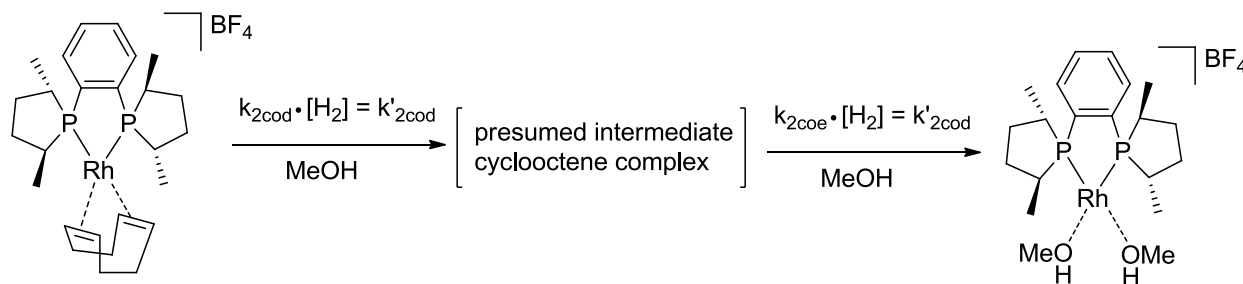


**Figure 9:** Generation of the solvate complex  $[\text{Rh}(\text{Me-DuPHOS})(\text{MeOH})_2]\text{BF}_4$ .

cod= cyclooctadiene; coe = cyclooctene<sup>25</sup>

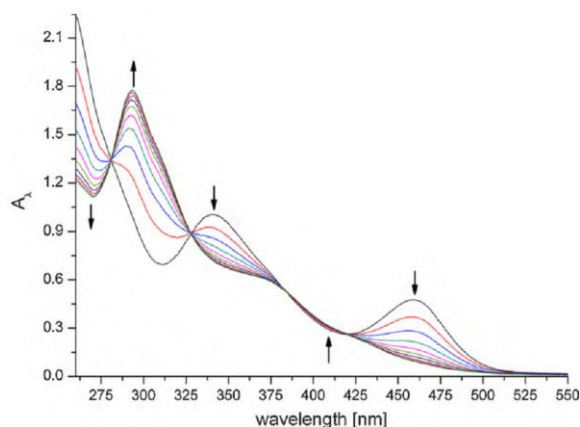


**Figure 10:** Reaction data for the stoichiometric hydrogenation of 0.01 mmol  $[\text{Rh}(\text{Me-DuPHOS})(\text{cod})]\text{BF}_4$  in 15 mL MeOH at 25 °C and 1 bar overall pressure (cycle time 3 min, layer thickness 0.5 cm).<sup>25</sup>

Reprinted with permission from “Kinetic and mechanistic investigations in homogeneous catalysis using operando UV/vis spectroscopy” C. Fischer, T. Beweries, A. Preetz, H.-J. Drexler, W. Baumann, S. Peitz, U. Rosenthal and D. Heller, *Catalysis Today*, 2010, 155, 282-288. Copyright © 2009 Elsevier B.V.

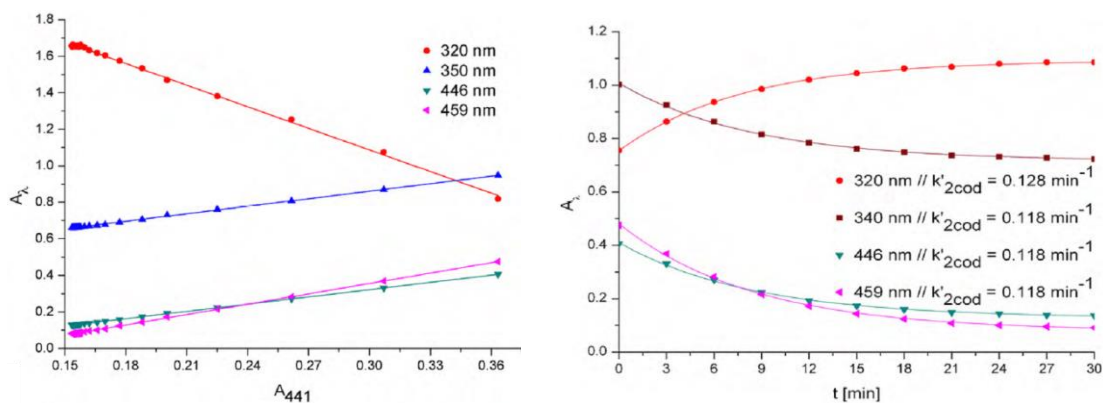


**Figure 11:** Extinction diagram (left) and comparison of spectroscopic values (points) and values fitted as pseudo-first order (solid line) for several wavelengths.<sup>25</sup> Reprinted with permission from “Kinetic and mechanistic investigations in homogeneous catalysis using operando UV/vis spectroscopy” C. Fischer, T. Beweries, A. Preetz, H.-J. Drexler, W. Baumann, S. Peitz, U. Rosenthal and D. Heller, *Catalysis Today*, 2010, 155, 282-288. Copyright © 2009 Elsevier B.V.

Gao *et al.*<sup>26</sup> reported the analysis of  $(\mu_4\text{-}\eta^2\text{-alkyne})\text{Rh}_4(\text{CO})_8(\mu\text{-CO})_2$  by using *in situ* UV/Vis spectroscopy together with band-target entropy minimization (BTEM) to reconstruct the pure spectra of the compound. Results show the combination of these two techniques is a good way to study organometallic species in solution that are air and water sensitive and hard to isolate.

Jaska *et al.*<sup>27</sup> reported mechanistic studies of Rh-catalyzed amine-borane and phosphine-borane dehydrocoupling reactions. Results they obtained from UV/Vis were compared with those obtained from well-defined Rh colloids  $\text{Rh}_{\text{colloid}}/[\text{Oct}_4\text{N}]\text{Cl}$ . A broad absorption was obtained by using  $\text{Me}_2\text{NH}\cdot\text{BH}_3$ , but there is no such absorption with  $\text{Ph}_2\text{PH}\cdot\text{BH}_3$ . This suggests the former solution contains Rh colloids while the latter doesn't.

Other organometallic studies using UV/Vis to examine catalytically-relevant reactions include Michael addition reactions,<sup>28</sup> hydrogenation,<sup>29</sup> oxidative addition<sup>30</sup> and electrochemical oxidation.<sup>31</sup>

### 1.2.3 IR Spectroscopy

IR spectroscopy is also an important analysis technique in organometallic catalysis research. For example, the IR spectrum of metal carbonyl complexes,  $\text{M}_n(\text{CO})_m$ , can be different based on the coordination mode, coordination number and geometry of the complex. Binding with the metal weakens the CO bond through back-bonding, and the CO stretching frequency moves to lower wavenumbers. The IR absorption of the CO stretching vibration is around  $1700\text{-}2100\text{ cm}^{-1}$  and this region is usually without interference from other vibrations.<sup>4</sup>

Conventionally, IR spectroscopy involves a sample preparation step. It can be achieved by taking an aliquot sample from the reaction or by flowing the reaction solution through a sampling cell. The cell must be very thin in order to avoid excessive absorption. This step can make IR spectroscopy inconvenient for organometallic catalysis, especially for intermediates characterization. To solve this problem, a new (Figure 12) technique called attenuated total reflectance (ATR) is integrated with IR spectroscopy (ATR-IR).<sup>32</sup>



ATR-IR is based on a mechanism that when the infrared beam reaches the solution surface, part of the light will go into the solution and reflect back. The reflected IR beam contains IR information of the solution that can be used for characterization of the solution. This technique allows *in situ* IR tests directly in the reaction solution without the need to take a sample.

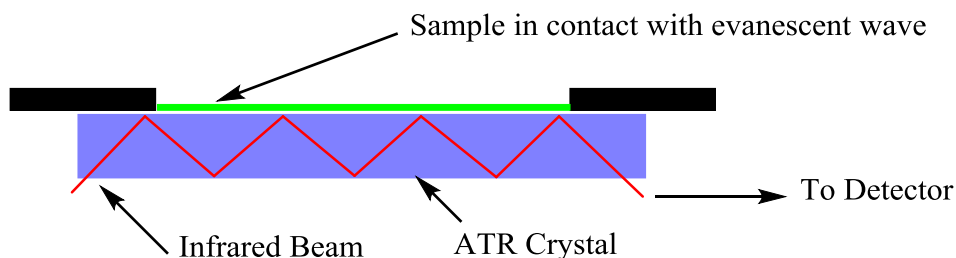


**Figure 12:** Attenuated Total Reflectance (ATR).

Currently there are a few applications by using IR-ATR for catalysis reaction study,<sup>33-35</sup> particularly using commercially available instruments such as the React-IR. React-IR is a product designed for *in situ* FTIR reaction analysis. It integrates attenuated total internal reflection (ATR) sensor with a fiber-optic probe. The probe directly contacts the reaction solution for IR analysis and the IR data of the whole reaction process can be detected and recorded in real time.<sup>36</sup>



**Figure 13:** Latest version of React-IR, the ReactIR™ 45m.<sup>36</sup>

In 2011, Barker *et al.*<sup>37</sup> utilized ReactIR spectroscopy for real time analysis of each step of a deprotonation-transmetalation-Negishi coupling reaction process. The carbon oxygen double bond from Boc group was found trackable by ReactIR. The addition of *s*-BuLi is responsible for a new C=O peak, which can also be monitored with ReactIR (Figure 14). The real time tracking also showed the reaction is much faster than what was previously thought.

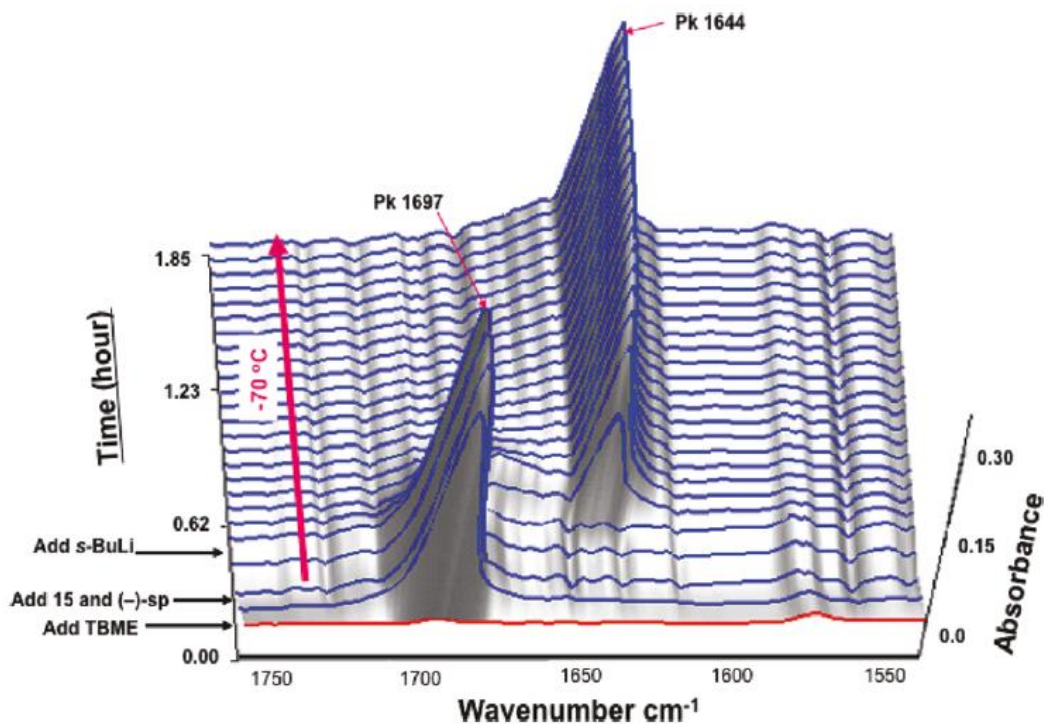


**Figure 14:** ReactIR spectrum of lithiation of *N*-Boc pyrrolidine compound.<sup>37</sup> Reprinted with permission from “Enantioselective, Palladium-Catalyzed  $\alpha$ -Arylation of *N*-Boc Pyrrolidine: In Situ React IR Spectroscopic Monitoring, Scope, and Synthetic Applications” G. Barker, J. L. McGrath, A. Klapars, D. Stead, G. Zhou, K. R. Campos and P. O’Brien, *The Journal of Organic Chemistry*, 2011, 76, 5936-5953. Copyright © 2011 American Chemical Society

In 2013, Gall *et al.*<sup>38</sup> reported using *in situ* infrared spectroscopy tracking of a Mannich-like reaction between amines, aldehydes and organozinc reagents by using ReactIR (Figure 15). In order to track different starting materials, products and intermediates, most of these species were first characterized individually. The authors managed to obtain enough information from spectroscopic data to propose two different pathways for the reaction, however, the key intermediate species are hard to identify due to stability issues.

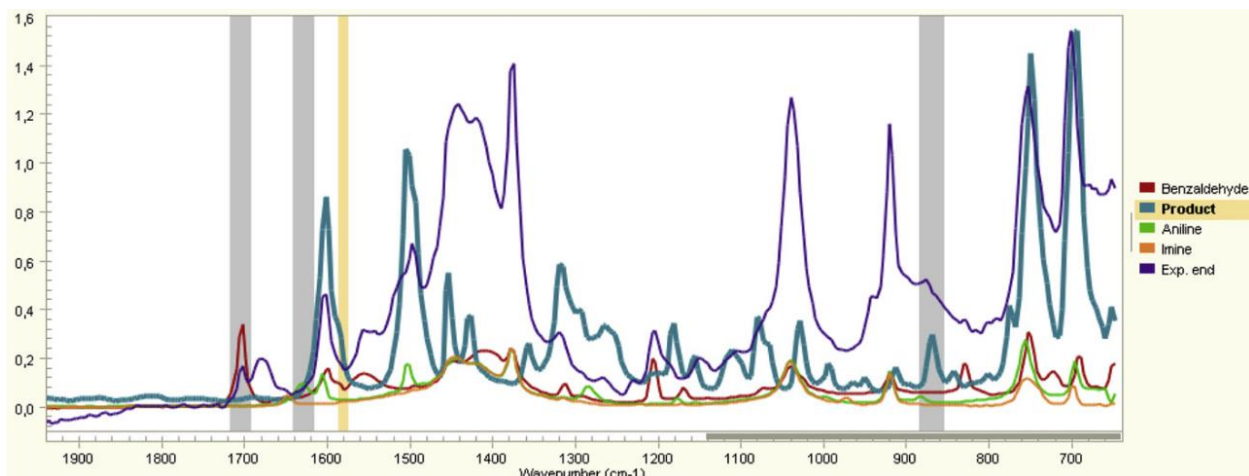


**Figure 15:** Overlay of different spectra including starting reagents, product and putative imine intermediate.<sup>38</sup> Reprinted with permission from “Mannich-like three-component synthesis of  $\alpha$ -branched amines involving organozinc compounds: ReactIR monitoring and mechanistic aspects” E. Le Gall, S. Sengmany, C. Hauréna, E. Léonel and T. Martens, *Journal of Organometallic Chemistry*, 2013, 736, 27-35. Copyright © 2013 Elsevier B.V.

### 1.2.4 Mass Spectrometry

A mass spectrometer converts a sample into gas phase ions, and electric (and sometimes magnetic) fields are applied to separate the ions by their mass-to-charge ratio.<sup>39</sup> Mass spectrometry is an outstanding analytical technique due to its high sensitivity (low detection limit),<sup>40</sup> high accuracy and the low amount of analyte it requires. With modern soft ionization techniques, MALDI (Matrix Assisted Laser Desorption Ionisation) –left side of Figure 16 and, ESI (Electrospray Ionisation) –right side of Figure 16<sup>41, 42</sup> little or even no fragmentation occurs during ionisation process, thus allowing the intact target molecule to be characterized.

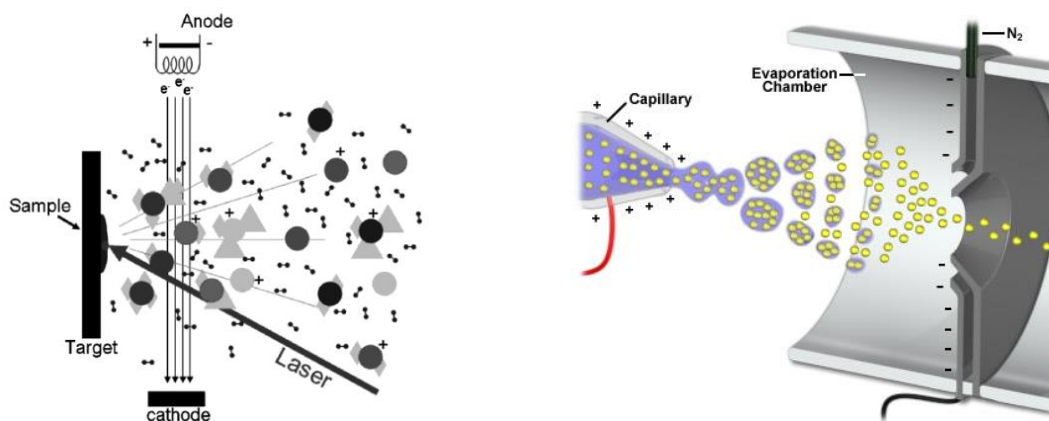


**Figure 16:** MALDI (left) and ESI sources.<sup>41, 42</sup> Reprinted with permission from “Electrospray and MALDI Mass Spectrometry: Fundamentals, Instrumentation, Practicalities, and Biological Applications, Second Edition” R. B. Cole, *Electrospray and MALDI Mass Spectrometry: Fundamentals, Instrumentation, Practicalities, and Biological Applications*, John Wiley & Sons, 2009. Copyright © 2010 John Wiley & Sons, Inc.

ESI-MS has become an increasingly popular tool for mechanistic studies of organometallic catalysis, especially in the area of short-lived reactive intermediates.<sup>43</sup> The reaction solution can be directly introduced into the instrument without pre-treatment. A more important advantage is that ESI-MS can quantitatively detect short life time, low concentration, and air-sensitive intermediates. However, in order to be detectable by MS, the species must be intrinsically charged such as a positive or negative ion. The synthetic introduction of charged tags into the target molecule is one of the best ways to achieve this goal. Currently ESI-MS has been successfully used in the study of catalytic oxidation,<sup>44-46</sup> palladium cross-coupling,<sup>47-49</sup> the Pauson-Khand reaction,<sup>50</sup> and many other reactions.<sup>51-57</sup>

Santos *et al.*<sup>58</sup> reported a mechanistic investigation of a Lewis base-catalyzed Baylis-Hillman reaction by using ESI-MS. The reason to use ESI-MS for this reaction is that the key intermediates in the proposed Baylis-Hillman reaction catalytic cycle (Figure 17) are monocations. The reaction intermediates as shown in Figure 17 can be transformed into gas phase and characterized by ESI-MS. The final results of Santos *et al.* confirmed this proposal.

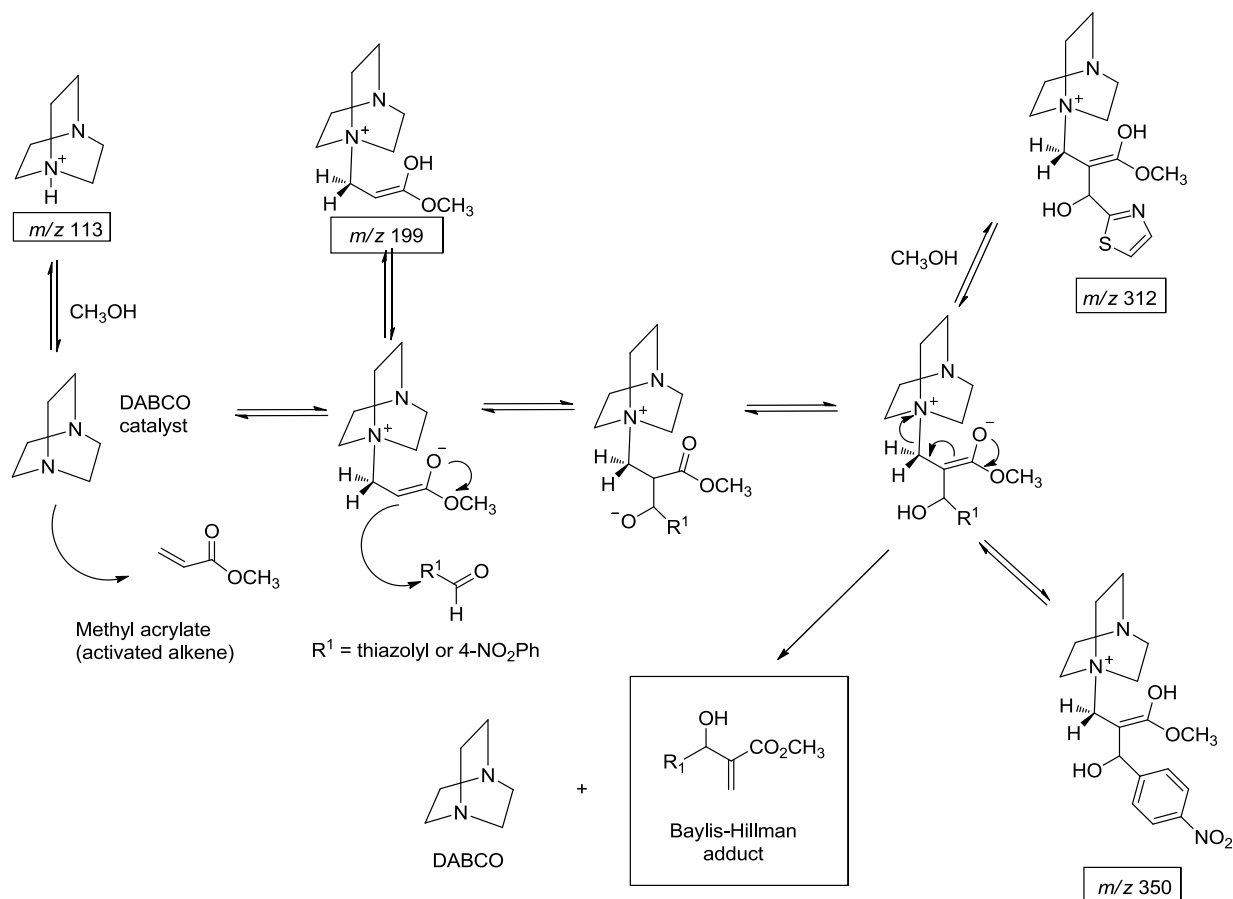


**Figure 17:** ESI-MS study of the mechanism of a Baylis-Hillman reaction catalyzed by DABCO.<sup>58</sup>

Shvo's catalyst<sup>59</sup> is a ruthenium complex reported as capable of achieving chemo-enzymatic dynamic kinetic resolution (DKR) of amines. Evidence of an intermediate from the proposed mechanism was characterized by NMR and IR, however, many key intermediates had not been detected, and there were two different pathways proposed. In order to find out the correct pathway, Vaz *et al.*<sup>60</sup> investigated this reaction by using ESI-MS and ESI-MS/MS. Many intermediates were captured and characterized (Figure 18), and the reaction process was continuously monitored. Results show evidence to support an inner-sphere H-transfer mechanism (Figure 19).

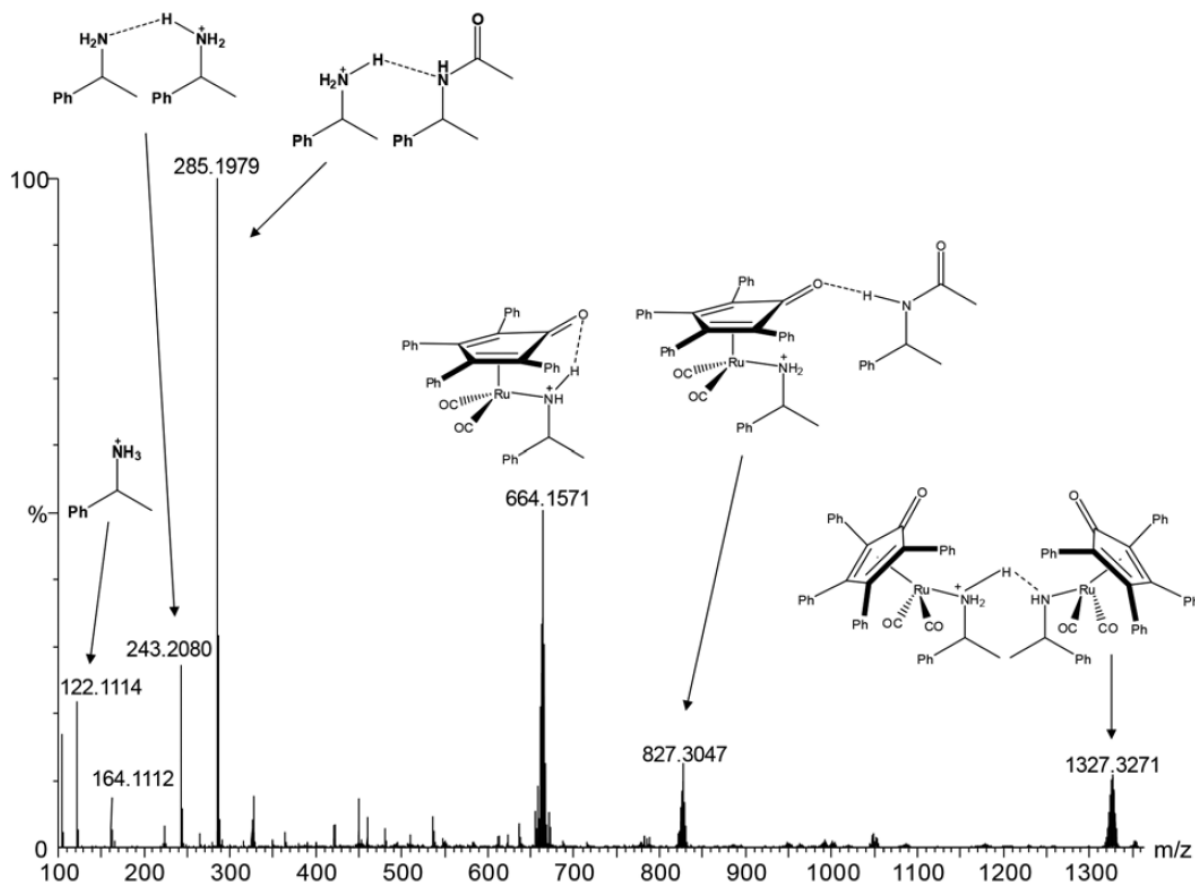


**Figure 18:** Charged intermediates were detected during the DKR of amines reaction, each intermediate can be represented by a characteristic peak.<sup>60</sup> Reprinted with permission from “Shvo's catalyst in chemoenzymatic dynamic kinetic resolution of amines – inner or outer sphere mechanism?” B. G. Vaz, C. D. F. Milagre, M. N. Eberlin and H. M. S. Milagre, *Organic & Biomolecular Chemistry*, 2013, 11, 6695-6698. Copyright © The Royal Society of Chemistry 2013

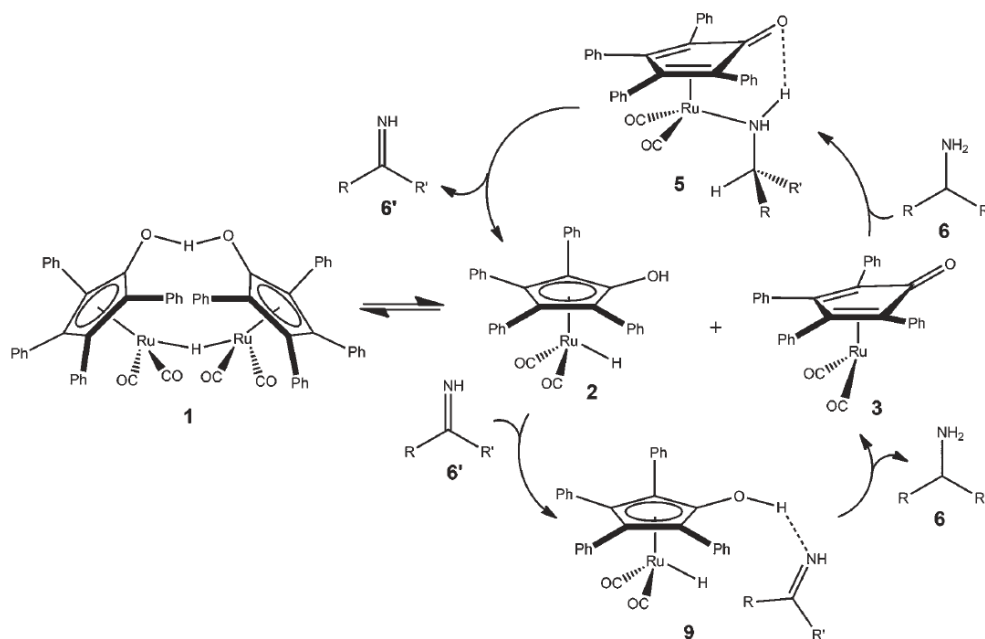


**Figure 19:** Shvo's catalyst catalyzed amine racemization mechanism revealed by ESI-MS.<sup>60</sup> Reprinted with permission from "Shvo's catalyst in chemoenzymatic dynamic kinetic resolution of amines – inner or outer sphere mechanism?" B. G. Vaz, C. D. F. Milagre, M. N. Eberlin and H. M. S. Milagre, *Organic & Biomolecular Chemistry*, 2013, 11, 6695-6698. Copyright © The Royal Society of Chemistry 2013

Ghoochany *et al.*<sup>61</sup> proposed a new mechanism for a Ru(II) complex-catalyzed base-free transfer hydrogenation of acetophenone by using a combination of ESI-MS and other techniques. ESI-MS played a key role in the clarification of C-H activation process. Under mild conditions, the key intermediates were detected. When collision-induced dissociation (CID) was applied, fragmentation shows the loss of HCl from these intermediates. Isotope labeling experiments were also carried out in ESI-MS. Combining all these data, the authors found the position of the C-H activation on the molecule.

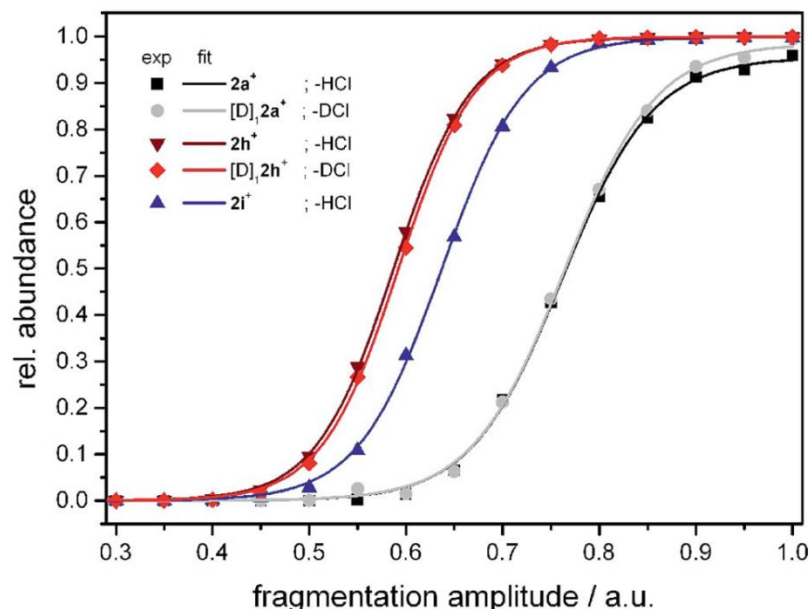


**Figure 20:** Collision-induced fragmentation of cationic species.<sup>61</sup> Reprinted with permission from “C–H Activation at a Ruthenium(II) Complex – The Key Step for a Base-Free Catalytic Transfer Hydrogenation?” L. Taghizadeh Ghoochany, C. Kerner, S. Farsadpour, F. Menges, Y. Sun, G. Niedner-Schatteburg and W. R. Thiel, *European Journal of Inorganic Chemistry*, 2013, 2013, 4305-4317. Copyright © 2013 WILEY-VCH Verlag GmbH & Co. KGaA, Weinheim

Machado *et al.*<sup>62</sup> reported detection of possible intermediates of “dba-free” Heck reaction by using ESI-MS. Pd(OAc)<sub>2</sub> was used instead of Pd<sub>2</sub>(dba)<sub>3</sub>•dba (Figure 21). Machado’s data was used as a comparison to the dba version of the Heck mechanism in order to gain additional insight into the world famous C-C cross-coupling reaction. Based on the detected intermediates, the authors proposed an expanded Heck catalytic cycle and also found evidence of “dba-free” intermediates in “dba-involved” Heck reaction.



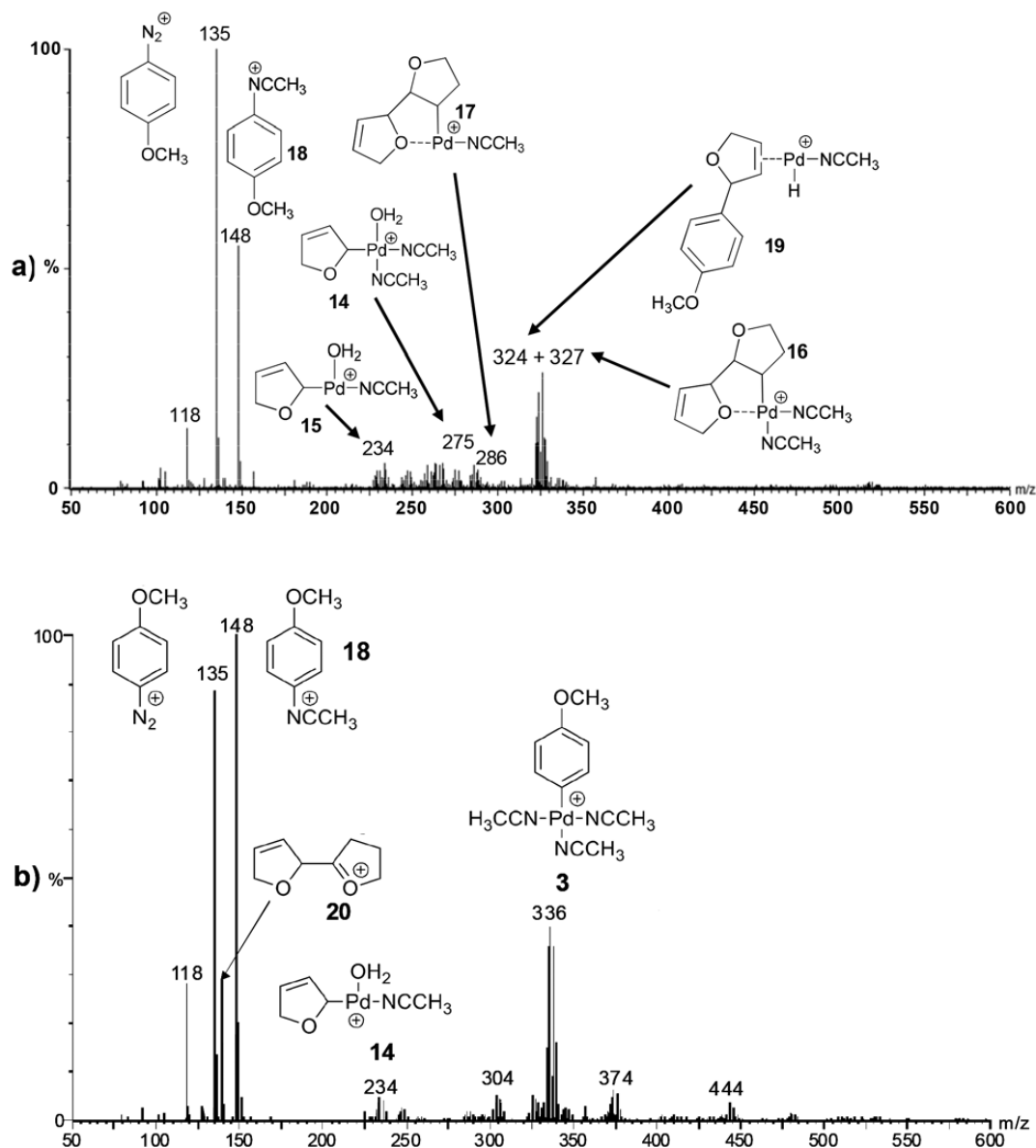


**Figure 21:** ESI-MS of dba-free arylpalladium species.<sup>62</sup> Reprinted with permission from ““Dba-free” palladium intermediates of the Heck–Matsuda reaction. A. H. L. Machado, H. M. S. Milagre, L. S. Eberlin, A. A. Sabino, C. R. D. Correia and M. N. Eberlin, *Organic & Biomolecular Chemistry*, 2013, 11, 3277-3281. Copyright © The Royal Society of Chemistry

ESI-MS can also be used to study extremely air sensitive organometallic chemistry. Trefz *et al.*<sup>63</sup> reported poly(methylaluminumoxane) (MAO) research by using ESI-MS. MAO is an important polymerization catalyst activator, however, the composition and structure are poorly characterized due to its oligomeric nature and very high air- and moisture- sensitivity. The authors developed an air sensitive setup by connecting ESI-MS with glovebox. The reactions

were carried out in fluorobenzene, and experiments were done in both positive and negative modes of ESI-MS. The results provided evidence that MAO is best thought of as a source of the small, highly reactive cation  $[\text{Me}_2\text{Al}]^+$ .

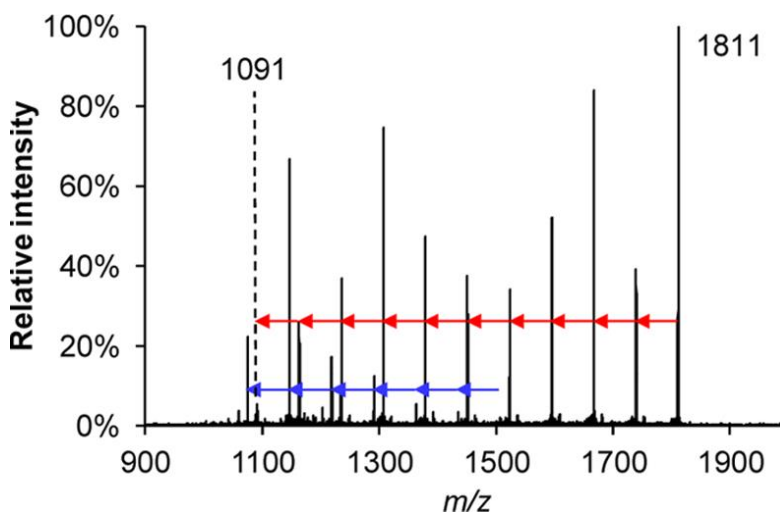


**Figure 22:** MS/MS of MAO anion  $m/z$  1881.<sup>63</sup> Ten losses of 72 Da from the parent ion are indicated by red arrows with a second series of fragment ions occurring at  $-16$  Da, between  $m/z$  1075 and 1507, depicted by blue arrows. Reprinted with permission from "Mass Spectrometric Characterization of Methylaluminoxane" T. K. Trefz, M. A. Henderson, M. Y. Wang, S. Collins and J. S. McIndoe, *Organometallics*, 2013, 32, 3149-3152. Copyright © 2013 American Chemical Society

ESI-MS is also a great tool to study rhodium chemistry. Parera *et al.*<sup>64</sup> were able to provide a great example in this field. A charged Rh(I) catalyst was used for a  $[2+2+2]$  cycloaddition reaction of diynes and monoynes. This was the first example of a mechanistic study of this reaction by ESI-MS, (Figure 23) and the intermediates from onoyne-rhodacyclopentadiene insertion were detected. The author used density functional theory (DFT) to help determine the structure of the intermediates.

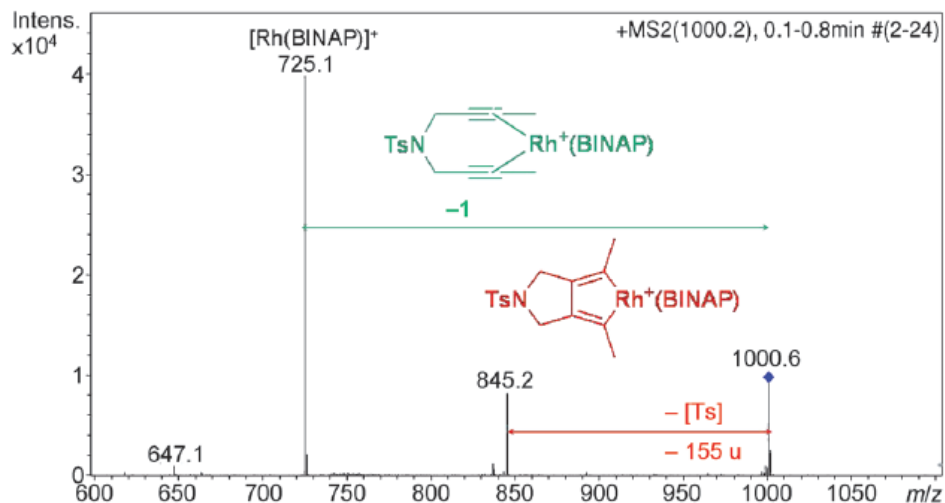


**Figure 23:** CID (collision induced dissociation) mass spectrum of the ion at  $m/z=1000.3$ , a Rh(I) intermediate.<sup>64</sup> Reprinted with permission from “Direct Detection of Key Intermediates in Rhodium(I)-Catalyzed [2+2+2] Cycloadditions of Alkynes by ESI-MS” M. Parera, A. Dachs, M. Solà, A. Pla-Quintana and A. Roglans, *Chemistry – A European Journal*, 2012, 18, 13097-13107. Copyright © 2012 WILEY-VCH Verlag GmbH & Co. KGaA, Weinheim

## 2. Techniques and methodologies

### 2.1 Introduction

Mass spectrometry is a classic technique in analytical chemistry. It has three main components: 1, the ion source where sample molecules get ionized and converted into gas phase charged particles; 2, the mass analyzer where ions are sorted and separated based on their mass-to-charge ratio ( $m/z$ ); 3, the detector, where the sorted ions are counted to get the ion intensity.

Mass spectrometry is originated from the field of physics; in the early 1900's the research of J.J Thomson on cathode rays established the foundation of MS field. Together with Francis Aston, he built the world's first mass spectrometer for atom mass measurement.<sup>65</sup> Since then, different types of mass spectrometer were created. All the three components of MS have been constantly innovated over the past 110 years.

The first ionization source was electron ionization (EI) developed by Dempster.<sup>66</sup> In the EI source, when vaporized sample molecules pass through a beam of high energy electrons, an electron of the analyte molecule is forced out of its orbital due to the powerful external electron beam. This leads to the production of the molecular ion  $[M]^{*+}$ . This ionization process is so energetic that only a very small portion of intact sample molecules can survive and the spectrum contains mainly fragments of the parent ion.

Since this method only gives limited information on the parent molecule, "soft" ionization methods were developed. Chemical ionization (CI)<sup>67, 68</sup> utilizes a reagent gas as a bridge between a highly energized electron beam and sample molecules, so the charge transfer is not directly between electron beam and sample which is the case of EI. In CI at first the electron beam hits the reagent gas (e.g.  $CH_4$ ) to ionize it, which then charge transferred to the adjacent analyte. As there is no direct contact between beam and sample, the fragmentation of the analyte is decreased significantly; more parent ion data can be obtained, but CI still has limited ability to detect large molecules because, like EI, it is limited by sample volatility.

Many other ionization methods were developed as well, such as Field Desorption (FD)<sup>69</sup>, Fast Atom Bombardment (FAB)<sup>70, 71</sup>, and Atmospheric Pressure Chemical Ionization (APCI)<sup>72</sup> etc.

Among them there are two techniques developed especially worth emphasizing: Electrospray Ionization (ESI) and Matrix Assistance Laser Desorption Ionization (MALDI). They are both “soft” ionization methods. Due to their importance in analytical chemistry, their inventors (Fenn and Tanaka, respectively) were awarded the Nobel Prize for Chemistry in 2002.<sup>73-75</sup>

In matrix-assisted laser desorption ionization (MALDI), the analyte is co-crystallized or coated with an organic matrix (usually an aromatic acid) and then energized with a pulsed UV laser. This ionization method is based on a solid sample and the charge transfer happens between matrix and the analyte. The laser blasts the matrix into the gas phase, and protons are transferred from matrix molecules to analyte molecules, so the analyte is mostly singly charged. The matrices developed by Karas and Hillenkamp<sup>76</sup> helped MALDI to become very popular (more so than Tanaka’s metal powders). The recently developed MALDI imaging<sup>77-79</sup> technique brings the application of MALDI in biology related studies into a new stage. MALDI can also be used on organometallic catalysis reaction research.<sup>80</sup>

## 2.2 Electrospray Ionization Mass Spectrometry

Electrospray ionization (ESI) was developed in the late 1960s by Dole and co-workers. At that time, Dole was trying to characterize non-volatile polymers, but there was no suitable soft ionization method to achieve his goal. Later, he was inspired by electrospray car painting when he visited a car manufacturer. Then he applied the electrospray process for ionization and got very promising results<sup>81, 82</sup>. In the 1980s, Yamashita and Fenn improved this technique and combined it with a modern mass spectrometer.

The electrospray ionization process is considered as the “softest”<sup>83</sup> ionization technique. The whole ionization process is shown in Figure 24. A dilute solution containing the target molecule or ion is introduced into the ESI source by using different types of mechanical pumps. In the ESI source, the solution travels through a capillary which is under highly positive or negative voltage (usually 2500 V to 5000 V). In positive mode, the high voltage will oxidize the capillary, solvent or analyte, and when the solution gets out of the capillary, the droplets will deform into a unique Taylor cone.<sup>84</sup> The solution will break down into fine droplets, all of which carry an excess of

positive charge. As the charges repel each other, they will all relocate on the surface of the fine droplet. During the flying of the droplets, they are surrounded by a warm drying gas which will help solvent molecules evaporate. This evaporation will cause the charge density of the droplet to increase and once the charge density reaches a Coulomb explosion threshold, the droplet split into smaller droplets with lower charge density, this splitting process will repeatedly occur in a very short time frame.<sup>85</sup> Eventually, all the solvent molecules evaporate and the positive charges stay with sample molecule ions in gas phase and enter into the MS analyzer.

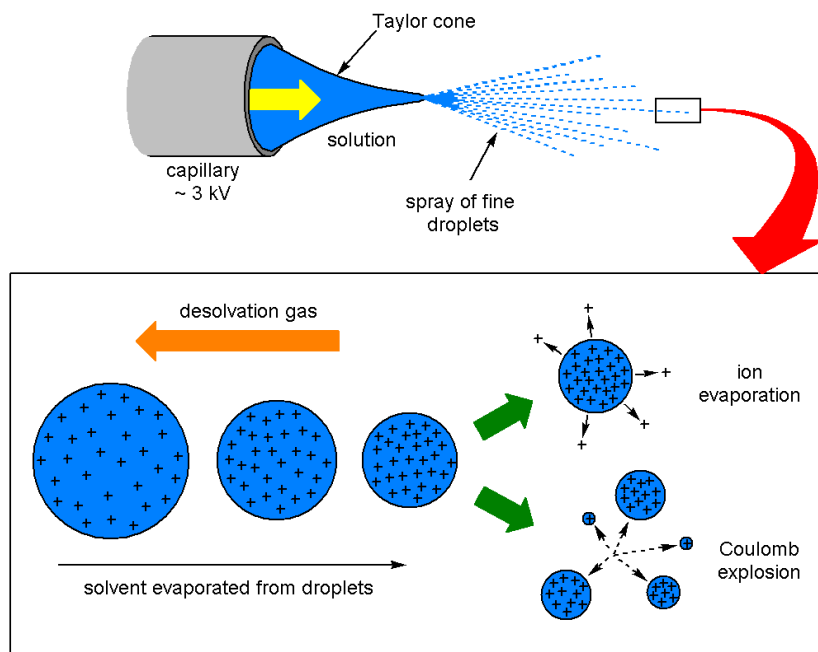


**Figure 24:** The desolvation process in electrospray ionization. Modified with permission of the author from Henderson, W., McIndoe J. S., *Mass Spectrometry of Inorganic and Organometallic Compounds*. John Wiley & Sons, Ltd. West Sussex: 2005, p. 92.

When the target molecules are separated from the rest of solvent molecules, there are two models to explain this final stage of ionization. The Ion Evaporation Model (IEM) and Charged Residue Model (CRM).<sup>86</sup> Small ions (<5000 Da) tend to transfer into the gas phase by evaporating from the surface of droplet, while large ions are likely to stay inside the droplet until all the surrounding solvent molecules evaporate (Figure 25). The whole process of ESI enables the target molecule to stay intact rather than generate many fragments. So information of the intact molecule can be captured.

Note that molecules associate with charged species (protons, alkali metal ions, etc) with wildly different affinities and as a result, equal quantities of two molecules usually do not generate the same abundance of ions. Furthermore, ions themselves are represented unevenly depending on how “surface active” they are (i.e. how likely they are to find themselves at the surface of the droplet, and hence to appear in the spectrum due to IEM). In practice, because ESI-MS is usually performed in polar solvents, the most over-represented ions are those that are especially greasy and hydrophobic.

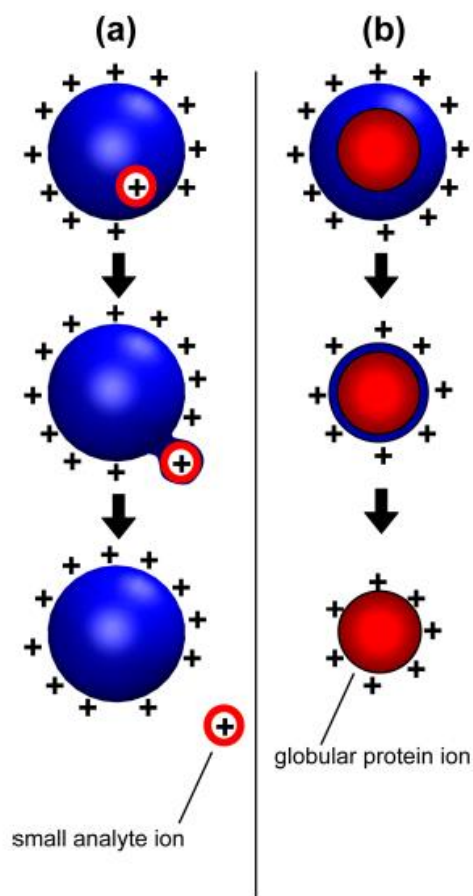


**Figure 25:** (a) IEM: Small ion ejection from a charged nanodroplet. (b) CRM: Release of a globular protein into the gas phase.<sup>86</sup> Reprinted with permission from “Unraveling the Mechanism of Electrospray Ionization” L. Konermann, E. Ahadi, A. D. Rodriguez and S. Vahidi, *Analytical Chemistry*, 2012, 85, 2-9.

Copyright © 2012 American Chemical Society

### 2.3 Quadrupole –Time of Flight (Q-TOF)

The ESI instrument used in this work was a Waters Q-TOF-Micro tandem mass spectrometer. Once gas phase ions are generated from the ESI source, they will be drawn into the sample cone due to the pressure difference as shown in Figure 26. The ESI source chamber is under slightly higher than atmospheric pressure, but the pressure inside of the sample cone is much lower. As from this part, the MS machine is under vacuum. Voltage difference is another driving force for the ion traveling process. However, not all of the ions get into the sample cone; a large proportion hits the cleanable baffle. If small droplets get into the sample cone, remaining solvent will be evaporated and pumped away. After that, ions traverse a right angle turn and enter the extraction cone which leads to an RF hexapole. RF lens chamber and analyzer part is under high vacuum ( $2 \times 10^{-7}$  mbar). This setup is to make sure there is a minimum amount of neutral molecules get into the analyzer.

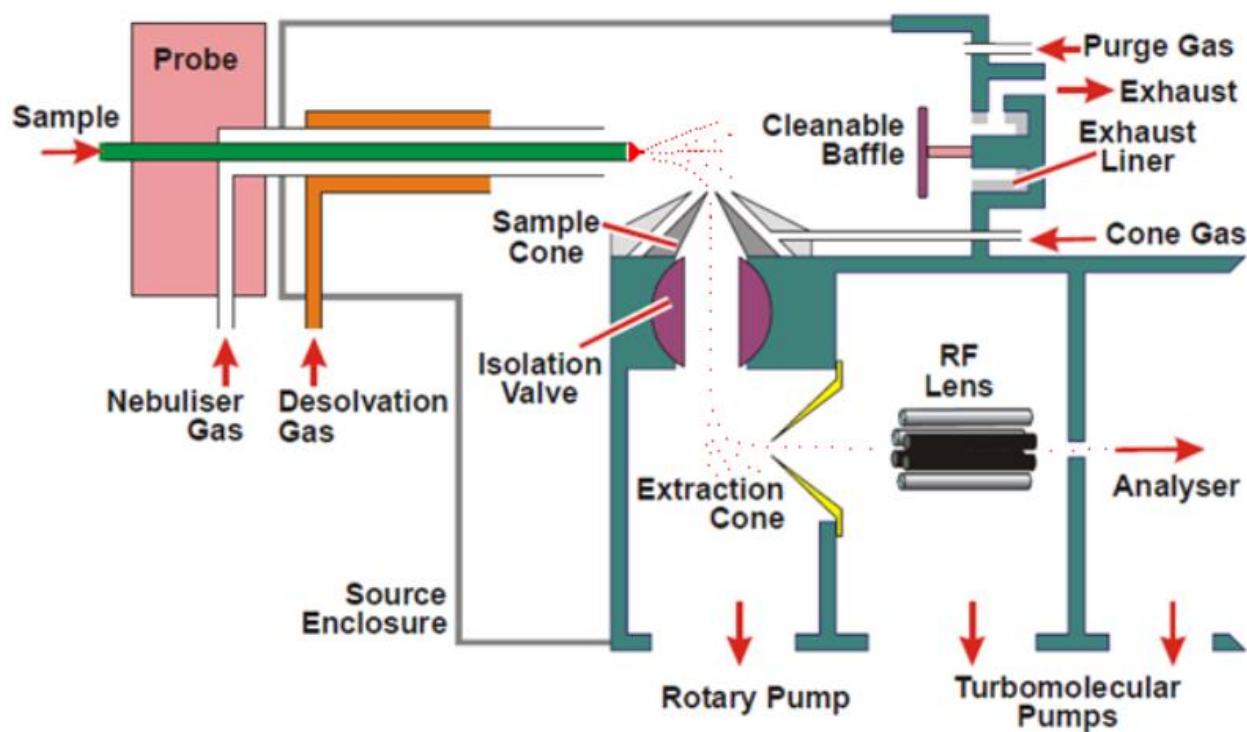


**Figure 26:** Electrospray source with QTOF-Micro scheme.<sup>87</sup> Reprinted with permission from “Micromass Q-TOF micro Mass Spectrometer Operator’s Guide” Copyright © 2012 Waters Corporation

As shown in Figure 27,<sup>87</sup> ions pass through a hexapole RF lens, in this part, ions will be confined into a narrow beam. In the next step, ions will enter into pre-filter, to get rid of low mass molecules before they enter the main quadrupole analyser as shown in Figure 28.<sup>87</sup>



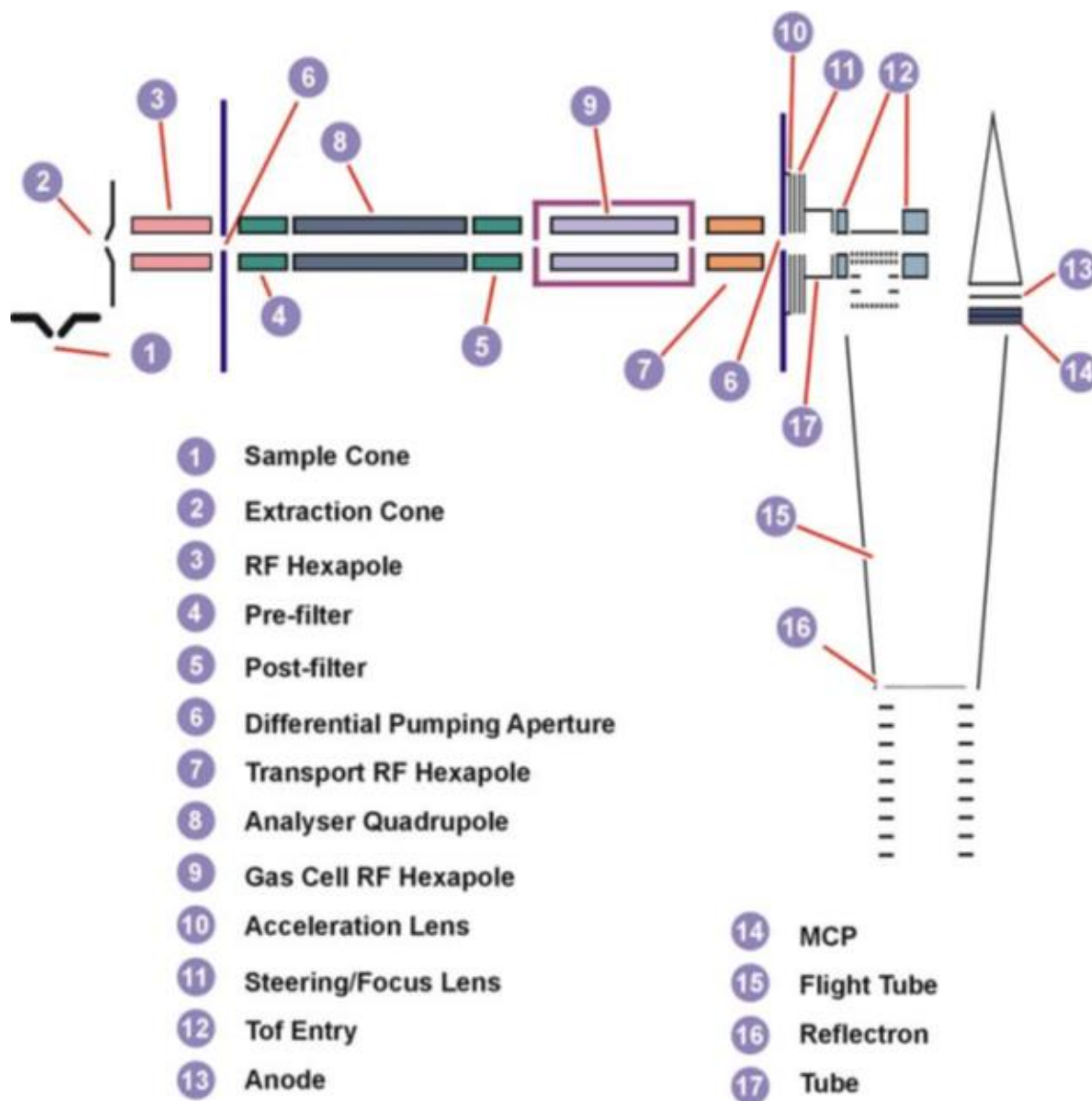


**Figure 27:** The Ion Optical System of the Q-TOF micro.<sup>87</sup> Reprinted with permission from “Micromass Q-TOF micro Mass Spectrometer Operator’s Guide” Copyright © 2012 Waters Corporation

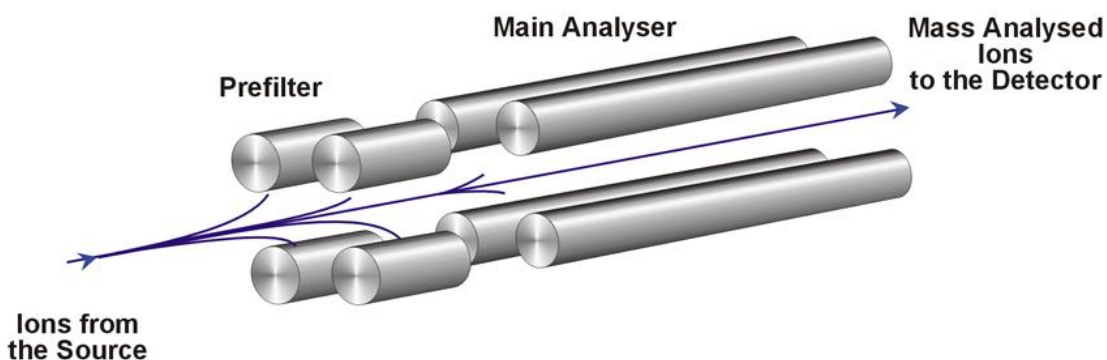


**Figure 28:** The Prefilter and Main Analyser of the Q-TOF *micro*<sup>87</sup> Reprinted with permission from “Micromass Q-TOF micro Mass Spectrometer Operator’s Guide” Copyright © 2012 Waters Corporation

The quadrupole analyzer has two functions. First, it can be used to focus on a specific  $m/z$  range, for example, from  $m/z$  50 to 2000. Second, it can be used to focus on a target  $m/z$  value, this is useful for MS/MS analysis, in other word, analyze the product ions by using collision induced dissociation (CID) to break the precursor ions apart.

Before ions enter the Time Of Flight analyzer, they will pass through collision gas cell, which contains Ar gas. Collision Induced Dissociation (CID) happens in this cell. In MS mode, this gas cell just works as a hexapole RF lens to help ions pass through to the second analyzer, but in MS/MS mode, the collision voltage can be set to higher value and this will lead to higher collision energy, and the ions will start generating fragments as the ions hit the collision gas and break apart. And the fragments will provide important structural information of the parent ions.

CID can also provide bond strength information; there are different types of bonds inside a molecule, the bond strength information can be detected by CID. Stronger bonds take higher collision energy to break. Energy dependent ESI (EDES) is an important type of reaction that can be achieved by CID. EDES is shown as contour map, on this map, the  $m/z$  of a give ion will be shown as well as the stability of each fragment at a certain collision voltage (Figure 29).<sup>88</sup> It provides information about bonding strength of ligands for a target molecule.

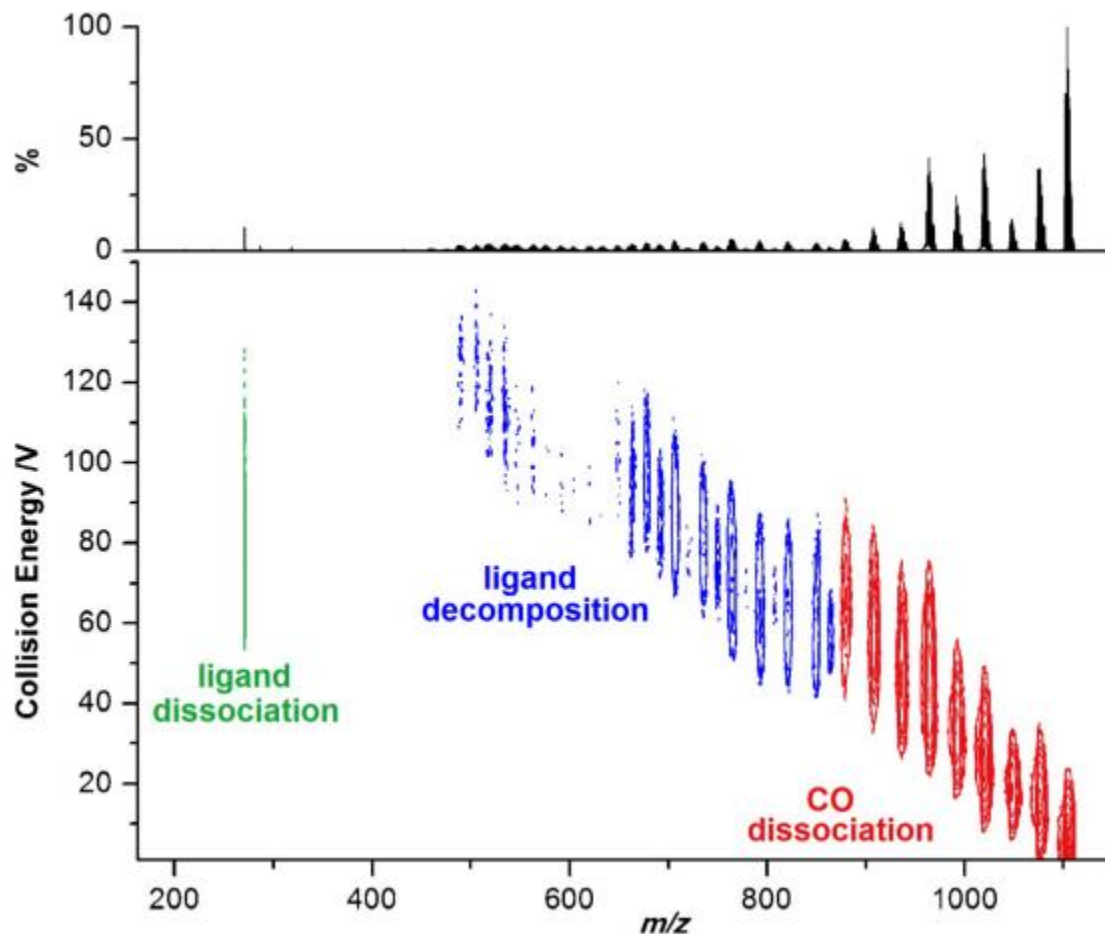


**Figure 29** Positive-ion energy-dependent ESI-MS of a representative example. X axis is the  $m/z$ , Y axis is collision energy in voltage, the red and blue dots are the detected signal of a certain species at the applied voltage.<sup>88</sup> Reprinted with permission from “Synthesis and characterization of a new class of anti-angiogenic agents based on ruthenium clusters” A. A. Nazarov, M. Baquié, P. Nowak-Sliwinska, O. Zava, J. R. van Beijnum, M. Groessl, D. M. Chisholm, Z. Ahmadi, J. S. McIndoe, A. W. Griffioen, H. van den Bergh and P. J. Dyson, *Sci. Rep.*, 2013, 3. Copyright © 2013 Macmillan Publishers Limited

In the next step, ions will enter into an orthogonal time-of-flight analyzer. When ions reach a device called the pusher, they are pulsed down a flight tube in a perpendicular direction. However, same mass-to-charge ratio ions within each group may contain different kinetic energy and their moving directions are also different, these must be corrected before they hit detector, otherwise the mass accuracy will suffer. The reflectron is the device to correct this; it works like an ion mirror, repelling ions back down the flight tube, as shown in Figure 30. Ions with higher kinetic energy will travel deeper into the reflectron than those with lower kinetic energy. After the reflection, the ions with same  $m/z$  will all hit the ion detector at the same time.

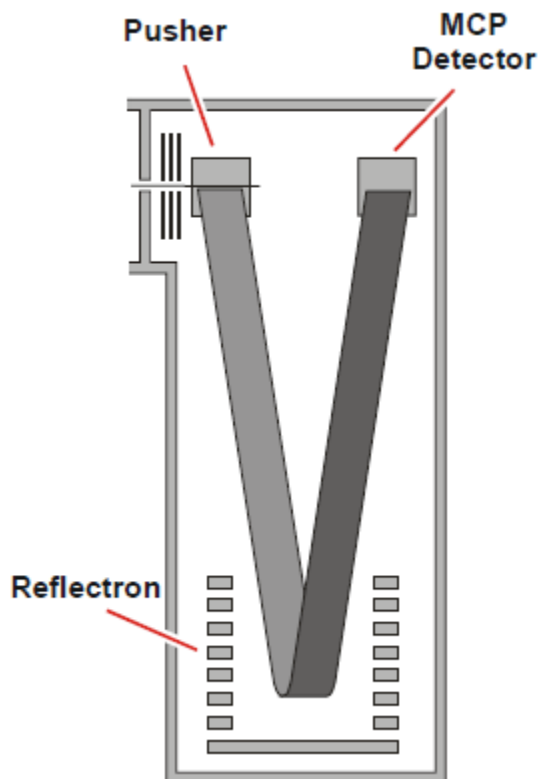


**Figure 30** Time of Flight analyzer<sup>87</sup> Reprinted with permission from “Micromass Q-TOF micro Mass Spectrometer Operator’s Guide” Copyright © 2012 Waters Corporation

The microchannel plate detector (MCP) is the final destination for the ions. It contains thousands of electron multipliers. When an ion hits the MCP, it will trigger an electron multiplier to generate a current. The strength of the current depends on the number of ions that arrives at MCP. Ions arrive at the same time have the same  $m/z$ . The more ions that arrive at the same time, the stronger the current will be, and it will be converted into computer data for future processing. The output signal will be transferred into Waters’ analysis software MassLynx where ion intensity and  $m/z$  is displayed in a Microsoft Windows system.

## 2.4 Continuous reaction monitoring with ESI-MS

ESI-MS cannot only detect the  $m/z$  of a target analyte, it can also detect the quantity of it in a given reaction because the MCP can detect both ion mass-to-charge ratio and ion intensity. The ion intensity represents the number of analytes which reach the MCP and this number is proportional to the concentration of the analyte in solution. When analyte concentration changes,

ion intensity also changes, it makes ESI-MS a perfect instrument for tracking target species in a dynamic reaction.

All the analytical techniques introduced in Chapter 1 can be used to track the whole process of a reaction. However, ESI-MS has unique advantages over all the other instruments in organometallic catalytic reactions. Any catalytic reaction can be a complicated mixture; it contains starting materials, catalysts, different intermediates, products and by-products as well as decomposed compounds. Usually the catalyst has low concentration, all of the compounds are in a dynamic environment which changes every second. It requires instrument with ability to detect, identify and track all the individual species in real time with very short interval time between each sampling (per second). In some cases, the reactions are air and moisture sensitive and the sample has to be protected under inert atmosphere. Mass spectrometry is an appropriate technique to achieve all of these goals.

Continuous reaction monitoring can be carried out using a technique called pressurized sample infusion (PSI) which was invented and developed by our previous group member Dr. Krista Vikse<sup>89, 90</sup>. The setup is shown in Figure 31. PSI is a cannula system that transfers a small amount of continuously flowing reaction solution from a slightly pressurized (1-10 psi) Schlenk flask to ESI-MS through PEEK tubing.

The pressure source of the system can be different depend on what the type of reaction to be monitored. For air and moisture sensitive reactions, the gas can be N<sub>2</sub> or Ar; for hydrogenation reaction H<sub>2</sub> will be used. Other examples include O<sub>2</sub>, CO, condensed air, CO<sub>2</sub>, C<sub>2</sub>H<sub>4</sub> etc. The flow rate based on the flask pressure and tube length and diameter was calculated based on the Hagen-Poiseuille equation, and tested under practical conditions.<sup>72</sup> The ideal pressure is 3 psi which is calculated based on Hagen–Poiseuille equation,<sup>91</sup> this pressure allows us to obtain a flowrate 30 to 60μL per minute. The pressure can be also set from 1 to 10 psi based on different reaction purposes.

The Schlenk flask is the reaction container, so for reactions that require high temperature, a condenser is necessary for cooling. The Schlenk flask has to be well sealed if the reaction is air

sensitive. Rubber septa and Teflon tape are commonly used. Grease can also be used but with caution as it can dissolve in certain solvent to interfere with reactions.

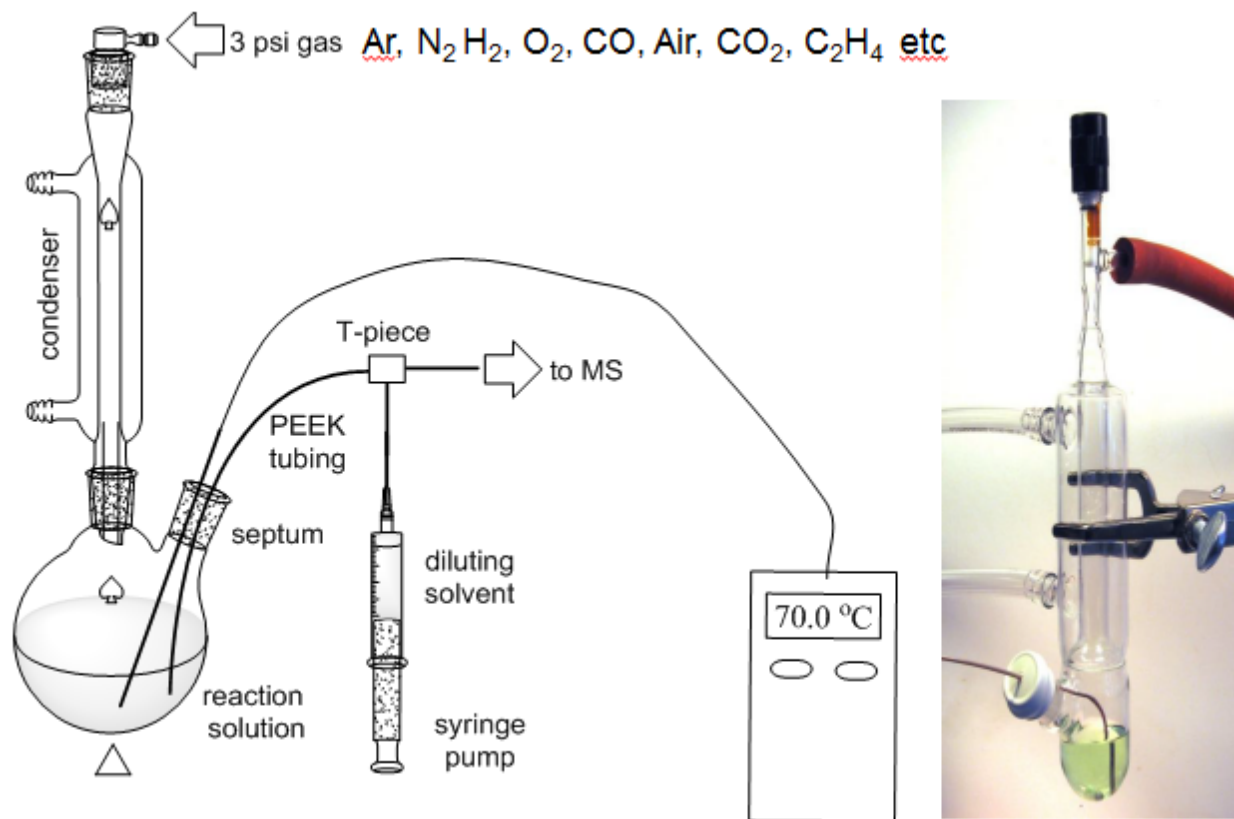


**Figure 31** Pressurized sample infusion system setup.

A short length of PEEK tubing (0.4 m) is used for cannula transfer. If the concentration of the reaction solution is too high, it can saturate the MS detector. In such cases, an online dilution system can be installed by using a T-piece. Diluting solvent can decrease the concentration to 1% of the original concentration. If the dilution solvent is different from reaction solvent or same solvent but with different temperature, it will help to quench the reaction, so the reaction will be stopped at the T-piece but the flow will keep going.

Once the system is set up, the reaction solution will be pushed into ESI-MS by the slight over pressure. Sampling time is set to 1 second per spectrum in most cases. The absolute intensity of each species in the reaction will be normalized against total ion current. An example of standard PSI-ESI-MS continuous reaction monitoring result is shown in Figure 32.<sup>72</sup> In this example, we

can see a silane redistribution reaction. When the catalyst is added; the starting material is converted into product over time.

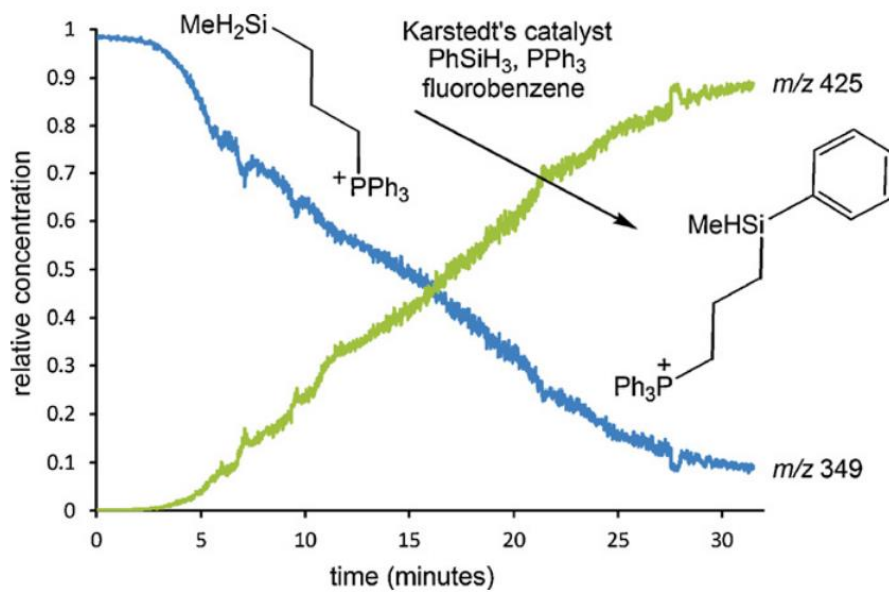


**Figure 32:** Normalized intensity vs. time trace for a charged silane ( $m/z$  349) and appearance of the product of redistribution ( $m/z$  425).<sup>72</sup>

### 3. Methodological innovations

#### 3.1 Numerical modeling

In order to simulate the proposed catalytic reaction mechanism and match the simulation with experimental result, we used different computer programs: Powersim<sup>92</sup> and COPASI<sup>93</sup>.

Powersim is system dynamic software originally used for financial and business simulation. But we chemists found a way to run reaction related simulations with it (Figure 33)<sup>94-96</sup>. The reasons that chemists can use financial software for chemistry kinetic studies is because Powersim simulation pathway design is based on graphic symbols and arrows rather than lines of codes as in Maple (Maplesoft Inc). And Powersim models can be built based on pure mathematical equations, chemical reaction process can be converted into these equations as elemental steps. This saves a lot of time not having to learn a programming language. With a few hours' design, a Powersim numerical model can be built (Figure 34) based on a proposed mechanism (Figure 33).

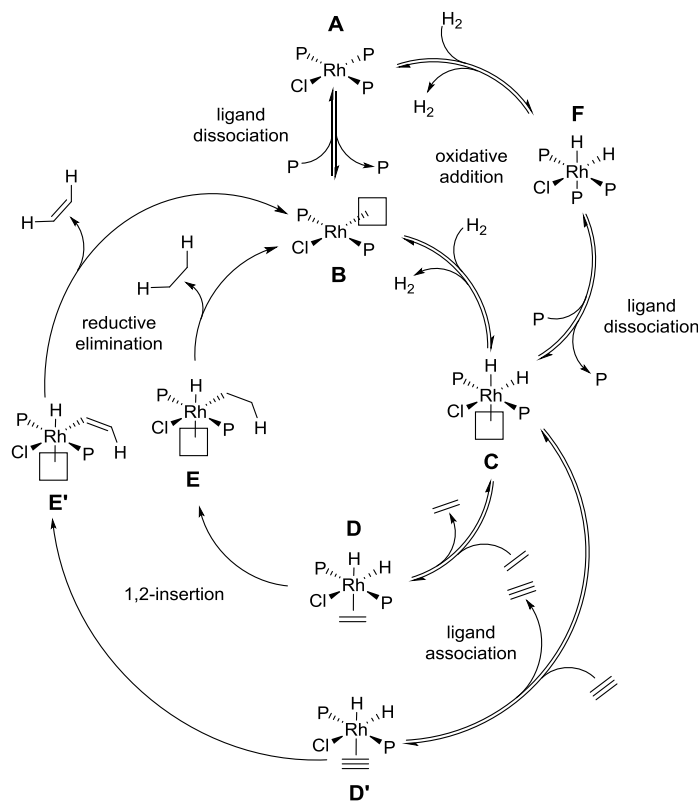


**Figure 33:** Proposed mechanism for hydrogenation of alkyne by Wilkinson's catalyst.<sup>95</sup>



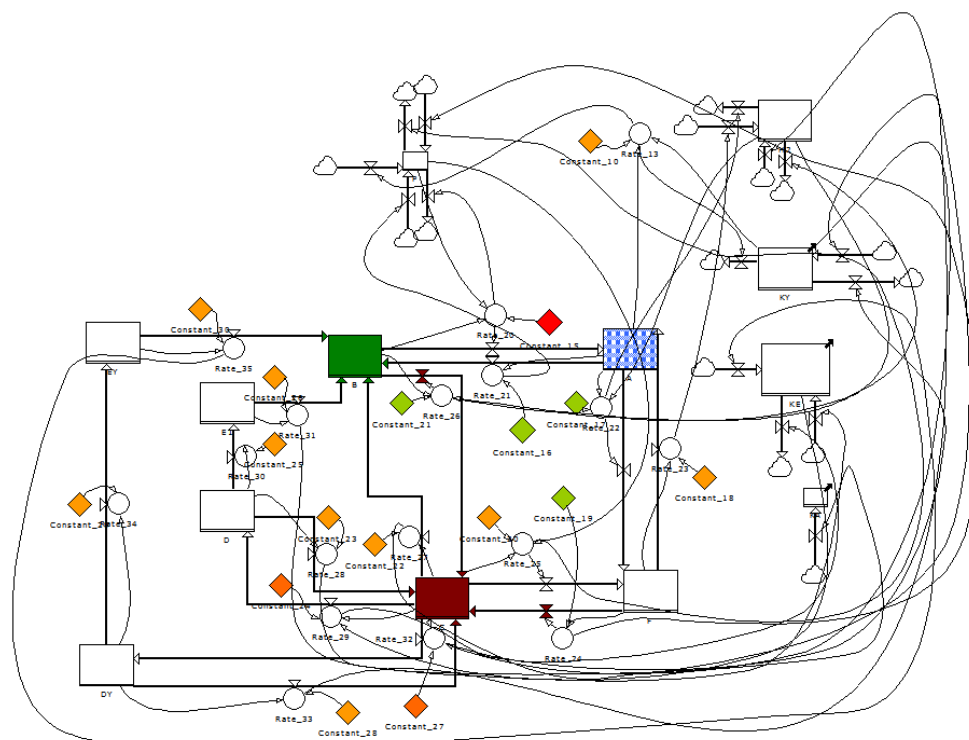


**Figure 34:** Powersim Numerical model<sup>95</sup>, this figure represents a Wilkinson's hydrogenation reaction.

After a Powersim model is built, the next step is rate constants estimation. This is the most difficult part for establishing a good model. For a proposed mechanism, the reasonable way to estimate a rate constant is to do literature research on related reactions and specific studies on a specific step of the whole reaction, and for rest of the steps, manual optimization is required. By appearance of simulated results, the rate constants will be revised to make it fit better into the experiment results.

Another numerical modeling software that we are using is called COPASI<sup>93</sup>. It stands for Complex Pathway Simulator. COPASI is open-source software which can be downloaded from the authors' website. COPASI has a simple interface and it is designed for biology and chemistry related simulations.

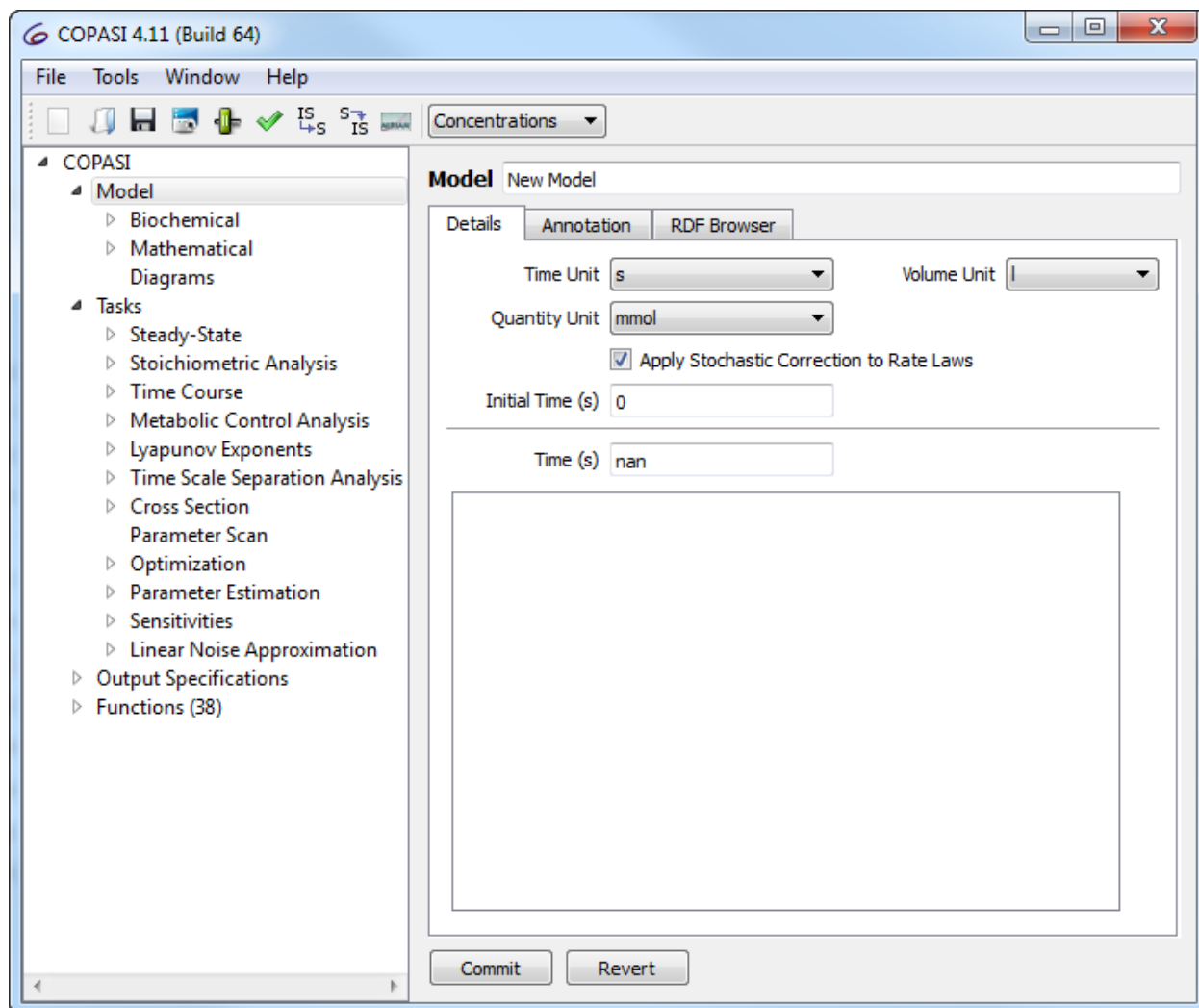
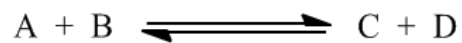


**Figure 35:** COPASI interface

For the same reversible reaction:



all you need to do is to type in a few characters, in this example, the model is  $A + B = C + D$ , the symbol “=” means it is a reversible reaction. If it is irreversible, we can use “->” instead of “=”.

**Reaction**

Details

Reaction

Reversible  Multi Compartment

Rate Law

Flux (mmol/s)

Symbol Definition

| Description | Name                               | Value | Unit       |
|-------------|------------------------------------|-------|------------|
| Parameter   | k1 <input type="checkbox"/> global | 0.1   | l/(mmol*s) |
| Substrate   | substrate                          |       | mmol/l     |
|             | A                                  |       |            |
|             | B                                  |       |            |
| Parameter   | k2 <input type="checkbox"/> global | 0.1   | l/(mmol*s) |
| Product     | product                            |       | mmol/l     |
|             | C                                  |       |            |
|             | D                                  |       |            |

**Figure 36:** COPASI model for reversible reaction

COPASI allows users to import real reaction data and do automatic matching calculations based on different mathematical methods (Figure 37) to find the rate constants that best fit the reaction. The software will do 30-100 calculations per second. Based on the complexity of the model, the whole calculation process may last from a few seconds to hours. This function is very important for rate constants optimization and it can speed up the whole model building process greatly. While does not have the graphical user interface of Powersim overall it is a much more powerful tool for building numerical models for catalytic mechanisms.

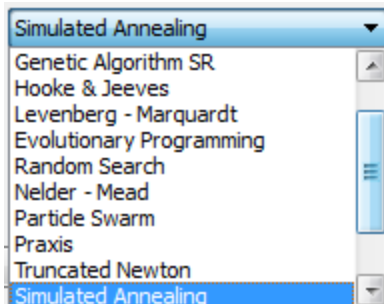


Figure 37: simulation method of COPASI

### 3.2 Powersim model design

Powersim software was originally designed for financial and business simulations, therefore, in order to apply it to chemistry a great deal of translation needs to be done. The meaning of the numbers has to be transferred into chemistry terms. For example, by converting from a dollar to a mole, a money transfer process is converted into a chemical process. The order of a reaction is represented in the program through connecting symbols with arrows.

The following Powersim models are built for use in catalytic reactions.

For a simple irreversible first order reaction:

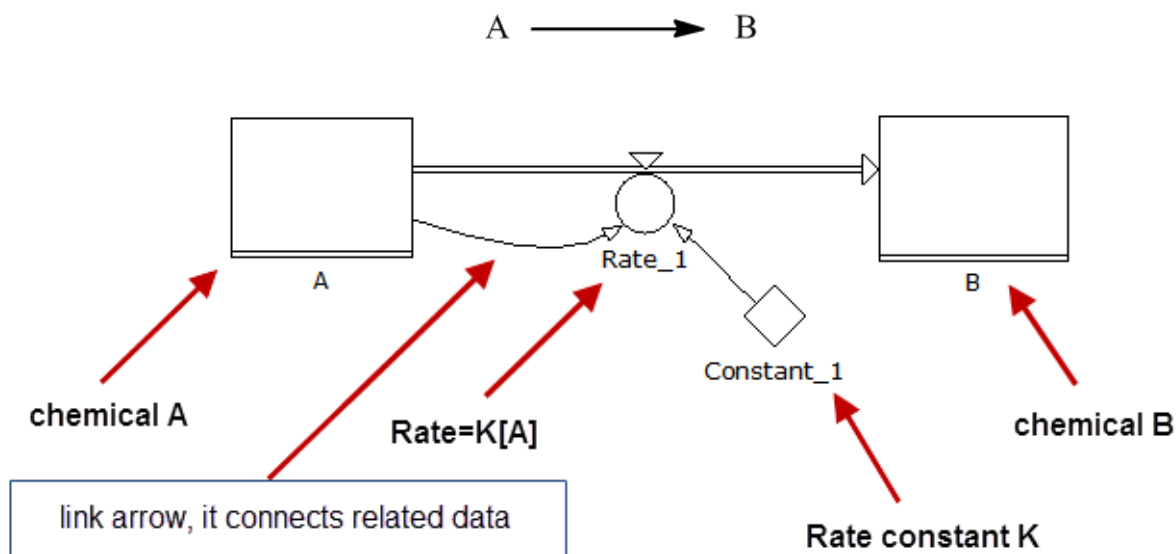
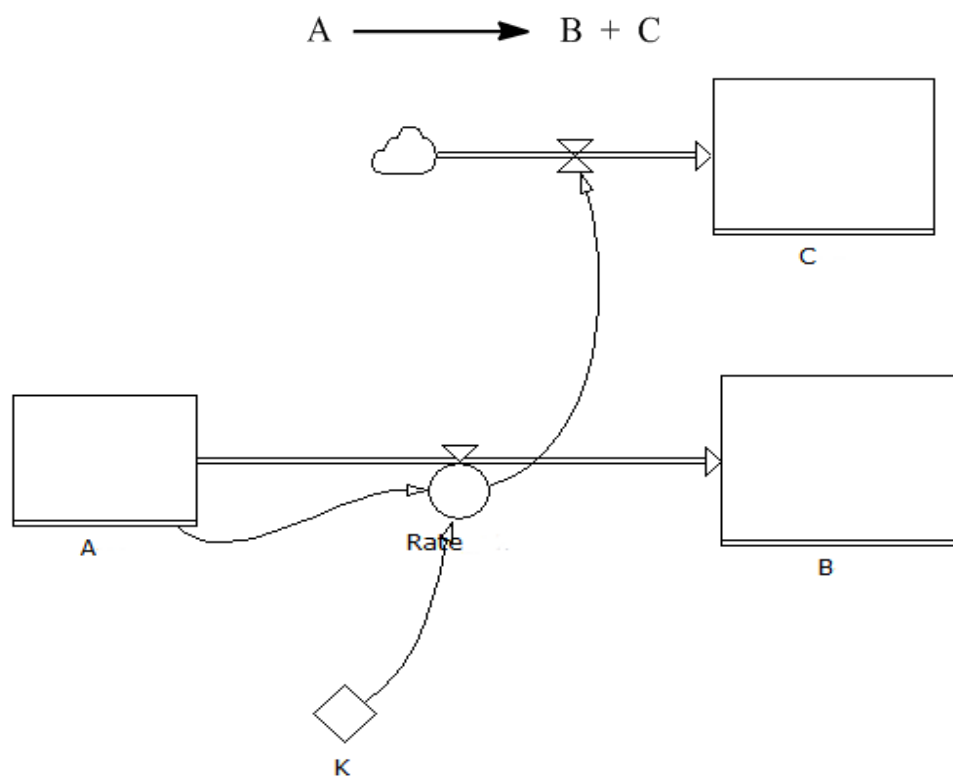


Figure 38: Powersim model for irreversible first order reaction.

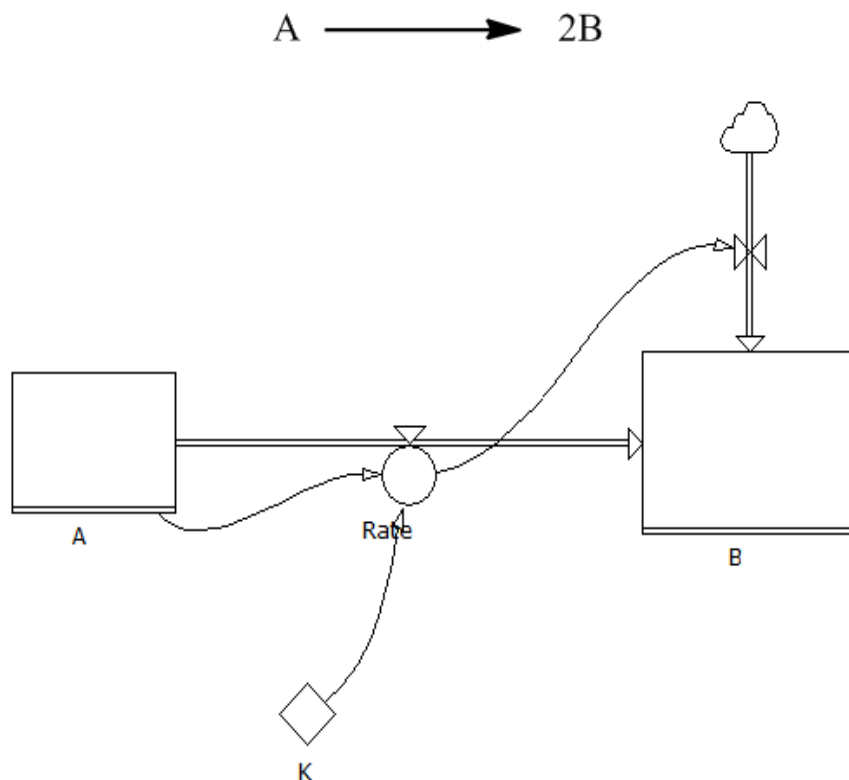
The model includes A and B as components for concentration of two species. They are connected by a one directional arrow; indicating A will convert into B. Constant\_1 is a variable used to set the rate constant of the reaction. Level A and Constant\_1 are connected with Rate\_1 by a small arrow indicating that the rate of the reaction is related to A and Constant\_1. After the model is built, the value and unit for each component can be set by clicking on them. This is the most basic Powersim model for a chemical reaction. The conversion rate equals  $k[A]$ .

The second example shows a reductive elimination process, where one reactant converts into two products. Similar to the example above, the A variable is connected with B by an arrow. The Rate variable controls the disappearance of A and appearance of B and C. The rule is the reactant can only connect with one product. For C, the second product, it has to connect with a cloud symbol by an arrow. This means there is a source for the generation of C and that the generation rate is the same as **Rate**, so there is a small arrow connects **Rate** and the arrow to C as shown in Figure 39. The conversion rate equals to  $k[A]$ .



**Figure 39:** Reductive elimination

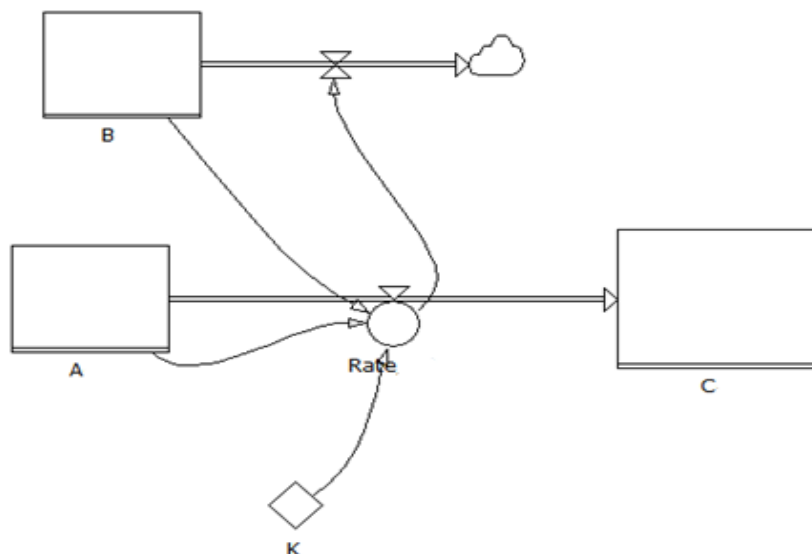
The process of a dimer splitting into two monomers is shown in Figure 40. There are two arrows connecting with B, the first one is from A, the second one is from the “cloud” symbol. And the rate constants for these two arrows are the same, meaning for each A consumed, two B will be produced. If it is A to 3B, there will be three arrows and so on. The conversion rate equals  $k[A]$ .



**Figure 40:** Dimer splits into two monomers

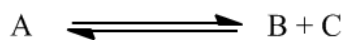
An oxidative addition process can be represented by Figure 41. As already demonstrated, one reactant can only connect with one product. A is connected with C, and B connects with a cloud. The conversion rate equals to  $k[A][B]$ .

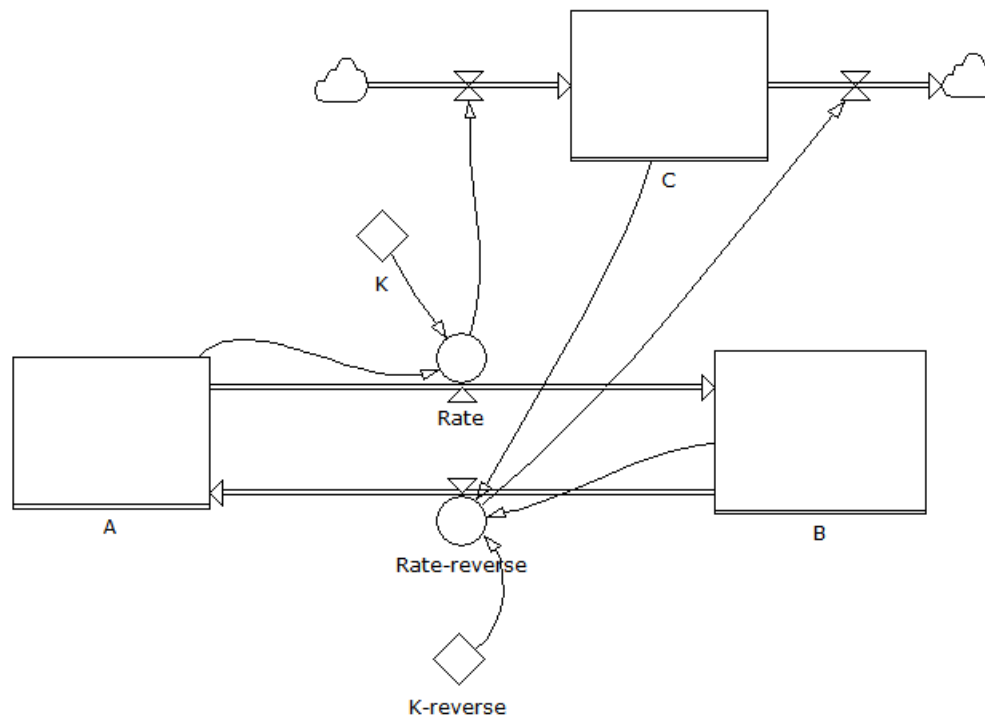




**Figure 41:** Oxidative addition

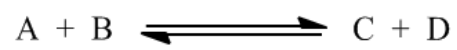
Figure 42 shows a reversible reductive elimination reaction. There are two big arrows between A and B, one towards B, the other towards A. These represent the reversibility of the reaction. There are two rate constants,  $K$  and  $K$ -reverse, for the forward and backward reaction, respectively.  $K$  equals to the production of C, so there is a small arrow connecting the Rate and the cloud-to-C arrow. Analogously,  $K$ -reverse equals to the consumption of C, so there is a small arrow connecting the Rate-reverse and C-to-cloud arrow. For the backward reaction, the concentration  $[B]$  and  $[C]$  contribute to the backward reaction rate Rate-reverse, so there is a small arrow connects the Rate-reverse and C and another one connects Rate-reverse and B. Rate =  $k[A]$ , Rate-reverse =  $k$ -reverse $[B][C]$ .





**Figure 42:** Reversible reductive elimination

For the following reaction:





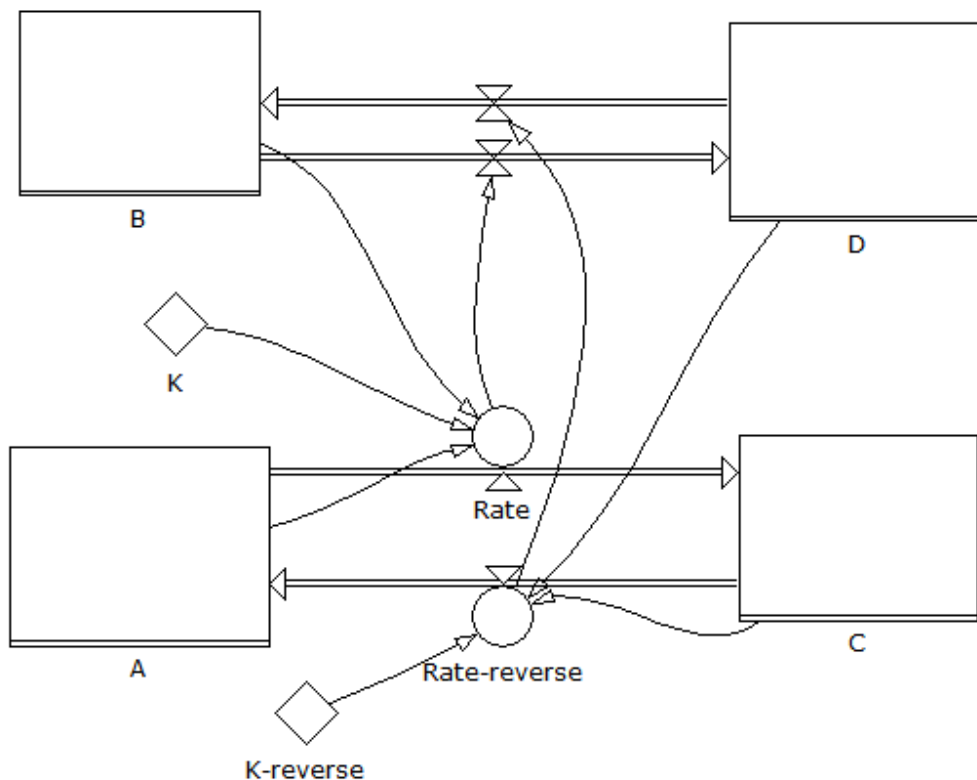


**Figure 43:** Powersim model for second order reversible reaction.

In this second order reversible reaction, we have two reactants and two products. When we try to build this model, the first step is to connect one reactant with one product. In this example, A connects with C, and B connects with D. There are 2 big arrows between A and C in two directions, which means A can convert into C and C can convert back into A. B is involved in the A-C conversion, so A, B and rate constant k are all connected with Rate. The Rate controls the decrease of A and B and increase of C and D. For the reverse reaction, it is the same method.  $\text{Rate} = k[A][B]$ ,  $\text{Rate-reverse} = k\text{-reverse}[C][D]$ .

For a complicated catalytic mechanism, these six elementary reactions make up the building blocks of the catalytic cycle.

### 3.3 Handling air and moisture sensitive reactions

When investigating air and moisture sensitive catalytic reactions using ESI-MS, there is a high chance the sample will be exposed to air. The analyser and detector are under vacuum, but the

source and the injection parts are not. In our group, our previous group members designed a positive pressure chamber; it is filled with nitrogen to protect the source from air leaking into the source. An airtight syringe is used for sample protection. However, this is not enough protection for extremely air-sensitive chemicals such as methylaluminumoxane (MAO). A glovebox is installed next to the MS (Figure 44), so extremely air sensitive reactions can be set up within and the sample can be injected into the MS via PEEK tubing through a small opening on the glovebox side wall.

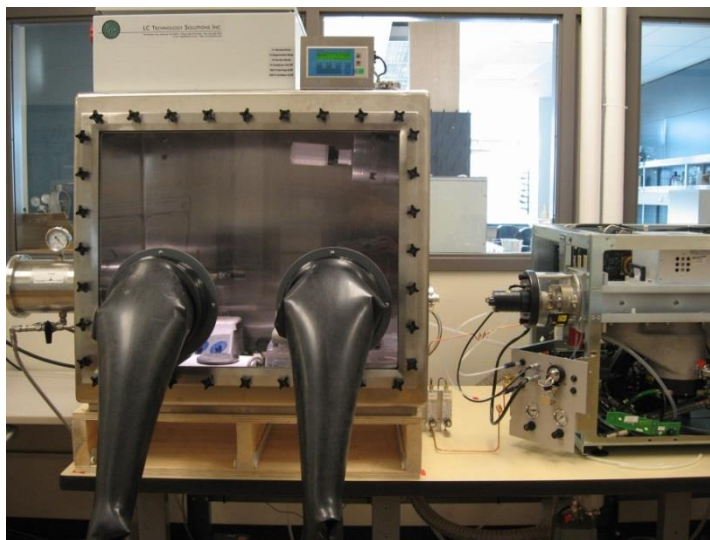


**Figure 44:** Glovebox next to MS

The instrument setup is one part of the protection system. The other important part is to get the reaction solution dry and degassed. In the case of most of our research (primarily online ESI-MS reactions) we only require less than 20 mg of the reactants and less than 10 mg of catalysts, and 2 to 20 mL of solvent. If the solvent is not dry, the small amount of water in a solvent is enough to decompose all the catalyst and significantly influence the reaction. Traditional solvent drying techniques are not enough for online MS reactions; we have to bring solvent drying to the next level. For example, the solvent from a Solvent Purification system (SPS) contains 5 ppm of water, for a reaction with 10 g of solvent; this equates to 50  $\mu\text{g}$  of water, which is equal to the molar amount of catalyst used in most reactions. Not to mention other sources including glassware residue and operationally introduced water.

The method we use to dry solvent is to set the still under constant reflux with  $\text{CaH}_2$  over two days before collection. After that, solvent will be taken into glovebox and loaded with activated molecular sieves, and left for another two days before use.

### 3.4 PSI-ESI-MS optimization

Since the development of pressurized sample infusion ESI-MS, we have applied it to a variety of reactions. These reactions are under different conditions, some require different temperatures, some have solubility issues, and some are conducted with very low volumes. These require the PSI-ESI-MS to be adjustable to fit all the conditions. In order to make PSI-ESI-MS a better method for online monitoring, we have optimized the system in many ways.

#### 3.4.1 PSI-ESI-MS filter

One of the most important optimization is the filtration system. For a PSI-ESI-MS reaction, the reaction solution will be pushed into MS continuously through PEEK tubing and ESI capillary for a period ranging from a few minutes to eight hours. If any insoluble particles get stuck in the pathway during the reaction, the ion intensity vibrates or even pauses for lack of incoming solution. In most cases, the reagent cannot be pre-filtered. Furthermore, it is possible that insoluble products, by-products or decomposed catalyst may precipitate out during the reaction, increasing the chance of blocking of the pathway.

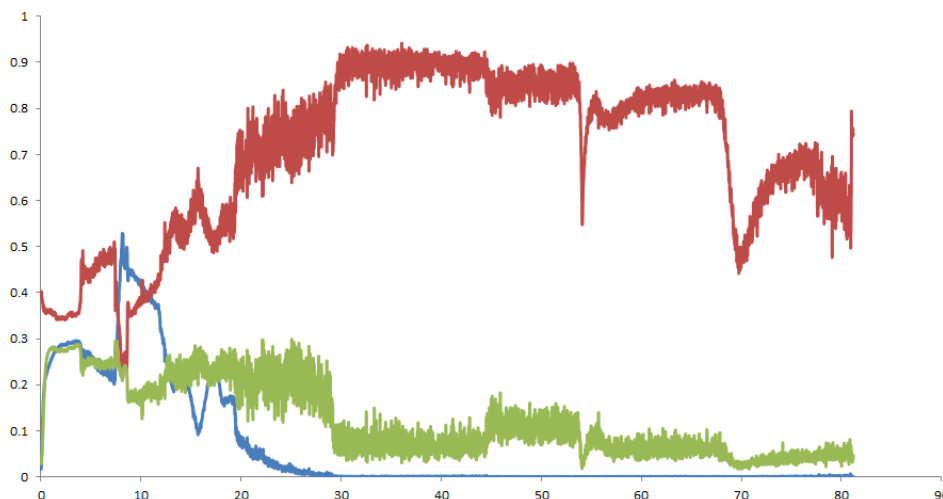


**Figure 45:** Online monitoring with blocked PEEK tubing

In order to solve this problem, I developed and refined eight generations of filters (Figure 46).

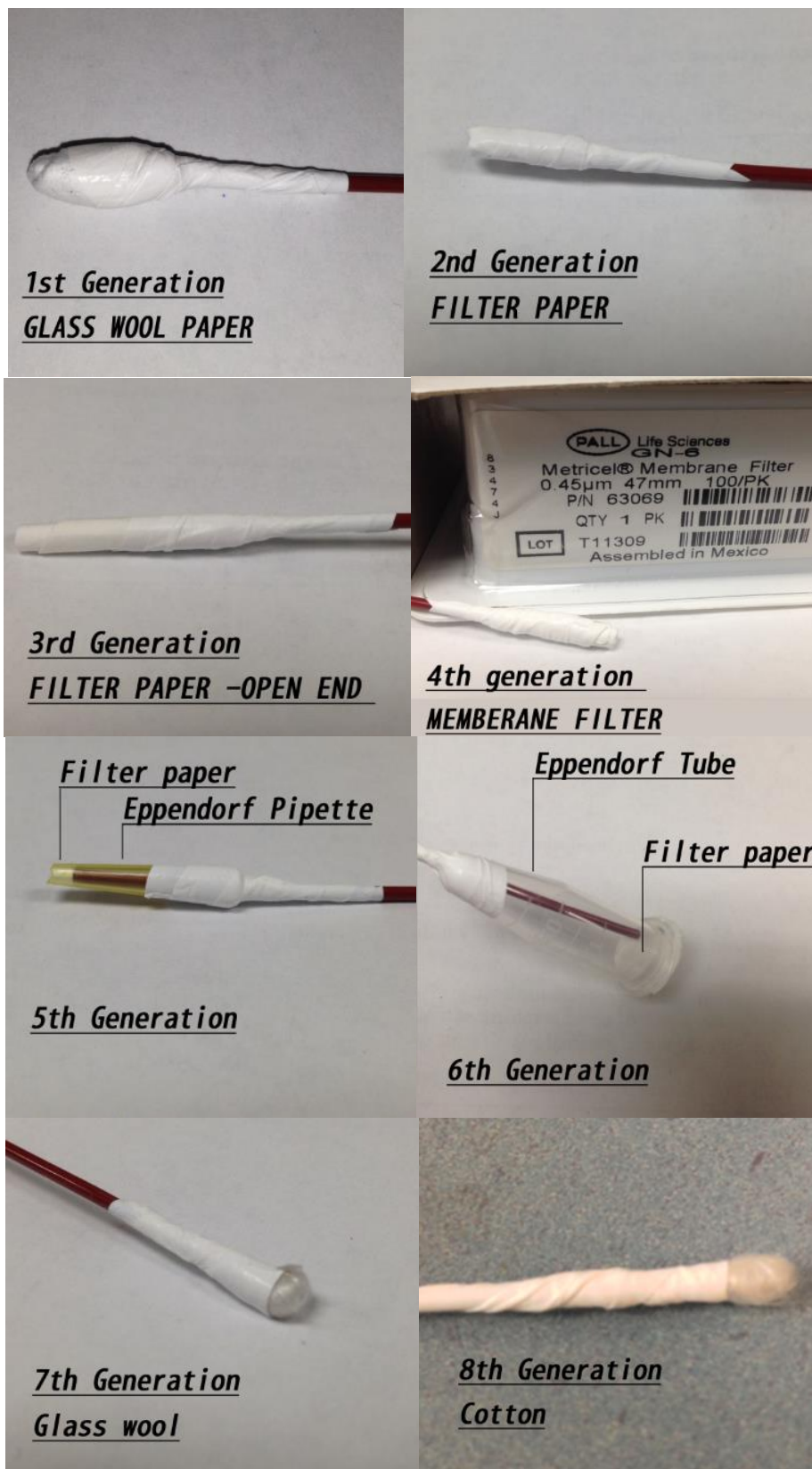


**Figure 46:** Eight generations of filter

Filters are made by connecting a material with PEEK tubing by Teflon tape. The ideal filter needs to meet a few requirements. It should filter off insoluble particles, it should not appreciably influence the flow rate or in other words increase the retention time. It should not create an area with different concentration, and it also should not interfere with the reaction. Based on these criteria, we can see the performance of these 8 types of filter. After years of tests, the cotton filter was found to be the best, as different solvent can go through it quickly and the filtration efficiency is excellent. However, cotton is still not the perfect material for all reaction purpose, as the main component is cellulose, which contains many OH bonds and can therefore interfere with a reactive compound such as MAO. Also, it is impossible to dry cotton in an oven so it has to be dried by other methods. The best filter for a given scenario can be chosen by consulting Table 2, the measurements for the performance are based on MS experimental results.

**Table 2:** Filter performance table

|                                   | 1          | 2            | 3            | 4            | 5            | 6          | 7            | 8            |
|-----------------------------------|------------|--------------|--------------|--------------|--------------|------------|--------------|--------------|
| <b>Filtration efficiency</b>      | <b>OK</b>  | <b>Bad</b>   | <b>Bad</b>   | <b>Great</b> | <b>Great</b> | <b>OK</b>  | <b>Great</b> | <b>Great</b> |
| <b>Retention time</b>             | <b>Bad</b> | <b>Great</b> | <b>Great</b> | <b>Great</b> | <b>Bad</b>   | <b>Bad</b> | <b>Bad</b>   | <b>Great</b> |
| <b>Concentration interference</b> | <b>Ok</b>  | <b>Great</b> | <b>Great</b> | <b>Great</b> | <b>OK</b>    | <b>Bad</b> | <b>Great</b> | <b>Great</b> |
| <b>Reaction interference</b>      | <b>No</b>  | <b>No</b>    | <b>No</b>    | <b>Yes</b>   | <b>No</b>    | <b>No</b>  | <b>No</b>    | <b>No</b>    |

### 3.4.2 PSI-ESI-MS dilution system

A dilution system designed for a highly concentrated catalysis reaction has been designed and tested. The detection limit of ESI-MS makes it difficult to conduct mechanistic investigations in such concentrated solution. Our previous group members have already designed a dilution system as shown in Figure 31, in which up to 1:100 dilution ratio can be achieved.<sup>90</sup> However, the problem here is that the more dilute the solution is, the more solution will pass through ESI capillary and reach the source. This is acceptable for a short experiment but for a long reaction, it

will increase the degree of contamination of the instrument. In order to solve this problem and boost the dilution efficiency, I designed a new setup (Figure 47 and Figure 48).

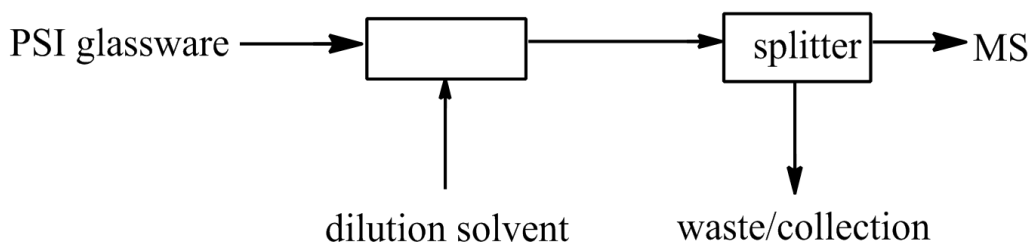


**Figure 47:** The new online dilution system.

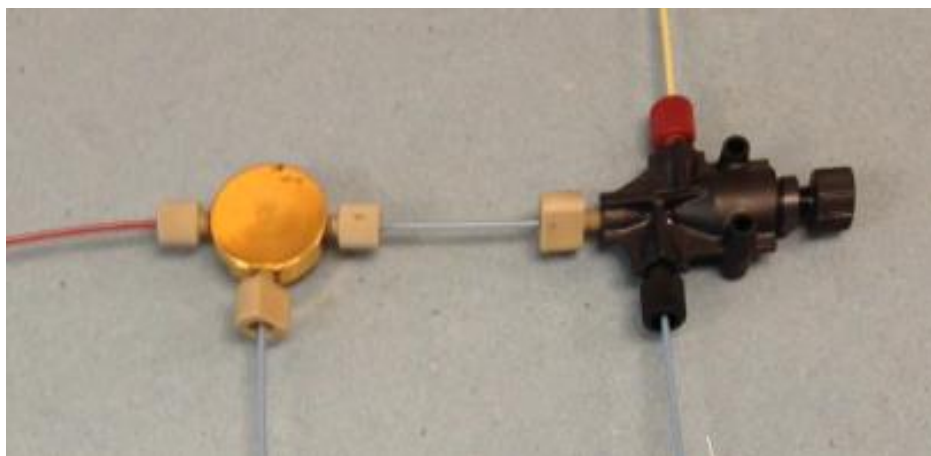


**Figure 48:** Photo of online dilution system.

The adjustable splitter can be set to any ratio between the two output PEEK tubes, it is important to protect the ESI-MS from signal overloading. With 1:100 diluted solution and a small portion of flow, PSI-ESI-MS was tested with up to 2 M reaction solution and the test results were good (i.e. minimal source contamination, no overloading of the detector). The larger portion of the flow can go to collection, waste, or it can be used for other online monitoring technique including UV and flow IR etc.

### 3.4.3 PSI glassware

For an air-sensitive catalytic reaction, the most-used PSI glassware is a Schlenk flask. It is usually used for reactions with volume 2 to 50 mL. For a smaller scale reaction, it is not

convenient. For example, an NMR tube reaction may only contain 0.7 mL of solution and enough solution is required to remain at the end of the reaction to allow NMR spectra to be obtained. In order to follow the same NMR tube reaction by NMR and MS, a new PSI NMR tube was designed. Two PEEK tubes can be plugged into a rubber NMR septum as shown in Figure 49. When low pressure is applied, the solution in the NMR tube can be infused into the mass spectrometer. Testing results show 1 psi pressure can push 0.1 mL solution per hour. This flow rate will not influence NMR tests so NMR and MS data can be obtained under near-identical conditions.

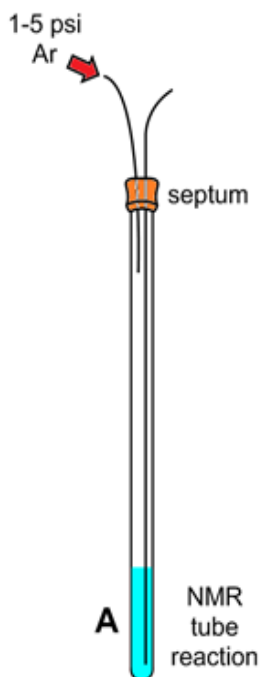


**Figure 49:** PSI NMR tube

Air-sensitive small volume sample tests can also be done by another setup that we designed. It is called PSI vial. The samples (trace amount to 1 mg) can be prepared in a glovebox and sealed with septum, similar to a PSI NMR tube, and the septum is good enough to hold 3 psi pressure.

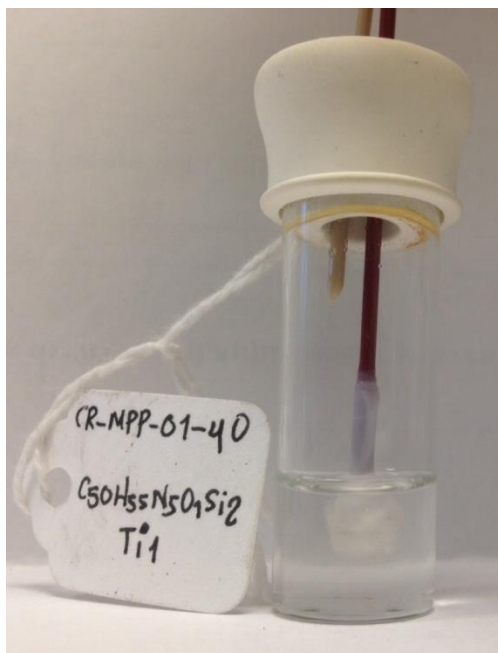


**Figure 50:** PSI sample vial. In a glovebox, small amounts of solid sample can be introduced into a vial capped with a septum, then taken out of the glovebox and solvent injected into it. Two PEEK tubes pierce through a septum into the vial. The yellow PEEK tube is connected to a pressure supply (e.g. Ar or N<sub>2</sub>), and the red PEEK tube is dipped into the solution and the other end is connected to the ESI-MS. If the sample is not soluble enough, a filter must be installed on the red PEEK tube and the septum fitted before the vial is capped.



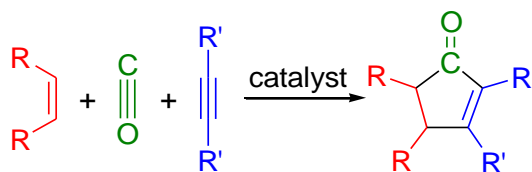
## 4. The Pauson-Khand Reaction

Portions of this chapter have been previously published, and are reproduced in part with permission from “The Pauson-Khand Reaction: A Gas-Phase and Solution-Phase Examination Using Electrospray Ionization Mass Spectrometry” M. A. Henderson, J. Luo, A. Oliver and J. S. McIndoe, *Organometallics*, 2011. Copyright © 2011 American Chemical Society

I performed all experimental work related with ligand synthesis, PSI and kinetics study, produced figures and co-wrote the paper with Matthew Henderson, JS McIndoe. AG Oliver performed the crystal structure determinations. Matthew Henderson performed gas phase reaction and crystallization.

### 4.1 Introduction

The Pauson-Khand reaction (PKR) is a [2 + 2 + 1] cycloaddition reaction involving three components - an alkene, an alkyne, and a carbon monoxide molecule that generates a cyclopentenone ring using  $\text{Co}_2(\text{CO})_8$  as catalyst (Equation: 2). It was reported in 1971 by Pauson and Khand during screen reactions on different substrates using this catalyst.<sup>97, 98</sup> Cycloaddition is one of the most attractive methods for synthesizing ring-structured pharmaceutical compounds. The Pauson-Khand reaction is a perfect reaction to achieve this goal because of its good yield, atom economy and high stereoselectivity.<sup>99-101</sup>

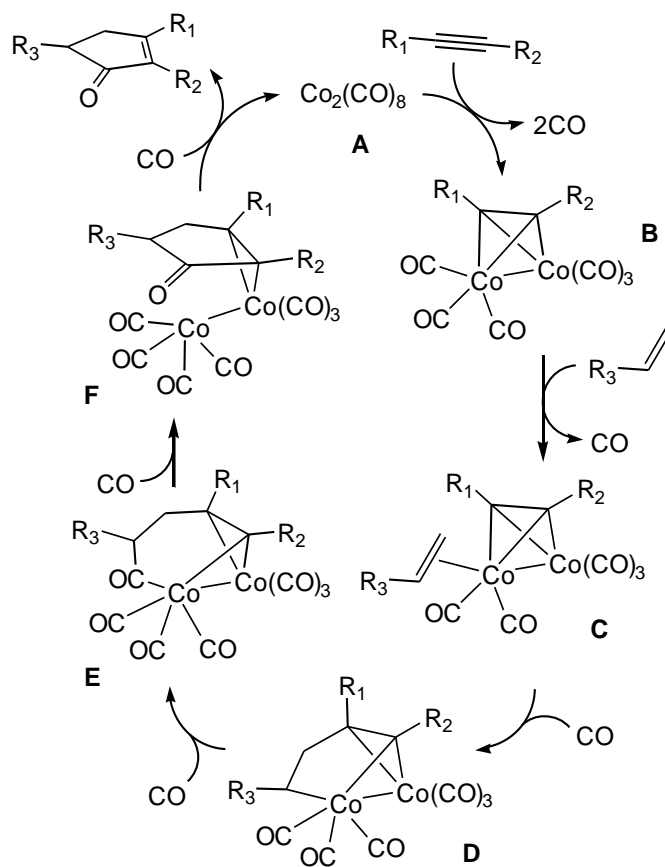


Equation: 2

During the early development of the Pauson-Khand reaction, the efficiency of the dicobalt catalyst was not high. The main strategy involves synthesizing the hexacarbonyl alkyne intermediate using a stoichiometric amount of  $\text{Co}_2(\text{CO})_8$ , and mixing it with an alkene and CO to generate the final product. A high pressure of CO and an extended reaction time were required during the reaction.<sup>79,102</sup>

Since 1998, there have been 40 to 80 papers per year focusing on the Pauson-Khand reaction. Many improvements have been made. Different activators that allow less CO pressure have been reported, including amine oxides, cyclohexylamine,<sup>103</sup> sulfides,<sup>104</sup> phosphine oxides,<sup>105</sup> and water.<sup>106</sup> Other metal complexes have also been reported including Co/Rh heterobimetallic nanoparticles,<sup>107</sup>  $[\text{RhCl}(\text{CO})_2]_2$ ,<sup>108</sup>  $[\text{Rh}(\text{dppp})_2\text{Cl}]$ ,<sup>109, 110</sup>  $\text{Ru}_3(\text{CO})_{12}$ ,<sup>111</sup>  $\text{MoCp}_2(\text{CO})_4$ ,<sup>112</sup>  $[\text{Ir}(\text{COD})\text{Cl}]_2$ ,<sup>113</sup>  $\text{CpTi}(\text{CO})_2$ .<sup>114, 115</sup> The reaction has also been performed in ionic liquids, enabling recycling of the catalyst.<sup>116</sup>

Magnus and co-workers proposed a stoichiometric mechanism based on their observations of the unique stereospecificity of the cyclization.<sup>117</sup> This catalytic cycle is widely accepted but only one intermediate was captured (B in Scheme 1,<sup>118</sup> the well-known dicobalt hexacarbonyl-alkyne).



**Scheme 2:** Proposed catalytic cycle for the intermolecular Pauson-Khand reaction.

## 4.2 Selected studies

Density functional studies by Yamanaka *et al.* showed a large energy barrier from  $\text{Co}_2(\text{CO})_6(\text{alkyne})$  to  $\text{Co}_2(\text{CO})_5(\text{alkyne})$ , while subsequent steps proceeded quickly (Figure 51).<sup>119</sup> This energy profile explained why previous research did not successfully detect any of the intermediates C to F.<sup>120</sup>

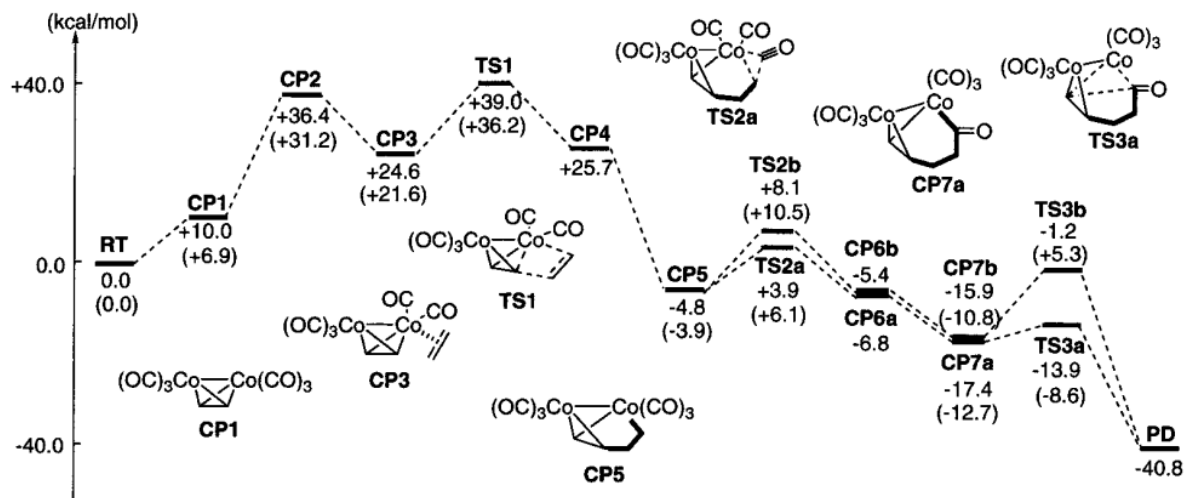


**Figure 51:** Energetics of the PK reaction. Reprinted with permission from “Density Functional Studies on the Pauson–Khand Reaction” M. Yamanaka and E. Nakamura, *Journal of the American Chemical Society*, 2001, 123, 1703-1708. Copyright © 2001 American Chemical Society

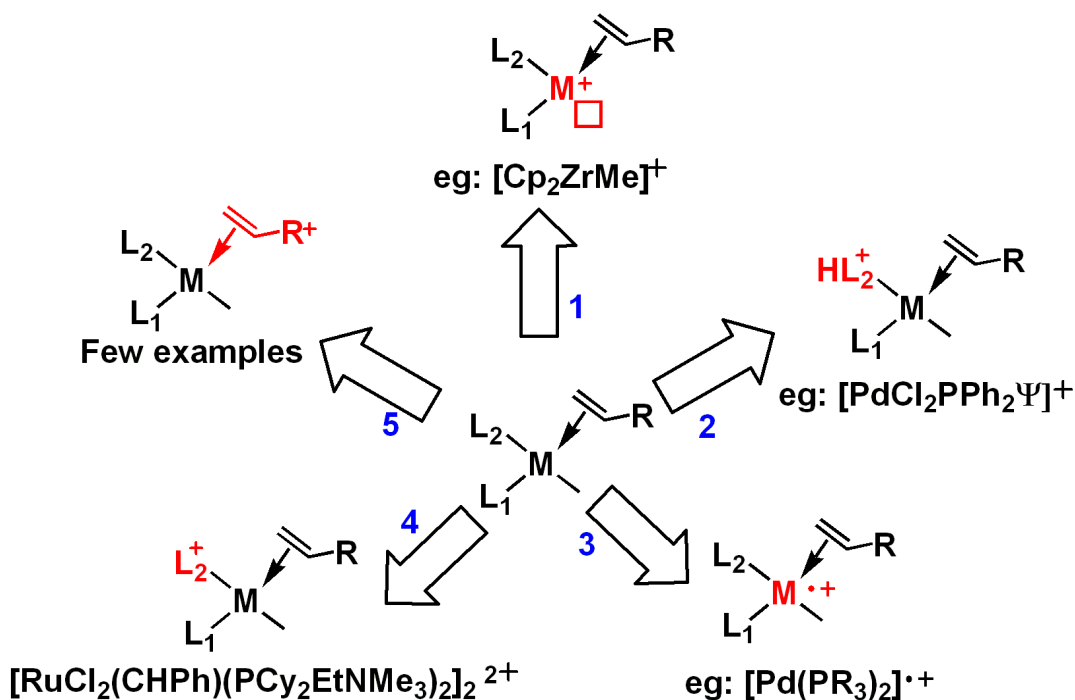
Gordon *et al.* were also working to capture the later intermediates.<sup>121</sup> Evans and co-workers were able to crystallize a pentacarbonyl dicobalt-ene complex with an (intramolecular) alkene filling the sixth coordination site, but the subsequent insertion reaction did not work.<sup>122</sup> Pallerla *et al.* investigated regioselectivity in Pauson-Khand reactions of cyclopropenes by X-ray crystallographic studies of isolated Co-complexes. They employed a chiral cyclopropene complex to react with a  $\text{Co}_2(\text{CO})_6(\text{alkyne})$  complex, and an inserted by-product was captured in which the cyclopropene ring had opened.<sup>123</sup> Another research group worked on the reactivity difference among olefin reagents in the PK reaction; the result shows that when the alkene binds with a favourable orientation, alkene insertion follows along with CO insertion and then reductive elimination of the product.<sup>124</sup> When the alkene binds in an unfavourable geometry, alkene insertion follows because this reaction is not dependent on the stereochemistry of the alkene. However, the subsequent CO insertion was prevented, meaning that stereospecificity is dictated by the CO insertion reaction. In order to satisfy the valencies of both cobalt atoms, the

cyclopropene ring opens for anionic coordination of the third carbon atom. Other reports have shown evidence of pentacarbonyl complexes by using alkynes with sulphur as the donor atom, one of the CO ligands was replaced by the donor atom.<sup>124, 125</sup>

In terms of kinetic studies of the Pauson-Khand reaction, there is only one report after four decades. In this report,<sup>126</sup> (trimethylsilyl)-ethyne and norbornadiene (NBD) were used for reaction progress kinetic analysis<sup>127</sup> to determine the rate =  $k[\text{Co}_2(\text{CO})_8]^{1.3}[\text{NBD}]^{0.3-1.2}/[\text{CO}]^{1.9}$ . Two important conclusions were made. Firstly, the starting material alkyne is not involved in the rate equation. This means the alkyne is not involved in the rate determining step, and higher concentrations of alkyne have no effect on the rate of the reaction. Secondly, more carbon monoxide will make the reaction slow down.

### 4.3 Challenges of ESI-MS for Pauson-Khand studies

ESI-MS is an analytical technique for ion detection. Any neutral compound is undetectable, and for any organometallic catalysis reaction mechanism study using ESI-MS, the conversion from neutral metal complexes to ionized metal complexes has always been a challenge.



Scheme 3: Five different ways of ionizing neutral metal complexes.

As shown in Scheme 3,<sup>128</sup> there are a variety of different ways to charge a neutral metal complex. (1) loss (or gain) of an anionic ligand such as  $X^-$  to become an inherently charged complex;<sup>129</sup> (2) a ligand with donor atoms that can form adducts with ions such as  $H^+$ ,<sup>130, 131</sup>  $Na^+$ ,<sup>132</sup> or  $Ag^+$ ;<sup>133</sup> (3) an electron rich oxidizable ligand that can lose an electron in reaction solution.<sup>134</sup> (4) a charged ancillary ligand, most often a phosphine;<sup>135</sup> (5) a charged substrate, in which case the metal complexes can only be detected when the substrate is bound to the metal.<sup>136, 137</sup>

In order to use ESI-MS for the study of the Pauson-Khand reaction, the reaction system requires positive or negative ions in solution phase. The catalyst  $Co_2(CO)_8$  is a neutral compound and cannot be detected in mass spectrometry. It has only one ligand that can be ionized, and its reactivity will be changed if one of the CO ligands is replaced by an ionisable ligand. One of the substrates, carbon monoxide, is in the gas phase and has no charge, so the alkyne or alkene will be the only option.

The metal complexes will fall into the fifth category – the charged substrate –as we can synthesize alkynes or alkenes with a charged tag.

#### 4.4 Advantages of ESI-MS for the Pauson-Khand Reaction studies

There are two advantages in using ESI-MS in the study of this reaction. First, even though  $Co_2(CO)_8$  and one of the substrates CO cannot be ionized, the alkyne and alkene functional group can be easily integrated into a charged tag system. The charged tag can be far away from the reaction center, so the catalysis reactivity will not be influenced by the ion, and the result will represent the reaction under real conditions. When the charged alkene and alkyne react with  $Co_2(CO)_8$ , the intermediates will have a charged tag on them. This allows ESI-MS to detect main intermediates and short-lived intermediates. Second, a previous study using ESI-MS provided valuable information and proved this charged tag method is valid. Gimbert and coworkers have employed a bis(diphenylphosphino)methane (dppm) ligand and a phenylacetylene to make  $Co_2(CO)_4(DPPM)(\mu^2-HC_2C_6H_5)$ .<sup>138</sup> Under ESI conditions, the dppm ligand deprotonates to generate a  $[M-H]^-$  anionic species which is detectable by MS. However, charging the ligand

gives only information on the catalyst, not on the overall progress of the reaction. Charging the substrate does both.

## 4.5 Results and Discussion

### 4.5.1 Design of charged substrate

In this project strategy (5) was used to prepare a series of charged pyrrolidinium and piperidinium salts with alkyne and/or alkene functionality.

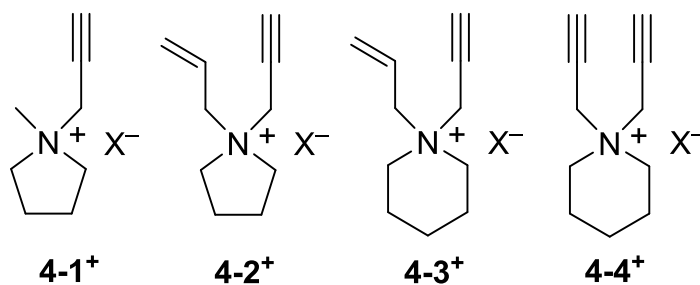
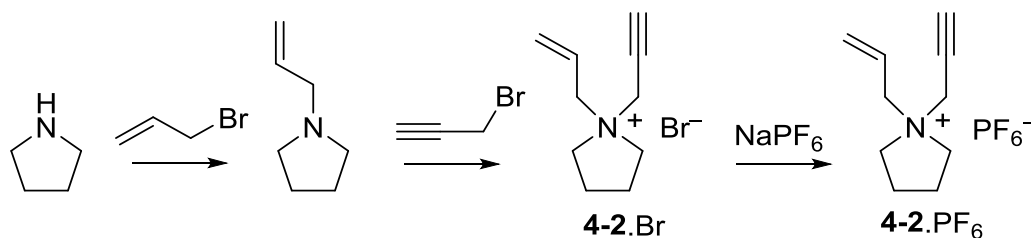


**Figure 52:** Functionalized pyrrolidinium and piperidinium salts.  $X^- = \text{Br}^-, \text{PF}_6^-, \text{BPh}_4^-, \text{Tf}_2\text{N}^-$ .

These salts were prepared by me with good yields starting from secondary or tertiary amines. The synthesis of these salts contains three steps as shown in Scheme 4. In the first step, two equivalents of secondary amine reacted with one equivalent of 3-bromopropene in a nucleophilic substitution reaction to generate one equivalent of pyrrolidinium bromide salt and one equivalent of 1-allylpyrrolidine. This reaction was done in ether at room temperature. The pyrrolidinium bromide salt by-product was insoluble in ether, so it was easy to filter out. The filtrate was forwarded to the second step where one equivalent of propargyl bromide was introduced at room temperature. The bis-functionalized product was insoluble in ether.

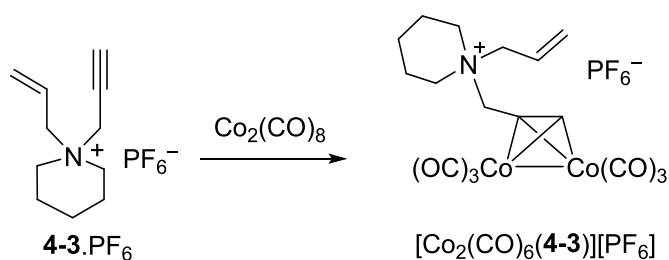
After simple filtration, the solid compound was obtained and ready for the next and final step – the salt metathesis with sodium hexafluorophosphate, sodium tetrphenylborate or sodium trifluoromethanesulfonimide. All of the metatheses were performed open to the atmosphere in water.



**Scheme 4:** Synthetic strategy applied to the charged acetylene substrates.

#### 4.5.2 Synthesis of cobalt complexes

In order to obtain detailed structural information of intermediate cobalt complexes, the synthesized charged salts were introduced to one equivalent of  $\text{Co}_2(\text{CO})_8$  in dichloromethane at room temperature to form the corresponding  $\text{Co}_2(\text{CO})_6(\mu\text{-alkyne})$  complex. The synthetic strategy is exemplified in Scheme 5 for the preparation of  $[\text{Co}_2(\text{CO})_6(\mathbf{4-3})][\text{PF}_6]$ . High quality ESI-MS spectra were obtained for  $[\text{Co}_2(\text{CO})_6(\mathbf{4-3})][\text{PF}_6]$  and the rest of the complexes where the observed peak corresponded to the expected ionic product of Scheme 5.



**Scheme 5:** Synthetic strategy for ionizing neutral metal complexes.

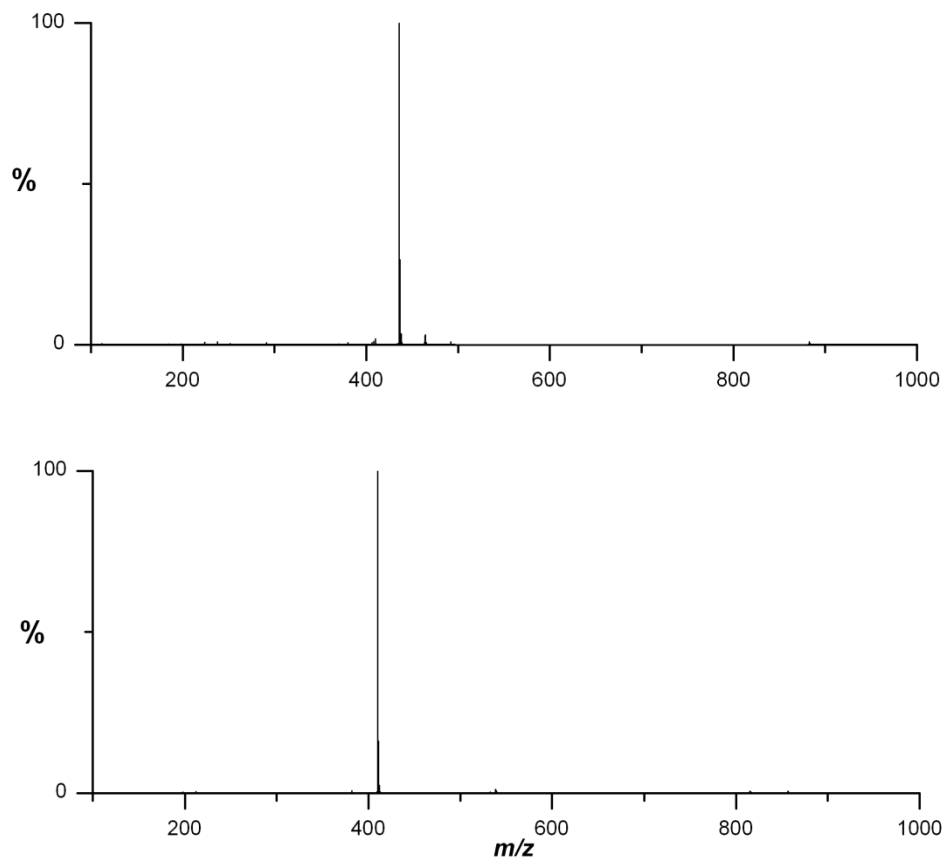


**Figure 53:** Positive-ion ESI-MS in dichloromethane  $[\text{Co}_2(\text{CO})_6(\mathbf{4-3})][\text{PF}_6]$  (top) and  $[\text{Co}_2(\text{CO})_6(\mathbf{4-1})][\text{PF}_6]$  (bottom). In both cases, the single peak corresponds to the intact cation.

$\mathbf{4-1}^+$  has a single alkyne functional group. As the hexafluorophosphate or tetrphenylborate salt, it reacted well with  $\text{Co}_2(\text{CO})_8$  to form  $[\text{Co}_2(\text{CO})_6(\mathbf{4-1})][\text{X}]$ , and a single-crystal X-ray structure was obtained for  $[\text{Co}_2(\text{CO})_6(\mathbf{4-1})][\text{BPh}_4]$  (Figure 54).<sup>50</sup>



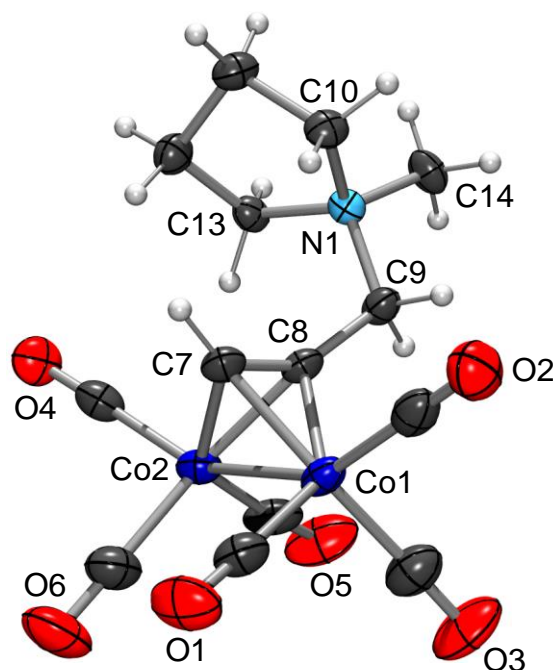


**Figure 54:** Single crystal X-ray structure of the cationic part of  $[\text{Co}_2(\text{CO})_6(\mathbf{4-1})]^+$   $[\text{BPh}_4]^-$ . The tetraphenylborate anion is not shown for the sake of clarity. Key bond lengths: Co1-Co2 2.461 Å; C7-C8 1.334 Å; C8-C9 1.488 Å; 1.311 ± 0.01 Å; Co-C 1.96 ± 0.01 Å; C-O 1.13 ± 0.01 Å; Co-CO 1.81 ± 0.02 Å; C-N 1.52 ± 0.02 Å. Key bond angles: C6-C7-C8 146.2°; Co-Co-C 51 ± 1°, Co-C-Co 77.5 ± 0.3°.

#### 4.5.3 Previous gas phase reaction

Previous gas phase studies on probing intermediates, showed  $[\text{Co}_2(\text{CO})_6(\mathbf{4-1})]^+$  can undergo an intermolecular Pauson-Khand reaction in the gas phase with different alkene gases.<sup>128</sup>

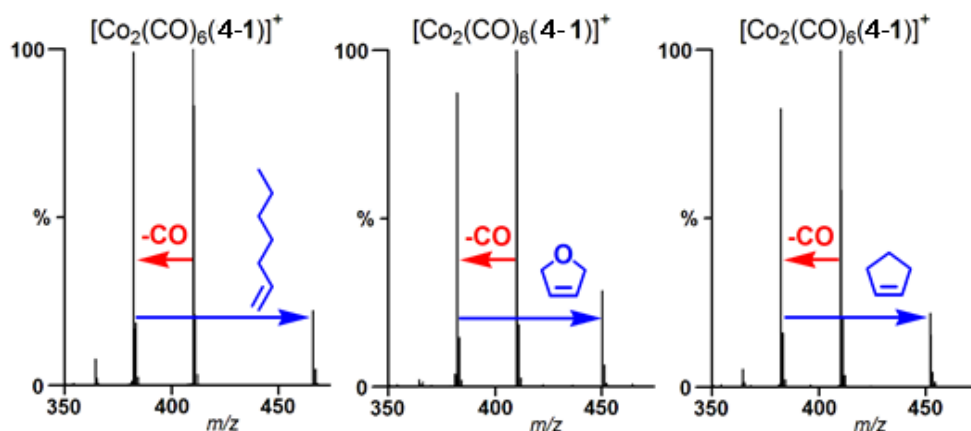


**Figure 55:** Gas phase reactions of  $[\text{Co}_2(\text{CO})_6(\mathbf{4-1})]^+$  with three different alkenes at a cone voltage of 20 V. In each case, one CO ligand is removed and the alkene adds to  $[\text{Co}_2(\text{CO})_5(\mathbf{1})]^+$ . The alkene does *not* add to the fully saturated ion.

The intermediates that were captured in these reactions are  $[\text{Co}_2(\text{CO})_5(\mathbf{4-1})(\text{alkene})]^+$ . In order to convert into this species, one CO ligand has to dissociate from the starting material  $[\text{Co}_2(\text{CO})_6(\mathbf{4-1})]^+$ . A second conclusion from Figure 55 is that different in bond strains or electronic effects of alkenes does not influence the reactivity of this coordination process because the results show all three alkenes have similar reactivity. In other words, alkene coordination is independent of the subsequent insertion reaction.

The following MS/MS reactions on  $[\text{Co}_2(\text{CO})_5(\mathbf{4-1})(\text{alkene})]^+$  showed the loss of an alkene as the first fragment in all three cases. This suggests the alkene is weakly bonded, the bond is weaker than that of CO to low oxidation state Co, and the insertion is trapped with additional CO. Therefore, the fact that a complete gas-phase Pauson-Khand transformation could not be observed was unsurprising, as was the ready loss of alkene upon reactivation using CID.

#### 4.5.4 Intramolecular Pauson-Khand reaction

Charged salts (**4-2**) and (**4-3**) have both alkyne and alkene functional groups. This can help to keep the weakly bonded alkene close to the reaction center to complete the Pauson-Khand reaction in a simple solution phase analysis.

With the pressurized sample infusion (PSI) online monitoring system, we designed a series of reactions that were constantly monitored under “real” conditions using ESI-MS. For this experiment, we used CO as the pressurizing gas. All the chemicals and glassware were initially protected under  $\text{N}_2$  and then flushed with CO.

Many experiments were performed before reproducibly good results were obtained. Solubility differences among starting material, catalyst, by-product and intermediates were the main issues in these tests. The charged salts have good solubility in polar solvents such as dichloromethane, methanol, ethanol, acetone, and acetonitrile but they cannot dissolve in nonpolar solvents; the  $\text{Co}_2(\text{CO})_8$  catalyst can be dissolved easily in apolar solvents such as benzene and toluene, but many polar solvents will decompose it or replace the CO ligands. All the solvents mentioned above were tested, and none of them met our experimental requirements.

Fluorobenzene showed better stability for both starting materials and catalyst, and the intermediates had good solubility in it. Also, fluorobenzene has a high boiling point, enabling

high-temperature reactions to be carried out. However, testing indicated that though the solubility improved, the starting material was still difficult to dissolve. This conclusion was made when dissolving the starting material **(4-3)** PF<sub>6</sub> and **(4-3)** Tf<sub>2</sub>N in 60 °C solvent; the starting material melted rather than dissolved, so it appeared to be a transparent solution. On closer inspection, however, slightly yellowish oil beads had formed.

The best solvent was found to be chlorobenzene. **(4-3)** Tf<sub>2</sub>N easily dissolved in PhCl, and PhCl has a high boiling point and meets all the experimental requirements except that it is not a very polar solvent; it has low sensitivity for ESI-MS. The detection of **(4-3)**<sup>+</sup> in this solvent was challenging; **(4-3)**<sup>+</sup> ion current per second was below 50, whereas a good ion current range is between 200 and 800 per second. Below this range, data fluctuation is significant, and obtained data cannot be used for kinetic studies. Ion current above this range leads to MS ion detector MCP (Micro Channel Plate) saturation, where the actual concentration is higher than the detector can tolerate, so the high intensity peaks will plateau and the result will misrepresent the true value. In order to increase the ion current, acetone was used as a diluent. As shown in Figure 31, acetone was used to dilute the chlorobenzene reaction solution, increasing the polarity of the mixed solvent and boosting the ion current significantly. While acetone is not a good solvent for the Pauson-Khand reaction, it is satisfactory as a dilution solvent because it is only in contact with the catalyst and intermediates for less than 2 seconds before they reach the ESI-source, which is insufficient time for catalyst decomposition to occur. There is another effect of acetone – when it mixes with chlorobenzene, the reaction will be quenched, meaning the reaction will be stopped at the T-piece mixer and no further reaction will occur beyond the mixer.

Because the reaction produces Co<sub>4</sub>(CO)<sub>12</sub> as a by-product, and this cluster is rather insoluble, we found crystallization of this compound caused the ion current to drop steadily over the course of the reaction and eventually the PEEK tubing would block completely. Spectra were normalized to the total ion current (TIC) to correct for these spray irregularities.

Therefore, a PSI-ESI-MS experiment was performed in chlorobenzene, with online dilution using acetone. Co<sub>2</sub>(CO)<sub>8</sub> was added to a solution of [**4-3**][Tf<sub>2</sub>N] under a CO atmosphere, and the reaction was monitored for 75 minutes (Figure 56). The appearance of only one intermediate was

observed, the expected  $[\text{Co}_2(\text{CO})_6(\mathbf{4-3})]^+$ . It in turn was consumed, with the appearance of the product,  $[\mathbf{4-3} + \text{CO}]^+$ . No intermediates were observed in the reaction (i.e. species with more or less CO ligands than six, collision voltage was also taken into consideration as shown in Figure 57), again consistent with the ligand dissociation step being rate-determining.

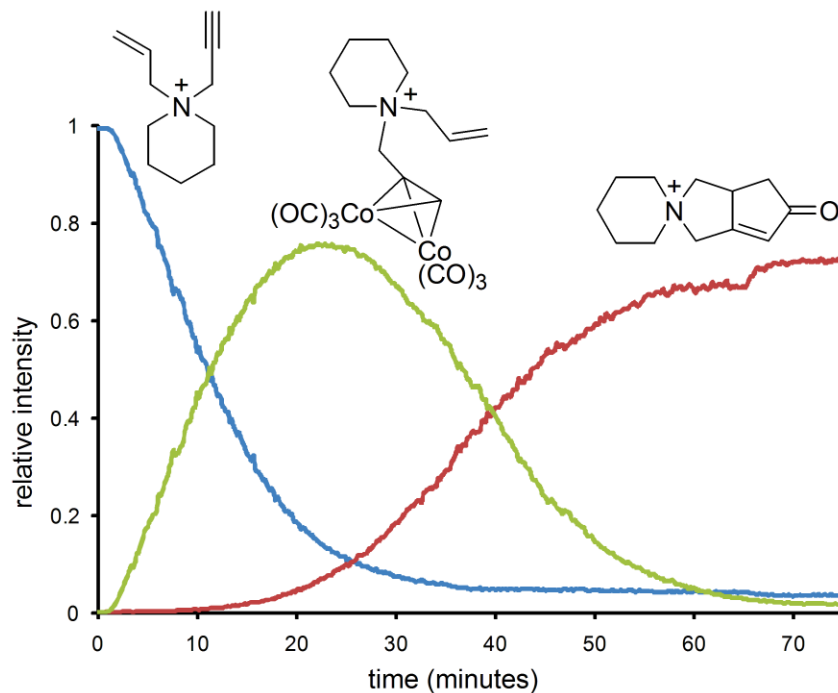


**Figure 56:** Abundance vs. time data for  $[\mathbf{4-3}]^+$  (starting material),  $[\text{Co}_2(\text{CO})_6(\mathbf{4-3})]^+$  (intermediate) and  $[\mathbf{4-3} + \text{CO}]^+$  (product). Data collected using positive ion PSI-ESI-MS in chlorobenzene, online dilution with acetone, Schlenk flask saturated and pressurized with CO. Data has been normalized to the total ion current. Scan time of 10 seconds per spectrum. Approximately 20% of the total ion current at the end of the reaction consisted of numerous low abundance by-products, none of which exceeded 5% of the total.

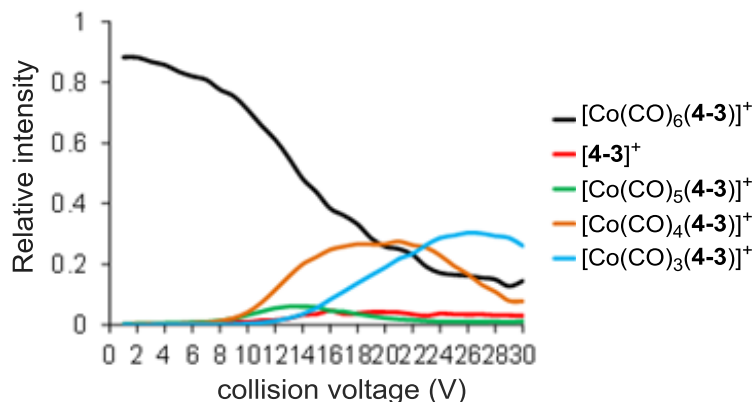


**Figure 57:** During the PSI-ESI-MS, the collision voltage was set to 2 V. The breakdown graph shows  $[\text{Co}_2(\text{CO})_6(\mathbf{4-3})]^+$  is a stable species at this voltage and it can only be fragmented when the collision voltage reaches 8 V.

The reaction was repeated at different temperatures, this time starting with the pre-prepared complex  $[\text{Co}_2(\text{CO})_6(\mathbf{4-3})][\text{Tf}_2\text{N}]$ , which was injected directly into a hot, CO-saturated solution. The reaction was conducted at 65.0, 70.0, and 75.0 °C. The temperature was well controlled within a  $\pm 0.2^\circ\text{C}$  range. Speciation was complicated due to the appearance of aggregates and solvent adducts, but these signals could be combined to obtain traces of reaction progress (Figure 58). The rate increases with temperature; the first 20% of the reaction is slow, but after that point each trace follows (pseudo) first-order kinetics. Plotting the natural log of the concentration of  $[\text{Co}_2(\text{CO})_8(\mathbf{4-3})]^+$  vs. time for each experiment produced a plot which was initially curved but that had a straight line region in the middle (covering conversions from 25% to at least 80% - reactions were stopped when the total ion current dropped too low to obtain good data), with  $k_{\text{obs}} = 0.050, 0.099, \text{ and } 0.245 \text{ s}^{-1}$  at 65, 70, and 75°C respectively.

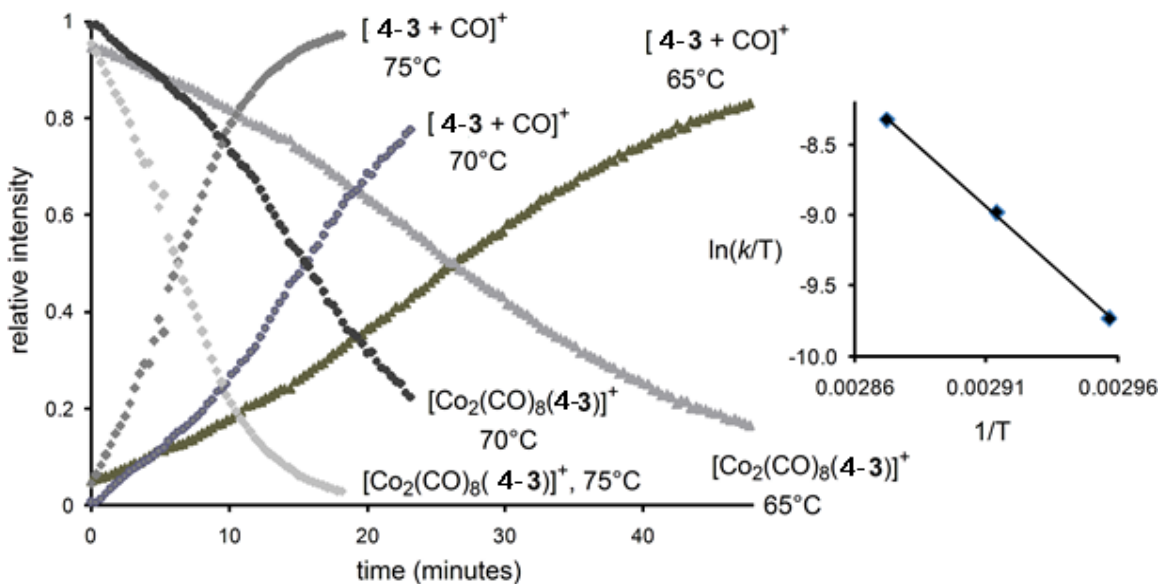


**Figure 58:** Intensity vs. time data for  $[\text{Co}_2(\text{CO})_6(\mathbf{4-3})]^+$  (starting material) and  $[\mathbf{4-3} + \text{CO}]^+$  (product), collected at three different temperatures. Inset: Eyring plot for the three different temperatures.

Enthalpy and entropy of activation were determined using an Eyring plot (Figure 58), which provided the activation parameters:  $\Delta H^\ddagger = 160 \pm 10 \text{ kJ mol}^{-1}$  and  $\Delta S^\ddagger = 130 \pm 30 \text{ J mol}^{-1} \text{ K}^{-1}$ . These relatively large values are consistent with the rate-determining step being ligand dissociation. They compare with values of  $\Delta H^\ddagger = 123.6 \pm 11.0 \text{ kJ mol}^{-1}$  and  $\Delta S^\ddagger = 72.4 \pm 37.3 \text{ J mol}^{-1} \text{ K}^{-1}$  for the rate of reaction of  $\text{Rh}_4(\text{CO})_{12}$  with an alkyne, another reaction thought to be limited by dissociation of a CO ligand.<sup>139</sup> A positive  $\Delta H^\ddagger$  indicates an endothermic reaction, and a positive  $\Delta S^\ddagger$  indicates entropy increases. Both of these are consistent with a rate-determining step of ligand dissociation.



It is also possible that the species we see as  $[\text{Co}_2(\text{CO})_6(\mathbf{4-3})]^+$  actually corresponds to intermediate **D** in the cycle (see Scheme 2) because in the intramolecular Pauson-Khand reaction this species has the same mass as the starting material, intermediate **B**. This may account for the initial slower rate of reaction (as it takes time for the process **B**  $\rightarrow$  **C**  $\rightarrow$  **D**). However, buildup of **D** would suggest that the next step, insertion of a CO ligand into a Co-C bond, is slow, and that this step is unlikely to have a large positive entropy of activation.

## 4.6 Conclusion

The investigations support the prediction that the rate-determining step of the intramolecular Pauson-Khand reaction is CO dissociation. Gas-phase studies by Matt Henderson on the early steps in the reaction scheme showed that CO dissociation and alkene coordination can both be readily achieved, and that the coordination of an alkene is influenced by the nature of the alkene. This suggests that the effect of the nature of the alkene operates on some later step in the reaction. Turning to the solution phase, the intramolecular reaction could be monitored using PSI-ESI-MS, and no intermediates apart from the dicobalt hexacarbonyl ion were observed, suggesting that the later steps in the reaction are relatively fast. Positive values of  $\Delta H^\ddagger$  and  $\Delta S^\ddagger$  suggest that the rate-determining step is ligand dissociation, consistent with early loss of CO that allows the alkene to coordinate and the rest of the reaction to proceed.

## 4.7 Experimental

All solvents were dispensed from an MBraun solvent purification system and used within minutes. Inert atmosphere techniques were used for all syntheses involving  $\text{Co}_2(\text{CO})_8$ . Methyl pyrrolidine, pyrrolidine, piperidine, allyl bromide, propargyl bromide, sodium hexafluorophosphate, sodium tetraphenylborate, sodium hydride, sodium chloride, sodium hydroxide, and dicobalt octacarbonyl were purchased from Aldrich and used without subsequent purification. NMR spectra were obtained on a Bruker AC 300 spectrometer (1H and 13C).

All mass spectra were collected by using a Micromass Q-TOF *micro* mass spectrometer in positive ion mode using pneumatically assisted electrospray ionization: capillary voltage, 2900 V; extraction voltage, 0.5 V; source temperature, 80 °C; desolvation temperature, 150 °C; cone gas flow, 100 L/h; desolvation gas flow, 100 L/h; collision voltage, 2 V (for MS experiments); collision voltage, 2–40 V (for MS/MS experiments); low and high mass resolution, 10.0; MCP voltage, 2700 V. Gas-phase ion–molecule reactions were carried out by a published method.<sup>140</sup>

**4-1** Br. Methyl pyrrolidine (3.8 g, 45.1 mmol) and diethyl ether (30.0 mL) were cooled to 0°C in a 100.0 mL round bottom flask. Propargyl bromide (5.0 mL of an 80% solution in toluene, 6.9 g, 57.5 mmol) in ether (25.0 mL) was added dropwise. The mixture was subsequently allowed to warm to room temperature and stirred overnight. The solvent was then evaporated and the white product dried under vacuum for 24 hours. (9.0 g, 44.0 mmol, 97%) M.P.: 62-68°C. <sup>1</sup>H NMR

(CD<sub>3</sub>OD):  $\delta$  (ppm) 4.50 (d, 2H, 3.63Hz); 3.75 (m, 4H); 3.52 (m, 1H); 3.29 (s, 3H); 2.31 (m, 4H).  
<sup>13</sup>C NMR (CD<sub>3</sub>OD):  $\delta$  (ppm) 81.96; 73.33 (f); 65.25; 54.50; 50.44; 23.20.

**4-1** PF<sub>6</sub>. An aqueous solution (20.0 mL H<sub>2</sub>O) of **1.Br** (1.4 g, 7.0 mmol) and sodium hexafluorophosphate (1.2 g, 7.1 mmol) was prepared. The mixture was heated to facilitate dissolution, and cooled to room temperature. The white crystals were filtered with a cold water wash and dried overnight under vacuum. (0.6 g, 2.3 mmol, 33%) M.P.: 146-147°C. <sup>1</sup>H NMR (CD<sub>3</sub>OD):  $\delta$  (ppm) 4.33 (d, 2H, 3.63 Hz); 3.67 (m, 4H); 3.45 (m, 1H); 3.22 (s, 3H); 2.28 (m, 4H). <sup>13</sup>C NMR (CD<sub>3</sub>OD):  $\delta$  (ppm) 81.78; 73.05; 65.15; 54.27; 50.24; 23.08. <sup>31</sup>P NMR (CD<sub>3</sub>OD):  $\delta$  (ppm) -143.22 (septet for PF<sub>6</sub><sup>-</sup>).

**Allyl pyrrolidine.**<sup>141</sup> Allyl bromide (6.0 mL, 8.4 g, 69.4 mmol) in diethyl ether (20.0 mL) was added dropwise to pyrrolidine (5.1 g, 71.7 mmol) in ether (20.0 mL) at 0°C over 30 minutes. The solution was then allowed to warm to room temperature and stir overnight before performing a potassium hydroxide extraction (3 × 25.0 mL of a 3.0M solution). The subsequent aqueous phase was then extracted with dichloromethane and all organic portions were combined, dried with anhydrous magnesium sulfate, and filtered. The solvent was removed on the rotary evaporator, and the orange liquid was distilled (fraction that boiled at 120 °C was retained) to give a colorless product. (3.5 g, 31.5 mmol, 45.0 %) <sup>1</sup>H NMR (CDCl<sub>3</sub>):  $\delta$  (ppm) 5.88 (m, 1H); 5.21 (m, 2H); 3.02 (d of t, 2H, 6.66Hz, 1.26Hz); 2.43 (m, 4H); 1.71 (m, 4H) <sup>13</sup>C NMR (CDCl<sub>3</sub>):  $\delta$  (ppm) 136.23, 116.53, 59.22, 53.96, 23.40.

**4-2** Br. Allyl pyrrolidine (0.67 g, 6.0 mmol) and propargyl bromide (0.80mL, 1.1 g, 7.2 mmol) were stirred in ether (30.0 mL) overnight. The white product was filtered and collected (0.45 g, 1.7 mmol, 31.0%). M.P.: 140-146°C. <sup>1</sup>H NMR (CD<sub>3</sub>OD):  $\delta$  (ppm) 6.11 (m, 1H); 5.76 (m, 2H); 4.30 (s, 2H); 4.16 (d, 2H, 7.29Hz); 3.68 (m, 4H); 3.49 (t, 1H); 2.28 (m, 4H). <sup>13</sup>C NMR (CD<sub>3</sub>OD):  $\delta$  (ppm) 129.40; 126.55; 82.03; 73.04; 64.55; 63.10; 51.25; 23.22.

**4-2** PF<sub>6</sub>. An aqueous solution of **2.Br** (0.27 g, 1.2 mmol, 20.0 mL H<sub>2</sub>O) was added to an aqueous solution of sodium hexafluorophosphate (0.21 g, 1.2 mmol, 10.0 mL H<sub>2</sub>O). The mixture was



reduced to a volume of 10.0 mL and left overnight in the fridge at 5 °C. The white crystals were filtered with a water wash and the filtrate was then reduced again to a smaller volume and transferred back into the fridge for further crystallization. The combined yield of both aliquots was 0.09 g, 0.31 mmol, 27%. M.P.: 78-80 °C. <sup>1</sup>H NMR (CD<sub>3</sub>OD): δ (ppm) 5.96 (m, 1H); 5.70 (m, 2H); 4.15 (s, 2H); 4.01 (d, 2H, 7.26Hz); 3.55 (m, 4H); 3.36 (t, 1H); 2.16 (m, 4H). <sup>13</sup>C NMR (CD<sub>3</sub>OD): δ (ppm) 129.37; 126.43; 81.96; 72.95; 64.53; 63.03; 51.10; 23.13. <sup>31</sup>P NMR (CD<sub>3</sub>OD): δ (ppm) -143.2 (septet).

**Allyl piperidine.** Allyl bromide (15.6 g, 128.9 mmol), piperidine (10.5 g, 123.3 mmol), and sodium hydride (3.3g, 145.9 mmol) were combined as described in the literature to yield allyl piperidine (11.9 g, 95.0 mmol, 77.0 %) after a partial dynamic vacuum distillation. <sup>1</sup>H NMR (CDCl<sub>3</sub>): δ (ppm) 5.82 (m, 1H); 5.05 (m, 2H); 2.89 (d of t, 2H, 6.75Hz, 1.2Hz); 2.30 (s, 4H); 1.52 (m, 4H); 1.37 (m, 2H). <sup>13</sup>C NMR (CDCl<sub>3</sub>): δ (ppm) 135.5, 117.33, 62.56, 54.37, 25.86, 24.26.

**4-3 Br.** Propargyl bromide (2.4 g of 80.0% solution in toluene, 16.2 mmol) in toluene (20.0 mL) was added to allyl piperidine (1.9 g, 15.5 mmol) in toluene (20.0 mL). The mixture was stirred at room temperature for 48 hours, and the resulting white product was vacuum filtered, and dried by vacuum overnight. (2.5 g, 10.1 mmol, 67.0%) M.P.: 154-156°C <sup>1</sup>H NMR (CD<sub>3</sub>CN): δ (ppm) 5.99-5.70 (m, 3H); 4.43 (s, 2H); 4.15 (d, 2H, 7.32Hz); 3.53 (m, 4H); 3.27 (q, 1H, 1.70Hz); 1.91 (m, 4H); 1.69 (m, 2H). <sup>13</sup>C NMR (CD<sub>3</sub>CN): δ (ppm) 129.88; 125.01; 82.68; 71.77; 62.33; 59.23; 50.38; 21.39; 20.31.

**4-3 PF<sub>6</sub>.** To 30.0 mL of water was added **3.Br** (0.45 g, 1.9 mmol) and sodium hexafluorophosphate (0.37 g, 2.2 mmol). The mixture was stirred for fifteen minutes and the white product was filtered (0.22 g). The filtrate was boiled to reduce the volume down to 15.0 mL and transferred to the freezer (-10 °C) for four hours. These crystals were then filtered (0.17 g) to give a combined yield of 0.39 g, 1.3 mmol, 68%. M.P.: 85-86°C. <sup>1</sup>H NMR (CD<sub>2</sub>Cl<sub>2</sub>): δ (ppm) 5.76 (m, 3H); 3.99 (s, 2H); 3.95 (d, 2H, 7.32Hz); 3.36 (m, 4H); 2.85 (t, 1H); 1.86 (m, 4H);

1.70 (q, 2H).  $^{13}\text{C}$  NMR ( $\text{CD}_2\text{Cl}_2$ ):  $\delta$  (ppm) 131.46; 122.74; 82.22; 70.17; 62.73; 59.22; 49.45; 20.90; 20.15.  $^{31}\text{P}$  NMR ( $\text{CD}_2\text{Cl}_2$ ):  $\delta$  (ppm) -143.82 (septet).

**Propargyl piperidine.** Piperidine (7.5 mL, 6.5 g, 75.9 mmol) in tetrahydrofuran (50.0 mL) was added to a slurry of sodium hydride (2.1 g, 85.5 mmol) in tetrahydrofuran (75.0 mL) over 1 hour. The mixture was allowed to stir at room temperature for another hour. A mixture of propargyl bromide (9.9 g of an 80.0% toluene solution, 66.2 mmol) in tetrahydrofuran was then added dropwise over an hour and the mixture was left to stir overnight. The mixture was quenched with a sodium chloride solution ( $1.0 \text{ mol L}^{-1}$ ) and the organic phase separated. The aqueous phase was then extracted with ethyl acetate ( $3 \times 50.0 \text{ mL}$ ) followed by tetrahydrofuran ( $2 \times 50.0 \text{ mL}$ ) and combined with the original organic fraction. After drying with anhydrous magnesium sulfate, and filtering with a THF wash, the solvent was removed on a rotary evaporator and the orange product distilled to give a light yellow liquid (5.4 g, 43.9 mmol, 66.0%).  $^1\text{H}$  NMR ( $\text{CDCl}_3$ )  $\delta$  (ppm): 4.24 (m, 1H); 3.16 (d, 2H, 2.28Hz); 2.39 (m, 4H); 1.51 (m, 4H); 1.34 (m, 2H).  $^{13}\text{C}$  ( $\text{CDCl}_3$ )  $\delta$  (ppm): 72.80, 68.36, 52.98, 47.43, 25.73, 23.74.

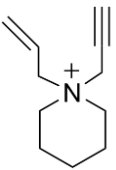
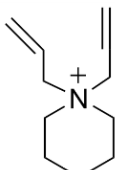
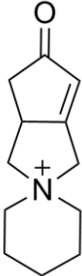
**4-4 Br.** Propargyl piperidine (1.0 g, 8.1 mmol) was added to propargyl bromide (1.4 g of an 80.0% toluene solution, 9.2 mmol) along with toluene (30.0 mL) and allowed to stir at room temperature for 24 hours. The solution was then refluxed for 1 hour, and the brown product was vacuum filtered with a toluene wash and dried under vacuum overnight. (0.84 g, 3.5 mmol, 43.0 %) M.P.: 200 °C (dec.).  $^1\text{H}$  NMR ( $\text{CD}_3\text{OD}$ ):  $\delta$  (ppm) 4.50 (d, 4H, 2.37Hz); 3.62 (t, 4H, 5.67Hz); 3.55 (t, 2H, 2.49Hz); 1.95(m, 4H); 1.72(m, 2H).  $^{13}\text{C}$  ( $\text{CD}_3\text{CN}$ ):  $\delta$  (ppm) 83.00; 71.09; 59.45; 51.01; 21.19; 20.29.

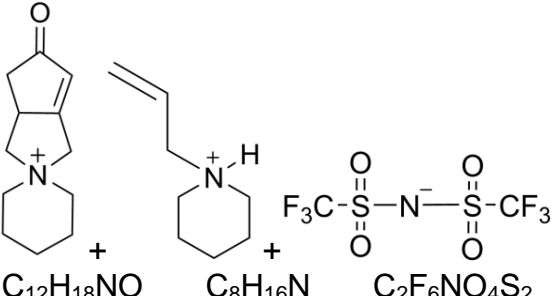
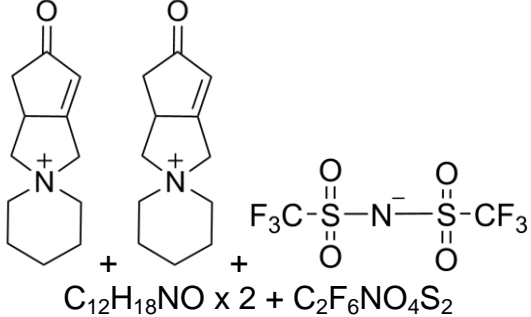
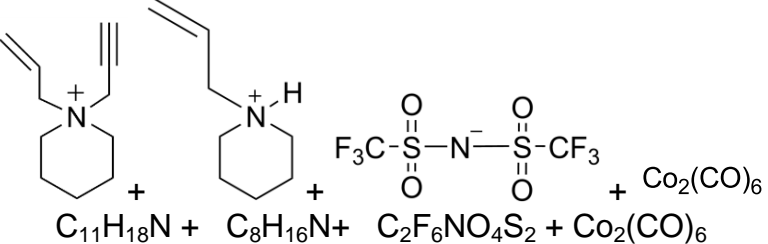
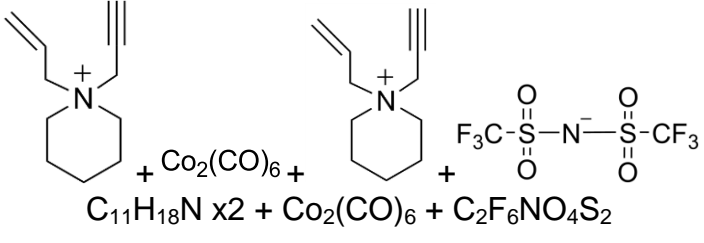
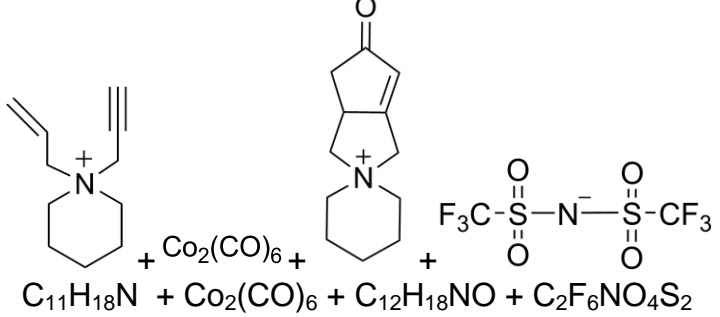
**4-4 PF<sub>6</sub>.** As for **1.PF<sub>6</sub>** with the following amounts of reagents and solvents: **4.Br** (0.17 g, 0.69 mmol), sodium hexafluorophosphate (0.18 g, 1.1 mmol), water (30.0 mL), isolated product (0.080 g, 0.26 mmol, 38.0 %). M.P.: 160-161.  $^1\text{H}$  NMR ( $\text{CD}_3\text{OD}$ ):  $\delta$  (ppm) 4.46 (s, 4H); 3.62 (t, 4H, 5.73Hz); 3.53 (t, 2H, 3.27Hz); 1.97 (m, 4H); 1.74 (m, 2H).  $^{13}\text{C}$  NMR ( $\text{CD}_3\text{OD}$ ):  $\delta$  (ppm) 83.39; 71.33; 59.90; 51.05; 21.81; 20.68.  $^{31}\text{P}$  ( $\text{CD}_3\text{OD}$ ):  $\delta$  (ppm) -143.24 (septet).

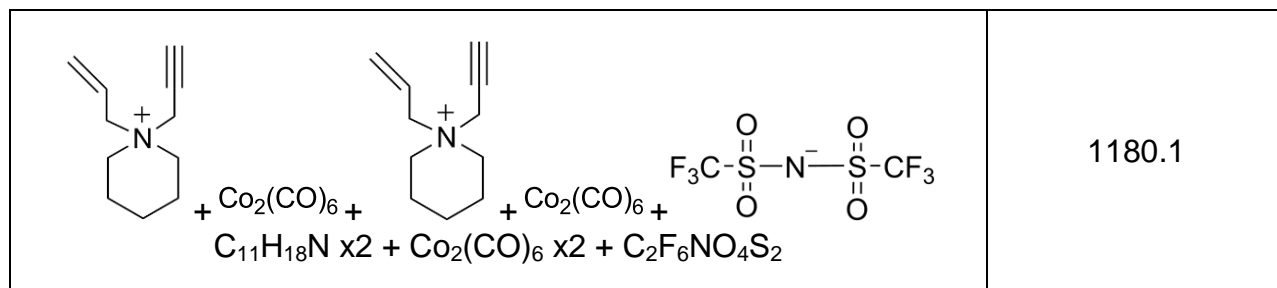
$[\text{Co}_2(\text{CO})_6(\mathbf{4-3})][\text{PF}_6]$ . Dicobalt octacarbonyl (0.15 g, 0.44 mmol) and **3b** (0.087 g, 0.28 mmol) were added to a Schlenk flask as solids against a dry nitrogen atmosphere. Dry dichloromethane

(10.0 mL) was then added and the mixture was allowed to react for two hours. The solvent was then evaporated, and the red solid was washed with ether (3 x 8.0 mL) and then dried under vacuum for 2 hours. The dark red product (0.13 g, 0.22 mmol, 78.0%) was collected and X-ray quality crystals were grown by dichloromethane and ether solvent diffusion in the freezer, with a small layer of 1-butanol between them. M.P. 90 °C (dec.).  $^1\text{H}$  NMR ( $\text{CD}_2\text{Cl}_2$ ):  $\delta$  (ppm) 6.38 (s, 1H); 5.74 (m, 3H); 4.70 (s, 2H); 4.00 (d, 2H); 3.42 (m, 4H); 1.88 (m, 4H); 1.72 (m, 2H).  $^{13}\text{C}$  NMR ( $\text{CD}_2\text{Cl}_2$ ):  $\delta$  (ppm) 130.91, 122.91, 75.25, 74.03, 62.69, 62.10, 58.86, 20.96, 20.32.  $^{31}\text{P}$  NMR ( $\text{CD}_2\text{Cl}_2$ )  $\delta$  (ppm) -143.79 (septet). IR ( $\text{cm}^{-1}$ ,  $\text{CH}_2\text{Cl}_2$ ): 2105 (st), 2066 (vs), 2045 (vs). UV-Vis: 356 nm, 364 nm, 421 nm.

**Table 3:** Aggregates and species in the reaction solution:

| Species   | Mass  |
|---|-------|
| $\text{C}_8\text{H}_{16}\text{N}^+$               | 125.5 |
| $3^+ \text{C}_{11}\text{H}_{18}\text{N}^+$       | 164.2 |
| Product $\text{C}_{12}\text{H}_{18}\text{NO}^+$  | 192.1 |

|  |       |
|--|-------|
|  <p> <math>C_{12}H_{18}NO + C_8H_{16}N + C_2F_6NO_4S_2</math> </p>                    | 598.2 |
|  <p> <math>C_{12}H_{18}NO \times 2 + C_2F_6NO_4S_2</math> </p>                        | 664.2 |
|  <p> <math>C_{11}H_{18}N + C_8H_{16}N + C_2F_6NO_4S_2 + Co_2(CO)_6</math> </p>      | 856.0 |
|  <p> <math>C_{11}H_{18}N \times 2 + Co_2(CO)_6 + C_2F_6NO_4S_2</math> </p>         | 894.1 |
|  <p> <math>C_{11}H_{18}N + Co_2(CO)_6 + C_{12}H_{18}NO + C_2F_6NO_4S_2</math> </p> | 922.1 |



## 5. Detailed kinetic analysis of rhodium-catalyzed alkyne hydrogenation

Portions of this chapter have been previously published, and are reproduced in part with permission from “A detailed kinetic analysis of rhodium-catalyzed alkyne hydrogenation” J. Luo, A. G. Oliver and J. Scott McIndoe, *Dalton Transactions*, 2013, 42, 11312-11318. Copyright © The Royal Society of Chemistry 2013

I performed all experimental work, produced all figures and co-wrote the paper with JS McIndoe. AG Oliver performed the crystal structure determinations. The wilkinson’s hydrogenation part was published, the Weller’s hydrogenation part is in preparation.

Hydrogenation of alkynes and alkenes mediated by rhodium complexes is a classic catalytic organometallic reaction.<sup>142</sup> The mechanism of these reactions has been studied extensively by different methods. In this chapter, a variety of hydrogenation reactions were performed and analyzed using PSI-ESI-MS.

### 5.1 Hydrogenation of olefins by Rh (PPh<sub>3</sub>)<sub>3</sub>Cl

#### 5.1.1 Introduction

Homogeneous hydrogenation of olefins was first introduced by Wilkinson.<sup>143</sup> Since the reports of the now well-known catalyst Rh(PPh<sub>3</sub>)<sub>3</sub>Cl in 1965,<sup>143-145</sup> Wilkinson and others have studied its catalytic capabilities in the hydrogenation of unsaturated substrates. Since then, this catalyst has been widely used due to its high efficiency and high sensitivity as well its ability to function under virtually unrestricted conditions. It has become one of the most famous catalysts in the world, and is known as “Wilkinson’s catalyst”.

The mechanism of the reaction has been studied by a wide range of different methods and it has become the most well-understood organometallic catalytic reaction. Every step of the catalytic cycle has been reported. Halpern *et al.* reported a detailed kinetic study and investigated the

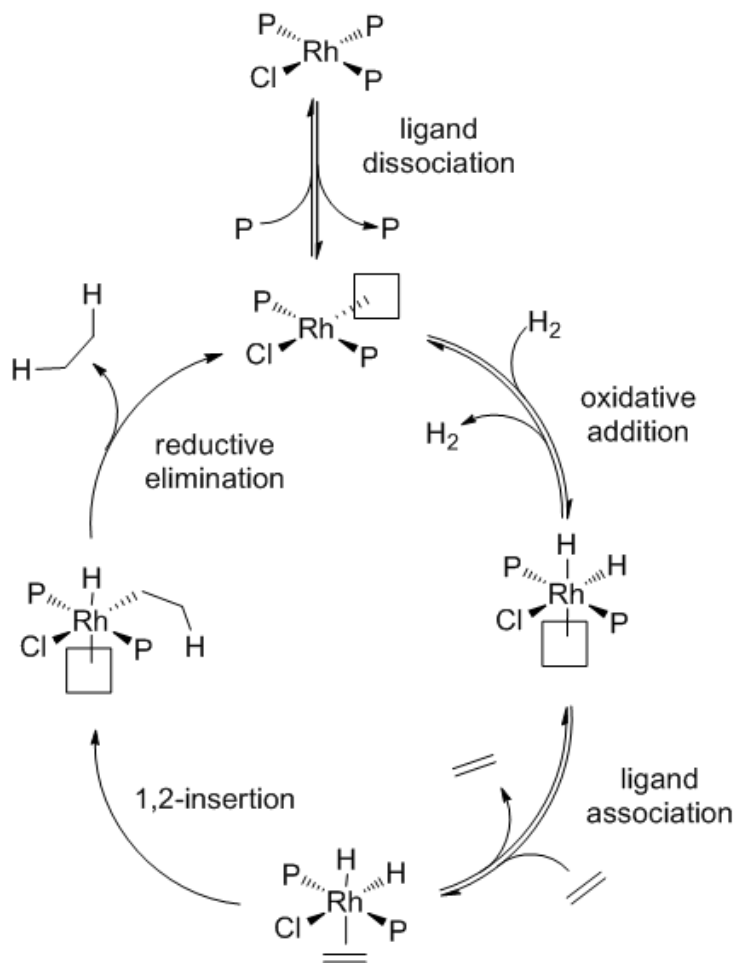
mechanism of oxidative addition of  $\text{Rh}(\text{PPh}_3)_3\text{Cl}$  with  $\text{H}_2$  and cyclohexene. NMR and UV/Vis spectroscopy were used for acquiring experimental data, and a number of rate constants were obtained. The authors also indicated the rate determining step involved Rh-H bond breakage by measuring kinetic isotope effect through replacing  $\text{RhH}_2(\text{PPh}_3)_3\text{Cl}$  with  $\text{RhD}_2(\text{PPh}_3)_3\text{Cl}$ .<sup>146</sup> In a recent study, Cabrera and co-workers used experimental data to build kinetic models of this hydrogenation by using avermectins  $\text{B}_{1a}$  and  $\text{B}_{1b}$  as substrates and  $\text{Rh}(\text{PPh}_3)_3\text{Cl}$  as catalyst. The kinetic model includes a proposed catalytic cycle and all the rate constants of all the steps of the reaction.<sup>147</sup>

In another study, the electronic and steric effects on nucleophilic addition to the alkene double bond were investigated to help reveal the reasons behind the selectivity towards different types of  $\pi$  bonds during the hydrogenation reaction.<sup>148</sup>

Bowker *et al.* used temperature programmed desorption to compare homogeneous Wilkinson's hydrogenation with heterogeneous hydrogenation on compound Rh(III). They concluded that the homogeneous and heterogeneous hydrogenation mechanisms have certain similarities.<sup>149</sup>

Koga *et al.* reported the first energy profile study of the whole catalytic cycle of Wilkinson's hydrogenation in 1986.<sup>150</sup> Wink and Ford performed a flash photolysis investigation on the key intermediate  $\text{Rh}(\text{PPh}_3)_2\text{Cl}$  and its reaction with CO,  $\text{C}_2\text{H}_4$ ,  $\text{PPh}_3$  and  $\text{H}_2$ ; various important equilibrium constants were acquired.<sup>151, 152</sup> Para-hydrogen induced polarisation NMR techniques provided important information on probing previously unobserved intermediates, especially dihydride species in the dynamic reaction system.<sup>153-155</sup>

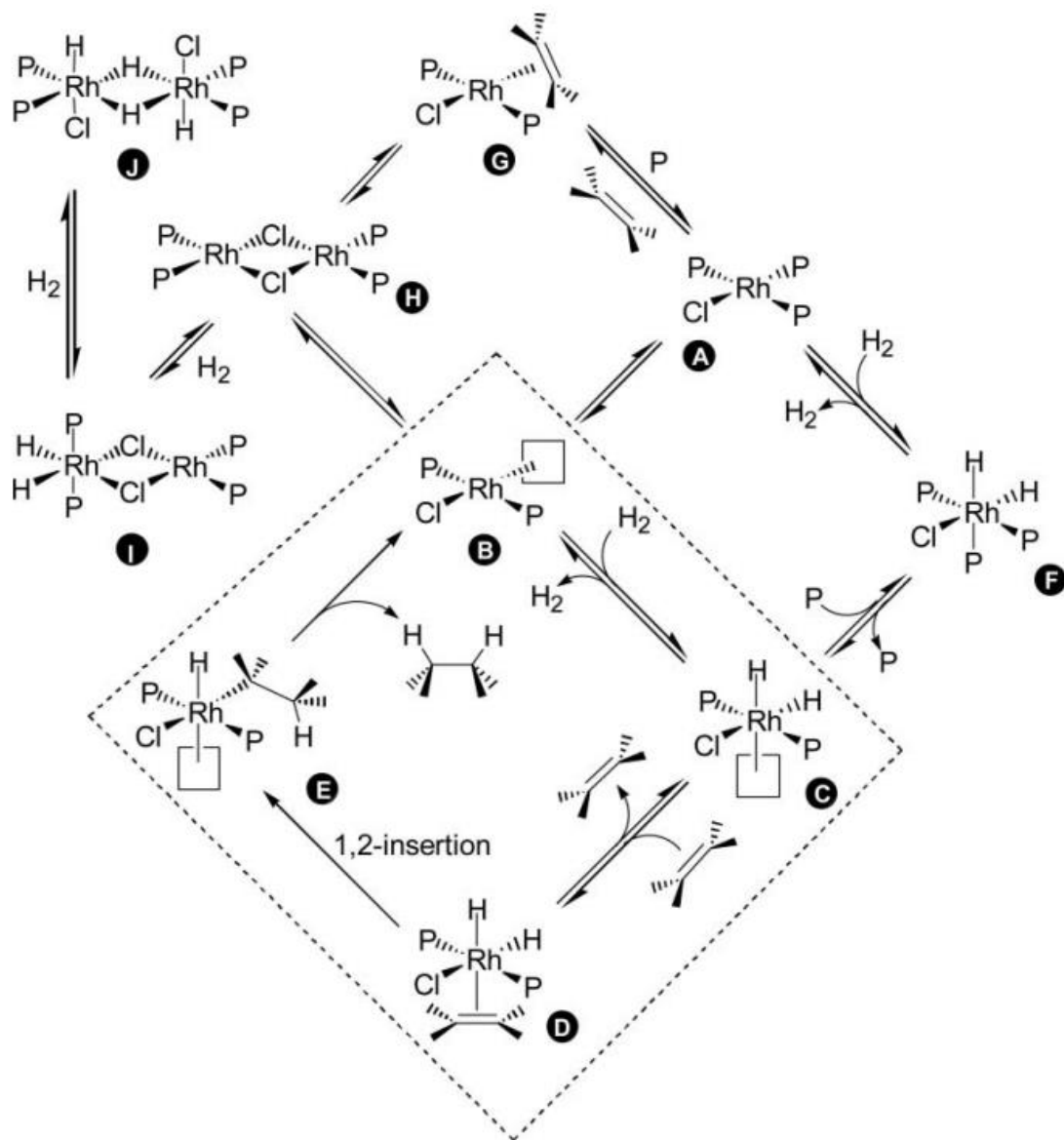
All the techniques that were mentioned above, when combined together gave us a clear picture of the Wilkinson's hydrogenation catalytic cycle. The generally accepted main cycle is shown in Scheme 6.<sup>156</sup> The  $\text{PPh}_3$  ligand dissociation to generate intermediate  $\text{Rh}(\text{PPh}_3)_2\text{Cl}$  is the first step of catalysis. The intermediate with a vacant site is more reactive, it is ready to undergo oxidative addition with  $\text{H}_2$  followed by ligand association of the olefin. After 1,2 insertion of the olefin, there is a reductive elimination to finish the catalytic cycle. The product alkane is released to the medium and the catalyst is converted back into the  $\text{Rh}(\text{PPh}_3)_2\text{Cl}$  species.



**Scheme 6:** Mechanism of alkene hydrogenation using Wilkinson's catalyst, adapted from Halpern.<sup>156</sup>

However, if off-cycle and dimerization processes are considered, it will be shown as a more complicated pathway (Scheme 7).<sup>135</sup>



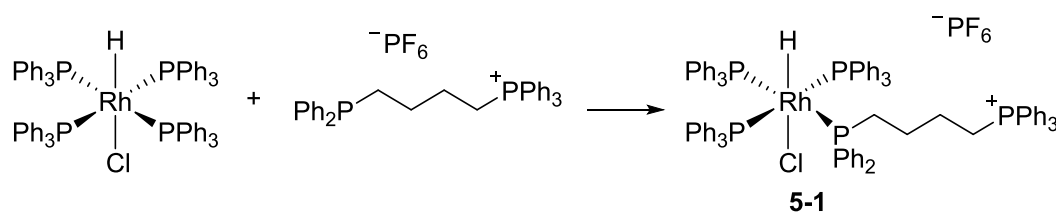


**Scheme 7** Mechanism of alkene hydrogenation using Wilkinson's catalyst with dimerization and off-cycle processes. Reprinted with permission from "Mono-alkylated bisphosphines as dopants for ESI-MS analysis of catalytic reactions" D. M. Chisholm, A. G. Oliver and J. S. McIndoe, *Dalton Transactions*, 2010, 39, 364-373. Copyright © 2010 Royal Society of Chemistry

### 5.1.2 Previous investigation with ESI-MS

Even though the hydrogenation of olefins by Wilkinson's catalyst has been around for 50 years, we still want to take advantage of our unique methodology to investigate the reaction to get more detailed kinetic data. Similar to the Pauson-Khand reaction, Wilkinson's catalyst is invisible in ESI-MS. So a method is needed to ionize it. In a previous project by our former group member

Dr. Danielle Chisholm, sub-stoichiometric quantities of a charged phosphine ligand  $[\text{Ph}_2\text{P}(\text{CH}_2)_4\text{PPh}_2\text{Bn}]^+ [\text{PF}_6]^-$  were added into the reaction.<sup>157</sup> The introduction of this charged phosphine ligand substituted one of the  $\text{PPh}_3$  ligands to generate a charged version of Wilkinson's catalyst (Equation 3). Hydrogenation was performed in chlorobenzene, and various rhodium complexes were observed consistent with the known speciation of this reaction mixture (Figure 59).<sup>135</sup>



Equation 3

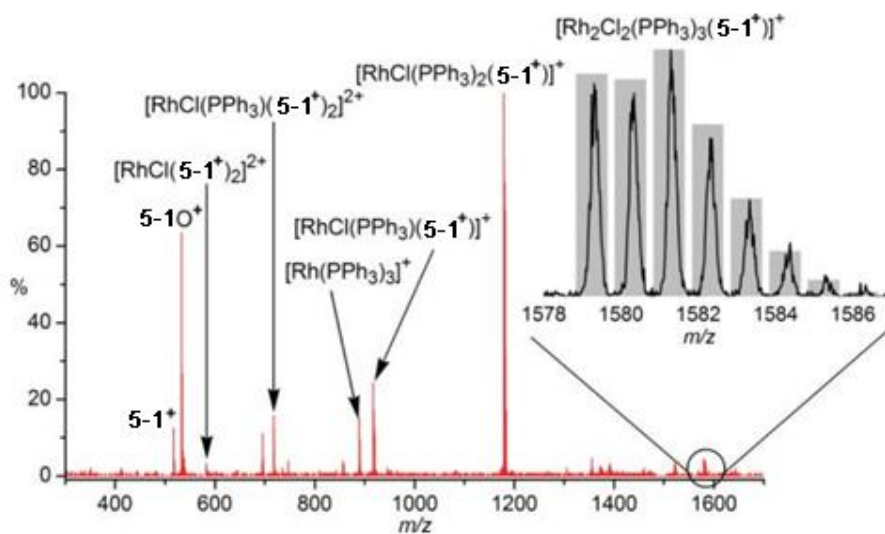


**Figure 59:** Positive ions of ionized Wilkinson's catalyst, where **5-1<sup>+</sup>** is  $[\text{Ph}_2\text{P}(\text{CH}_2)_4\text{PPh}_2\text{Bn}]^+$ . Reprinted with permission from "Mono-alkylated bisphosphines as dopants for ESI-MS analysis of catalytic reactions" D. M. Chisholm, A. G. Oliver and J. S. McIndoe, *Dalton Transactions*, 2010, 39, 364-373.

Copyright © 2010 Royal Society of Chemistry

However, because ESI-MS operates only on ions, only catalyst-containing species are observed, so the overall progress of the reaction was not tracked and therefore the concentration of intermediates cannot be matched to activity. It is unable to decide if the observed species are truly reactive intermediates, resting states or decomposition products. Although the system can

be combined with other techniques to get correlated data, the methodology should be modified to make it an independent standalone analysis technique to measure intermediates and track reaction progress. Based on the Pauson-Khand reaction, we have found that if the substrate is charged, we can achieve this goal. So here we have used a charge-tagged alkyne to enable us to track the progress of the reaction as well as detect any appreciable quantities of intermediates that include the charged tag.

### 5.1.3 Results and Discussion

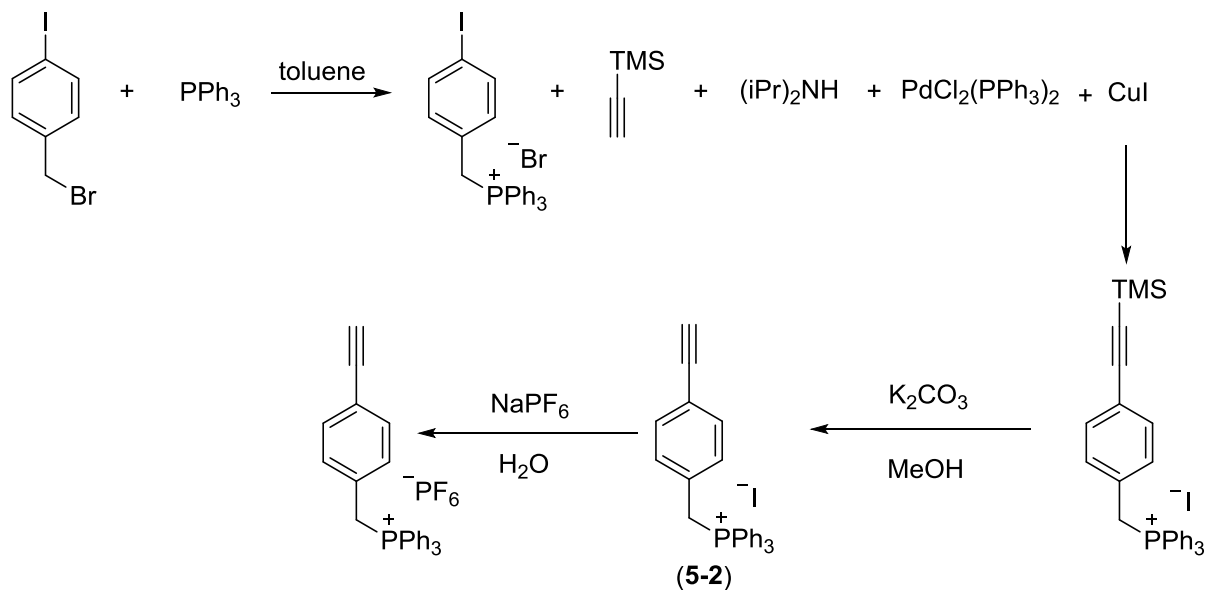
#### 5.1.3.1 Design of charged substrate

There are many strategies to integrate a charged tag with an alkyne. For an ideal charged alkyne that has conveyed amenability for ESI-MS analysis, it must meet the following requirements: 1) the charged tag itself should not be involved in the reaction or influence reactivity of the catalyst or the alkyne or any other functional groups; 2) it should be easy to prepare, ideally, the synthesis route should be under four steps, the less the better. Even though the reaction only takes a very small quantity of the substrate, it has to be simple. It should represent a widely used olefin substrate in other Wilkinson's hydrogenation research; 3) it should be easy to purify, and the purity has to be high after purification, so the final product should be a single peak in ESI-MS spectrum; 4) It should be high in mass (higher than  $m/z$  200) and have high surface activity, so it will dominate spectral intensity and providing very similar response factors for all ions involving that tag; 5) It should have a relatively non-coordinating anion, to maximally reduce the extent of ion pairing, improving sensitivity and minimizing the appearance of complicating aggregate ions.

Initially, a triphenylphosphonium salt in which the alkyne was remote from the charge,  $[\text{Ph}_3\text{P}(\text{CH}_2)(\text{C}_6\text{H}_4)\text{C}_2\text{H}]^+[\text{PF}_6]^-$  (**5-2**), was tried (Scheme 8). The synthesis is straightforward, in order to get pure product, we chose to convert the starting material into charged salt in the first step. The second step is a Sonogashira coupling reaction with CuI as co-catalyst. In the third step,  $\text{K}_2\text{CO}_3$  was used to remove TMS, however, the reaction time must be controlled accurately, in our case, the reaction took 70 minutes. Over 70 minutes, the dimerized byproduct will form and we found if this happens, the following purification step is very hard. The reaction was

tracked with ESI-MS to prevent the product dimerization. The final step was to convert it to the  $\text{PF}_6^-$  version.

This salt proved impervious to reaction other than at the alkyne and crystalline (see supporting information for crystal structure of the bromide salt of this cation), but proved to be too insoluble in the solvents of interest, even with a variety of different alkynes. While ESI-MS is sensitive enough to detect these salts in solution, the low solubility led to real problems in accurately establishing catalyst loadings because of the low concentrations required and the difficulty inherent in avoiding decomposition of the catalyst.



**Scheme 8:** Synthesis route of (5-2)

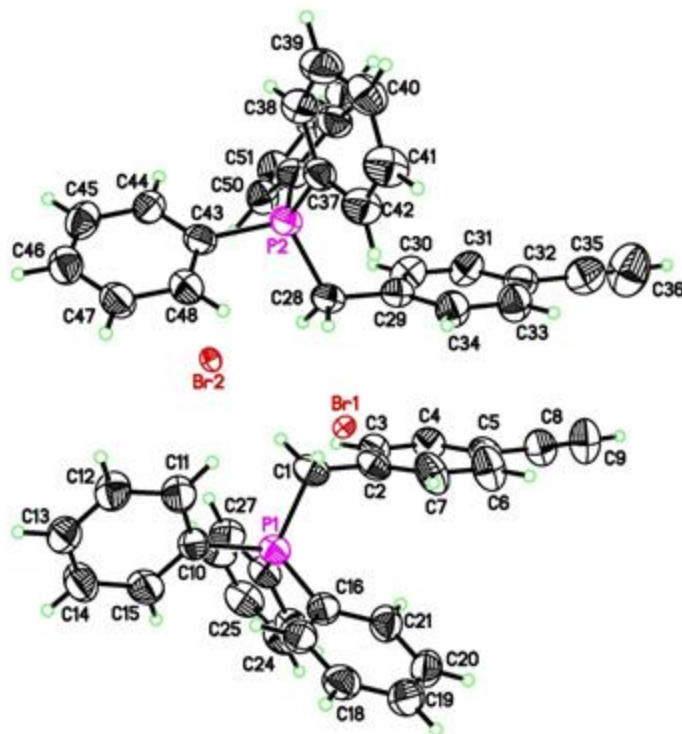
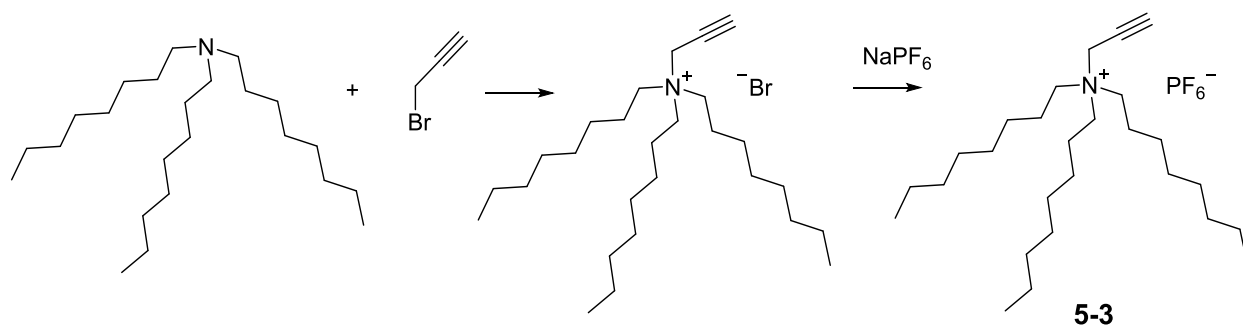


**Figure 60:** X-ray crystal structure of  $[\text{Ph}_3\text{P}(\text{CH}_2)_4\text{C}_2\text{H}]^+ \text{Br}^-$ . Key structural parameters: C5-C6 1.118 Å; C4-C5-C6 177.51°.

The second charged alkyne synthesized was the alkyne-functionalized trioctylamine salt,  $[\text{N}(\text{C}_8\text{H}_{17})_3(\text{CH}_2\text{C}_2\text{H})]^+ [\text{PF}_6]^-$  (**5-3**). The two-step synthesis is shown in Scheme 9.

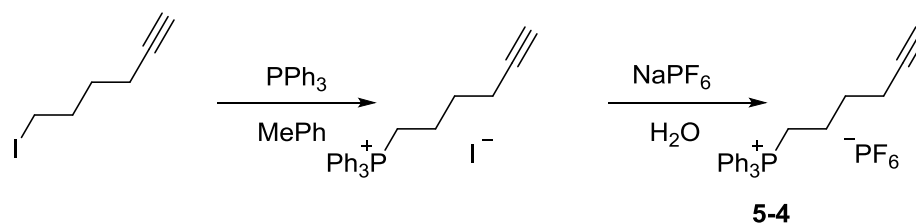


**Scheme 9:** Synthesis route of (**5-3**)

(**5-3**) has great solubility, however, further tests revealed that this substrate failed to meet the required criteria as the ammonium tag was readily cleaved to form  $[\text{N}(\text{C}_8\text{H}_{17})_3\text{H}]^+$  at a rate that was competitive with hydrogenation of the alkyne, and generated numerous Rh-containing

catalyst decomposition products. **5-3** also produced significant amounts of aggregates of the form [(cation)<sub>n</sub> + (anion)<sub>n-1</sub>]<sup>+</sup>,<sup>158</sup> making the analysis complicated.

Another charged alkyne  $[\text{Ph}_3\text{P}(\text{CH}_2)_4\text{C}_2\text{H}]^+[\text{PF}_6]^-$  (**5-4**) was readily prepared from 6-bromo-hexyne and triphenylphosphine, followed by salt metathesis with  $\text{Na}[\text{PF}_6]$ .



**Scheme 10:** Synthesis route of (**5-4**)

**5-4** had no problems related to solubility, reactivity or aggregation as the  $[\text{PF}_6]^-$  salt, and all experiments described used this phosphonium-tagged terminal alkyne as the substrate.

Crystals of  $[\text{Ph}_3\text{P}(\text{CH}_2)_4\text{C}_2\text{H}]^+\text{I}^-$  (the alkyne starting material, before metathesis of the iodide salt for  $[\text{PF}_6]^-$  to make **5-4**) were obtained and used to acquire an X-ray crystal structure (Figure 61). Structural parameters are entirely ordinary, in keeping with the idea that there is nothing exceptional about the alkyne functional group - it is remote enough from the charged tag that its chemistry is unaffected by the distant modification.

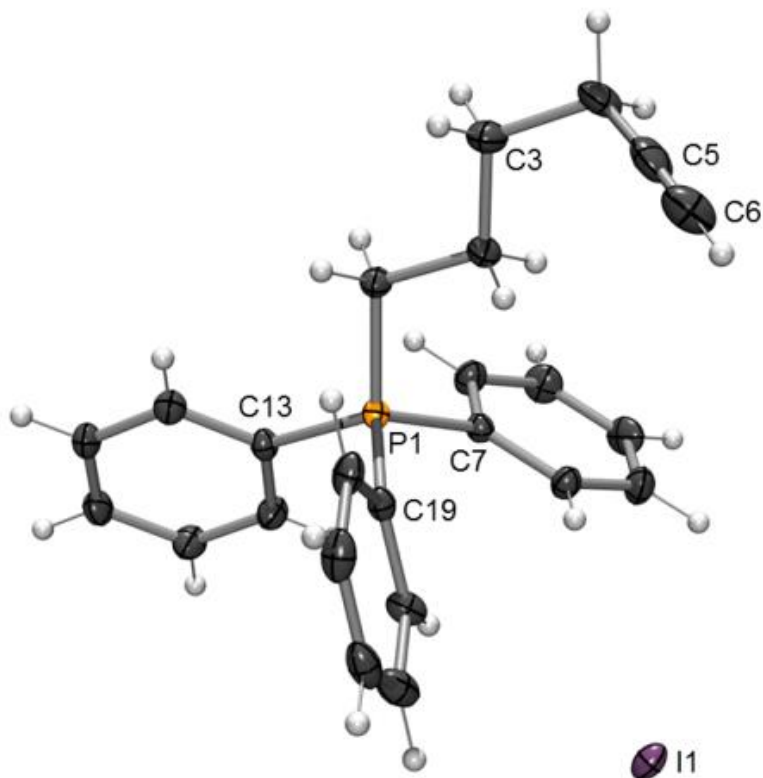


**Figure 61:** X-ray crystal structure of  $[\text{Ph}_3\text{P}(\text{CH}_2)_4\text{C}_2\text{H}]^+ \text{I}^-$  (the precursor to **5-4**). Key structural parameters: C5-C6 1.118 Å; C4-C5-C6 177.51°.

#### 5.1.3.1 Alkyne hydrogenation with Wilkinson's catalyst by PSI-ESI-MS

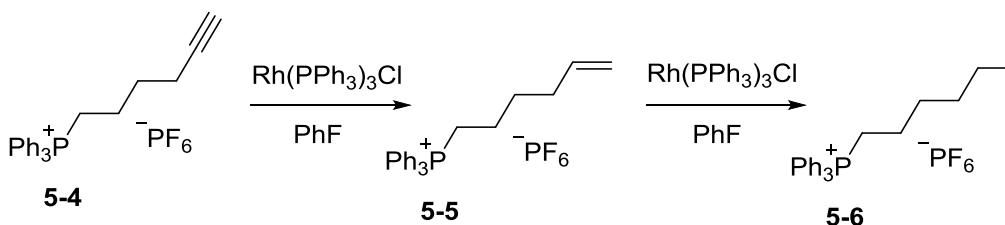
The reactions were done with **5-4** as substrate in fluorobenzene with Wilkinson's catalyst; high purity  $\text{H}_2$  gas was used as the pressure source as well as  $\text{H}_2$  source. Different solvents were tested and fluorobenzene was finally chosen as **5-4** has good solubility in it.

In order to detect any catalytic intermediates containing Rh and charged-tagged alkyne, many experiments were carried out with high loadings of Wilkinson's catalyst. The reaction speed benefited from the high equivalent of catalyst loading as well. To simplify the analysis and data processing, all the experiments were run under the same pressure of hydrogen as is usually employed in the PSI-ESI-MS experiment, i.e. 3-5 psi above atmospheric pressure (i.e. ~ 130 kPa).<sup>89</sup> This overpressure also represents a large excess of hydrogen; the reaction was conducted

at 0.0082 mmol in 10 ml, i.e. a  $0.82 \text{ mmolL}^{-1}$  concentration, so one equivalent of hydrogen required just 0.4 ml of gas, and the experiment used a Schlenk flask with a volume of 100 ml.

As mentioned above, in previous studies using ESI-MS and a charged phosphine ligand,<sup>159</sup> no intermediates containing the alkene were observed, though a variety of off-cycle species such as  $\text{Rh}_2\text{P}_4\text{Cl}_2$  and  $\text{RhP}_3\text{ClH}_2$  were detected. The predominant Rh-containing species was  $\text{RhP}_3\text{Cl}$ .

The reaction process is shown in Scheme 11, the charge-tagged alkyne **5-4** led to production of the corresponding alkene (**5-5**) and alkane (**5-6**). The result is shown in Figure 63. At room temperature the reaction was finished within one hour, the highest percentage that alkene can reach is about 60% of relative intensity whereas both alkyne and alkane are at 20% each. This observation suggested that the conversion from alkyne to alkene is faster than from alkene to alkane.



**Scheme 11:** Hydrogenation of alkyne to alkene and then to alkane.



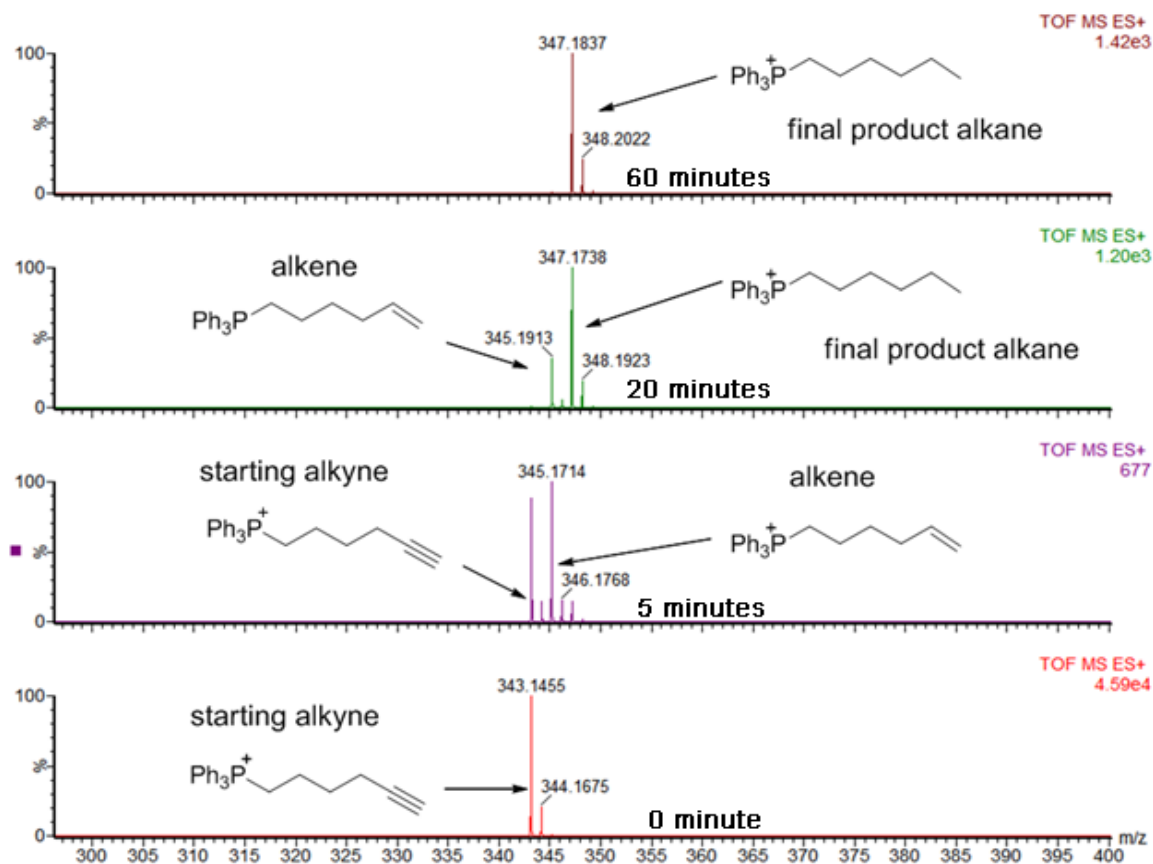


**Figure 62:** Positive-ion ESI-MS in fluorobenzene, [PPh<sub>3</sub>P(CH<sub>2</sub>)<sub>4</sub>CCH]PF<sub>6</sub> (bottom) is the starting material. [PPh<sub>3</sub>P(CH<sub>2</sub>)<sub>5</sub>CH<sub>3</sub>]PF<sub>6</sub> (top) is the final product.

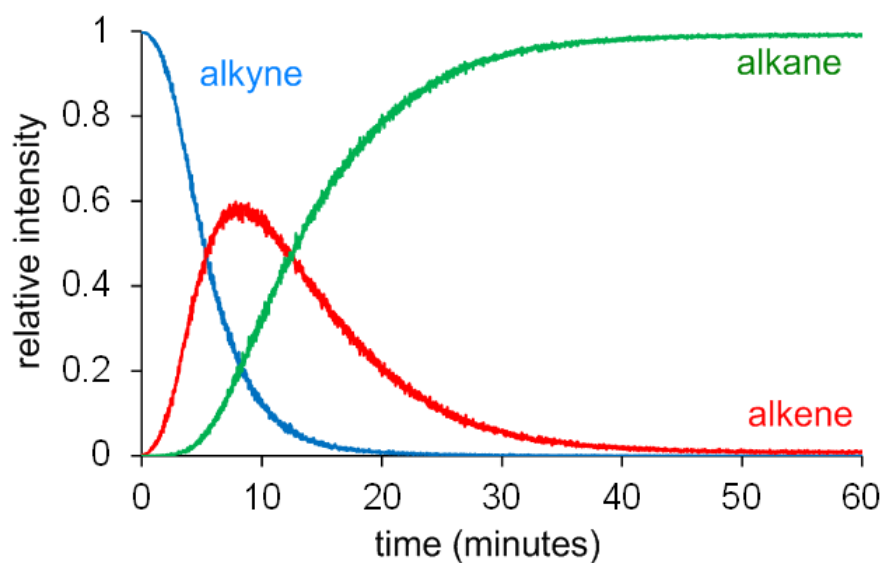


**Figure 63** Relative intensity vs time traces for alkyne (5-4), alkene (5-5) and alkane (5-6).

This reaction was run at room temperature with a high catalyst loading to maximize the chances of observing a rhodium-containing intermediate that included the charged tag, different cone

voltages were tested as well as cone gas flow rate and other ESI and TOF parameters. But no such intermediates were observed. The results are similar to a previous ESI study. This negative result tells us that the 1,2-insertion and the reductive elimination are not turnover limiting steps as we would expect the intermediates prior to each of these steps should have a fairly high and detectable intensity. It does not tell us whether the phosphine dissociation, oxidative addition of dihydrogen, or alkyne/alkene binding are turnover-limiting steps, because the tagged ligand is not involved in any of these steps.

The experiment was conducted at different temperatures in order to exclude the possibility that the reactivity observed is some sort of fact of the electrospray process itself or a gas-phase phenomenon. Cooks noted that certain reactions are greatly accelerated during supersonic expansion in the ESI process (by several orders of magnitude in one example).<sup>160</sup> However, if that were the case in these reactions, we would expect to see similar reactivity regardless of the reaction flask temperature. However, this is not the case; the reaction is very fast at high flask temperatures, and very slow at cold flask temperatures, and both were collected under ESI source conditions that were identical. This observation is strong evidence for the data representing solution rather than gas-phase conditions. The three temperatures examined were 0.0 °C, 23.0 °C (ambient) and 58.2 °C. The temperature of the solution was not controlled when it goes through the PEEK tubing between flask and ESI source, so in each case, there was a brief period (on the order of a few seconds) in which the reaction temperature was altered.

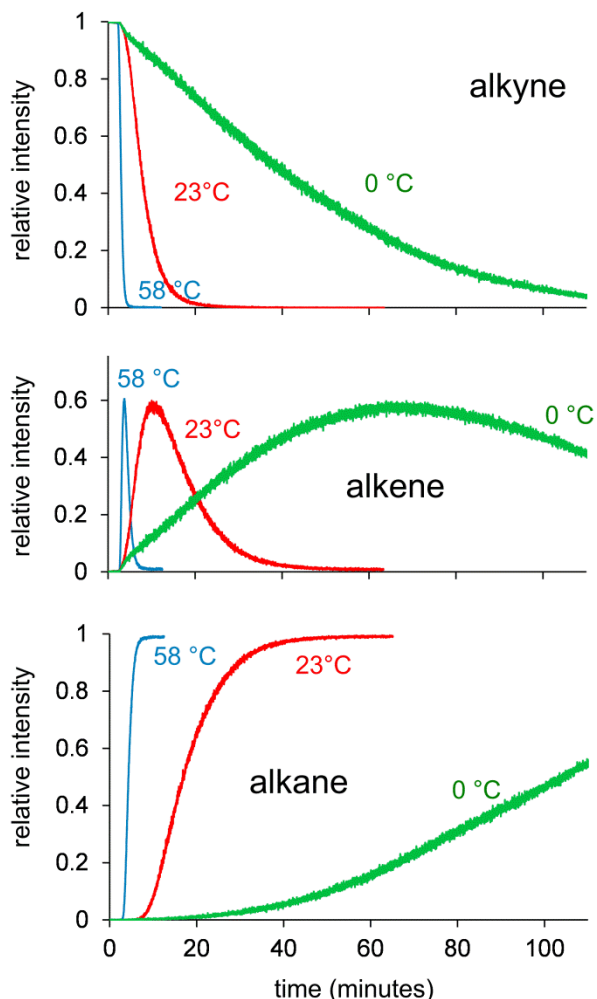


**Figure 64:** Traces for disappearance of alkyne (top), appearance and disappearance of alkene (middle), and appearance of alkane (bottom) at temperatures of 0°C, 23°C and 58°C.

From the reaction results we can find that reduction of the alkyne and alkene happened at the same time, meaning these two reduction reactions compete with each other, i.e. once alkyne converts to alkene, the alkene will start to convert to alkane, there is no selectivity for alkyne hydrogenation to complete before alkene hydrogenation starts. In order to get better understanding of the process, we built a numerical model to simulate the whole process and estimate the key rate constants. The model itself is complicated as we had to build both alkyne and alkene hydrogenation cycles, then make both of them operate simultaneously and in competition with one another.

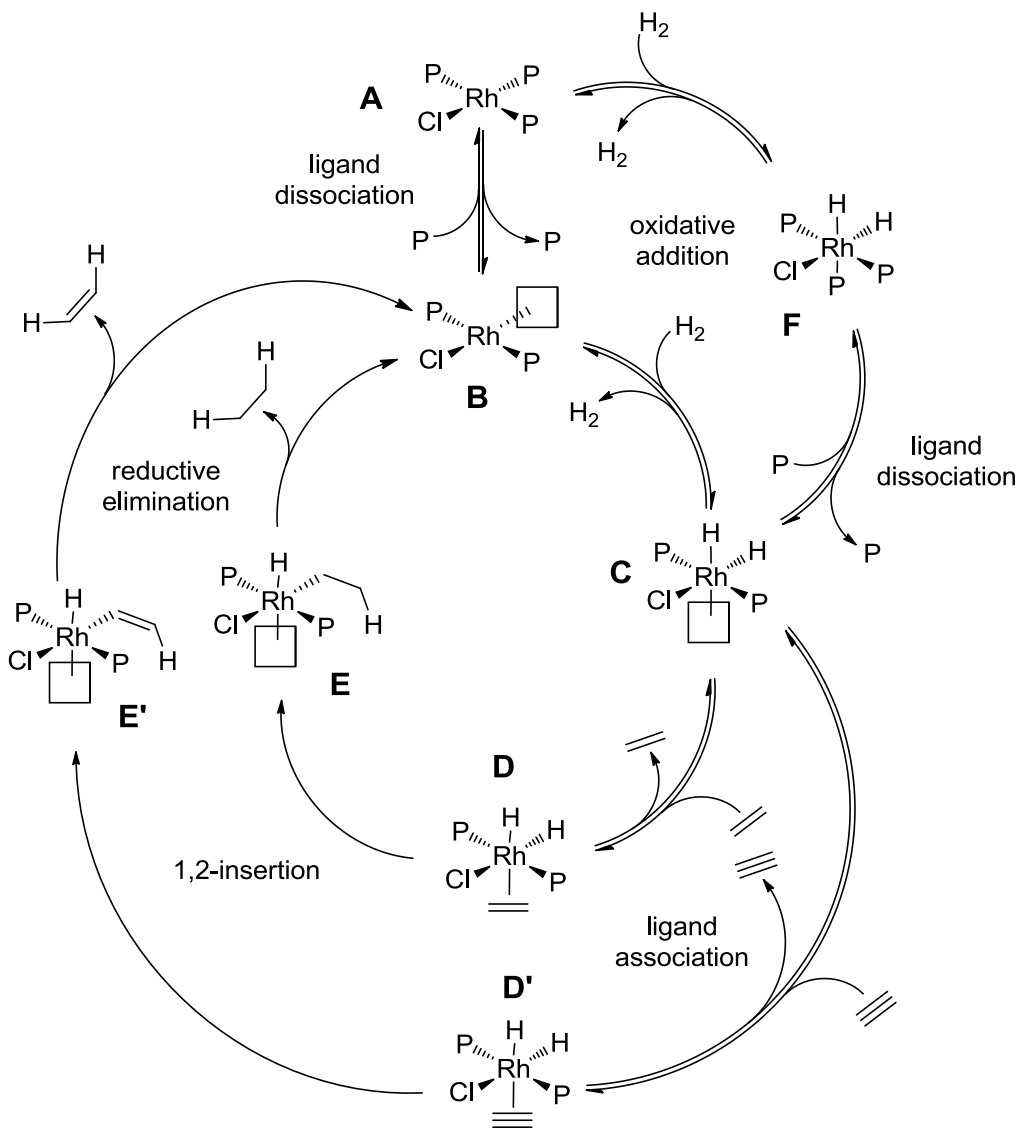


**Figure 65:** Catalytic cycle for hydrogenation of alkyne to alkane, where the two hydrogenations compete with one another.

The program PowerSim<sup>161</sup> was used to model each of the steps and published references were consulted to find rate constants as a starting point for as many steps as possible.<sup>146, 162, 163</sup> For all the other parameters, manual adjustment was done. Manual adjustments were time consuming, and later on with the acquisition of COPASI, models could be constructed in much less time. For the reaction at 23 °C and 17% catalyst loading, the modelled rates that provided the best match with experimental data are listed in Table 4. During the estimation process, the large number of independent parameters have to be tested and the numbers need to be treated with some

reservations. But they provide a satisfying solution to the experimental data based on the accepted mechanism (Figure 66).

**Table 4:** Rate constants for the numerically modelled reaction at 23°C.

| Rate constant, $k$ | Rate constant, $k$ for forward reaction | Rate constant, $k$ for back reaction |
|--------------------|---|--------------------------------------|
| <b>A → B</b>       | 0.00385                                 | 13.6                                 |
| <b>A → F</b>       | 0.0001                                  | $1 \times 10^{-8}$                   |
| <b>F → C</b>       | 0.0033                                  | 13.6                                 |
| <b>B → C</b>       | 4000                                    | 1                                    |
| <b>C → D</b>       | 47                                      | 5000                                 |
| <b>C → D'</b>      | 141                                     | 4000                                 |
| <b>D → E</b>       | 10000                                   | 0                                    |
| <b>E → B</b>       | 10000                                   | 0                                    |
| <b>D' → E'</b>     | 10000                                   | 0                                    |
| <b>E' → B</b>      | 10000                                   | 0                                    |

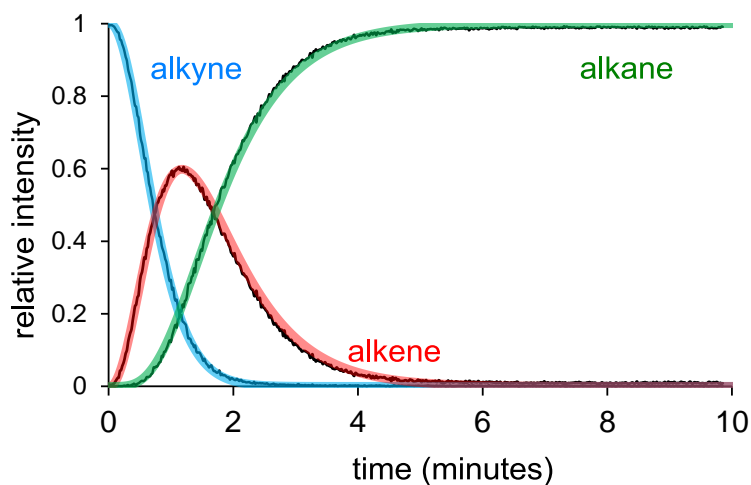


**Figure 66:** Match between simulated and experimental reaction progress curves. The thin black lines are the experimental curves; the thick transparent lines are the calculated curves.

From the estimated parameter we can find out that the initial ligand dissociation from **A** to **B** is slow as the rate constant for the back reaction is much larger than the forward reaction. To match accurately to the rest of the reaction, the final steps of the reaction proved to be fast (modelled as irreversible reactions with rates of 10000 units, but the model is essentially insensitive to changes in these rates once they are faster than the earlier reactions in the cycle). The slowest steps of the productive part of the cycle are ligand association of alkene or alkyne with the unsaturated 16e Rh<sup>III</sup> complex, P<sub>2</sub>Rh(H)<sub>2</sub>Cl, **C**. That a ligand association should be slow is somewhat counterintuitive unless the fact that a solvent molecule needs to be displaced first is taken into account (solvent involvement was not explicitly modelled). The model predicts that the ligand association reaction lies a long way towards the unsaturated (= solvent coordinated) complex, and that the forward reaction is approximately three times faster for the alkyne over the alkene (the back reactions are much faster and both of similar magnitude). This low level of selectivity means that partial hydrogenation<sup>164-167</sup> is not feasible with Wilkinson's catalyst, at least without the addition of modifying agents.<sup>168</sup>

Because the key rate constant is the ligand dissociation step to generate the unsaturated 14 electron RhP<sub>2</sub>Cl from RhP<sub>3</sub>Cl, we would expect the reaction to be inhibited by the addition of PPh<sub>3</sub> (the mechanism predicts a reaction rate that is inversely first order in triphenylphosphine concentration). That proves to be true; the reaction slows substantially with added PPh<sub>3</sub>. The experiments were conducted with 5% catalyst at 91.0 °C, in order to expedite the analyses. Extra PPh<sub>3</sub> was loaded before the catalyst solution was added, with 0 eq, 1 eq to catalyst and 2 eq to catalyst. The changes in reaction rate were predicted well by our numerical model when we altered only the initial concentration of PPh<sub>3</sub> (Figure 67), adding confidence to its accuracy.

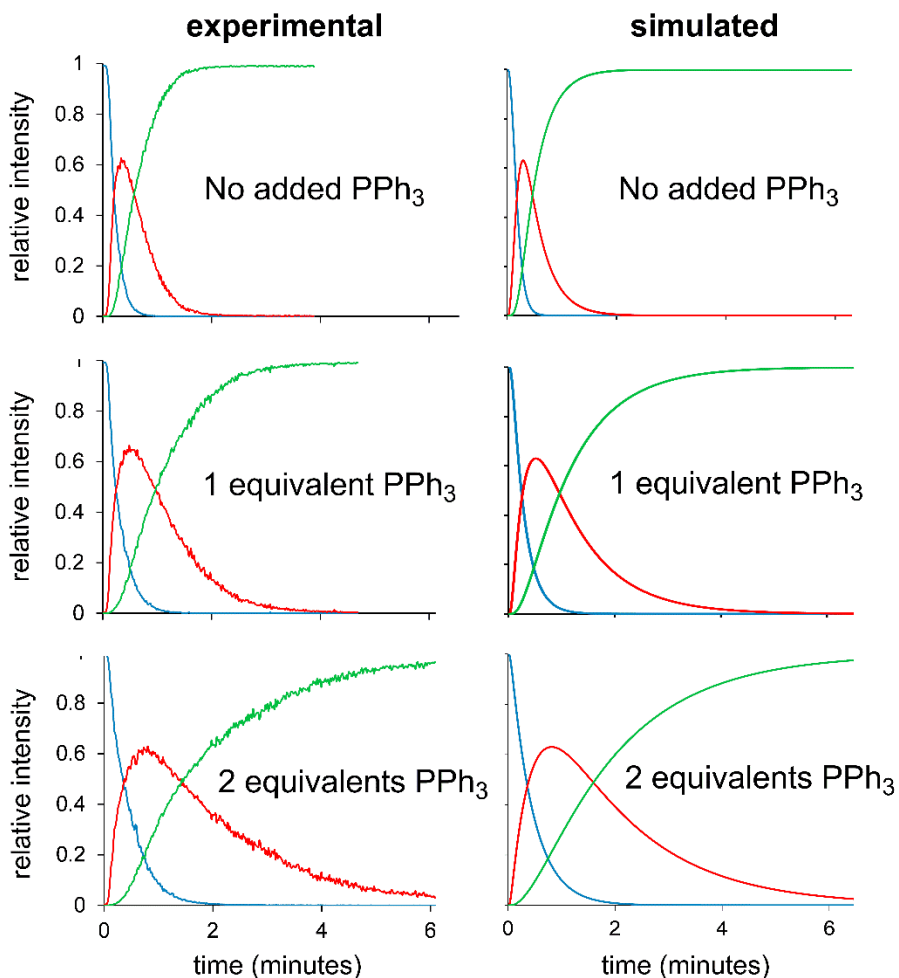


**Figure 67:** Experimental traces for hydrogenation of **5-4** using Wilkinson's catalyst (5 mol%) at 91°C in the presence of (a) no added PPh<sub>3</sub>, (b) one equivalent of PPh<sub>3</sub>, and (c) two equivalents of PPh<sub>3</sub>. The right-hand column shows the corresponding traces calculated by the numerical model, wherein only the starting concentration of PPh<sub>3</sub> has been altered.

#### 5.1.4 Conclusion

Alkyne hydrogenation by Wilkinson's catalyst can be studied in dense kinetic detail using pressurised sample infusion to continuously and directly monitor the reaction using ESI-MS. Due to the high frequency of data collection, reactions that finish in short time can be monitored. This shows the unique advantage of pressurised sample infusion over other techniques on reaction monitoring. Confidence in the quality and reliability of the data so obtained is enhanced by the excellent matches between experimental data and that obtained by numerically modelling the reaction based on a well-established mechanism. Both the model and the experimental data

responded in the same way to perturbations to the concentration of free phosphine, which predictably slows the reaction given that the turnover-limiting step involves dissociation of the phosphine from Wilkinson's catalyst to generate the unsaturated, 14-electron complex that rapidly oxidatively adds hydrogen.

## 5.2 Hydrogenation of olefins by Weller's catalyst

### 5.2.1 Introduction

In the first part of the chapter, Wilkinson's catalyst was used for the study of alkyne hydrogenation where it was confirmed that the turnover-limiting step was ligand dissociation from the precatalyst to generate the unsaturated, 14-electron species  $\text{Rh}(\text{PPh}_3)_2\text{Cl}$ . We also used the charged alkyne to make the whole reaction detectable in mass spectrometry; however, we saw no metal-containing intermediates during the reaction. We went looking for a charged catalyst that would perform the same transformation, and decided on a cationic rhodium complex. A cationic rhodium complex will give us a chance to detect any charged Rh peak in MS. These are well known to be excellent selective hydrogenators of alkynes, from the classic work of Schrock and Osborn from the 1970s.<sup>169</sup> Finally the cationic catalyst,  $[\text{Rh}(\text{PCpr}_3)_2(\text{PhF})]^+[\text{B}[3,5-(\text{CF}_3)_2\text{C}_6\text{H}_3]_4]^-$  ( $\text{P}^{\text{C}}\text{pr}_3$  = triscyclopropylphosphine, PhF = fluorobenzene) was chosen.<sup>170</sup> Because the catalyst was firstly synthesized and provided by Professor Andrew Weller from University of Oxford, here we call this catalyst, "Weller's catalyst".

Cationic rhodium complexes of the type  $[\text{Rh}(\text{diene})(\text{PR}_3)_2]\text{PF}_6$  are known for hydrogenation of alkynes from Schrock and Osborn's work,<sup>169</sup> and since then these type of complexes have served as precursors in various studies of homogeneous catalysis. Bis(ditertiaryphosphine) chelate complexes of rhodium(I) were studied as catalytic hydrogenators of methylene succinic acid, and cationic and hydrido versions of the complex were found to be more active than corresponding chloro versions with activity increasing with increasing chain length of the diphosphine.<sup>171</sup> Additionally the complex  $[\text{Rh}(\text{NBD})(\text{PPh}_3)_2][\text{BF}_4]$  (NBD = 2,5-norbornadiene) was found to selectively catalyze phenylacetylene to styrene without reduction of the diolefin of the catalyst, proof that the active species is diolefin coordinated instead of dihydrido and monohydrido derivatives.<sup>172</sup> Semihydrogenation of internal alkenes such as diphenylacetylene



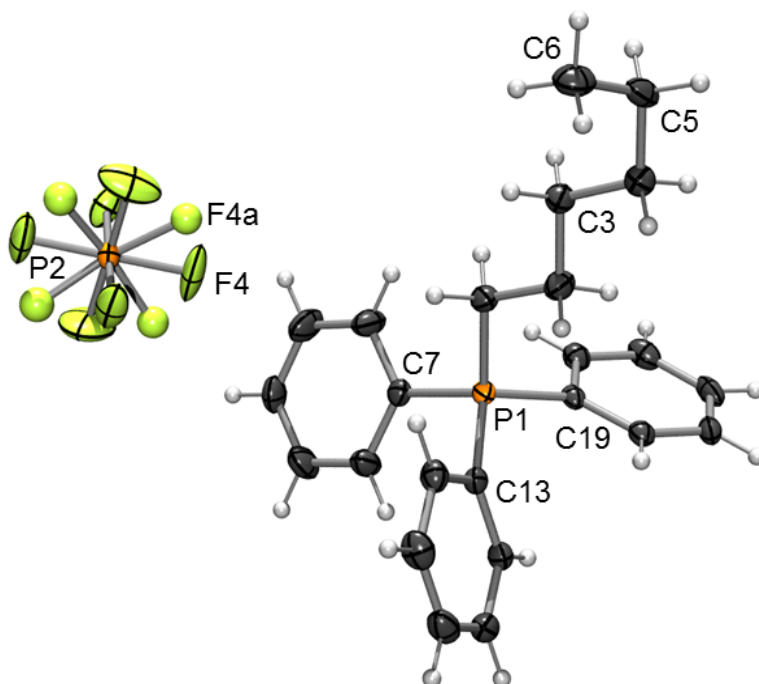
has also been developed with good selectivity with use of trinuclear cationic rhodium complexes.<sup>173</sup> Innately linked to cationic rhodium hydrogenation is catalytic asymmetric synthesis to produce enantiomerically pure compounds due to the possibility of introducing a degree of chirality in the ligands on the metal center. Extensive work has been done in this area with rhodium originally, but more recently iridium and ruthenium complexes.<sup>174-177</sup> With the work of Wilkinson *et al.* the scope of these  $[\text{Rh}(\text{diene})(\text{PR}_3)_2]\text{PF}_6$  precursors was further extended to the hydrogenation of imines,<sup>178</sup> and since then the hydrogenations of prochiral imines for the production of a chiral amines has become a promising route for synthesis of chiral nitrogen containing compounds.<sup>179, 180</sup>

So for the first time, in combining the charged alkyne with the cationic rhodium catalyst for the hydrogenation reaction and monitoring the process by PSI-ESI-MS, the intention was to detect Rh containing intermediates and track the behaviour of each species.

### 5.2.2 Results and Discussion

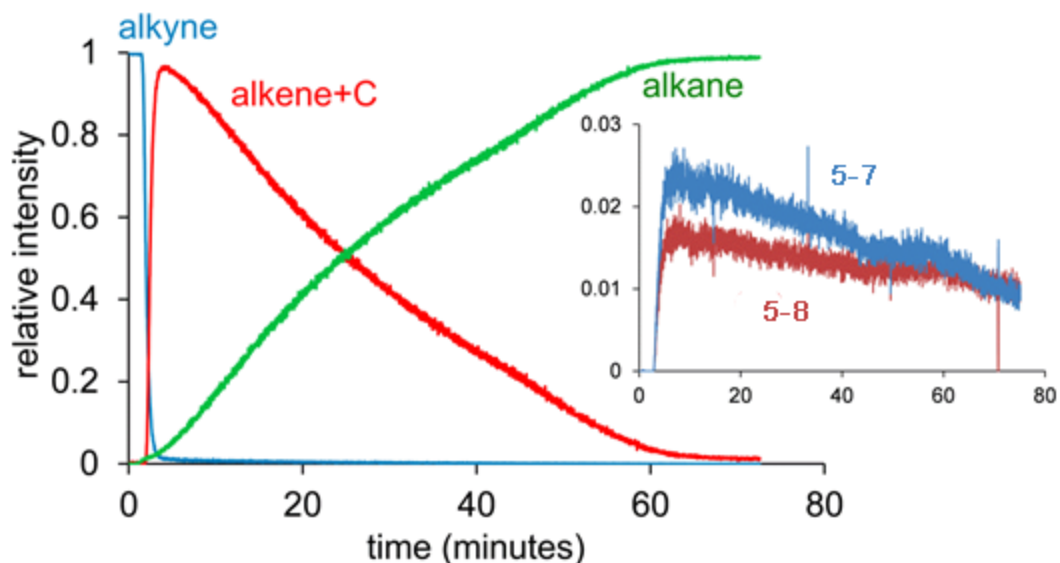
Cationic rhodium(I) complexes are known to be active hydrogenation catalysts,<sup>181-184</sup> and electronically unsaturated versions can be stabilized using bulky phosphines. They also have the advantage of being readily detected by ESI-MS. The example studied was  $[\text{Rh}(\text{P}^c\text{Pr}_3)_2(\text{FPh})]^+[\text{BAr}^{\text{F}}_4]^-$  (R = cyclopropyl,  $\text{Ar}^{\text{F}}$  = 3,5-bis(trifluoromethyl)phenyl).<sup>170</sup>

The charged substrate used was the same as for Wilkinson's hydrogenation in the first part of the chapter:  $[\text{Ph}_3\text{P}(\text{CH}_2)_4\text{C}_2\text{H}][\text{PF}_6]$  (**5-4**), which proved to have the right combination of solubility, high ESI-MS response factor, and lack of reactivity of the tag for the purposes of reaction analysis.<sup>95</sup> The product alkane,  $[\text{Ph}_3\text{P}(\text{CH}_2)_5\text{CH}_3][\text{PF}_6]$  (**5-6**), was isolated and crystallized to establish that the reactivity of the charge-tagged alkyne duplicates that of a regular terminal alkyne; the resulting structure of the triphenylhexylphosphonium salt was very ordinary in regard to a regular terminal alkyne (Figure 68).



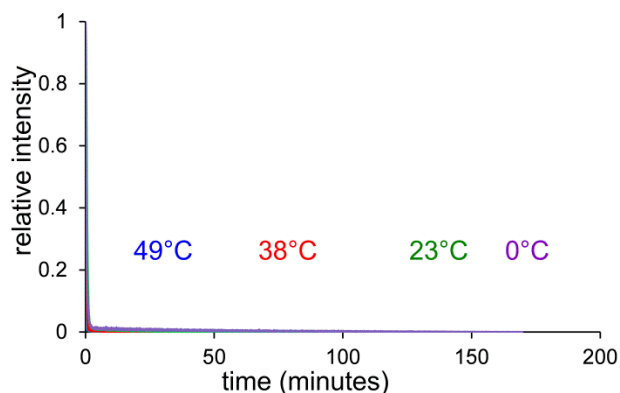
**Figure 68:** Alkane hydrogenation product. Key bond lengths and angles: C5-C6 1.500 Å; C4-C5-C6 113.83°.

The reactions were run with similar condition as Wilkinson's hydrogenation. But the kinetics of this reaction proved to be very different from that catalyzed by Wilkinson's catalyst,  $\text{Rh}(\text{PPh}_3)_3\text{Cl}$ .<sup>95</sup> For Wilkinson's catalyst, the rate of alkyne hydrogenation was only three times faster than the rate of alkene hydrogenation, and the turnover-limiting step was phosphine dissociation from the  $\text{Rh}(\text{PPh}_3)_3\text{Cl}$  precatalyst to generate the reactive 14-electron species  $\text{Rh}(\text{PPh}_3)_2\text{Cl}$ . However, for the cationic rhodium catalyst studied here, the alkyne hydrogenation was *much* faster than hydrogenation of the alkene,  $[\text{Ph}_3\text{P}(\text{CH}_2)_4\text{CH}=\text{CH}_2][\text{PF}_6]$  (**5-5**), and production of both appeared to be essentially zero order in alkyne (alkene). No intermediates were observed that included both rhodium complex and the charged tag, and the only observed rhodium-containing species were  $[\text{Rh}(\text{PR}_3)_2(\text{FPh})]^+$  (**5-7**) and  $[\text{Rh}(\text{PR}_3)_2]^+$  (**5-8**). These features are summarized in Figure 69.



**Figure 69:** Hydrogenation of  $[\text{Ph}_3\text{P}(\text{CH}_2)_4\text{CH}=\text{CH}_2][\text{PF}_6]$  under 3 psi of  $\text{H}_2$ , with 13.3% of  $[\text{Rh}(\text{PR}_3)_2(\text{FPh})]^+[\text{BAR}_4^{\text{F}}]^-$  as catalyst at room temperature with FPh as solvent. Inset: relative intensity vs time plot exhibiting behavior of  $[\text{Rh}(\text{PR}_3)_2(\text{FPh})]^+$  (**5-7**) and  $[\text{Rh}(\text{PR}_3)_2]^+$  (**5-8**).

The selectivity for alkyne over alkene is great (at least 50:1), but because the reaction is (close to) zero order in alkynes (alkene), we know that this substrate is not involved in the turnover-limiting step. This suggests that the alkyne (alkene) coordination to the Rh complex is fast, but that the alkyne still substantially out-competes the alkene. The reaction is sensitive to temperature (Figure 70), confirming that the reaction is taking place in solution rather than being some sort of artefact of the ESI-MS ionization process.



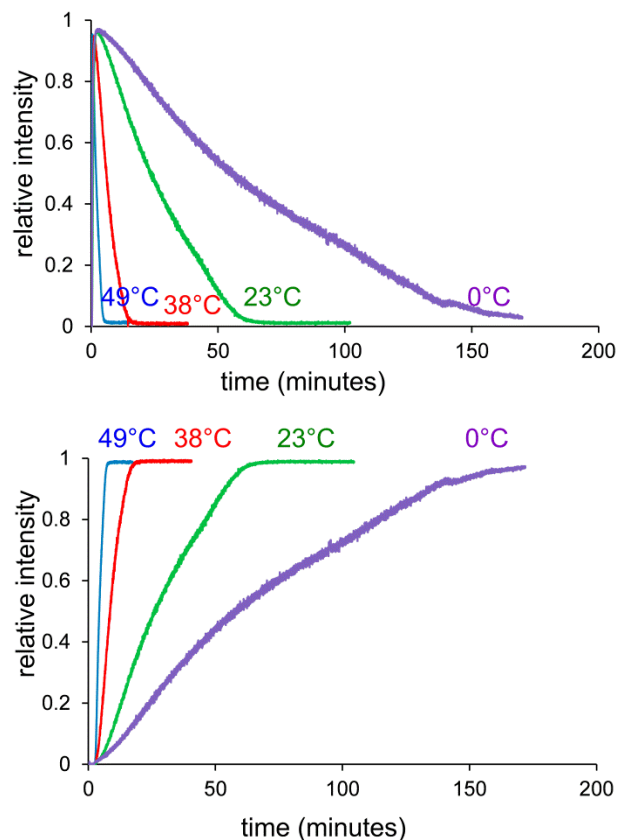


**Figure 70:** Top: disappearance of alkyne **5-4** at 0, 23, 38 and 49°C (fast at all temperatures). Middle: appearance and consumption of alkene **3**. Bottom: appearance of alkane **5-6**.

The reaction is first order in catalyst concentration (Figure 71), suggesting that the reaction involves a mononuclear rhodium species as catalyst. Hydrogen was present in large excess during the preliminary catalytic runs, so another experiment was carried out to establish the order of this compound.

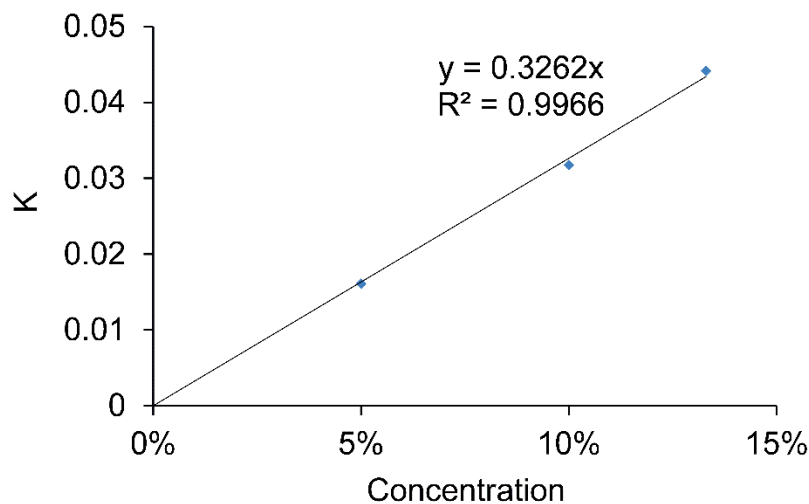


**Figure 71:** Reaction rate as a function of catalyst loading, illustrating that the reaction is first order in the concentration of  $[\text{RhP}_2(\text{FPh})]^+[\text{BAR}_4^-]$  used.

The experiment was re-examined using one equivalent of  $\text{H}_2$  (170  $\mu\text{L}$ ): the reaction was much slower and the kinetics cleanly displayed first order characteristics (Figure 72).

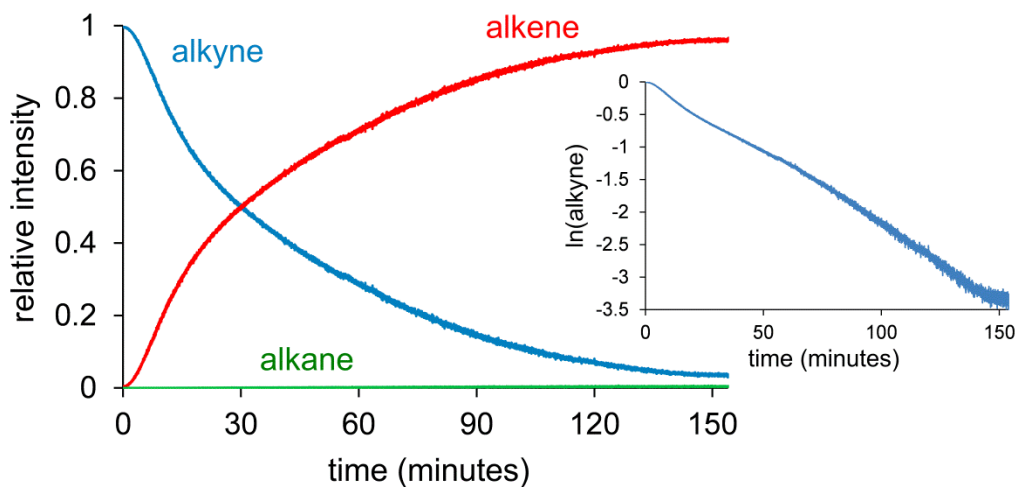


**Figure 72:** Selective hydrogenation of the charge-tagged alkyne in the presence of 1.1 equivalents of  $\text{H}_2$ . Inset:  $\ln[x]$  vs time plot exhibiting 1st order behavior.

This reaction is actually one of the hardest in the project. In other hydrogenation reactions, high purity hydrogen was used as the pressure source. In order to monitor the reaction with only one

equivalent of hydrogen, another inert gas must be used as the pressure source. The gas chosen was nitrogen, and a syringe was used to introduce one equivalent of  $\text{H}_2$  (170  $\mu\text{L}$ ).

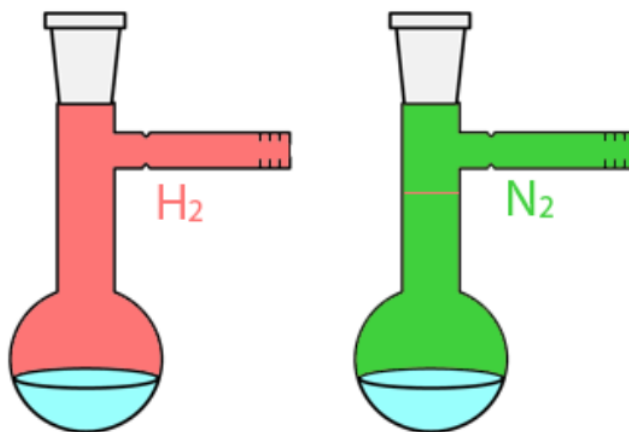


**Figure 73:** Comparison of hydrogenation with excess hydrogen and one equivalent of hydrogen.

Given that the turnover-limiting step involves hydrogen, it is reasonable to assume that a primary kinetic isotope effect (KIE) <sup>185, 186</sup> may be detectable in the reaction. As such, we ran the reaction using  $\text{D}_2$  instead of  $\text{H}_2$ , and found the alkene  $\rightarrow$  alkane reduction to be faster for  $\text{H}_2$ , by a factor of  $k_{\text{H}}/k_{\text{D}} = 2.1 \pm 0.2$  (Figure 74). This value is consistent with oxidative addition being the slow step, since concerted oxidative addition requires the breaking of an H-H (D-D) bond.

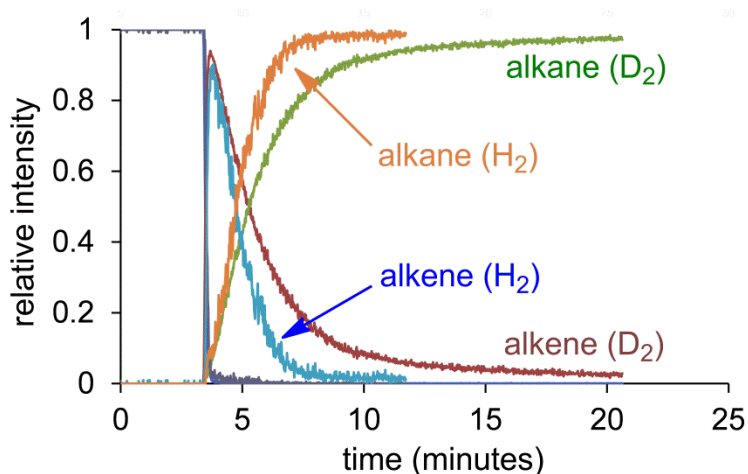


**Figure 74:** Reaction profiles for the reduction of alkyne to alkane using  $\text{H}_2$  (blue/yellow) vs.  $\text{D}_2$  (green/red).

So while the kinetics strongly point to the oxidative addition of H<sub>2</sub> being turnover-limiting, the fact we are unable to identify intermediates containing the charge-tagged alkyne or the alkene needs justifying. We can do so on several grounds.

(a) Monodentate alky(e)nes are difficult to characterize by ESI-MS at the best of times, because they are generally weakly bound and easily lost during the desolvation process.<sup>135</sup> This is exacerbated for a cationic metal complex binding a cationic alky(e)ne, as the charges repel each other.

(b) The catalyst on its own in fluorobenzene is distributed 20:1 between  $[\text{Rh}(\text{PR}_3)_2(\text{FPh})]^+$  (**5-7**) and the unsaturated  $[\text{Rh}(\text{PR}_3)_2]^+$  (**5-8**). However, during catalysis the ratio is closer to 1:1, suggesting that *something* is out-competing the fluorobenzene for coordination (Figure 75, Figure 76), and that most reasonable something is the alkyne or alkene.

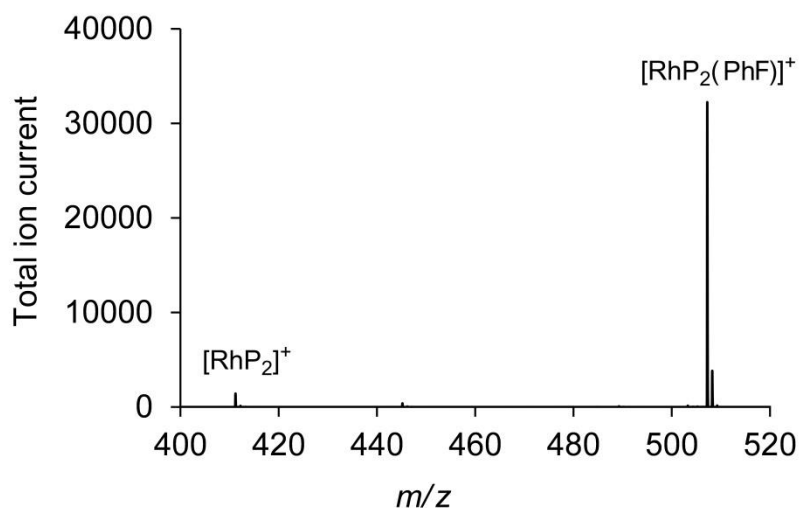


**Figure 75:** Precatalyst signal before hydrogenation started: mostly  $[\text{RhP}_2(\text{PhF})]^+$ .

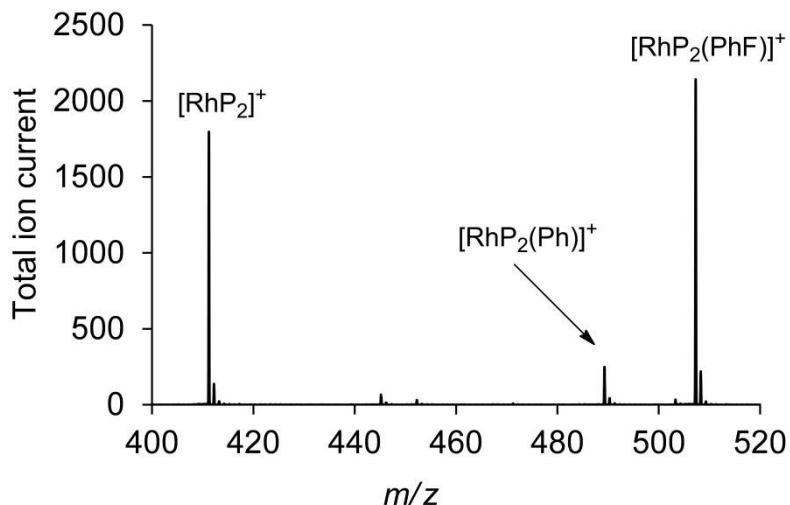


**Figure 76:** Precatalyst signal after hydrogenation started: a mix of  $[\text{RhP}_2]^+$  and  $[\text{RhP}_2(\text{PhF})]^+$ .

(c) Addition of octyne to  $[\text{Rh}(\text{PR}_3)_2(\text{FPh})]^+$  displaces the fluorobenzene and produces the ions  $[\text{Rh}(\text{PR}_3)_2(\text{octyne})_n]^+$  ( $n = 1$  or  $2$ , see Figure 77). This observation suggests that fluorobenzene is a relatively weakly bound ligand and is easily displaced by alkynes. Interestingly, with different, chelating ligands and  $\text{CH}_2\text{Cl}_2$  as solvent, PhF dissociation is slow.<sup>187</sup>

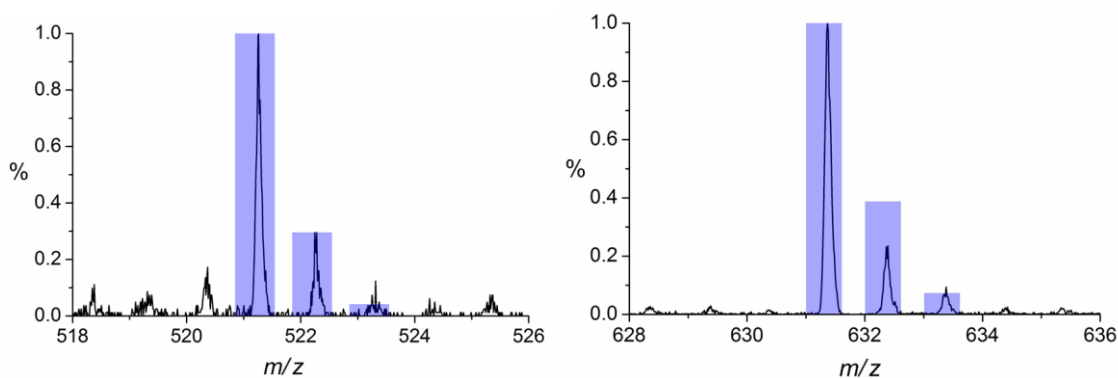


**Figure 77:** Mass spectrum of  $[\text{Rh}(\text{PR}_3)_2(\text{octyne})_n]^+$  ( $n = 1$ , left, and  $n = 2$ , right). Experimental data shown by line, calculated isotope pattern shown by columns.

(d) Mechanisms involving the alkyne (alkene) spending hardly any time coordinated to rhodium (i.e. when the equilibria  $\text{B} \leftrightarrow \text{C}$  and  $\text{B} \leftrightarrow \text{C}'$  lie a long way towards B) do not fit the observed kinetics.

(e) Ions of the form  $[\text{Rh}(\text{P}_2)\text{H}_2]^+$  were never observed in the mass spectrometer in the presence of  $\text{H}_2$ , suggesting that addition of  $\text{H}_2$  to the catalyst is either slow or lies a long way in the wrong



direction. In Professor Weller's lab, the complex was examined with  $^1\text{H}$  NMR under a pressure of  $\sim 4$  atm of  $\text{H}_2$ , and there were no observable changes at room temperature. Storage of this solution under  $\text{H}_2$  overnight led to the appearance of a doublet of multiplets at  $\delta$  4.33 ppm ( $^2J_{\text{HF}} = 48.8$  Hz) and several multiplets from  $\delta$  1.68 to 0.73 ppm characteristic of fluorocyclohexane<sup>188</sup> from the hydrogenation of fluorobenzene. This has been shown previously to proceed via a colloidal Rh catalytic route.<sup>189, 190</sup>

Osborn and Schrock outlined three possible mechanisms for the hydrogenation of alkenes by cationic rhodium complexes (Figure 78).<sup>169</sup>

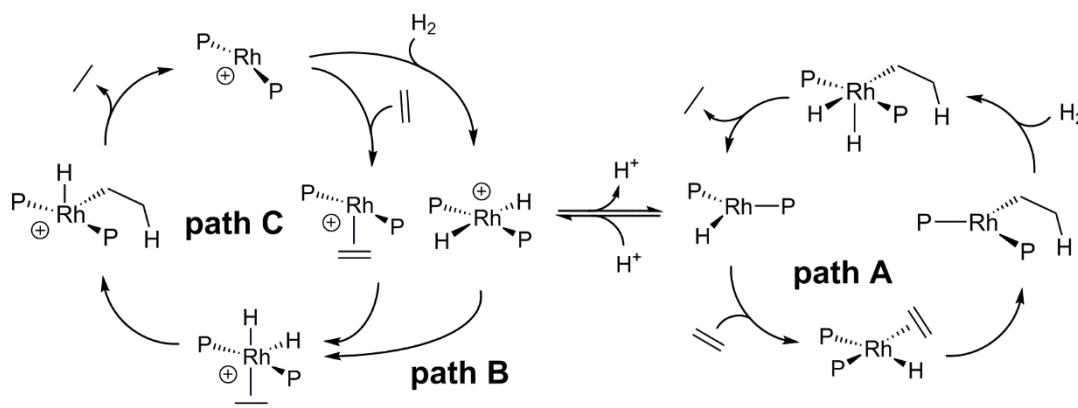


**Figure 78:** Pathways for alkene hydrogenation, after Schrock and Osborn.

Path A involved addition of  $\text{H}_2$  to  $[\text{RhL}_n]^+$  then deprotonation to form an active neutral catalyst of the form  $\text{RhHL}_n$ . Alkene coordination, migratory insertion,  $\text{H}_2$  addition, and reductive elimination of alkane followed. Path B involved addition of  $\text{H}_2$  then coordination of alkene to  $[\text{RhL}_n]^+$ , followed by migration and reductive elimination of the product alkane. Path C is the same as Path B, except the order of  $\text{H}_2$  and alkene reactivity is reversed. Osborn and Schrock considered path A as predominate, except where binding of the alkene was particularly strong, such as in the selective hydrogenation of dienes.<sup>169</sup>

All three mechanisms were considered as possible candidates to explain the observations, path C was ultimately settled on, for a number of different reasons:

(a) Neither  $\text{RhHL}_n$  (path A) nor  $[\text{RhH}_2\text{L}_n]^+$  (path B) could be detected by  $^1\text{H}$  NMR when examining  $[\text{RhP}_2(\text{fluorobenzene})]^+$  in the presence of  $\text{H}_2$ .

(b) If Path A was operative, any of the intermediates  $\text{RhHP}_2(\text{alkene})$ ,  $\text{RhRP}_2$  and  $\text{RhH}_2\text{RP}_2$  would be observable as monocations using ESI-MS, thanks to the charged tag. None of these species were in fact observed. If this path was operative, at least one should be (the one whose consumption is turnover-limiting).

(c) Addition of bases such as  $\text{NEt}_3$  ought to accelerate reactions proceeding via Path A, thanks to the deprotonation equilibrium being perturbed in the direction of  $\text{RhHP}_2$ . However, no such acceleration was observed. Indeed, the reaction was considerably *slowed* in the presence of  $\text{NEt}_3$  (Figure 79), and the reaction became much less selective for the alkyne. The reaction reached a maximum of 50% in alkene only, similar to the degree of selectivity exhibited by Wilkinson's catalyst.<sup>95</sup>

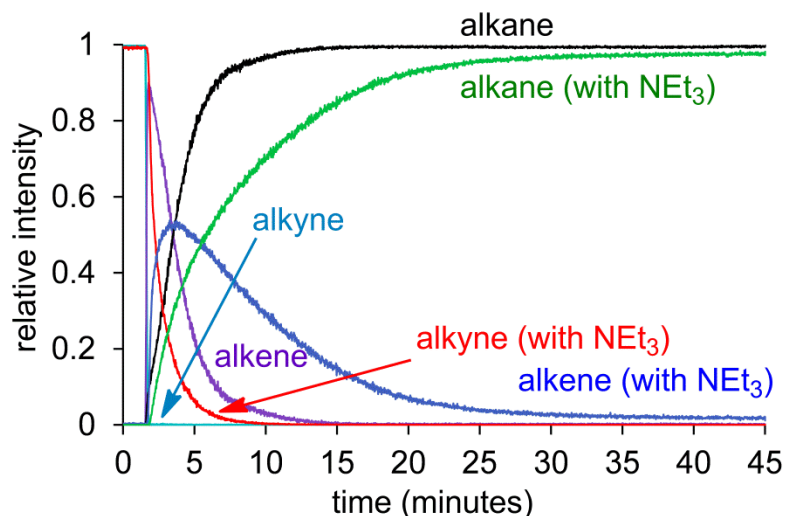


**Figure 79:** The effect of  $\text{NEt}_3$  on the rate and selectivity of hydrogenation.

Note that addition of  $\text{NEt}_3$  to  $[\text{RhP}_2]^+$  in the presence of  $\text{H}_2$  resulted in disappearance of  $[\text{RhP}_2]^+$  and the appearance of  $[\text{HNEt}_3]^+$  (Figure 80), suggesting the formation of neutral  $\text{RhHP}_2$ .

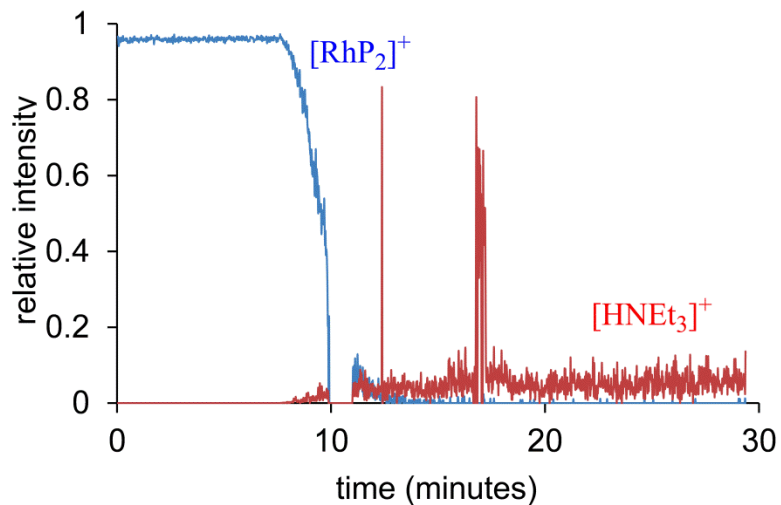


**Figure 80:** Addition of  $\text{NEt}_3$  leads to the disappearance of  $[\text{RhP}_2]^+$  and the appearance of  $[\text{HNEt}_3]^+$ .

(d) The ligand we used,  $\text{PCpr}_3$ , is more basic than those used by Schrock and Osborn ( $\text{PPhMe}_2$  and  $\text{PPh}_3$ ), favouring path B or C.

(e) The solvent used, fluorobenzene, is unfavourable to deprotonation compared to the polar solvents used by Schrock and Osborn (tetrahydrofuran, acetone, 2-methoxyethanol).

(f) The numerical modelling (*vide infra*) proved most tractable for Path C, providing excellent correlation with experimental data. Neither Path A nor Path B provided sensible solutions.

Path C has been redrawn in Figure 81 and elaborated to include the alkyne and the alkene on the same plot.

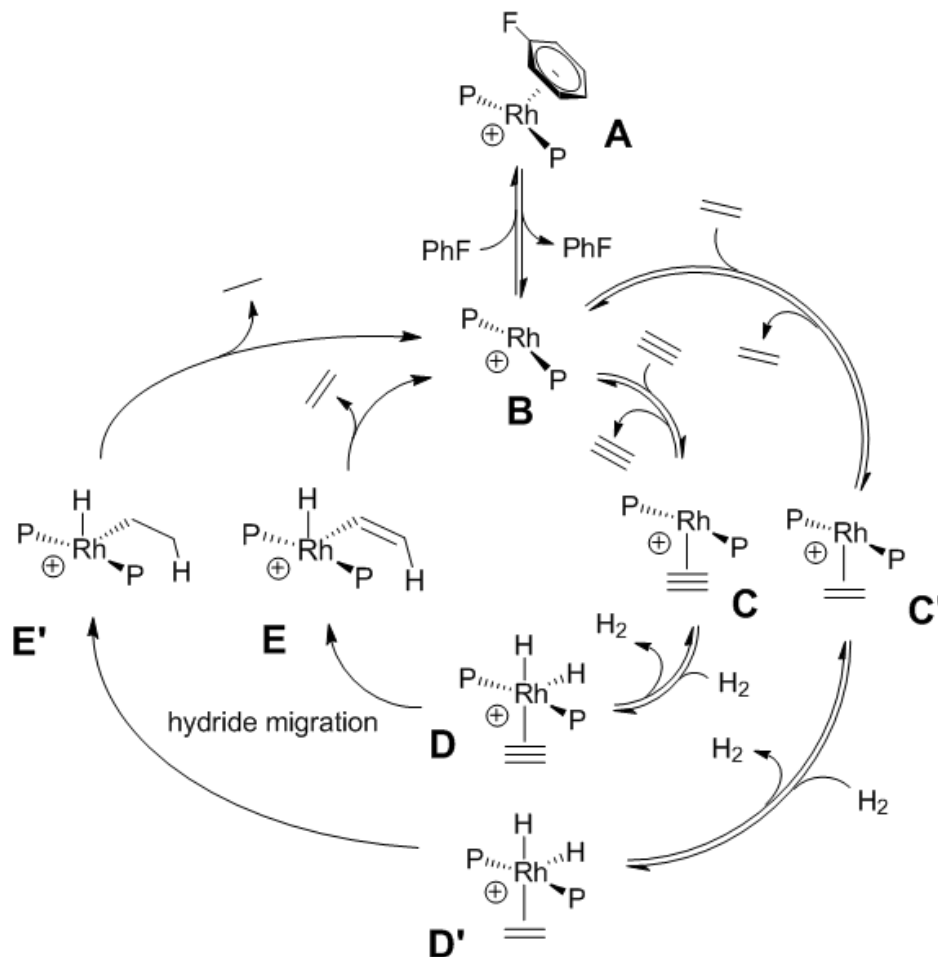


**Figure 81:** The mechanism of alkyne/alkene hydrogenation. P = P(cyclopropyl)<sub>3</sub>.

Using the cycle in Figure 81, a numerical model was constructed and the program Copasi<sup>93</sup> used to generate a set of rate constants compatible with the observed results. A variety of optimization methods and starting points were tested. Given the number of independent parameters - if all steps in the cycle were reversible, there are 18 rate constants to consider - the picture was simplified by assuming hydride migration and reductive elimination steps were fast and irreversible, leaving a more tractable 10 rate constants to optimize. 2 out of these 10 rate constants,  $A \rightarrow B$  and  $B \rightarrow A$  can be easily predicted based on the experimental measurements. These showed that a stable amount of B exists in the reacting solution and this can only be explained by having a much higher forward reaction from A to B. After these values were fixed to match the ESI-MS traces, the rest of the rate constants can be estimated by Copasi by using different mathematical methods. The sets of data in Table 5 were established by different

methods: two different genetic algorithms, simulated annealing, differential evolution, and evolutionary programming. For the computational methods, different starting points were randomly chosen in order to ensure a local minimum hadn't been found. All these methods mentioned above generated very similar rate constants and they all provided a good match for the experimental data.

**Table 5:** Estimated rate constants by different COPASI methods. First order rate constants are in units of  $\text{min}^{-1}$  and second order rate constants in units of  $\text{min}^{-1} \text{mmol}^{-1} \text{L}$ .

|                     | Genetic Algorithm | Genetic Algorithm SR | Simulated Annealing    | Differential Evolution | Evolutionary Programming |
|---------------------|-------------------|----------------------|------------------------|------------------------|--------------------------|
| $B \rightarrow C$   | 122               | 118                  | 118                    | 101                    | 116                      |
| $C \rightarrow B$   | 0.00364           | 0.122                | $1.175 \times 10^{-5}$ | 0                      | $4.37 \times 10^{-6}$    |
| $B \rightarrow C'$  | 4.79              | 4.43                 | 4.67                   | 3.39                   | 4.56                     |
| $C' \rightarrow B$  | 0.0475            | 0.0412               | 0.0427                 | 0                      | 0.0404                   |
| $C' \rightarrow D'$ | 1.92              | 2.01                 | 1.95                   | 2.06                   | 2.13                     |
| $D' \rightarrow C'$ | 2.00              | 329                  | 2.72                   | 0                      | 925                      |
| $C \rightarrow D$   | 0.0407            | 0.0408               | 0.0435                 | 0.0410                 | 0.0441                   |
| $D \rightarrow C$   | 206               | 103                  | 877                    | 0                      | 997                      |

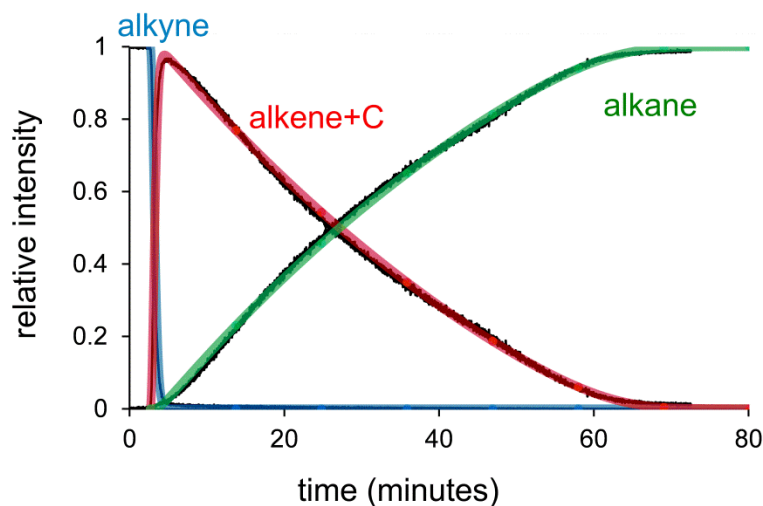


**Figure 82:** Direct comparison between simulated (coloured lines) and experimental results (black). The simulation is for the genetic algorithm, but similarly good matches were obtained for the other methods.

*Fluorobenzene dissociation:  $A \rightarrow B$*

The lack of any initiation time suggested to us that fluorobenzene dissociation was relatively fast. As such, trying to model this dissociation step added complexity to the model without adding anything to our understanding of the productive part of the cycle. Accordingly, the catalyst behavior was inspected over the course of the reaction and we selected rate constants that reflected the relative abundances of **5-7** and **5-8**. These values turned out to be  $10 \text{ min}^{-1}$  and  $0.1 \text{ min}^{-1} \text{ mmol}^{-1} \text{ L}$ .

*Alkene/alkyne association  $B \rightarrow C$*

All models predicted that binding of the alkene to **5-8** was slower than the binding of the alkyne to **5-8** by a factor of at about 40, but that both were relatively fast. However, this factor appeared to be just part of the reason for the selectivity for alkyne over alkene.

*Oxidative addition of hydrogen  $C \rightarrow D$*

This step is turnover-limiting, as predicted by the stoichiometric  $\text{H}_2$  addition, the overall zero-order kinetics, and the primary KIE established from the  $\text{D}_2$  experiment. As expected, the numerical modelling is in agreement: this step is slow, and especially so for the alkene, by a factor of about 40 compared to the alkyne.

*Migration and reductive elimination  $D \rightarrow E$  and  $E \rightarrow B$*

No attempt was made to model these steps, since they must be relatively fast from all the other evidence (most notably the observation of intermediates).

Further confirmation of the mechanism came through competition experiments. The charge-tagged alkyne  $[\text{Ph}_3\text{P}(\text{CH}_2)_4\text{CCH}]^+$  and a similar charge-tagged alkene,  $[\text{Ph}_3\text{P}(\text{CH}_2)_3\text{CH}=\text{CH}_2]^+$  were combined and an excess  $\text{H}_2$  reduction was conducted competitively. Neither alkene reacted until practically all of the alkyne was consumed, at which point the observed rates of alkene consumption were fairly similar (Figure 83).

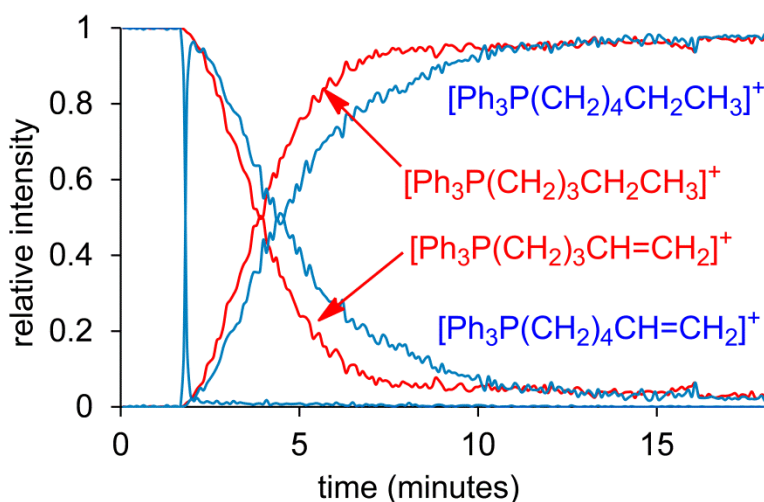


**Figure 83:** Competition reaction: reduction of alkyne vs. alkene. Note that the alkenes remain essentially untouched until the alkyne is completely consumed. Reduction of the two alkenes proceed at similar pace, though the hydrogenation of  $[\text{Ph}_3\text{P}(\text{CH}_2)_3\text{CH}=\text{CH}_2]^+$  was slightly faster than that of  $[\text{Ph}_3\text{P}(\text{CH}_2)_4\text{CH}=\text{CH}_2]^+$ .

The rate of reaction of the two alkenes are  $3.2 \times 10^{-4} \text{ mol L}^{-1} \text{ min}^{-1}$  for  $[\text{Ph}_3\text{P}(\text{CH}_2)_3\text{CH}=\text{CH}_2]^+$  and  $2.5 \times 10^{-4} \text{ mol L}^{-1} \text{ min}^{-1}$  for  $[\text{Ph}_3\text{P}(\text{CH}_2)_4\text{CH}=\text{CH}_2]^+$ . The fractionally faster rate for  $[\text{Ph}_3\text{P}(\text{CH}_2)_3\text{CH}=\text{CH}_2]^+$  is perhaps due to a small electronic effect due to the greater proximity of the charged tag.

Examination of catalyst behavior showed that the ratio of **5-7** to **5-8** stayed fairly constant and fairly similar in intensity throughout the reaction (see supporting information). The absolute

intensity reached a maximum soon after catalyst addition, and the intensity drops as the reaction proceeds, stabilizing at the completion of the reaction. This behavior was attributed to a competitive catalyst decomposition pathway stemming from a reaction intermediate (if the decomposition was from a catalyst precursor, the decomposition ought to continue after the cessation of the reaction). No charged rhodium-containing species were identified that could account for the disappearance of signal, suggesting that the decomposition product is neutral.  $\text{RhP}_2\text{H}$  is one such possibility; there was no colour change that might indicate the formation of metallic rhodium.

### 5.2.3 Conclusion

Analysis of alkyne hydrogenation using a charge-tagged alkyne and a cationic rhodium catalyst revealed the catalyst to be a highly efficient partial hydrogenator, with a rate of alkyne hydrogenation in excess of 50 times faster than alkene hydrogenation. The mechanism was shown by a combination of ESI-MS, NMR, isotope effects and numerical modelling methods to have a turnover-limiting step of oxidative addition of hydrogen following alkyne binding. Using a stoichiometric amount of hydrogen was shown to be an effective means of enabling selective hydrogenation to the alkene.

## 5.3 Experimental

Fluorobenzene was freshly distilled from  $\text{P}_2\text{O}_5$  before use. All other solvents were dispensed from an MBraun solvent purification system (SPS) immediately before use. All reactions were under nitrogen or argon atmosphere. Chemicals and solvents were purchased from Aldrich and used without subsequent purification. All mass spectra were collected by using a Micromass Q-TOF *micro* mass spectrometer in positive ion mode using pneumatically assisted electrospray ionization: capillary voltage, 3000 V; extraction voltage, 0.5 V; source temperature, 90°C; desolvation temperature, 180°C; cone gas flow, 100 L/h; desolvation gas flow, 100 L/h; collision voltage, 2 V (for MS experiments); collision voltage, 2-80 V (for MS/MS experiments); MCP voltage, 2700 V.



**ESI-MS reaction monitoring using pressurized sample infusion.** A Schlenk flask was used for these experiments, as described in Chapter 3.<sup>89, 90</sup> A solution of **[5-4][PF<sub>6</sub>]** (10-20 mg, 0.021-0.042 mmol) was monitored using the PSI-ESI-MS setup. The Schlenk flask was pressurized to 3 psi using 99.999% purity hydrogen gas or D<sub>2</sub> gas. Wilkinson's catalyst, Rh(PPh<sub>3</sub>)<sub>3</sub>Cl (1.0-4.0 mg, 0.0011-0.0043 mmol) or [Rh(PCpr<sub>3</sub>)<sub>2</sub>(FPh)]<sup>+</sup>[BAr<sup>F</sup><sub>4</sub>]<sup>-</sup> (1.0-6.0 mg, 0.75-4.5 μmol, 1.0-20.0% catalyst loading) was dissolved in 1.0 mL of fluorobenzene and injected into the PSI flask via a septum. The solution end of PEEK tubing was protected with a cannula filter system to avoid the tube being blocked by any insoluble by-products. Data were processed by normalizing the abundance of each species to the total ion count of all species identified as containing the tag. No smoothing of the data was performed.

**5-2.Br. (4-ethynylbenzyl)triphenylphosphonium bromide.** Triphenylphosphine (5.1 g, 19.6 mmol) and 4-iodobenzyl bromide (2.6 g, 8.7 mmol) were added to 10.0 mL toluene in a Schlenk flask and the mixture was stirred for 72 hours. The solid product was dried under high vacuum for 48 hours (4.9 g, 8.7 mmol, 99%). A portion of the product (0.30 g, 0.54 mmol) was mixed with diisopropylamine (0.55 g 5.4 mmol), PdCl<sub>2</sub>(PPh<sub>3</sub>)<sub>2</sub> (0.0019 g, 0.027 mmol), CuI (0.0010 g, 0.0054 mmol) and Me<sub>3</sub>SiC<sub>2</sub>H (0.11 g, 1.1 mmol) in a 12:5 mixture of MeOH and toluene and allowed to react for 2 hours. Silica flash column was applied for purification, and the desired product was isolated and dried to a brown powder (0.13 g, 0.28 mmol, 5.0%). Crystals for X-ray crystallographic analysis were grown by vapour diffusion of hexane into a chloroform solution. ESI-MS(+) *m/z* 377.1, (-) *m/z* 78.9.

**5-2.PF<sub>6</sub>. (4-ethynylbenzyl)triphenylphosphonium hexafluorophosphate(V).** Sodium hexafluorophosphate (0.10 g, 0.60 mmol) was dissolved in 2.0 mL of water, and a 1 mL methanol/water solution of **5-4.Br** (0.030 g 0.065 mmol) was added with stirring. The product was filtered and washed with water and dried under high vacuum for a week. The final product was a white powder (0.028 g, 0.054 mmol, 83%). <sup>1</sup>H NMR (CDCl<sub>3</sub>): δ (ppm) 7.82 (m, 3H); 7.68 (m, 7H); 7.55 (m, 7H); 6.89 (m, 2H); 4.61, (d, 2H, 14.4Hz); 3.10 (s, 1H). <sup>31</sup>P NMR (CDCl<sub>3</sub>): δ (ppm) 23.38 (singlet); -143.61 (septet). ESI-MS(+) *m/z* 377.1, (-) *m/z* 145.0.

**5-3.Br.** **N,N-dioctyl-N-(prop-2-yn-1-yl)octan-1-aminium bromide.** Trioctylamine (15.9 g, 45.1 mmol) and diethyl ether (10.0 mL) were introduced into an aluminium foil-wrapped Schlenk flask at room temperature. Propargyl bromide (5.0 mL of an 80.0% solution in toluene) was added, and the mixture stirred for 72 hours. The solvent was evaporated and the light brown liquid dried under vacuum for 10 h. The final product was a light brown solid (19.8 g, 41.8 mmol, 93.0%). ESI-MS(+)  $m/z$  392.6, (–)  $m/z$  78.9.

**5-3.PF<sub>6</sub>.** **N,N-dioctyl-N-(prop-2-yn-1-yl)octan-1-aminium hexafluorophosphate(V).** A methanol solution (10.0 ml) of **2.Br** (5.3 g, 11.2 mmol) and sodium hexafluorophosphate (2.8 g, 16.7 mmol) was prepared. The mixture was added dropwise into 500.0 mL of distilled water and stirred for 1 h. The yellow oily product was washed twice with 100.0 mL of distilled water under sonication and dried under vacuum. Final product was a yellowish white powder (5.2 g, 9.7 mmol, 86.0%). <sup>1</sup>H NMR (CDCl<sub>3</sub>): δ (ppm) 4.08 (d, 2H, 2.45Hz); 3.26 (m, 6H); 2.78 (m, 1H); 1.66 (m, 6H); 1.27, (m, 33H); 0.88 (m, 6H). ESI-MS(+)  $m/z$  392.6, (–)  $m/z$  145.0.

**5-4.I.** **Hex-5-yn-1-yltriphenylphosphonium iodide.** Triphenylphosphine (5.0 g, 19.0 mmol) was dissolved into 10.0 mL of toluene in a Schlenk flask at 75°C, and 6-iodo-1-hexyne (1.0 g, 4.8 mmol) added dropwise over 10 minutes. The mixture was stirred for 72 hours, before the product was filtered off, washed with toluene and dried under high vacuum. Final product was a white powder (2.2 g, 4.7 mmol, 98.0%). Crystals for X-ray crystallographic analysis were grown by vapour diffusion of hexane into a chloroform solution. ESI-MS(+)  $m/z$  343.1, (–)  $m/z$  126.9.

**5-4.PF<sub>6</sub>.** **Hex-5-yn-1-yltriphenylphosphonium hexafluorophosphate(V).** Sodium hexafluorophosphate (0.56 g, 2.1 mmol) was dissolved in 5.0 mL of water, and 5.0 mL of a methanol/water mixed solution of [Ph<sub>3</sub>P(CH<sub>2</sub>)<sub>4</sub>C<sub>2</sub>H]<sup>+</sup>[I]<sup>–</sup> (0.50 g 1.1 mmol) was added dropwise with stirring. The product was filtered and washed with water and dried under high vacuum for a week. Final product was a white powder (0.55 g, 1.1 mmol, 53%). <sup>1</sup>H NMR (CDCl<sub>3</sub>): δ (ppm) 7.81 (m, 3H); 7.70 (m, 12H); 3.22 (m, 2H); 2.29 (m, 2H); 1.86, (t, 1H, 2.64Hz); 1.81 (m, 3H); 1.26 (s, 1H). ESI-MS(+)  $m/z$  343.1, (–)  $m/z$  145.0.

**5-9.Br. Pent-4-en-1-yltriphenylphosphonium bromide.** Triphenylphosphine (5.5 g, 20.1 mmol) was dissolved into 10.0 mL of toluene in a Schlenk flask at 75°C, and 5-bromo-1-pentene (2.1 g, 13.4 mmol) added dropwise over 10 minutes. The mixture was stirred for 72 hours, before the product was filtered off, washed with toluene and dried under high vacuum. Final product was a white powder (0.50 g, 1.2 mmol, 9.1%). ESI-MS(+)  $m/z$  331.1, ESI-MS(-)  $m/z$  78.9.

**5-9.PF<sub>6</sub>. Pent-4-en-1-yltriphenylphosphonium hexafluorophosphate(V).** Sodium hexafluorophosphate (0.50 g, 3.0 mmol) was dissolved in 5.0 mL of water, and 5.0 mL of water solution of [Ph<sub>3</sub>P(CH<sub>2</sub>)<sub>3</sub>C<sub>2</sub>H<sub>3</sub>]<sup>+</sup>[I]<sup>-</sup> (0.50 g, 1.2 mmol,) was added dropwise with stirring. The product was filtered and washed with water and dried under high vacuum for a week. Final product was a white powder (0.5 g, 1.1 mmol, 91.0%). <sup>1</sup>H NMR (CDCl<sub>3</sub>): δ (ppm) 7.80 (m, 3H); 7.68 (m, 12H); 5.68 (m, 1H); 5.05 (m, 2H); 3.13 (m, 2H); 2.30 (m, 2H); 1.71 (m, 2H). ESI-MS(+)  $m/z$  331.1, ESI-MS(-)  $m/z$  145.0.

## 6. The use of charged substrates to investigate Si-H activation by ESI MS

I performed all experimental work, produced all figures and co-wrote the paper with JS McIndoe. AG Oliver performed the crystal structure determinations, publication under preparation.

Catalytic organosilicon chemistry has rapidly developed in recent years, especially Si-H activation reactions. Catalytic Si-H activation is the process of coordination of Si-H  $\sigma$  bonds with transition metals, followed by formation of a new Si-element bond, including dehydrocoupling of silanes to make Si-Si bonds, hydrosilation to make Si-C bonds, silane hydrolysis and alcoholysis to make Si-O bonds and so on. These reactions can be used to make functionalized silicon compounds that have potential industrial applications such as silicone oil, rubber and resin. However, structural control over the synthesis of the desired molecules remains limited by relatively basic understanding of the mechanisms. The success of catalytic carbon reactions cannot be directly copied into silicon because there are obvious differences in their electronic structures.<sup>191</sup> This chapter involves the preliminary investigation of catalytic reactions involving Si-H bonds using the methods and strategies developed earlier in the thesis.

### 6.1 Current research in the area of Si-H activation

#### 6.1.1 Dehydrocoupling of silane

Dehydrogenative coupling of silanes is a reaction involving breaking of Si-H bonds and formation of a Si-Si bond, accompanied by the elimination of hydrogen gas. The product usually involves the formation of oligo or polysilanes.<sup>192</sup> Dehydrocoupling of silanes is an important reaction because the products polysilanes have unusual thermal, photochemical, optical and electronic properties which arise from the delocalization of sigma ( $\sigma$ ) bonds in the backbone of the oligomer, and this leads to the absorption of specific UV wavelengths by the Si-Si chain.<sup>193</sup>

Dehydrocoupling of silanes was first reported by Harrod when he investigated the polymerization of organosilanes catalyzed by group IV complexes.<sup>194, 195</sup> The advantages of dehydrocoupling of silanes include easy purification (the main by-product is H<sub>2</sub>), the ability to add functional groups, and control over stereochemistry and chain length. Dehydrocoupling of silanes remains an active area of research, and catalysts used include early<sup>196,197</sup> and late<sup>198-202</sup>

transition metals, often in tandem with a co-catalyst such as Red-Al.<sup>196</sup> The mechanism is strongly dependent on the nature of the catalyst. Early transition metals (Ti, Zr Hf etc), are supposed to undergo two consecutive  $\sigma$  bond metatheses,<sup>203</sup> because in  $d^0$  complexes, oxidative addition is not possible. Most of catalysts in this category are metallocene complexes,  $Cp_2MR_2$ . Steric hindrance is an important limiting factor in the formation of Si-Si bonds. Primary hydrosilanes result in longer Si-Si chains than do secondary hydrosilanes, and tertiary silanes are most difficult to couple.<sup>203,204</sup>

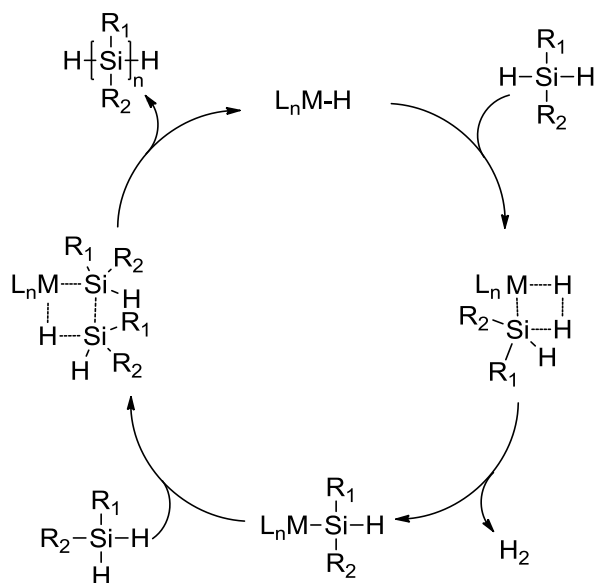


**Figure 84:** Dehydrocoupling of silanes for early transition metal complexes, following the  $\sigma$  bond metathesis mechanism.

For late transition metal complexes (Ni, Pd, Rh etc), the Si-Si bond forming step is unknown so far, and different mechanisms have been proposed.<sup>203</sup> Figure 85 shows a mechanism with a series of oxidative addition/reductive elimination steps. Figure 86 shows a 1,2 silyl migration with a highly reactive silylene intermediate. This mechanism is debated due to the lack of direct proof of observation of such intermediates.

Tilley used an alkyne to trap silylene into a 2+2 cycloaddition product, suggesting that silylene is forming during the reaction of rhodium phosphine complexes.<sup>205</sup> Milstein used another system to prove the existence of silylene; in his reaction,  $H_2SiPh_2$  formed dehydrocoupling products by using  $Rh(P^iPr_3)_2(OTf)$  as the catalyst, but when the substrate was switched to the tertiary silanes  $HSiPh_2Me$  and  $HSiPhMe_2$ , no coupling occurred even though  $Ph_2SiH_2$  has similar sterics and

electronics to these tertiary silanes. This is because 1,2 migration of group other than hydrogen atom is difficult.<sup>206</sup>

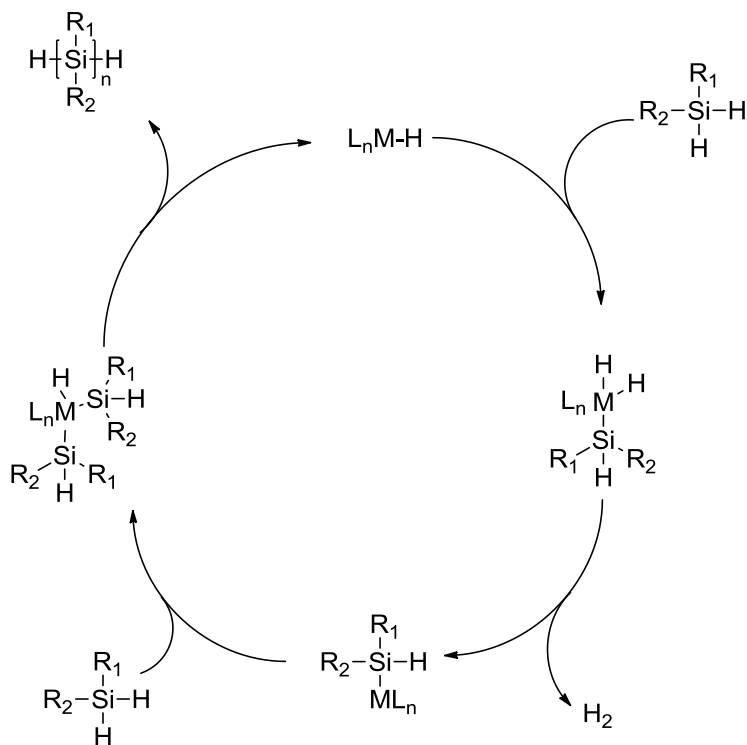


**Figure 85:** Dehydrocoupling of silanes for late transition metal complexes, following the oxidative addition/reductive elimination mechanism.

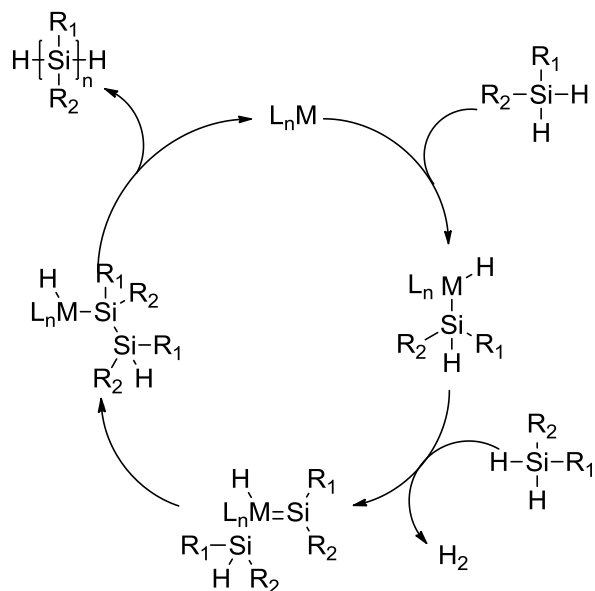


**Figure 86:** 1,2 silyl migration (or silylene insertion) mechanism for dehydrocoupling of silanes by late transition metal complexes.

Dehydrocoupling of silanes by late transition metals was first reported by Ojima using Wilkinson's catalyst,  $(PPh_3)_3RhCl$  with  $Ph_2SiH_2$  and  $MePhSiH_2$ .<sup>207</sup> Since then, various rhodium complexes have been found to be active in the dehydrocoupling of hydrosilanes. The Si-Si bond coupling is easier for primary silanes, it becomes more difficult for secondary silanes and does not work for tertiary hydrosilanes.<sup>203</sup> The Rosenberg group have reported a high-yielding route to  $(Ph_2SiH)_2$ .<sup>208</sup> Observations based on  $^{31}P$  NMR provided insights into the mechanism of silane dehydrocoupling.<sup>203</sup> This reaction was studied using ESI-MS by Danielle Chisholm from our group. In this paper, a catalysis mechanism cycle was proposed (Figure 87). The ESI-MS reaction was carried out by using a charged phosphine ligand (Figure 88) to replace one triphenylphosphine of Wilkinson's catalyst  $(PPh_3)_3RhCl$  in solution through a ligand dissociation-association process. By doing this, Wilkinson's catalyst gets a positive charge and it is detectable in ESI-MS. By using a syringe pump, the reaction solution was introduced continuously into the spectrometer, so the whole process of reaction could be monitored in real time. All the detectable species in the mechanism are in blue color in Figure 87.  $P_2RhH$  is found to be the active dehydrocoupling catalyst.

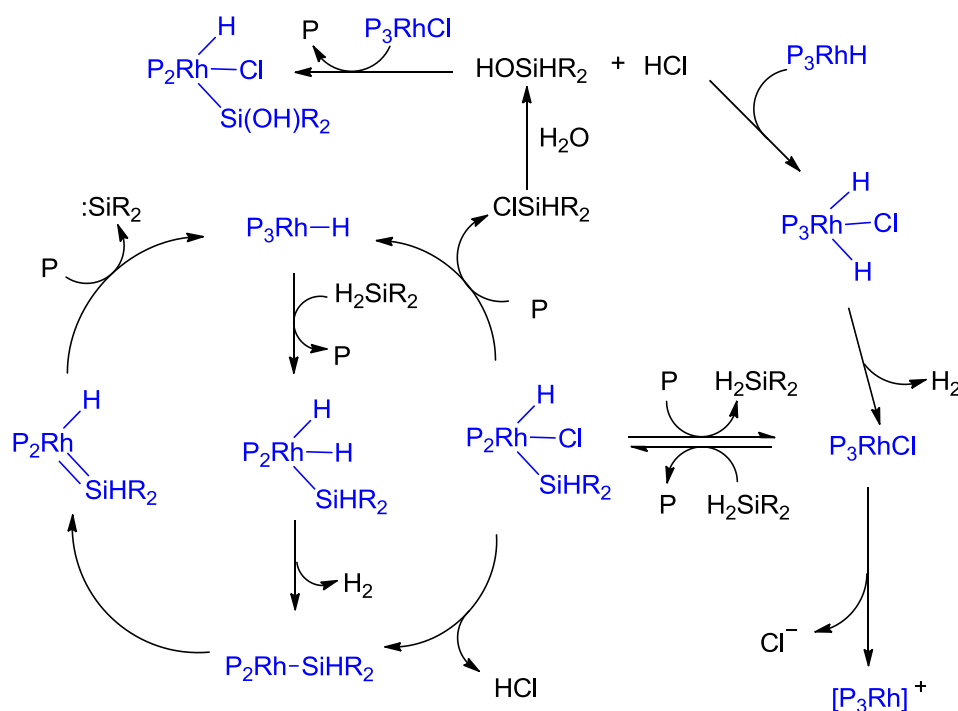


**Figure 87:** Proposed dehydrocoupling of silane mechanism based on observation.

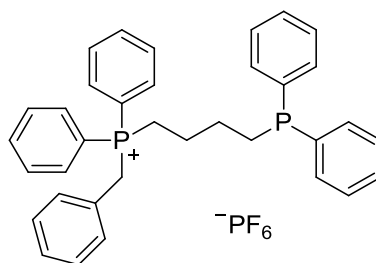


**Figure 88:** Charged phosphine ligand benzyl(4-(diphenylphosphino)butyl)diphenylphosphonium hexafluorophosphate(V).

This system can potentially detect M=Si silylene, but the  $R_2Si:$  silylene and the product are undetectable due to absence of a charge, and these are important species in the formation of Si-Si bond. In order to detect these species, it is necessary to develop a system to detect these species as well as previously detected species at the same time.

By using a charged silane, it should be possible to detect all the  $[Si-Rh]^+$  containing intermediates, as well as the starting material and final product. Figure 89 shows all the species that could potentially be visible in ESI-MS.

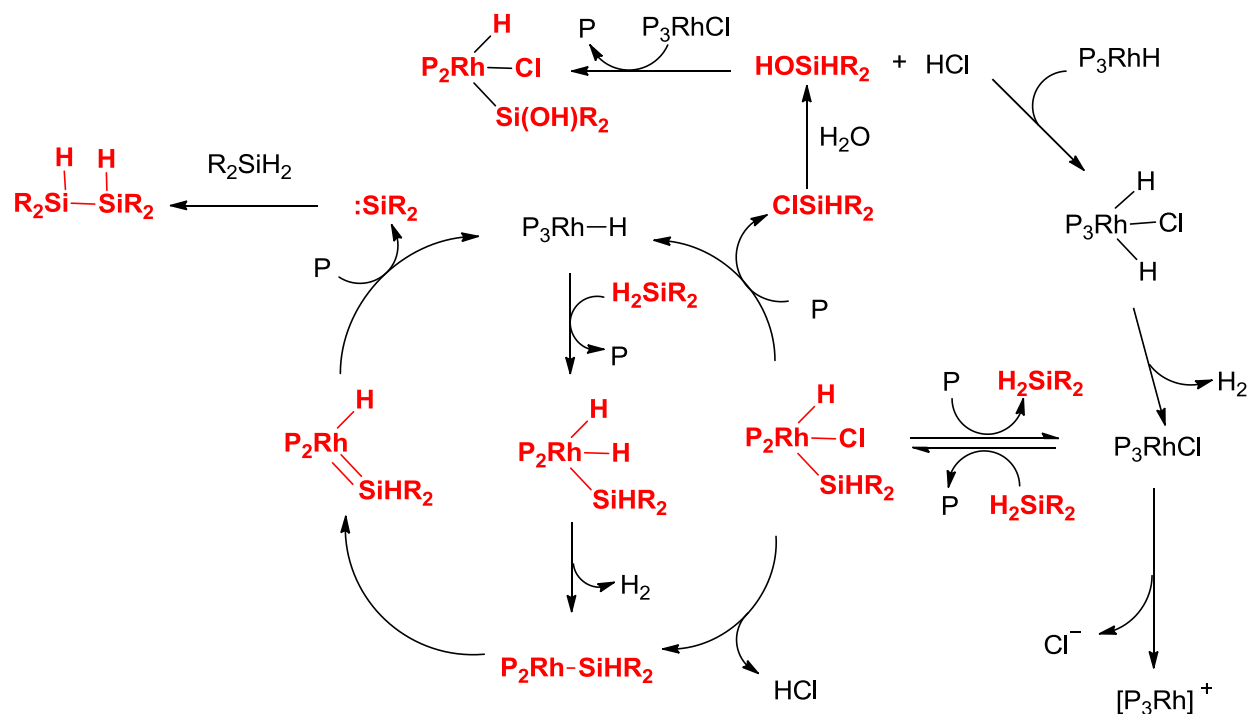


**Figure 89:** Red species should be visible in ESI-MS by using a charged silane substrate.



### 6.1.2 Hydrolysis of silanes

Siloxanes and polysiloxanes are valuable building blocks for silicon-based polymeric materials in industry.<sup>209</sup> Global demand for siloxanes and polysiloxanes was about 13.5 billion dollars in 2010<sup>210</sup>. Usually the synthesis involves the strongly exothermic hydrolysis of chlorosilanes by water to generate silanediols, which condense into polysiloxanes.<sup>211</sup> Corrosive HCl gas is released during the reaction (Figure 90).

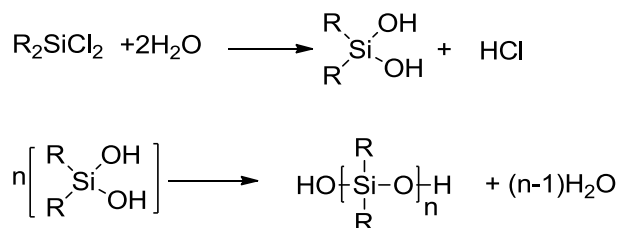


**Figure 90:** Hydrolysis of dichlorosilane

Another method to make these materials is by hydrolysis of hydrosilanes with water. This method will not generate HCl and the only by-product is hydrogen gas, so it is environmentally friendly and has high atom economy. However, even though there is huge bond energy difference between Si-H and Si-O bond, the conversion of Si-H into Si-O bond by water is quite slow in neutral conditions. Base and strong acid are commonly used as catalysts,<sup>211</sup> however metal catalysts become more popular because their highly efficient behaviour and mild reaction conditions.

Hydrolysis of silane with water by organometallic catalysts has become a hot topic in the last decade.<sup>209, 212-220</sup> By using different equivalents of water and various types of catalysts, hydrosilanes will react with water to generate siloxanes, polysiloxanes and hydrogen gas, and condensation reaction between siloxanes will generate polysiloxanes and water (Figure 91).<sup>221</sup>

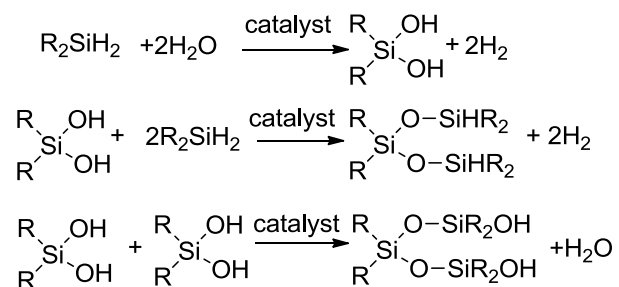


**Figure 91:** Hydrolysis and condensation of hydrosilanes.

Various catalysts were found to be effective in this reaction, and siloxanes and silicones were successfully prepared with different functional groups.<sup>213-217, 219-222</sup> Kinetic studies have been reported and different mechanisms have been proposed. For example, a cationic oxorhenium catalyst was used for hydrolysis of silane as a hydrogen storage method with 6% capacity by weight of hydrogen storage (Figure 92), and a mechanism was proposed based on isotope labelling and kinetic studies.<sup>220</sup>

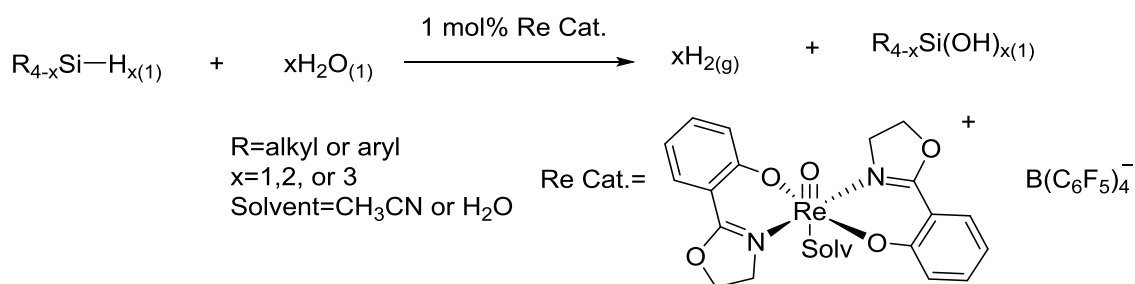


**Figure 92:** Cationic oxorhenium catalyst for hydrolysis of silane.

Sze Tat Tan *et al.* proposed a mechanism for a ruthenium catalyst based on NMR studies,<sup>214</sup> as did Ting Yan Lee *et al.* for a different ruthenium catalyst based on X-ray structures of isolated intermediates and NMR studies (Figure 93).<sup>215</sup> However, there is no commonly accepted mechanism so far.

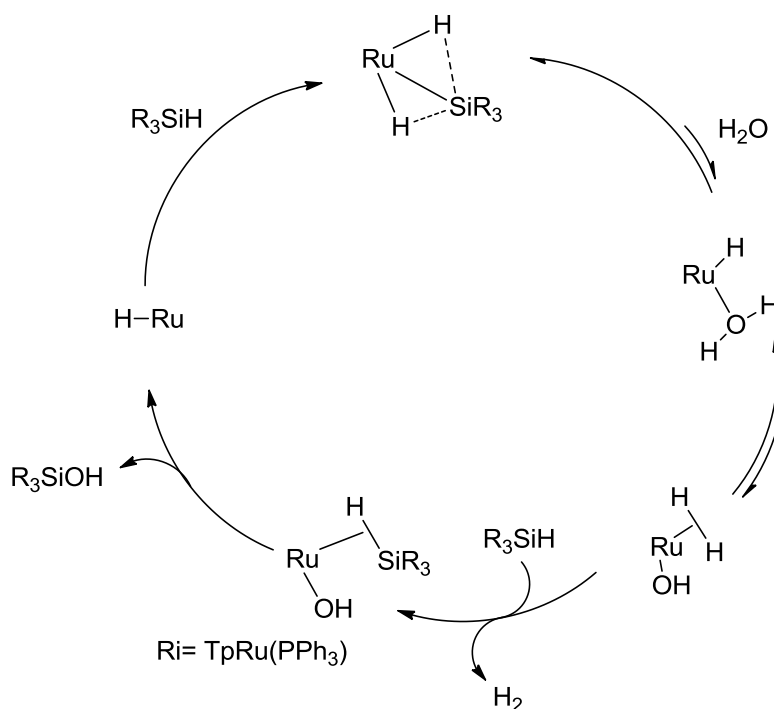
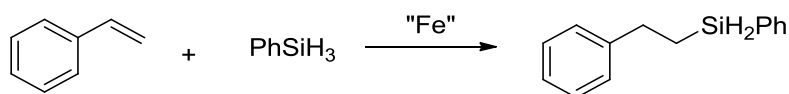


**Figure 93:** A ruthenium complex catalyzed hydrolysis of silane mechanism proposed by Lee *et al.*<sup>215</sup>

### 6.1.3 Hydrosilation

Hydrosilation is one of the most important techniques for making an Si-C bond as well as other silicon-heteroelement bonds by addition of Si-H to a  $\pi$  bond (C=C, C $\equiv$ C etc).<sup>211, 223</sup> It can introduce functionalized silanes or alkylsilanes into organic molecules (Si-Cl, Si-OR etc.). Hydrosilation can be mediated by radicals and transition metal catalysts.<sup>4</sup> In this thesis, transition metal catalyzed hydrosilation will be focused on.

Bart reported a new Fe(0) complex (Figure 94) that is efficient and regioselective for hydrosilation of terminal alkenes with PhSiH<sub>3</sub> and Ph<sub>2</sub>SiH<sub>2</sub>. After hydrosilation, styrene will only go to the terminal hydrosilation product (Scheme 12). This research showed how new ligands can be helpful for modulating metal activity, and how non-precious metals can effectively catalyze hydrosilation.<sup>224</sup>



**Scheme 12:** Exclusive terminal hydrosilation product.

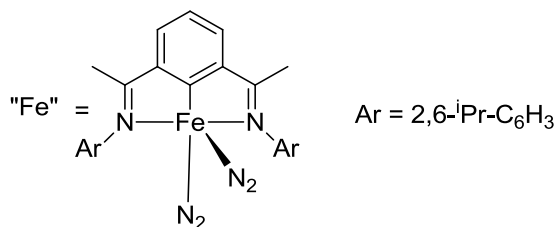


**Figure 94:** Fe complex for hydrosilation

Platinum catalysts, such Karstedt's catalyst, are very efficient in hydrosilation reactions.<sup>225-228</sup> [Cp\*Ru(MeCN)<sub>3</sub>][PF<sub>6</sub>] is very efficient for the hydrosilation of alkynes, with mainly  $\alpha$ -addition products.<sup>229-233</sup> Many other transition metals can also be used in hydrosilation, including Pt,<sup>234</sup> Fe,<sup>224</sup> Ru,<sup>235, 236</sup> Os,<sup>237</sup> Rh,<sup>238, 239</sup> Ir,<sup>240, 241</sup> and Ni.<sup>242</sup> However, for such a widely used reaction, there are still problems with hydrosilation catalyst design, especially in terms of stereoselectivity, partly because it is hard to isolate and characterize the extremely reactive intermediates. The commonly accepted mechanism for the hydrosilation was proposed by Chalk and Harrod, who made an analogy between isolated Ir complexes and their proposed reactive Pt catalyst species (Figure 95).<sup>223</sup>

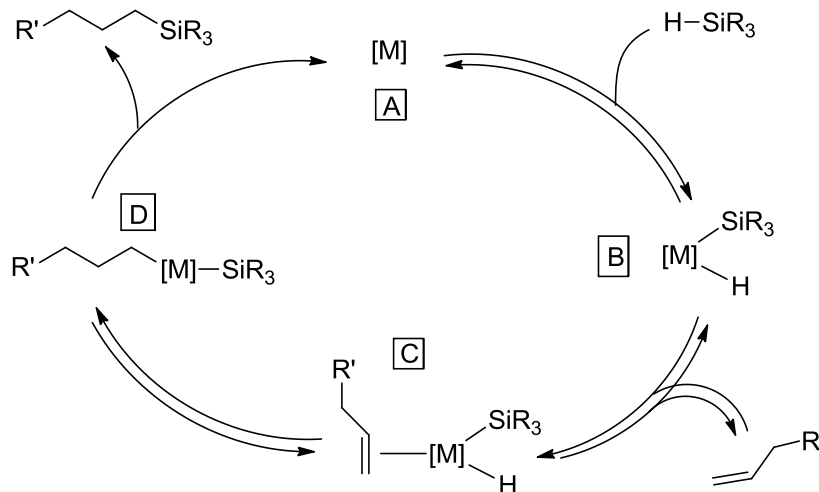
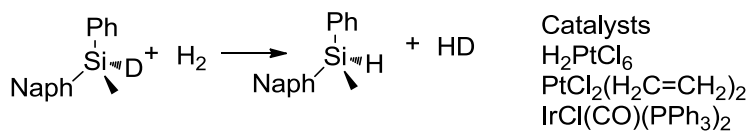


**Figure 95:** The Chalk-Harrod mechanism.

The whole catalytic cycle includes oxidative addition of Si-H to metal center, coordination of  $\pi$  bond to the metal center, ligand insertion and reductive elimination to give the product. This mechanism is simple but cannot explain a lot of experimental observations and hydrosilation by reactive metals other than Pt. For example, there is often an induction period;<sup>223</sup> oxidative addition of Si-H into metal center occurs with retention of configuration at Si (Scheme 13);<sup>211</sup> and the formation of vinylsilanes cannot be explained.



**Scheme 13** Oxidative addition of Si-H into metal center occurs with retention of configuration at Si.

Therefore, there are many modified Chalk-Harrod mechanisms proposed.

These modified mechanisms in which the order of some steps are changed can explain the formation of vinylsilanes.<sup>243</sup> Another type of possible active intermediates are silylenes. Tilley's group reported reversible 1,2-migration of hydrogen between Pt and Si which indicated a possible Pt-silylene intermediate.<sup>244</sup> They also observed unusually selective hydrosilation of olefins with primary silanes without by-product when using a Ru=Si based catalyst as precatalyst (Figure 96).<sup>245</sup>

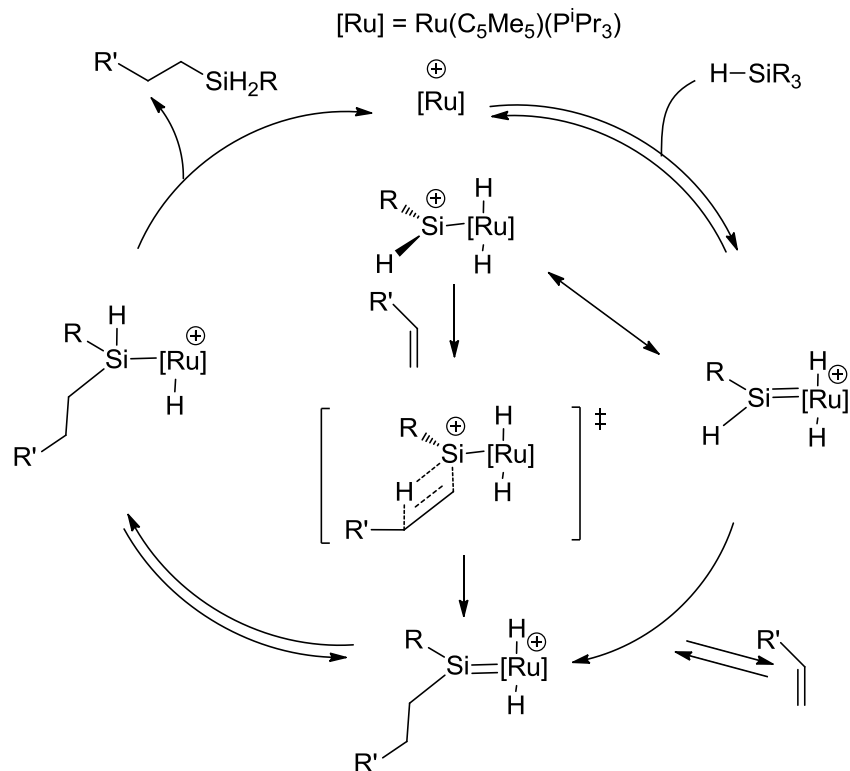
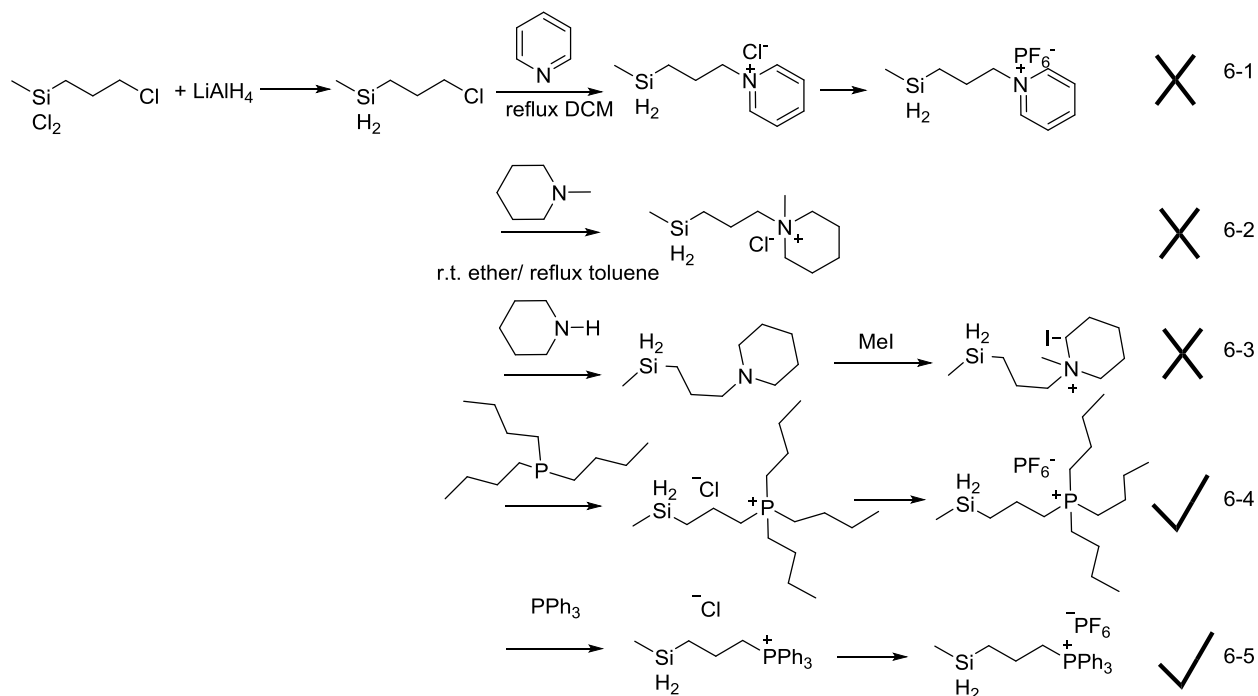


**Figure 96:** Proposed Ru-silylene-based catalytic cycle.

These are just a very small part of the whole mechanism investigation of hydrosilation research, and many new research results were published recently. However there are still many problems unexplainable so far, the understanding of catalytic cycle based on currently scientific methodology has been very slow and design of a good asymmetric catalyst is still largely dependent on “a mixture of luck, intuition and perseverance”.<sup>246</sup> It is necessary to get new techniques involved in the area.

## 6.2 Results and Discussion

For synthesizing charged hydrosilanes, different synthetic routes were attempted. (Scheme 14) Compound **6-4** and **6-5** are stable and easy to prepare, and Figure 97 shows the X-ray crystal structure of **6-5**.



**Scheme 14:** Attempted routes for making charged silane substrates.

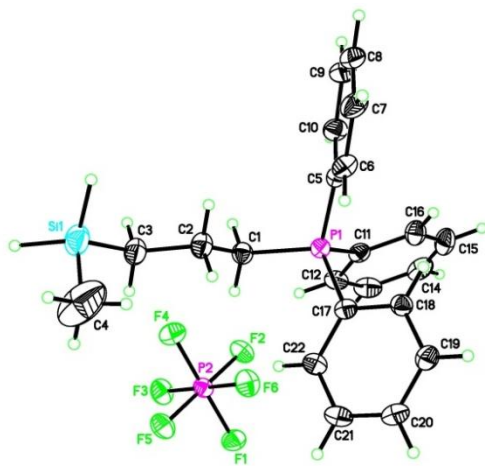


**Figure 97:** X-ray crystal structure of compound 6-5.

With the synthesized charged substrate **6-5**, PSI-ESI-MS<sup>89</sup> was used as sampling method. Comparing with syringe pump sampling method, PSI-ESI-MS gives much better results, and it can monitor the whole reaction from the very beginning. Figure 98 shows the reaction investigated. By adding 10 equivalents of di-*n*-hexylsilane, the chance of double charged species is decreased, the Si-Si chain can grow longer, and the concentration of the charged species is kept reasonably low.

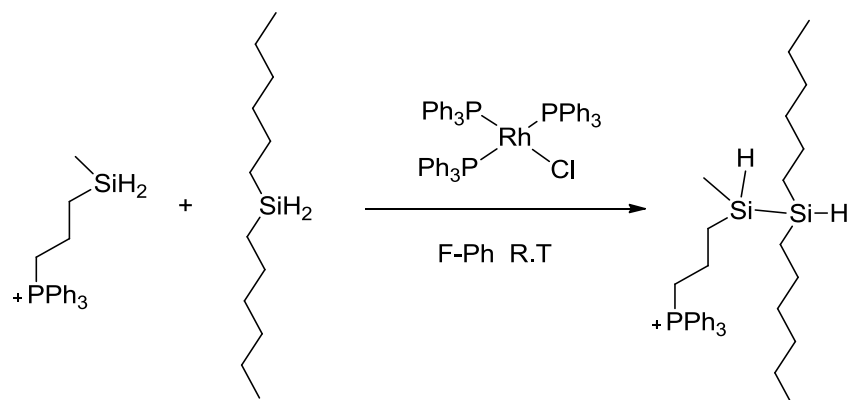


**Figure 98:** Dehydrocoupling of silanes catalyzed by Wilkinson's catalyst,  $\text{RhCl}(\text{PPh}_3)_3$ .

However, the reaction did not go well at the beginning of the project, the biggest issue was hydrolysis. Before we upgraded our drying technique, the reaction was repeated many times and always ended up with the hydrolysis of the silane (Figure 99, Figure 100).

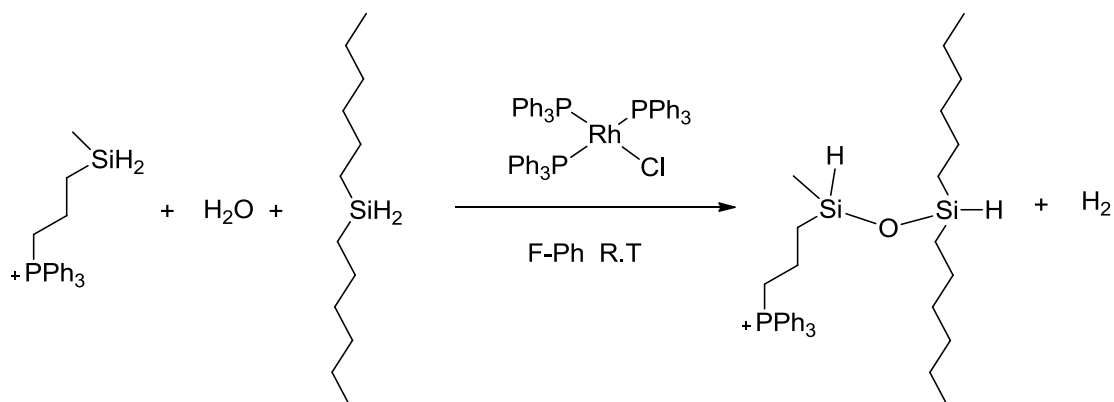


**Figure 99:** Hydrolysis of silanes catalyzed by Wilkinson's catalyst,  $\text{RhCl}(\text{PPh}_3)_3$ .

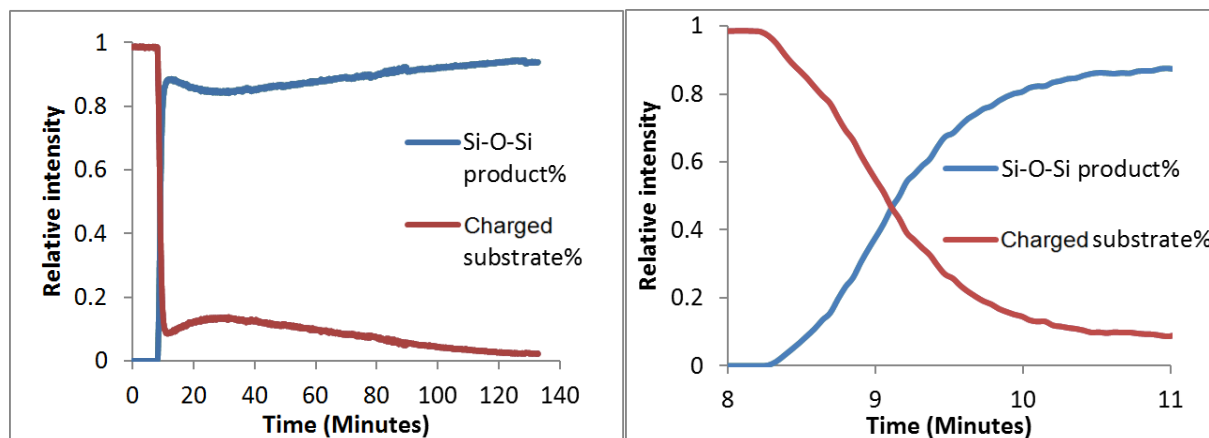
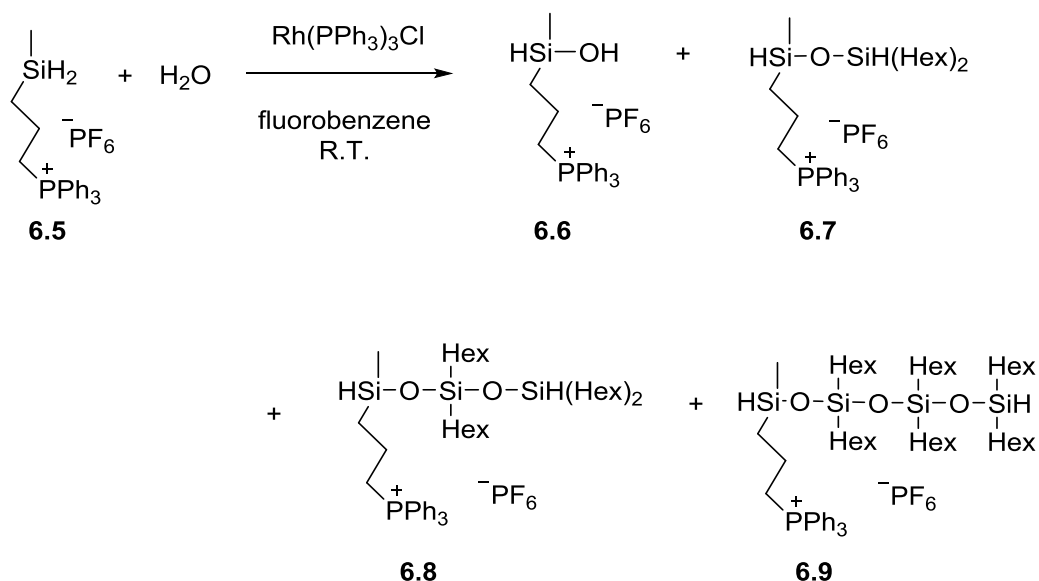


**Figure 100:** PSI-ESI-MS online monitoring result of hydrolysis of silane. Left: whole reaction process over 130 minutes. Reaction started when  $\text{RhCl}(\text{PPh}_3)_3$  was introduced into reaction system around the 8th minute. Right: enlarged graph of converting part. The whole reaction finished in 3 minutes.

In some cases, more water existed in solvent and with 20 equivalents of dihexylsilane, polysiloxane was produced (Equation 4). With PSI-ESI-MS, we are able to track the behavior of each species in the polymerization process. The starting silane was hydrolyzed first and then quickly converted into **6-7** and when the intensity of **6-7** started to drop, the polysiloxane chain started getting longer.



**Equation 4:** Hydrolysis of silanes by Wilkinson's catalyst  $\text{RhCl}(\text{PPh}_3)_3$ .



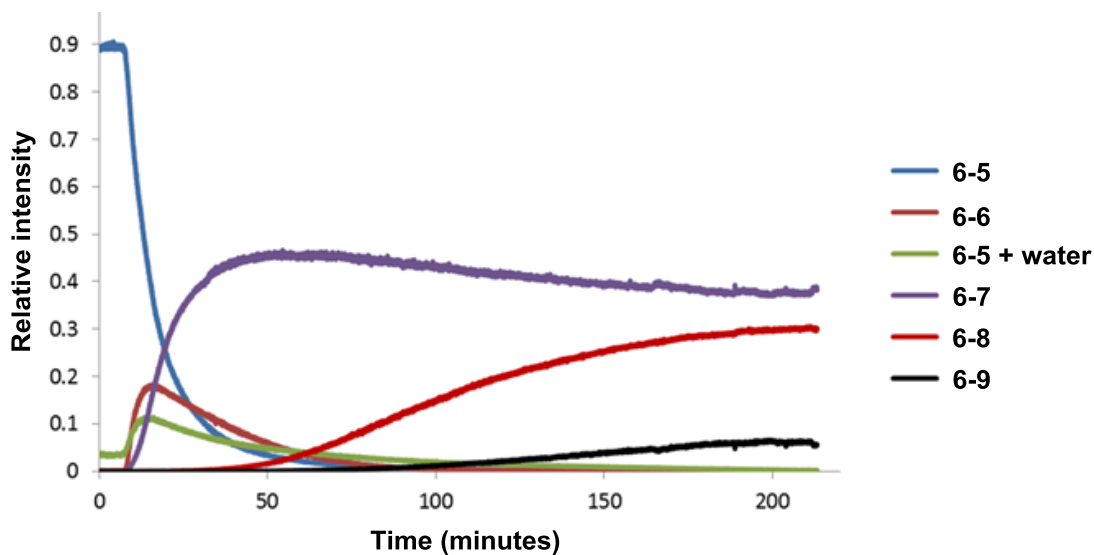


**Figure 101:** PSI-ESI-MS online monitoring result of hydrolysis of silane. Whole reaction process was over 210 minutes. Reaction started when  $\text{RhCl}(\text{PPh}_3)_3$  was introduced into reaction system around the 10th minute.

During the investigation of alkyne hydrosilation, a similar hydrolysis reaction was recorded (Figure 102, Figure 103). The oligomerization reaction kept going on as long as water was present.

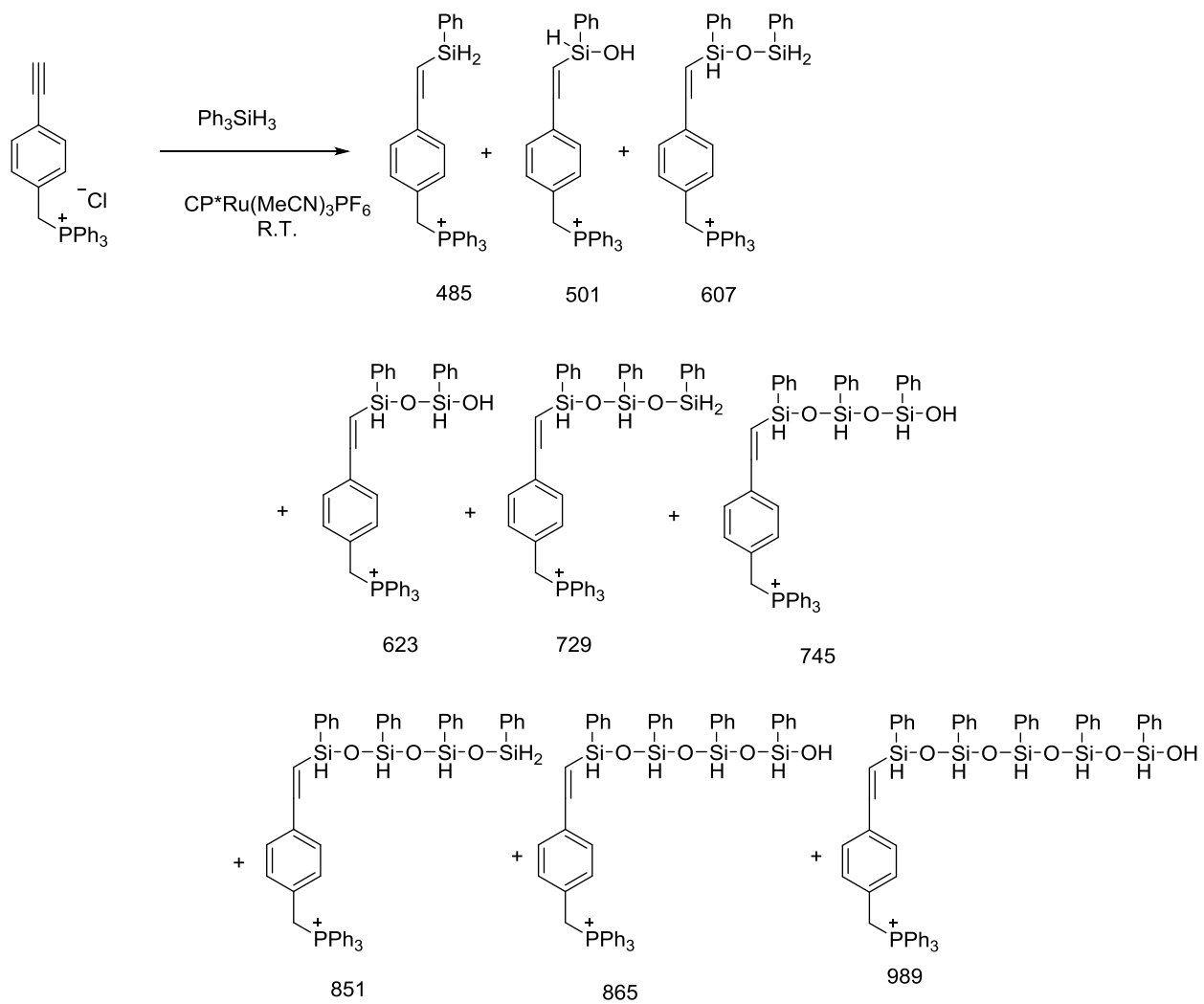


**Figure 102:** Hydrolysis of silanes, even longer oligomer products were detected.

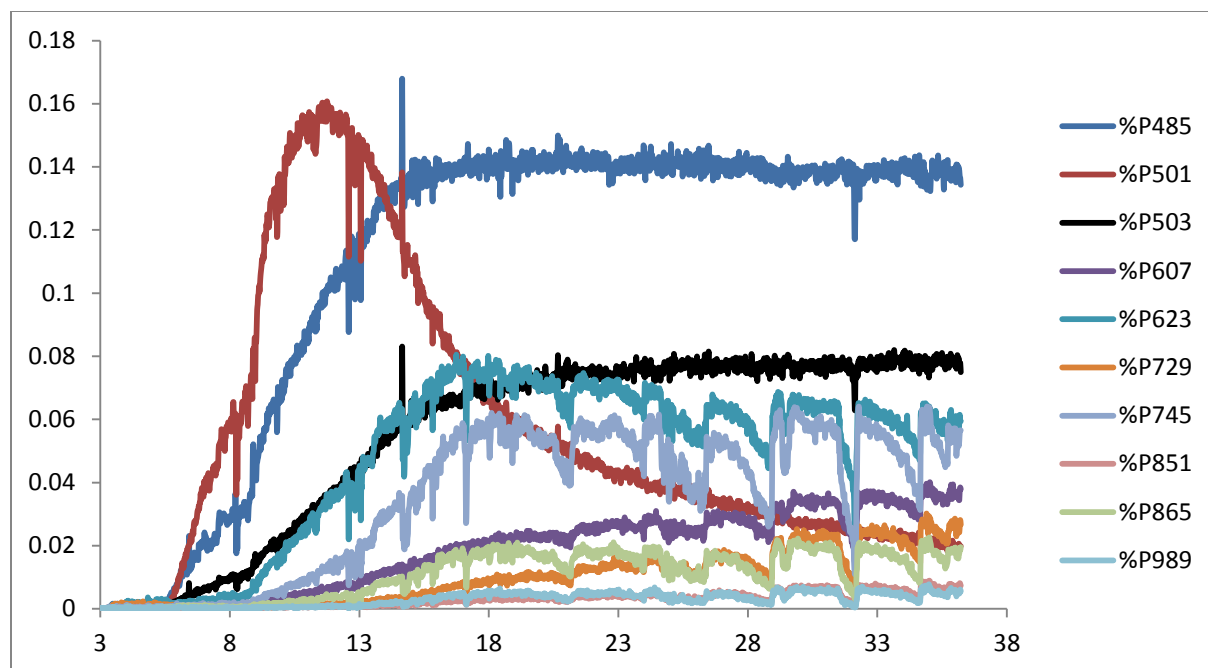


**Figure 103:** PSI-ESI-MS online monitor of hydrolysis of silane by  $[\text{Cp}^*\text{Ru}(\text{MeCN})_3][\text{PF}_6]$ . The data quality is poor because the PEEK tubing was partially blocked by large molecular weight oligomer products.

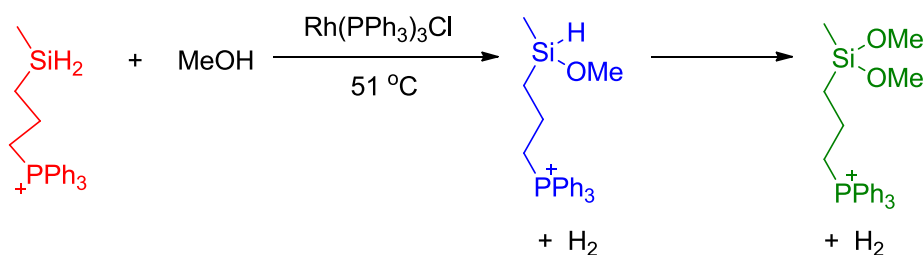
Target product %P485 is stable with water, no hydrolysis of silane.

As we are using small amounts of substrate, after calculation, 10  $\mu\text{g}$  of water is one molar equivalent to the silane we use in the reaction. If we use 10 g of solvent from solvent purification system (SPS), and it will contain 5 ppm of water, that is 50  $\mu\text{g}$  of water, which is 5 equivalents. So the solvent we use has to be 50 to 100 times drier than SPS solvent. So we set up a constant still with  $\text{CaH}_2$  as drying reagent to dry fluorobenzene. After distillation we use activated molecular sieve to store the distilled solvent for another 48 hours before use. By doing this, there is no more water problem.

However, dehydrocoupling of silanes reaction did not work between charged silane **6-5** and phenylsilane with Wilkinson's catalyst but gas generated during the process indicating dehydrocoupling of phenylsilane itself and  $\text{H}_2$  was produced. As phenylsilane is a primary silane, its reactivity is higher than the secondary silane **6-5**. So the dehydrocoupling of silanes reaction preferred to happen between two primary silanes.

As seen in Figure 101, the secondary silane **6-5** has higher reactivity with the O-H bond in water than the Si-H bond in silane, we assume it may also react with methanol as silane alcoholysis. In

order to prove this point, fluorobenzene was used as solvent with Wilkinson's catalyst, and 10 equivalents of methanol were added to the reaction.



**Equation 5:** Silane alcoholysis between **6-5** and MeOH.

Under higher temperature, the reaction finished quickly. **6-5** converted to monosubstituted silane within 30 seconds. And then it took over 10 minutes to fully convert into disubstituted silane. This could be due to steric hindrance of the first OMe group which made the second step slow down.

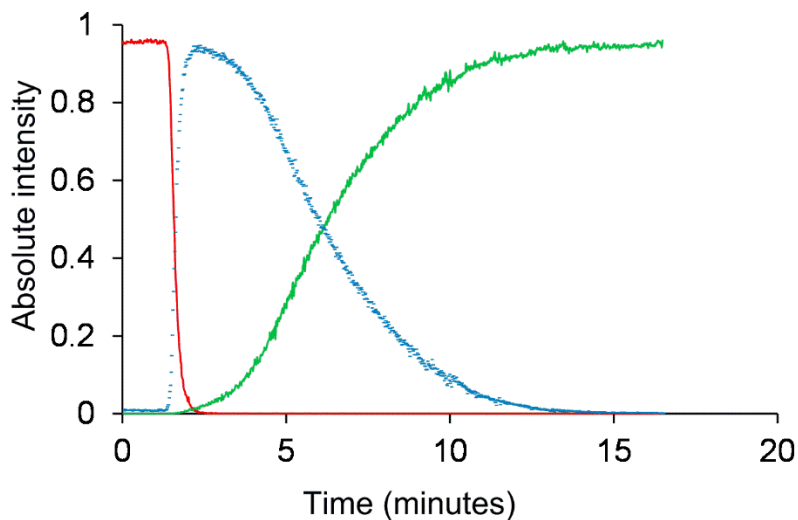
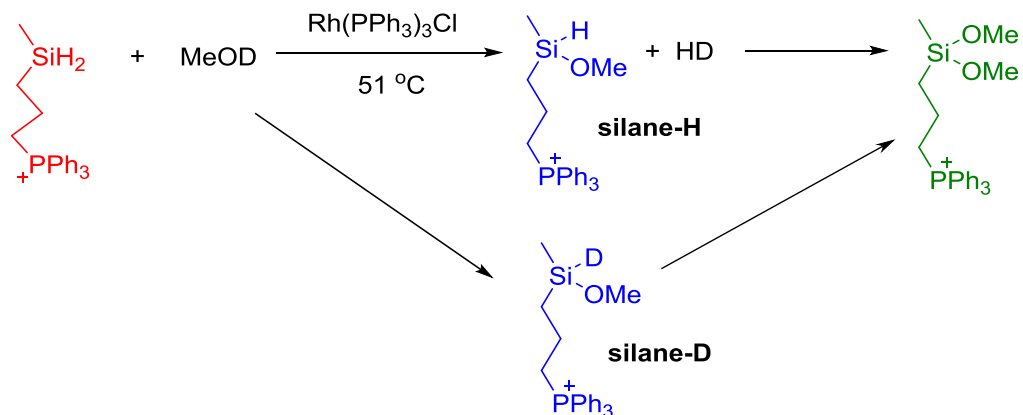


**Figure 104:** Silane alcoholysis between **6.5** and MeOH under 51 °C.

Then we looked into kinetic isotope effect by using MeOD instead of MeOH. When tracking the reaction, we found from the isotope pattern of monosubstituted silane that there is a high percentage of silane-D exists (silane-H : silane-D=1:0.6). This is due to fast proton exchange during the reaction. The first step of this KIE reaction is fast, the monosubstituted silane reached

100% within 30 seconds. But the second step took over 90 minutes, which is 8 times longer than alcoholysis with methanol.



**Scheme 15:** Silane alcoholysis between **6-5** and MeOD.

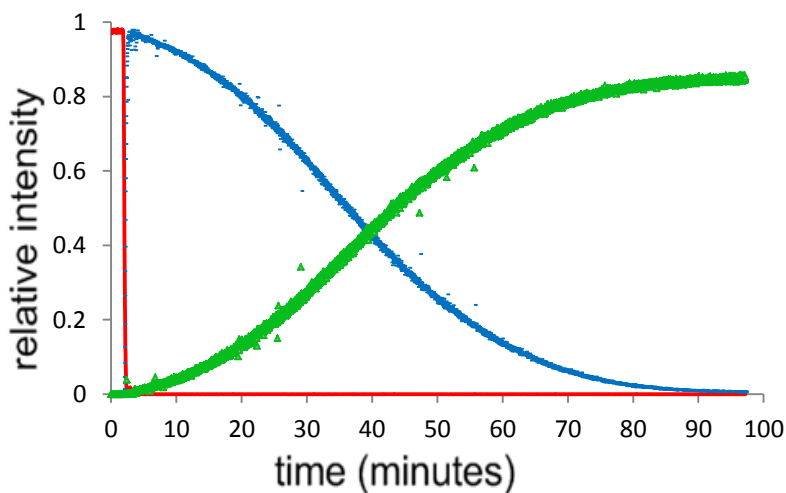


**Figure 105:** Silane alcoholysis between **6-5** and MeOD under 51 °C.

During the reaction, many intermediates were detected. A derivative of Wilkinson's catalyst,  $[\text{Rh}(\text{PPh}_3)_3]^+$  with  $m/z$  889.7 was clearly visible throughout. At the beginning of the reaction, the intensity of the peak started dropping. During the reaction, the intensity was maintained at a relatively low level, and when the reaction reached the end, the intensity started increasing as the catalyst released from the catalytic cycle.

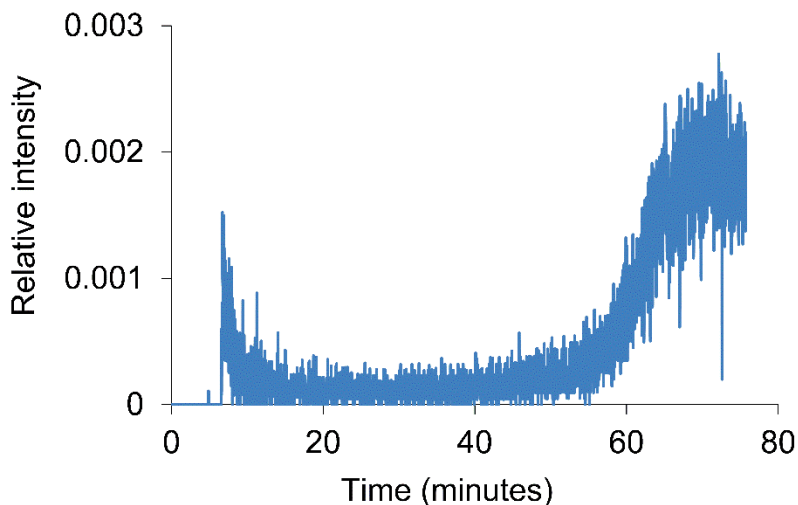


**Figure 106:** Relative intensity vs time for Wilkinson's catalyst fragment  $[\text{Rh}(\text{PPh}_3)_3]^+$  at  $m/z=889.7$ .

The behaviour of this species suggests that it is most likely a catalyst resting state.

A potential intermediate with  $m/z$  1041 was detected by tracking the time dependent behaviour of individual peaks. The peak is clearly (Figure 107) not impurity as it showed up when the reaction started, in other words when a was injected into the reaction flask. The intensity kept at stable level through the reaction and started dropping at the end of the reaction, when  $[\text{Rh}(\text{PPh}_3)_3]^+$  recovered as shown in Figure 106.

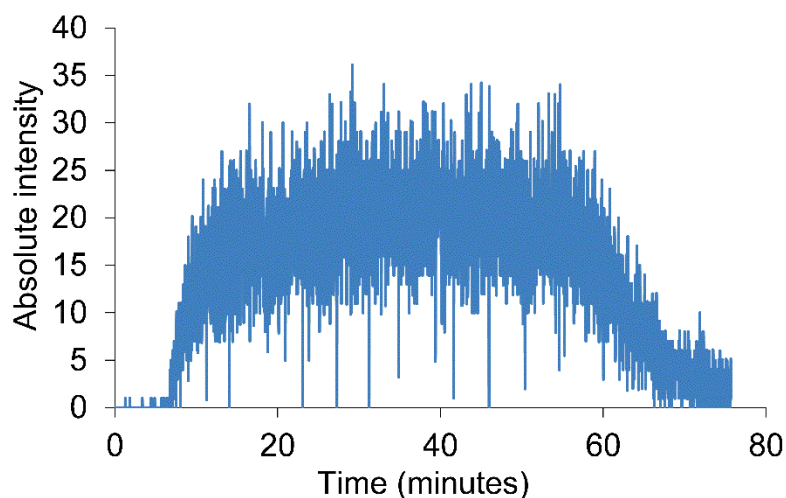


**Figure 107:** A potential intermediate of alcoholysis of silane by Wilkinson's catalyst.

The isotope pattern of the peak (Figure 108) suggests it is a mixture of two species, possible structures are shown in Figure 108.

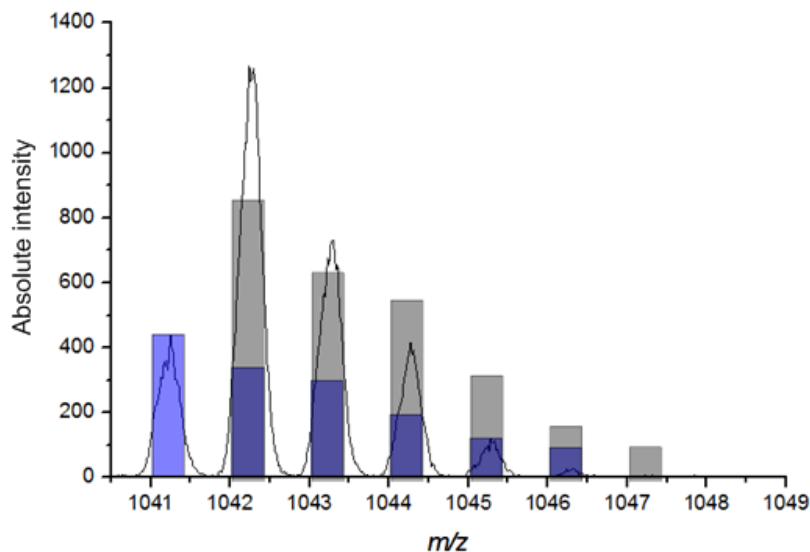


**Figure 108:** Mixture of potential intermediates, mixture of two potential intermediate with formular  $[(PPh_3)_2RhCl+MeSi(CH_2)_3PPh_3+H]^+$  (blue peaks) and  $[(PPh_3)_2RhCl+MeSi(CH_2)_3PPh_3+D]^+$  (gray peaks) at ratio 1:2.

Observation of this species and its behaviour suggests that it is most likely a catalyst resting state, that eventually is consumed when all of the substrate is gone. Because its abundance does not track with the overall rate of reaction, it is unlikely to be part of the catalytic cycle proper.

### 6.3 Future work

Si-H activation is a very difficult system to study and has to date received limited attention by ESI-MS analysis. This study provided one other report where ESI-MS can be used to get better understanding of the mechanism of these reactions. This work goes further though, in showing that by carefully designing the system to carry a charge on the substrate, meaningful data may be obtained that correlates closely with reactions that contains no charge.

One reaction that would reveal much more information of dehydrocoupling of silanes is to find or synthesize a secondary silane which has similar reactivity as charged silane **6.5**, so the dehydrocoupling reaction will happen between these two compounds. By doing so, the chance of detecting any key intermediates will increase, and the reaction behavior and kinetics information may also be revealed.

The silane alcoholysis reaction also has great potential for studying the mechanism, characterizing different intermediates and build numerical models. Different temperature and different alcohols can be used to see the influence of functional groups. CD<sub>3</sub>OD and other deuterated alcohol can be used for study of the kinetic isotope effect.

## 6.4 Experimental

Fluorobenzene was freshly distilled from CaH<sub>2</sub> and stored over molecular sieves before use. All other solvents were dispensed from an MBraun solvent purification system (SPS) immediately before use. All reactions were under nitrogen or argon atmosphere. Chemicals and solvents were purchased from Aldrich and used without subsequent purification. All mass spectra were collected by using a Micromass Q-TOF *micro* mass spectrometer in positive ion mode using pneumatically assisted electrospray ionization: capillary voltage, 3000 V; extraction voltage, 0.5 V; source temperature, 90°C; desolvation temperature, 180°C; cone gas flow, 100 L/h; desolvation gas flow, 100 L/h; collision voltage, 2 V (for MS experiments); collision voltage, 2-80 V (for MS/MS experiments); MCP voltage, 2700 V.

**ESI-MS reaction monitoring using pressurized sample infusion.** A Schlenk flask was used for these experiments, as described elsewhere.<sup>89, 90</sup> A solution of [6.5][PF<sub>6</sub>] (5-10 mg, 0.010-0.020 mmol) was monitored using the PSI-ESI-MS setup. The Schlenk flask was pressurized to 3 psi using 99.999% purity N<sub>2</sub> gas or Ar gas. Wilkinson's catalyst, Rh(PPh<sub>3</sub>)<sub>3</sub>Cl (1-4 mg, 0.0011-0.0043 mmol) was dissolved in 1 mL of fluorobenzene and injected into the PSI flask via a septum. The solution end of PEEK tubing was protected with a cannula filter system to avoid the tube being blocked by any insoluble by-products. Data were processed by normalizing the abundance of each species to the total ion count of all species identified as containing the tag. No smoothing of the data was performed.

**Dihexylsilane.** LiAlH<sub>4</sub> (6.2 g, 163.0 mmol) and 200.0 ml of tetraglyme were introduced into a three neck round bottom flask. Di-n-hexyldichlorosilane (25.0 ml, 81.5 mmol) was introduced into the same flask dropwise over 30 minutes in ice bath. The reaction was stirred at room temperature overnight. The mixture was vacuum distilled and the product fraction collected at



65-75°C. The final product was a colorless transparent liquid (13.9 g, 69.5 mmol, 85%).  $^1\text{H}$  NMR ( $\text{CDCl}_3$ ):  $\delta$  (ppm) 1.53 (s, 2H); 1.25 (m, 12H); 0.86 (m, 10H).

**6-5. Cl (3-(methylsilyl)propyl)triphenylphosphonium chloride.**  $\text{LiAlH}_4$  (5.0 g, 131.4 mmol) was introduced into a round bottom flask, 200.0 ml of ether was added, dichloro(3-chloropropyl)(methyl)silane (12.0 ml, 76.1 mmol) was added dropwisely into the flask in icebath. The reaction was stirred overnight, filtered under  $\text{N}_2$  protection, distilled under atmospheric pressure, and the fraction with boiling point 115 – 118°C was collected. 2.0 g of the liquid product and  $\text{PPh}_3$  (4.3 g, 16.4 mmol) was stirred in toluene for 96 hours at 108°C. The final product was filtered off as a white powder. ESI-MS(+)  $m/z$  349.5.

**6-5.  $\text{PF}_6$  (3-(methylsilyl)propyl)triphenylphosphonium hexafluorophosphate(V).** Dissolve **6-5 Cl**. (1.0 g, 2.6 mmol) in water and add  $\text{NaPF}_6$  (0.65 g, 3.9 mmol) stir for 10 minutes and filter. Dry at 70°C under high vacuum for 14 days. The final product is a white powder (0.43 g, 0.87 mmol, 34% ).  $^1\text{H}$  NMR ( $\text{CDCl}_3$ ):  $\delta$  (ppm) 7.74 (m, 2H); 7.63 (m, 8H); 7.26 (m, 5H); 3.56 (m, 2H); 3.19 (m, 2H); 1.65 (m, 2H); 0.95 (m, 2H); 0.02 (m, 3H); ESI-MS(+)  $m/z$  349.5.

## 7. Collaborative studies

Portions of this chapter have been previously published, and are reproduced in part with permission from “Copper-Mediated Fluorination of Arylboronate Esters. Identification of a Copper(III) Fluoride Complex” P. S. Fier, J. Luo and J. F. Hartwig, *Journal of the American Chemical Society*, 2013, 135, 2552-2559. Copyright © 2013 American Chemical Society

I performed all experimental work, produced all figures and co-wrote the paper with JS McIndoe and collaborators. Publications are under preparation.

As the importance of organometallic compounds increase every day, more and more air and moisture sensitive catalysts and molecules are synthesised. Scientists are seeking new ways to understand the behaviour and reactivity of their systems, and ESI-MS can often provide new and complementary information. Follow-up analyses may include MS/MS experiments that can provide further characterization of species of interest. However, many groups lack the infrastructure and expertise to conduct the necessary experiments, and seek to collaborate with us to provide unique insights. This chapter provides brief accounts of some of these collaborations; so far one paper has been published<sup>247</sup> and more are on the way.

### 7.1 CdSe-DHLA for H<sub>2</sub> production

Professor Patrick Holland and Professor Richard Eisenberg from the University of Rochester have been working on hydrogen production system by using water as solvent at pH 4.5, ascorbic acid (AA) (0.5-1 M) as the sacrificial donor, CdSe quantum dot (4.0 μM) capped with dihydrolipoic acid (DHLA ~400 μM) as the photosensitizer, and Ni(NO<sub>3</sub>)<sub>2</sub> (4.0 μM) as the pre-catalyst. Lots of work had been done to prove that the Ni was not attached to the CdSe. The hypothesis was that the Ni<sup>2+</sup> forms a complex with DHLA, which has been shown to be able to detach from CdSe under photolysis, but it was not known how much DHLA came off the CdSe surface and how it coordinated to the Ni<sup>2+</sup>.

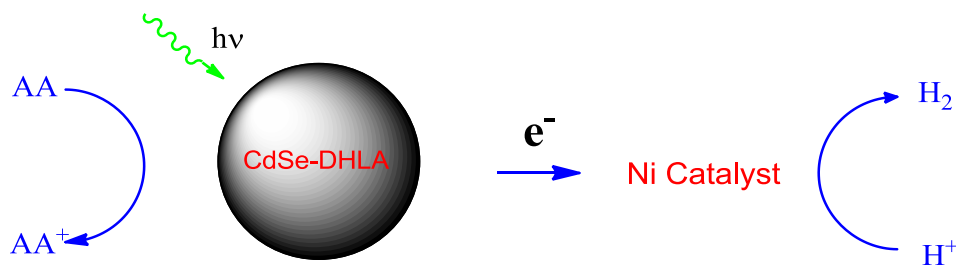


**Figure 109:** CdSe-DHLA for H<sub>2</sub> production.

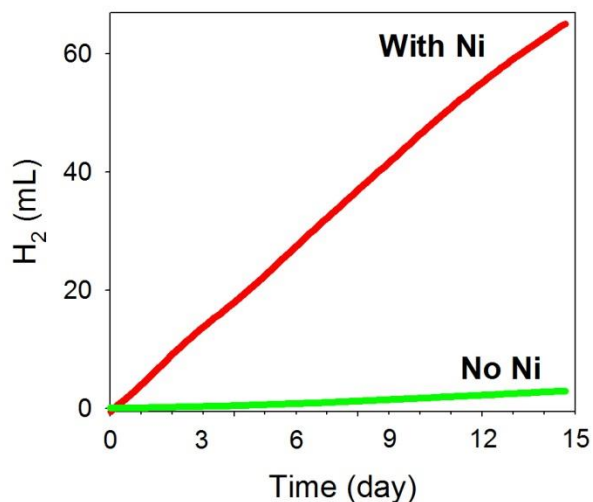


**Figure 110:** Difference between adding and not adding Ni in the hydrogen production system.

Four samples were provided as shown in Table 6, for which reasonably strong signals in methanol as solvent were obtained under anaerobic conditions, and MS/MS data were collected to assist in assignments. Ni has a characteristic isotope pattern, but there was little evidence of it. Any complex with Ni in it will be dominated by peaks 2 mass units apart (assuming a 1+ ion). There were hundreds of peaks, but they contained mostly C, H, N, O, and S (or other largely monoisotopic elements). There were some that looked like they might contain Ni, but they could also be coincidental overlap of two simpler patterns. At higher masses, the baseline was filled with low intensity peaks all over the spectrum. In ESI-MS, these peaks correspond to real species, and are characteristic of complex mixtures with large numbers of species with overlapping isotope patterns. In this case, it could be CdSe NPs with differing amounts of Cd, Se, Ni etc. Sample C is different from the other 3 and contains a lot of doubly charged species (the peaks in the isotope pattern were only  $m/z$  0.5 apart which indicates a double charge)

**Table 6:** Samples for CdSe-DHLA for H<sub>2</sub> production

|          | Ascorbic Acid | CdSe-DHLA  | Ni(NO <sub>3</sub> ) <sub>2</sub> | pH  | Reaction Time<br>(hv > 450 nm) |
|----------|---------------|------------|-----------------------------------|-----|--------------------------------|
| Sample A | 16 μM         | 4 μM       | 4 μM                              | 4.5 | 1 hour                         |
| Sample B | 16 μM         | 4 μM       | 4 μM                              | 4.5 | 5 hour                         |
| Sample C | 0.3 M         | 4 μM       | 4 μM                              | 4.5 | 5 hour                         |
| Sample D | 16 μM         | 20 μM DHLA | 4 μM                              | 4.5 | N/A                            |

After the disappointing results, samples contain only Ni and DHLA were tested (Table 7). A strong signal for the disulfide rather than for the dithiol was observed, suggesting that oxidation to the disulfide had occurred, precluding observation of DHLA/Ni complexes.

**Table 7:** Samples with Ni and DHLA only

|          | Ascorbic Acid | DHLA  | Ni(NO <sub>3</sub> ) <sub>2</sub> | solvent                   | pH |
|----------|---------------|-------|-----------------------------------|---------------------------|----|
| Sample A | 200μM         | 100μM | 20μM                              | 1:1 EtOH/H <sub>2</sub> O | 5  |
| Sample B | 200μM         | 100μM | 20μM                              | 1:1 EtOH/H <sub>2</sub> O | 6  |
| Sample C | 200μM         | 100μM | 0                                 | 1:1 EtOH/H <sub>2</sub> O | 5  |
| Sample D | 0             | 0     | 20μM                              | 1:1 EtOH/H <sub>2</sub> O | 5  |

After preparation of fresh samples in our lab, no Ni-containing species could be observed, but only an insoluble orange suspension was formed. The lack of Ni-containing species suggested that it was locked up in the precipitate. The conclusion was that the nickel present in the hydrogen production system was not free in solution, but instead was intimately involved with the CdSe nanoparticles. Our negative results meant that our work did not appear in the final paper,<sup>248</sup> but the referees were convinced that all possible attempts had been made to identify the key species by ESI-MS.

## 7.2 Fe<sub>4</sub>S<sub>4</sub> clusters

Professor Patrick Holland and coworkers from the University of Rochester (now Yale) have been working on synthetic FeS clusters. These clusters had been stored in a glovebox over four years until they crystallized. Since most of these compounds do not have any proton, have broad UV-vis spectra, and are air and moisture sensitive, ESI-MS is a good candidate for characterizing them.

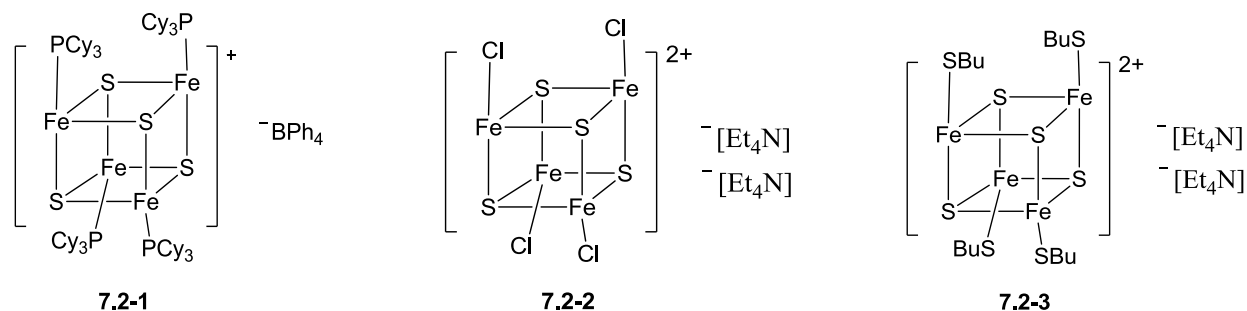


**Figure 111:** FeS cluster samples

MS of the samples, including some MS/MS on each of the clusters have been obtained (Figure 112-115), and we got good data on all of them (see supporting information for particularly nice MS/MS, in which we see clean loss of all 4 PCy<sub>3</sub>, Cy = tricyclohexylphosphine). The results are an indication of why they need gentle conditions - even using our SOP, we see a lot of free [PCy<sub>3</sub> + H]<sup>+</sup> from ligand dissociation.

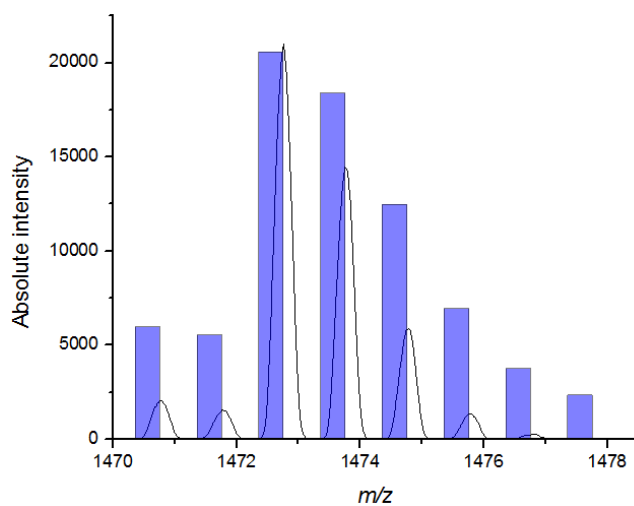


**Figure 112:** MS of the Fe<sub>4</sub>S<sub>4</sub>(Cy<sub>3</sub>)<sub>4</sub> cluster, the blue bar is the calculated isotope pattern, the line is the experimental data.

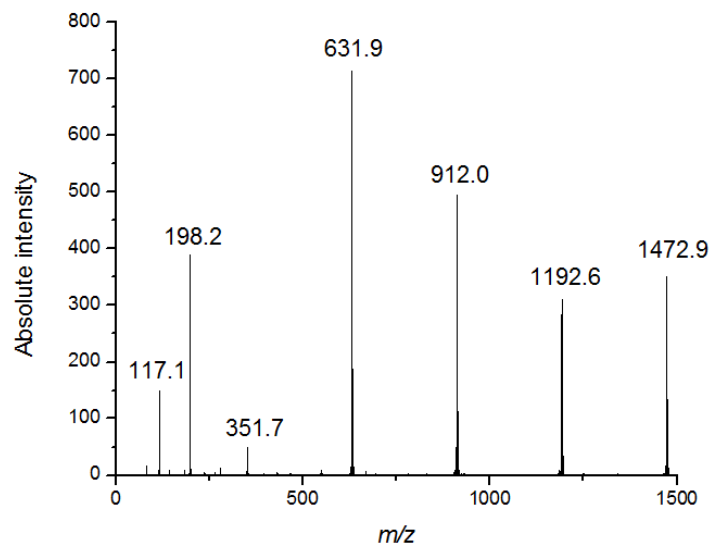


**Figure 113:** MS/MS of the **7.2-1**. We can see many fragments of the mother ion-1472.9, the daughter ions: 1192.6, 912.0, 631.9 and 351.7 are due to lose of  $\text{PCy}_3$ .

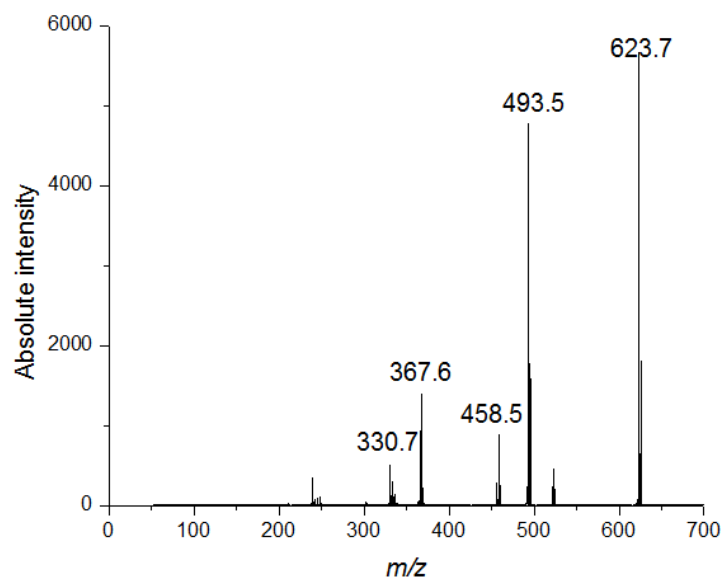


**Figure 114:** MS/MS of the **7.2-2**, 623.7 is  $[\mathbf{7.2-2} + \text{Et}_4\text{N}]^+$ , 493.5 is **7.2-2**, 458.5 is  $[\mathbf{7.2-2} - \text{Cl}]^+$ .

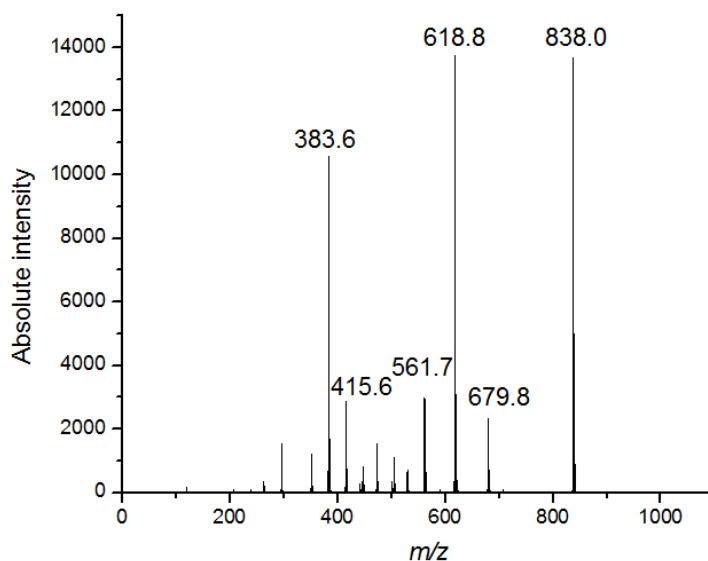


**Figure 115:** MS/MS of **7.2-3**, 838.0 is  $[\mathbf{7.2-2} + \text{Et}_4\text{N}]^+$ , 618.8 is  $[\mathbf{7.2-2} - \text{SBU}]^+$ , 383.6 is  $[\mathbf{7.2-2} - 3^*\text{SBU}]^+$

The  $[\text{Fe}_4(\text{SBU})_4]^{2-}$  dianions have more complicated spectra than the cation, because ionization can proceed in different ways, i.e.  $\text{X}^-$  loss to form  $[\text{M-X}]^-$  monoanions, and aggregation with a cation to form  $[\text{M} + \text{cation}]^-$  monoanions, as well as just the  $[\text{M}]^{2-}$  dianions. MS/MS were done of the highest  $m/z$  species only. The only puzzling aspect was the appearance of additional ions at 24 Da above the main species for the  $[\text{Fe}_4(\text{SBU})_4]^{2-}$  cluster. This is an unusual increment, and it probably does not mean addition of a small molecule, but rather a substitution (i.e. exchange of SBU for something 24 Da heavier than SBU). This species remained unassigned as an unknown impurity. This work has not yet been published.

### 7.3 Lactide polymerization by cationic zinc complexes

Professor Paul Hayes and coworkers from University of Lethbridge have been investigating lactide polymerization by cationic zinc complexes.<sup>249</sup> The air and moisture sensitive nature of their catalysts makes it hard to identify intermediates during the polymerization process.

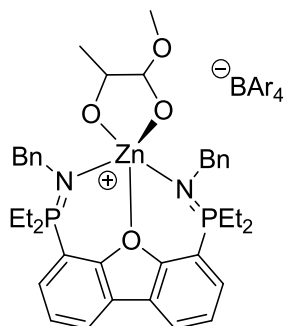


**Figure 116:** Structure of the cationic zinc complex.

At first, we successfully identified the complex by using positive mode of ESI-MS under inert atmosphere.

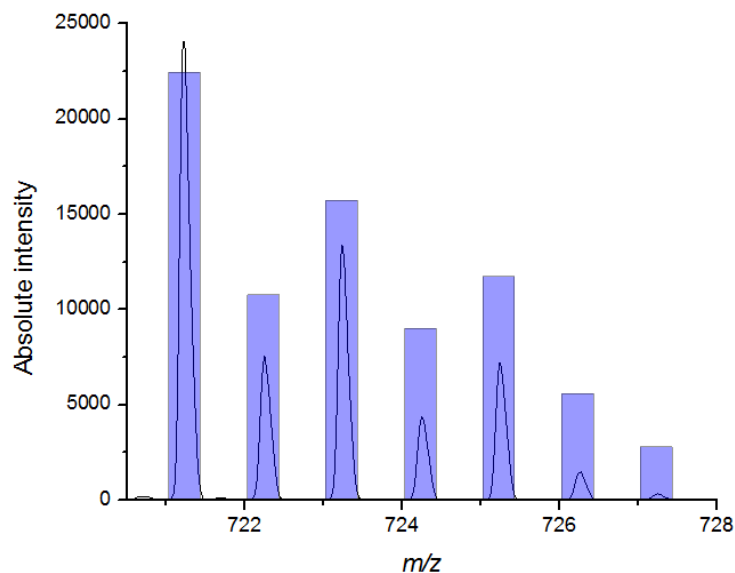


**Figure 117:** MS data of the Zn complex and the calculated isotope pattern (blue bars).

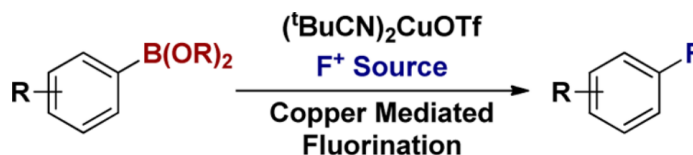
The polymerization reaction was initiated by injecting 5 to 200 equivalents of lactide to one equivalent of the Zn catalyst. When lactide was introduced into the reaction flask, the Zn complex disappeared and many new peaks showed up. A few of the peaks contained Zn, and many of them contained a repeating lactide unit. This means the polymerization reaction initiated. However the Zn containing species had very low intensity which made it difficult to identify the possible combinations. The species containing no Zn were identified as the ligand with hydrolyzed lactide. At this time, solvent from the SPS was being used, but as previously mentioned, SPS solvent contains enough water to kill a water sensitive reaction because of the low concentration of reactants. The system has not been reinvestigated for lack of sample and the



fact that the Hayes group has moved on from this catalyst, but any future work will require the additional drying precautions required to get the solvent to well below 1 ppm water.

#### 7.4 Copper-Mediated Fluorination of Arylboronate Esters. Identification of a Copper(III) Fluoride Complex

Professor John F. Hartwig and coworkers from University of California, Berkeley discovered a copper-mediated fluorination reaction that appears to occur via a Cu(III) fluoride complex (Scheme 16).<sup>247</sup> The species is not isolable and attempts to get a meaningful mass-spectrum with their department instrument have not been successful due, in part, to the lack of air-free equipment and the sensitivity of the copper complex to moisture.



**Scheme 16:** Copper-Mediated Fluorination of Arylboronate Esters. Reprinted with permission from “Copper-Mediated Fluorination of Arylboronate Esters. Identification of a Copper(III) Fluoride Complex” P. S. Fier, J. Luo and J. F. Hartwig, *Journal of the American Chemical Society*, 2013, 135, 2552-2559.

Copyright © 2013 American Chemical Society

The reaction was followed by ESI-MS under an inert atmosphere, by mixing a 1:1 ratio of  $(^t\text{BuCN})_2\text{CuOTf}$  and  $[\text{Me}_3\text{pyF}][\text{PF}_6]$  at room temperature, with a 1:1 ratio of THF and fluorobenzene as solvent, this was monitored for 10 minutes. The ions  $[(^t\text{BuCN})_2\text{Cu}]^+$  and  $[(\text{Me}_3\text{py})(\text{THF})\text{Cu}(\text{F})(\text{OTf})]^+$  were observed as the major peaks in the spectrum. One key intermediate with  $m/z$  424.10 was obtained and, was identified as  $[(\text{Me}_3\text{py})(\text{THF})\text{Cu}(\text{F})(\text{OTf})]^+$ .

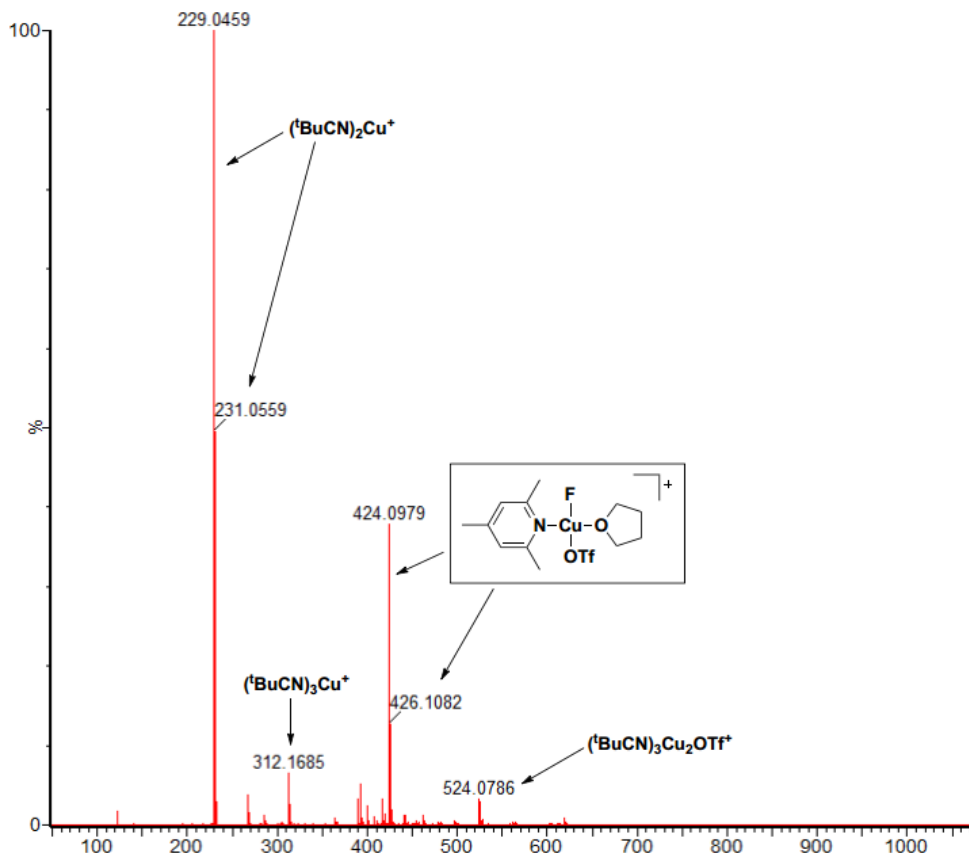
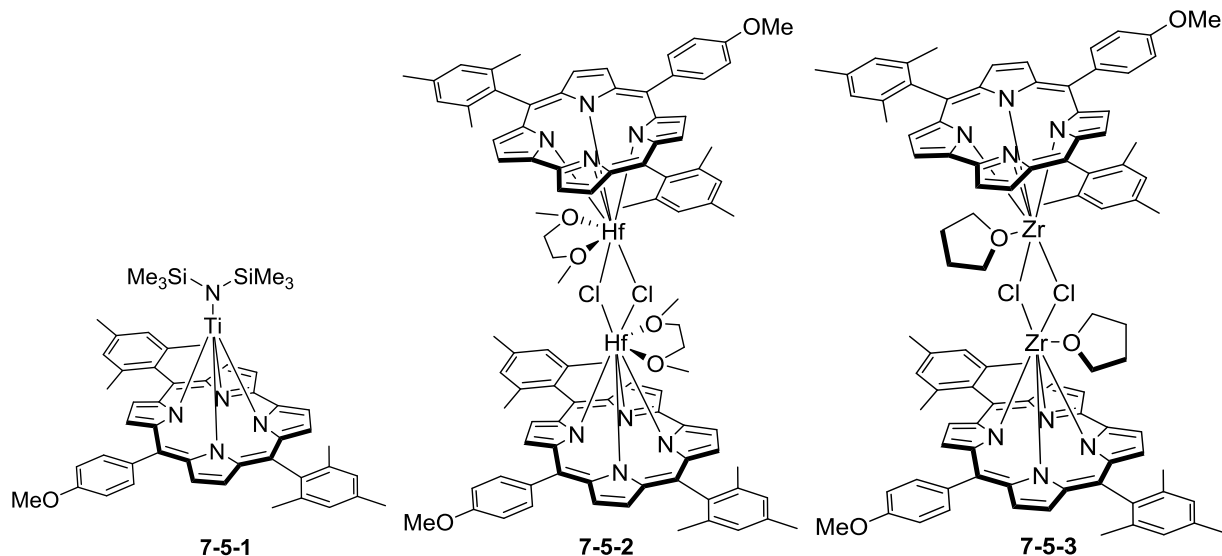


**Figure 118:** MS of intermediate in copper-mediated fluorination Reprinted with permission from “Copper-Mediated Fluorination of Arylboronate Esters. Identification of a Copper(III) Fluoride Complex” P. S. Fier, J. Luo and J. F. Hartwig, *Journal of the American Chemical Society*, 2013, 135, 2552-2559. Copyright © 2013 American Chemical Society

The result was published in the *Journal of the American Chemical Society*.<sup>247</sup>

## 7.5 Ti, Hf and Zr complexes

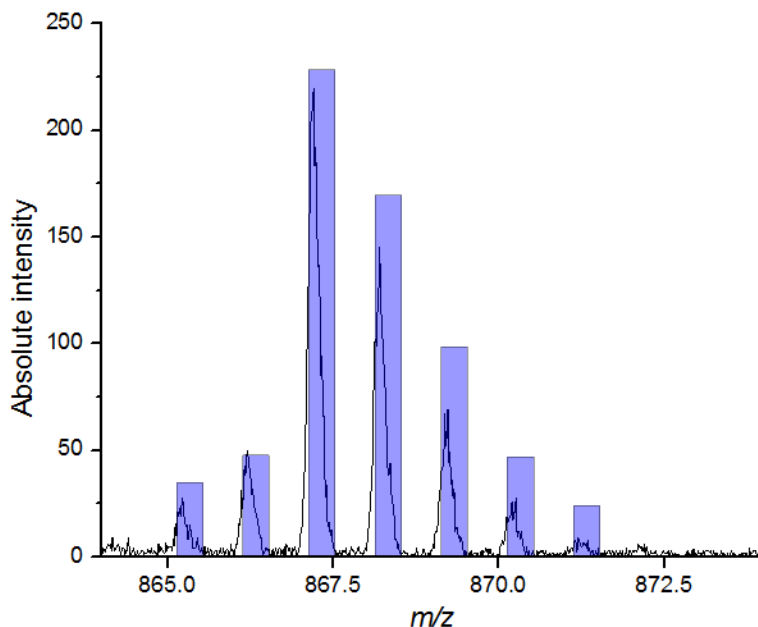
John Arnold and coworkers from University of California, Berkeley have been working on three different metal complexes (shown in Figure 119). The complexes are also air and moisture sensitive, and another challenge is that these complexes contain no charge, so theoretically they are invisible in ESI-MS.



**Figure 119:** Ti, Hf and Zr complexes

In order to characterize these compounds, inert atmosphere ESI-MS was used with  $\text{Na}[\text{BAr}^{\text{F}}_4]$  with the intention that these complexes would associate with  $\text{Na}^+$  via the methoxy functionality. By using pressurized sample vials, large Schlenk flasks could be avoided for these samples, and these vials are disposable, eliminating cross contamination.

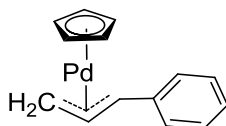
ESI-MS of **7-5-1** in positive mode generated a peak at  $m/z$  867.2, 1 off from the expected  $m/z$  868.3 for  $[\text{M}+\text{Na}]^+$  (Figure 120). For complexes **7-5-2** and **7-5-3**, only the monomer was observed instead of the dimer, suggesting that the dimer could not survive the ESI process or that the solution did not contain dimer. The Arnold group is still comprehending these results.

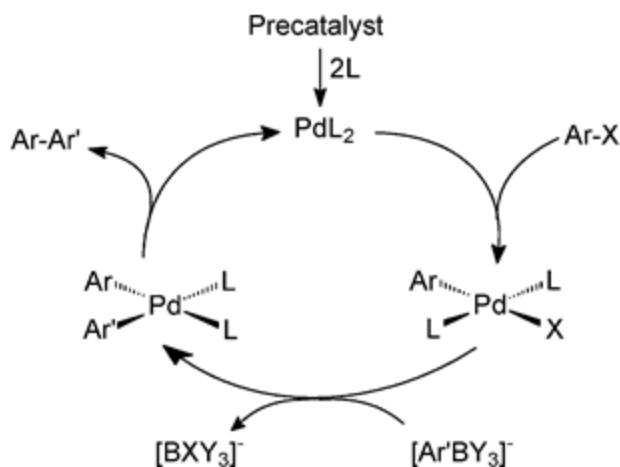


**Figure 120:** MS experimental data shows as  $[M+Na-H]^+$  of **7-5-1**, calculated isotope pattern of  $[M+Na-H]^+$

## 7.6 Unusually Effective Catalyst Precursor for Suzuki–Miyaura Cross-Coupling Reactions

Professor Michael Baird and coworkers from Queen’s University reported an unusually effective catalyst precursor for Suzuki–Miyaura cross-coupling reactions in the compound  $Pd(\eta^3\text{-1-Ph-C}_3\text{H}_4)(\eta^5\text{-C}_5\text{H}_5)$  (Scheme 17).<sup>250</sup> Addition of two equivalents of phosphine results in (presumably) reductive elimination of the allyl and cyclopentadienyl ligands. However, the exact process by which this occurred was not well understood, and the system was studied using PSI-ESI-MS using a negatively-charged and a neutral phosphine ligand.





**Scheme 17:** Widely accepted Suzuki reaction catalytic cycle.

Two ligands were investigated: **7-7-1**, a negatively charged version of the Buchwald ligand known as SPhos, and **7-7-2**, SPhos itself.<sup>251</sup>

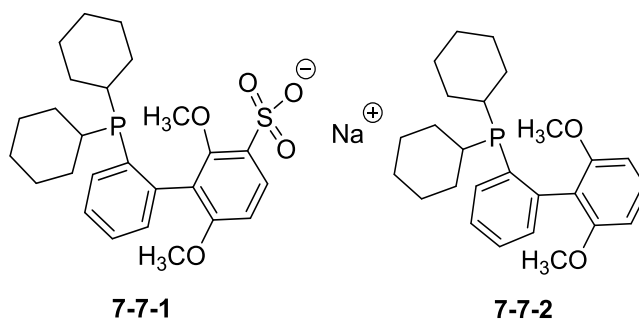


**Figure 121:** Ligands for Pd( $\eta^3$ -1-PhC<sub>3</sub>H<sub>4</sub>)( $\eta^5$ -C<sub>5</sub>H<sub>5</sub>) activation.

Addition of Pd( $\eta^3$ -1-Ph-C<sub>3</sub>H<sub>4</sub>)( $\eta^5$ -C<sub>5</sub>H<sub>5</sub>) to a solution of **7-7-1** caused the peak due to the phosphine ligand to completely disappear over the course of 20 minutes (Figure 124).

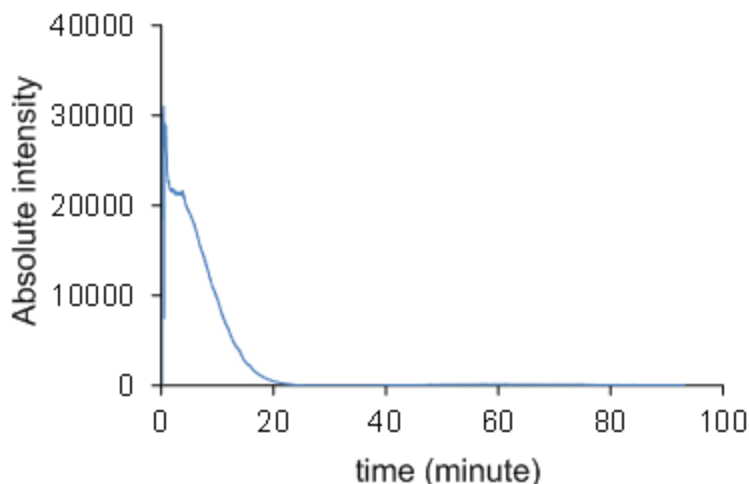


**Figure 122:** Negative mode, ESI-MS. Addition of  $\text{Pd}(\eta^3\text{-1-Ph-C}_3\text{H}_4)(\eta^5\text{-C}_5\text{H}_5)$  to charged ligand **7-7-1** makes ligand disappear over the course of about 20 minutes.

The most abundant species to appear was the expected Pd(0) catalyst,  $[\text{Pd}(\mathbf{7-7-1})_2]^{2-}$  (Figure 123), but its abundance was only a tiny fraction of that of the original ligand. This sort of disappearance of charged species suggests some sort of neutralization event. Therefore the reaction was studied again, this time with neutral Sphos, **7-7-2**.

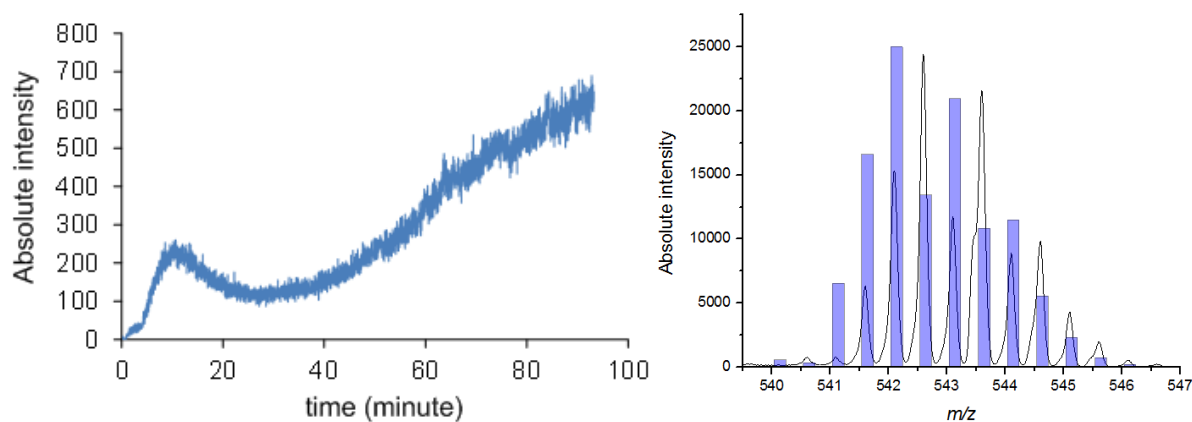


**Figure 123:**  $(\mathbf{7-7-1})_2\text{Pd}$  species is the main Pd containing peak in the reaction, however the calculated isotope pattern (blue bars) shows a extra H is present.

Addition of the neutral catalyst precursor to the neutral ligand did in fact generate charged species: one containing Pd, the cationic allyl complex  $[\text{Pd}(\eta^3\text{-1-Ph-C}_3\text{H}_4)(\mathbf{7-7-2})]^+$ , and the other the allyl phosphonium compound  $[(\text{C}_3\text{H}_4)\text{Ph}(\mathbf{7-7-2})]^+$ .

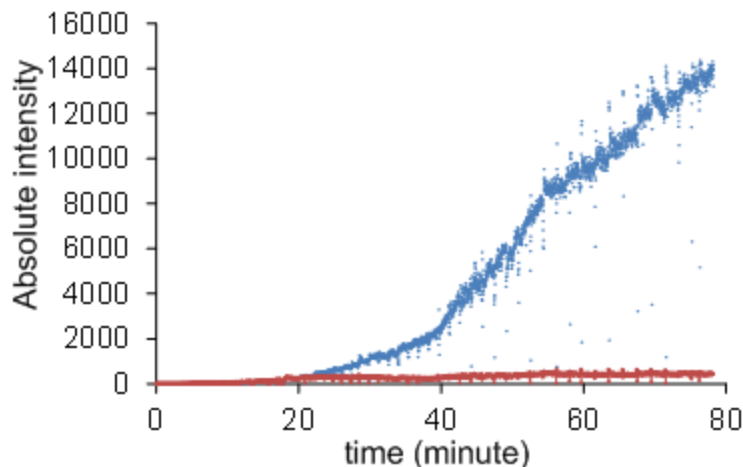
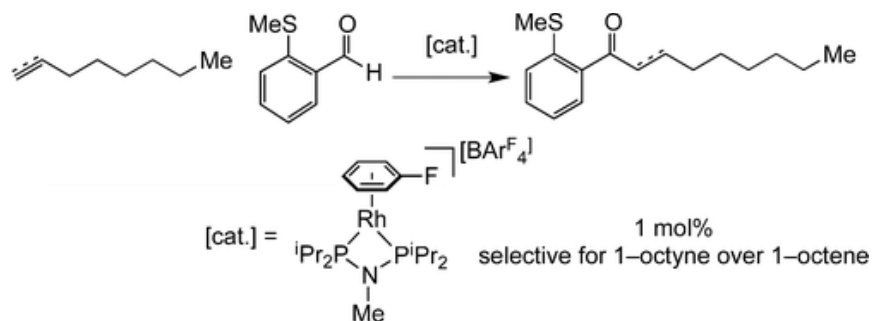


**Figure 124:** In positive mode of ESI-MS. Reaction with **7-7-2** as ligand. The blue species is  $[\text{PhC}_3\text{H}_4+\mathbf{7-7-2}]^+$ , the red species is  $[\eta^3\text{-1-PhC}_3\text{H}_4+\text{Pd}+\mathbf{7-7-2}]^+$

Formation of these complexes explains the disappearance of the anionic ligand, since both  $\text{Pd}(\eta^3\text{-1-PhC}_3\text{H}_4)(\mathbf{7-7-1})$  and  $(\text{C}_3\text{H}_4)\text{Ph}(\mathbf{7-7-1})$  would be zwitterionic and hence invisible to ESI-MS. These results leave some unanswered questions: What happens to the cyclopentadienyl ligand? Is the allyl phosphonium compound generated by reductive elimination from the Pd complex? More work is required on this system, and we await word from Queens on the complementary NMR experiments being conducted there. However, the initial PSI-ESI-MS results have provided some promising insights.

## 7.7 Rhodium complexes catalyzed hydroacylation reaction

Professor Andrew Weller and coworkers from University of Oxford have been investigating hydroacylation reaction catalyzed by rhodium complexes.<sup>22</sup> By using different chelating diphosphine ligands, the Rh complexes are efficient for reactions shown in Scheme 18. NMR studies provided evidence of the existence of some key intermediates; however, the detailed mechanism and the kinetic behavior studies of the reaction are still important for fully understanding this reaction.



**Scheme 18:** Rhodium complexes catalyzed hydroacylation reaction.

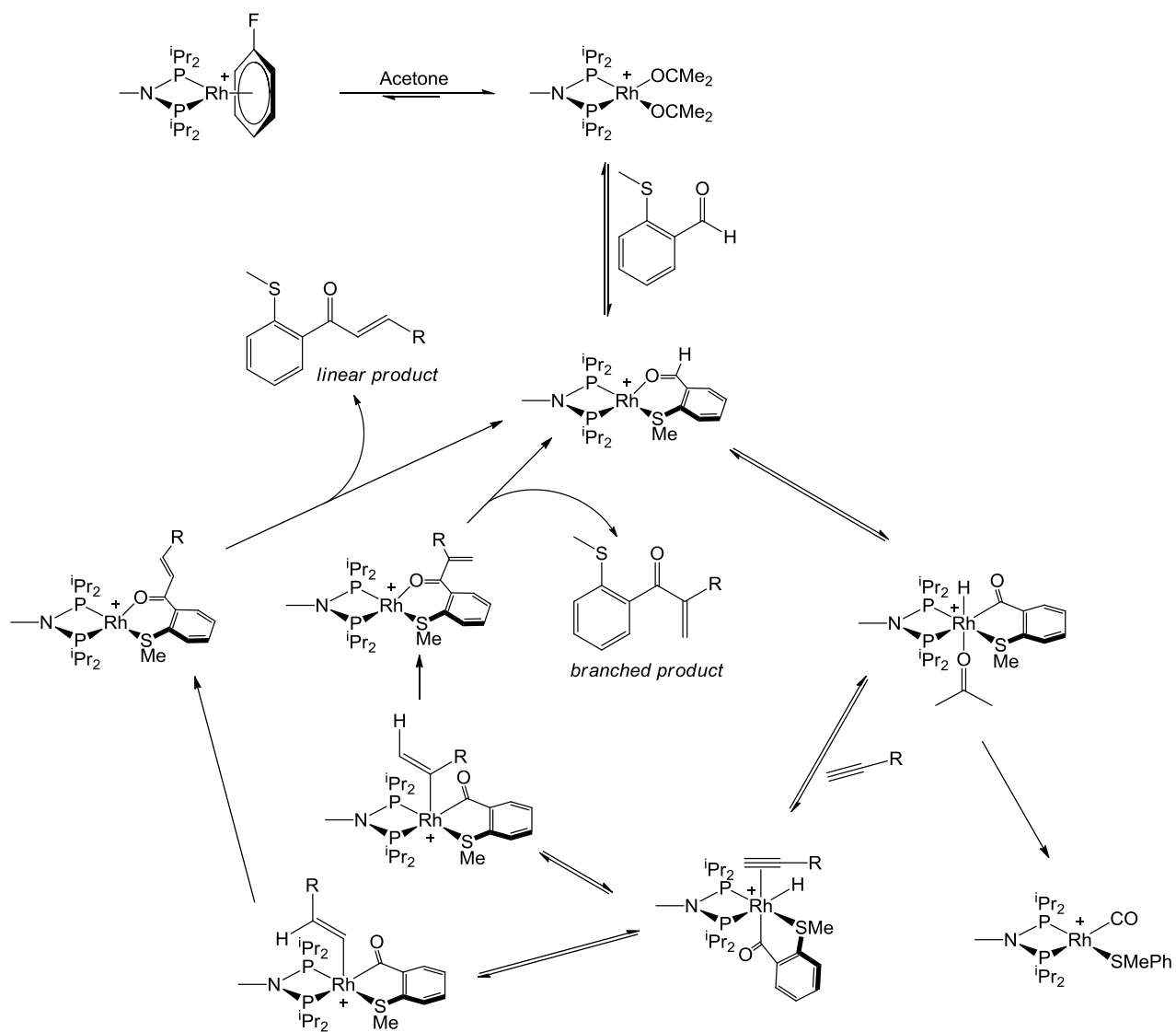
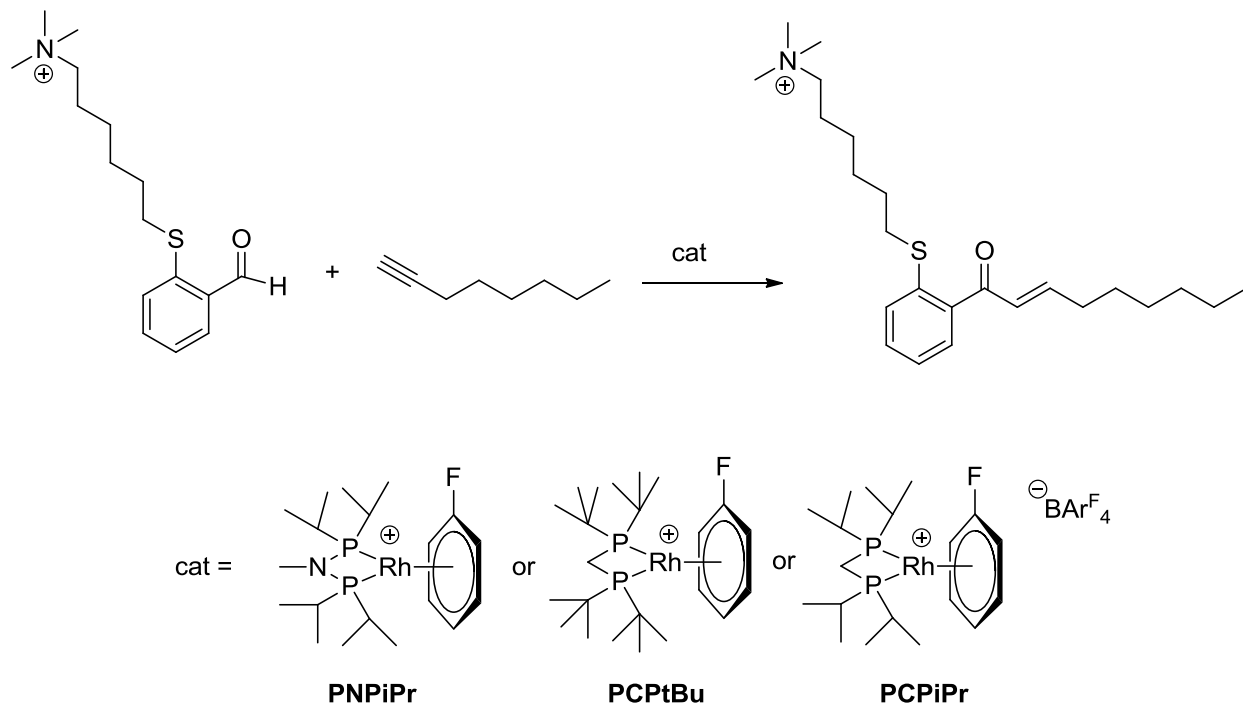


**Figure 125:** Proposed mechanism for hydroacylation by rhodium complexes.



We carried out the mechanistic investigation by using our PSI-ESI-MS. The catalysts and aldehyde we used are shown in Scheme 19. And we chose to use a charged aldehyde so that we can monitor the behavior of catalyst, intermediates, as well as final products and by-products.



**Scheme 19:** Hydroacylation reactions by different Rh catalysts.

We have successfully identified all except one the species in the catalytic cycle and obtained good time-dependent behavior data for each species in the reaction. Raw data was sent to Professor Weller for future analysis. In Figure 126, once the catalyst was introduced into the PSI-ESI-MS system, the reaction started. The catalyst showed up and converted into other species very quickly; all the intermediates in the catalytic cycle can be monitored as well as the final products.

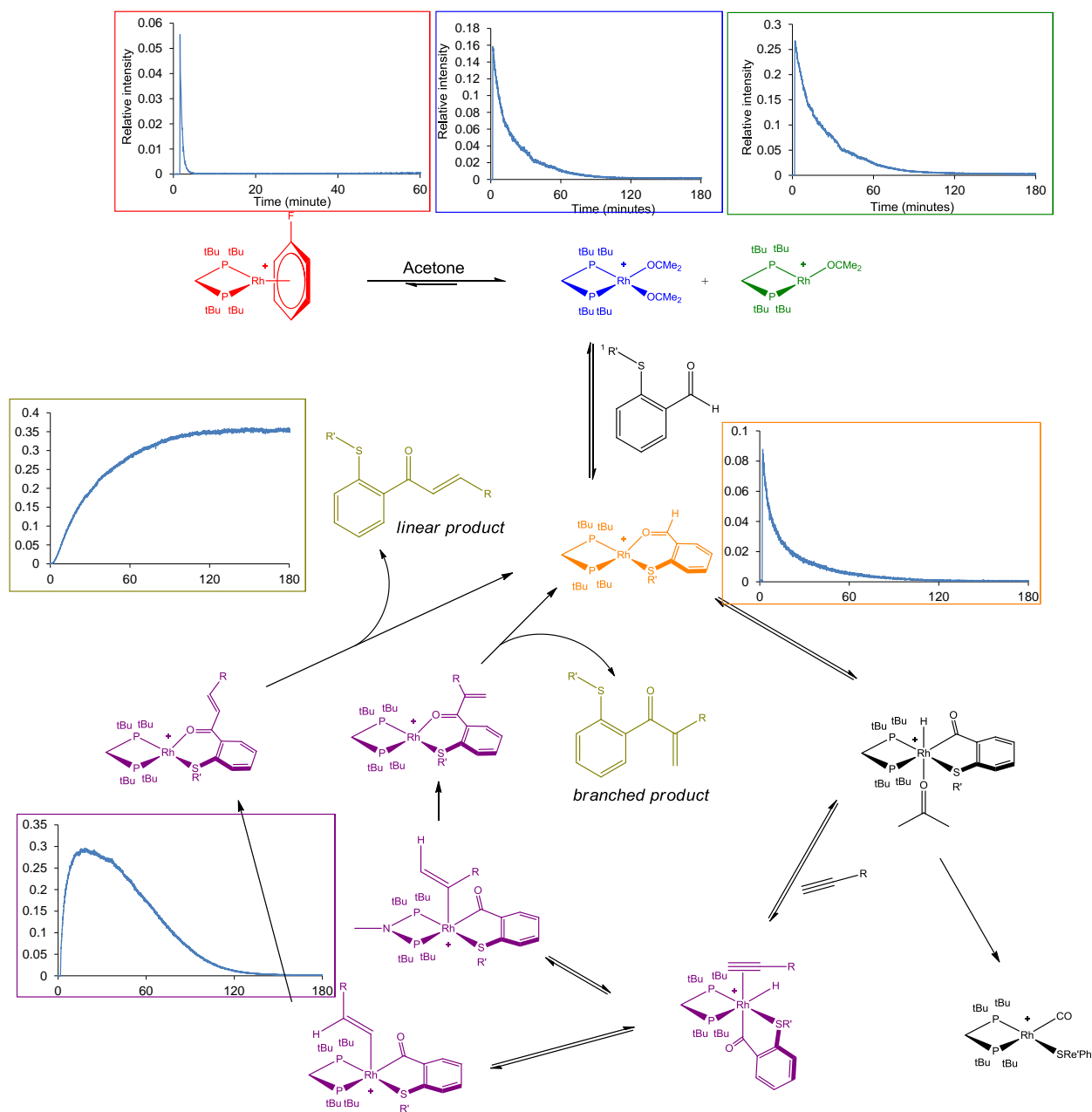


**Figure 126:** Hydroacylation catalytic cycle with reaction online monitoring results.

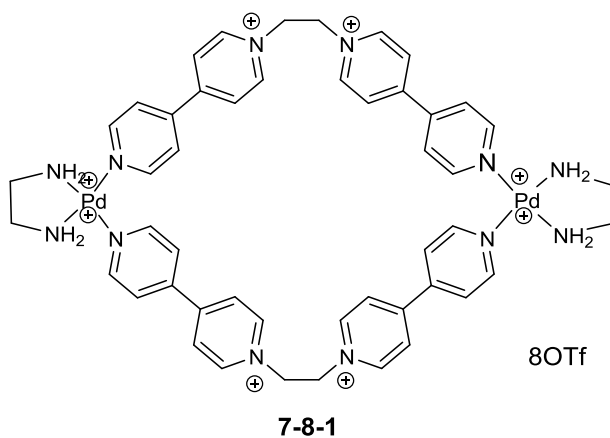
All except one on cycle species in the hydroacylation catalytic cycle were identified and kinetics data were obtained. In this figure, **PCPtBu** was used as catalyst, once the catalyst was introduced in the solution, reaction started processing. The time dependent behavior of each species has been portrayed in different colors, the color corresponds to the compounds of the same color.

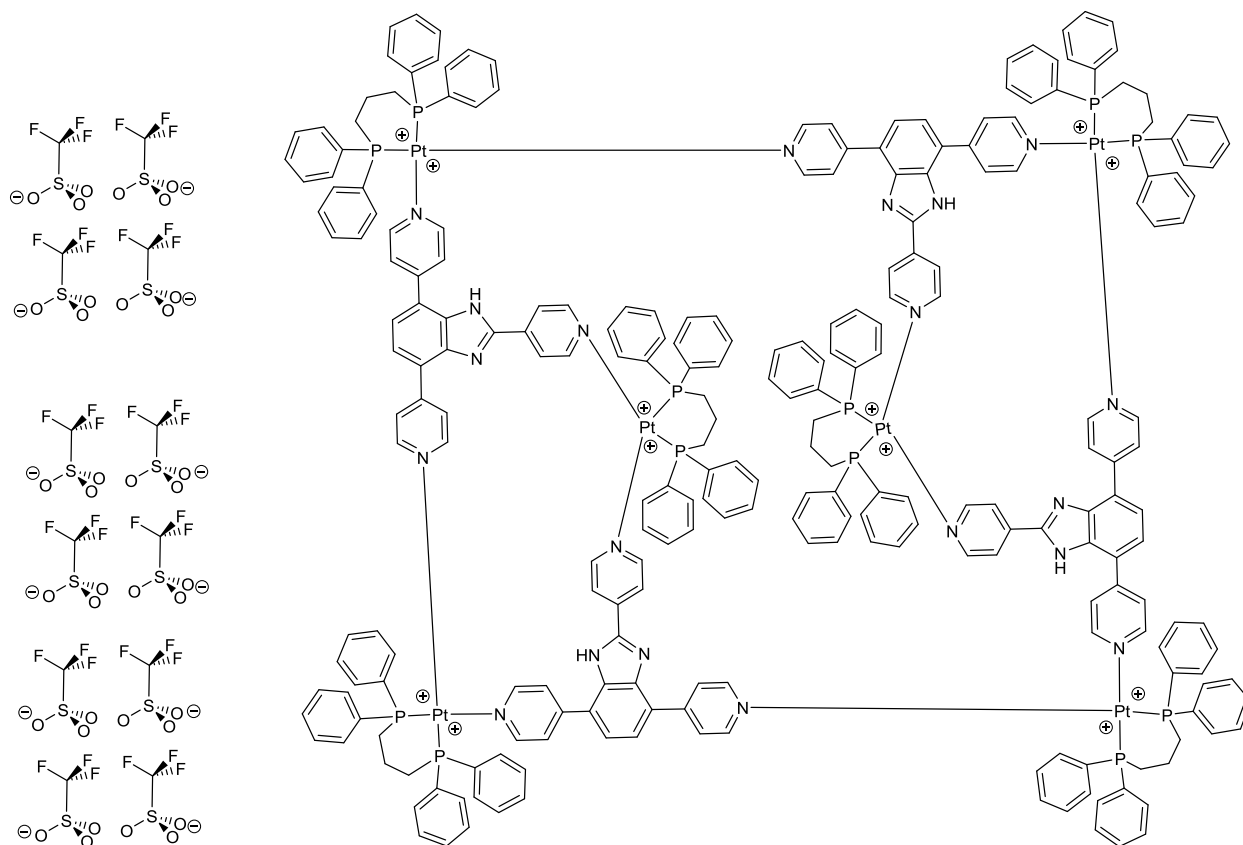
## 7.8 CryoSpray MS (CSI-MS)

I was honored to win a Quebec research fellowship for 6 months of study and research in Professor Garry Hanan's lab at University of Montreal. There, we mainly used Bruker MicroTOF high resolution MS for MS related studies; recently Hanan's group acquired the first CryoSpray ionization (CSI) source in Canada. Coldspray Ionization was first developed by Kentaro Yamaguchi in 2000.<sup>252</sup> The general technique is very similar to electrospray ionization, they have a similar ESI probe and desolvation chamber. CSI is a very soft ionization technique; it is even "softer" than ESI. It can solve the problem of decomposition of fragile compounds induced by high temperature during the ESI desolvation process. By using low temperature spray cone gas and drying gas, CSI can cool the source and desolvation chamber to reduce decomposition.

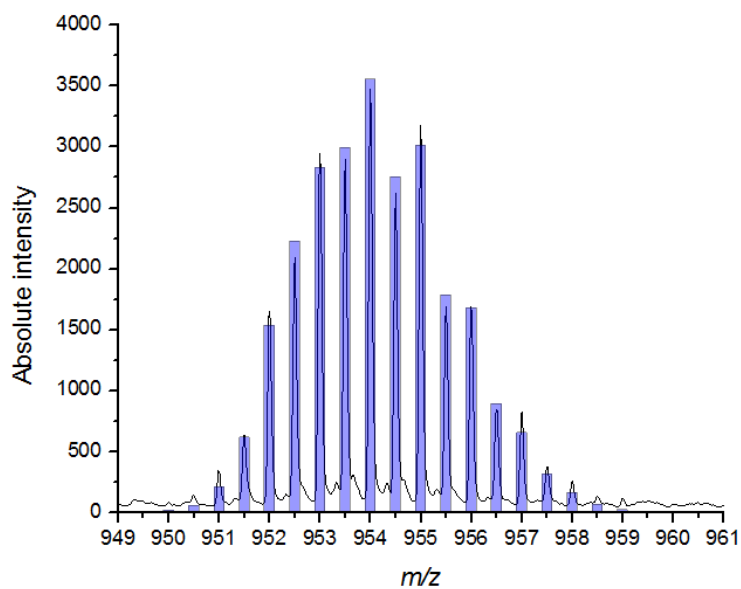
CSI-MS is a good technique for studying weak-interaction chemistry such as multiple charged and highly solvated ions; labile organic and organometallic complexes, DNA di-/tri-/quadru-plexes, and hyper-stranded DNAs.<sup>253</sup>

With CSI, we have successfully characterized over 80 weak non-covalent bonding supramolecular complexes, examples are shown below.





7-8-2

**Figure 127:** Weak bonding supramolecular complexes characterized by CSI.**Figure 128:** Experiment data of 7-8-1 (2+) and calculated isotope pattern (blue bars)

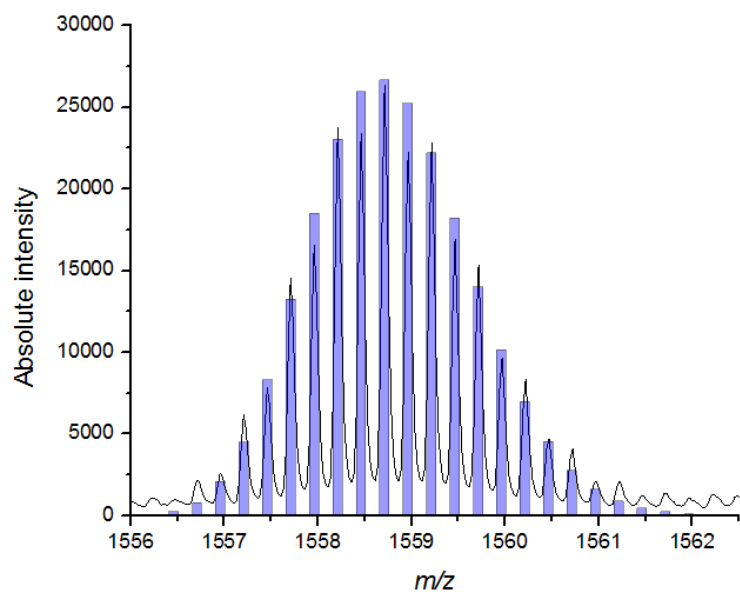


**Figure 129:** Experimental data of 7-8-2 (4+) and calculated isotope pattern (blue bars)

## 8. Conclusion

The work presented here describes the ongoing development and application of pressurized sample infusion (PSI) in catalysis reaction studies. Since the invention of the PSI-ESI-MS, the technique has been used on various projects.

Chapter one and two serve as an introduction to ESI-MS and organometallic catalysis. In chapter three, the optimization of pressurized sample infusion was discussed. In chapter four, we applied PSI to an intramolecular Pauson-Khand reaction; it is the first PSI-ESI-MS experiment to have been done with a reactive gas (CO) rather than protective gas such as N<sub>2</sub> and Ar. We overcame solubility problems by using a second solvent as a dilution solvent. This reaction was also the first time PSI-ESI-MS has been used for entropy and enthalpy calculations. We have demonstrated that PSI-ESI-MS is a powerful technique to study the Pauson-Khand reaction. A CO dissociation was confirmed as rate limiting step in the catalytic cycle.

In chapter five, we used H<sub>2</sub> gas for Rh-catalyzed hydrogenation kinetic studies. Conventional Wilkinson's catalyst was used and, for comparison, the more reactive Rh-based "Weller's catalyst" was also used. The two catalysts behave very differently in terms of hydrogenation. "Weller's catalyst" is capable of semi-hydrogenation as concluded from the PSI-ESI-MS results. Numerical modeling was integrated with PSI-ESI-MS, and calculated data matches the experimental data perfectly. In chapter six, where PSI was used for catalytic Si-H activation reaction studies, we were able to gain a deeper understanding of reactions such as dehydrocoupling of silanes and alcoholization of silane. However, since these are such complicated reactions, more work should be done in future including the use of lower reactivity secondary silanes for the dehydrocoupling of silanes and the use of different alcohols and reaction conditions for alcoholization of silanes.

Finally, in the past five years, over ten collaborative projects from different research institutes and industries have been carried out by using PSI technique. Good results were obtained, and many optimizations have been added to the PSI technique.

For future research, PSI-ESI-MS can be developed as a standard method for chemistry kinetics studies and the characterization of air-sensitive organometallic compounds. The combination of PSI-ESI-MS with other techniques such as NMR, UV, IR etc. for real-time monitoring will continue to be explored in the McIndoe group, along with the help of the numerical modelling methods I introduced to the group. Within the McIndoe group, techniques that I invented have become standard protocols, and are being applied in the study of a wide variety of reactions: palladium-catalyzed cross-couplings (Suzuki, Suzuki step polymerization, Heck, Hiyama), other rhodium-catalyzed transformations (hydroacylation, decarbonylation). As more reactions are studied and the technique gains further credibility, I expect these methods will find application in other laboratories who at present use more laborious and less sensitive approaches.

## References

1. P. T. Anastas and J. C. Warner, *Green Chemistry: Theory and Practice*, Oxford University Press, Incorporated, 1998.
2. M. Schlosser and L. S. Hegedus, *Organometallics in synthesis : a manual*, J. Wiley, Chichester; New York [etc.], 1994.
3. D. Astruc, *Organometallic chemistry and catalysis*, Springer, Berlin ; New York, 2007.
4. R. H. Crabtree, *The organometallic chemistry of the transition metals*, John Wiley, 2001.
5. E. V. Gusevskaya, *Quim. Nova*, 2003, **26**, 242-248.
6. [http://www.nobelprize.org/nobel\\_prizes/chemistry/laureates/2005/](http://www.nobelprize.org/nobel_prizes/chemistry/laureates/2005/), Accessed April 23, 2014.
7. P. Jean-Louis Hérisson and Y. Chauvin, *Die Makromolekulare Chemie*, 1971, **141**, 161-176.
8. [http://www.nobelprize.org/nobel\\_prizes/chemistry/laureates/2005/advanced.html](http://www.nobelprize.org/nobel_prizes/chemistry/laureates/2005/advanced.html), Accessed Dec 5, 2013.
9. [http://www.nobelprize.org/nobel\\_prizes/chemistry/laureates/2010/](http://www.nobelprize.org/nobel_prizes/chemistry/laureates/2010/), Accessed April 23, 2014.
10. R. F. Heck, *J. Am. Chem. Soc.*, 1969, **91**, 6707-6714.
11. M. Bradshaw, J. Zou, L. Byrne, K. Swaminathan Iyer, S. G. Stewart and C. L. Raston, *Chem. Commun. (Cambridge, U. K.)*, 2011, **47**, 12292-12294.
12. F. Ozawa, A. Kubo and T. Hayashi, *Chem. Lett.*, 1992, **21**, 2177-2180.
13. A. O. King, N. Okukado and E.-i. Negishi, *J. Chem. Soc., Chem. Commun.*, 1977, 683-684.
14. N. Miyaoura, K. Yamada and A. Suzuki, *Tetrahedron Lett.*, 1979, **20**, 3437-3440.
15. [http://en.wikipedia.org/wiki/Nuclear\\_magnetic\\_resonance\\_spectroscopy](http://en.wikipedia.org/wiki/Nuclear_magnetic_resonance_spectroscopy), Accessed May 15, 2014.
16. S. M. Jackson, D. M. Chisholm, J. S. McIndoe and L. Rosenberg, *Eur. J. Inorg. Chem.*, 2011, **2011**, 327-330.
17. C. Godard, S. B. Duckett, S. Polas, R. Tooze and A. C. Whitwood, *Dalton Trans.*, 2009, 2496-2509.
18. C. Zuccaccia, G. Bellachioma, S. Bolaño, L. Rocchigiani, A. Savini and A. Macchioni, *Eur. J. Inorg. Chem.*, 2012, **2012**, 1462-1468.
19. S. Mom, M. Beaupérin, D. Roy, S. Royer, R. Amardeil, H. Cattet, H. Doucet and J. C. Hierso, *Inorg. Chem.*, 2011, **50**, 11592-11603.
20. M. Boutain, S. B. Duckett, J. P. Dunne, C. Godard, J. M. Hernandez, A. J. Holmes, I. G. Khazal and J. Lopez-Serrano, *Dalton Trans.*, 2010, **39**, 3495-3500.
21. D. J. Darensbourg, S. J. Kyran, A. D. Yeung and A. A. Bengali, *Eur. J. Inorg. Chem.*, 2013, **2013**, 4024-4031.
22. I. Pernik, J. F. Hooper, A. B. Chaplin, A. S. Weller and M. C. Willis, *ACS Catalysis*, 2012, **2**, 2779-2786.
23. J. M. Larsson and K. J. Szabó, *J. Am. Chem. Soc.*, 2012, **135**, 443-455.
24. D. A. Skoog, F. J. Holler and S. R. Crouch, *Principles of instrumental analysis*, Thomson Brooks/Cole, 2007.
25. C. Fischer, T. Beweries, A. Preetz, H.-J. Drexler, W. Baumann, S. Peitz, U. Rosenthal and D. Heller, *Catal. Today*, 2010, **155**, 282-288.
26. F. Gao, M. B. Sullivan, G. M. Kuramshina, L. Guo and M. Garland, *ChemPhysChem*, 2012, **13**, 3139-3145.
27. C. A. Jaska and I. Manners, *J. Am. Chem. Soc.*, 2004, **126**, 9776-9785.
28. M. Bauer, T. Kauf, J. Christoffers and H. Bertagnolli, *Phys. Chem. Chem. Phys.*, 2005, **7**, 2664-2670.
29. M. V. Joshi, S. Vaidya, R. Pandey and D. Mukesh, *J. Catal.*, 1999, **183**, 102-106.



30. C. Amatore and A. Jutand, *J. Organomet. Chem.*, 1999, **576**, 254-278.
31. N. Matyasovszky, M. Tian and A. Chen, *The Journal of Physical Chemistry A*, 2009, **113**, 9348-9353.
32. H. Maskill, *The Investigation of Organic Reactions and Their Mechanisms*, Wiley, 2008.
33. S. Sarkar, S. Niyogi, E. Bekyarova and R. C. Haddon, *Chemical Science*, 2011, **2**, 1326-1333.
34. T. Zhang, W. Li and J.-P. Croue, *Environ. Sci. Technol.*, 2011.
35. L. Bini, E. J. E. Houben, E. A. Pidko, C. Müller and D. Vogt, *Catal. Today*, 2010, **155**, 271-278.
36. [http://us.mt.com/us/en/home/products/L1\\_AutochemProducts/L2\\_in-situSpectroscopy.html](http://us.mt.com/us/en/home/products/L1_AutochemProducts/L2_in-situSpectroscopy.html), Accessed Oct 26, 2011.
37. G. Barker, J. L. McGrath, A. Klapars, D. Stead, G. Zhou, K. R. Campos and P. O'Brien, *The Journal of Organic Chemistry*, 2011, **76**, 5936-5953.
38. E. Le Gall, S. Sengmany, C. Hauréna, E. Léonel and T. Martens, *J. Organomet. Chem.*, 2013, **736**, 27-35.
39. W. Henderson and J. S. McIndoe, *Mass spectrometry of inorganic and organometallic compounds*, J. Wiley, 2005.
40. M. N. Eberlin, *Eur. J. Mass Spectrom.*, 2007, **13**, 19-28.
41. R. B. Cole, *Electrospray and MALDI Mass Spectrometry: Fundamentals, Instrumentation, Practicalities, and Biological Applications*, John Wiley & Sons, 2009.
42. [http://www.magnet.fsu.edu/education/tutorials/tools/ionization\\_esi.html](http://www.magnet.fsu.edu/education/tutorials/tools/ionization_esi.html), Accessed Oct 07, 2011.
43. L. S. Santos, *Reactive Intermediates: MS Investigations in Solution*, Wiley-VCH, 2010.
44. M. Bonchio, G. Licini, G. Modena, O. Bortolini, S. Moro and W. A. Nugent, *J. Am. Chem. Soc.*, 1999, **121**, 6258-6268.
45. Z. Li, Z. H. Tang, X. X. Hu and C. G. Xia, *Chemistry – A European Journal*, 2005, **11**, 1210-1216.
46. B. C. Gilbert, J. R. Lindsay Smith, A. Mairata i Payeras, J. Oakes and R. Pons i Prats, *J. Mol. Catal. A: Chem.*, 2004, **219**, 265-272.
47. K. L. Vikse, Z. Ahmadi, C. C. Manning, D. A. Harrington and J. S. McIndoe, *Angewandte Chemie International Edition*, 2011, **50**, 8304-8306.
48. F. Wu, S. R. Foley, C. T. Burns and R. F. Jordan, *J. Am. Chem. Soc.*, 2005, **127**, 1841-1853.
49. L. S. Santos, *Eur. J. Org. Chem.*, 2008, **2008**, 235-253.
50. M. A. Henderson, J. Luo, A. Oliver and J. S. McIndoe, *Organometallics*, 2011.
51. C. Adlhart and P. Chen, *Helv. Chim. Acta*, 2003, **86**, 941-949.
52. Y.-M. Kim and P. Chen, *Int. J. Mass Spectrom.*, 1999, **185–187**, 871-881.
53. C. Hinderling, C. Adlhart and P. Chen, *Angewandte Chemie International Edition*, 1998, **37**, 2685-2689.
54. D. Feichtinger, D. A. Plattner and P. Chen, *J. Am. Chem. Soc.*, 1998, **120**, 7125-7126.
55. P. Chen, *Angewandte Chemie International Edition*, 2003, **42**, 2832-2847.
56. M. Eberlin, *Eur. J. Mass Spectrom.*, 2007, **13**, 19-28.
57. J. A. Lessa, A. Horn, É. S. Bull, M. R. Rocha, M. Benassi, R. R. Catharino, M. N. Eberlin, A. Casellato, C. J. Noble, G. R. Hanson, G. Schenk, G. C. Silva, O. A. C. Antunes and C. Fernandes, *Inorg. Chem.*, 2009, **48**, 4569-4579.
58. L. S. Santos, C. H. Pavam, W. P. Almeida, F. Coelho and M. N. Eberlin, *Angewandte Chemie International Edition*, 2004, **43**, 4330-4333.
59. Y. Blum, D. Czarkie, Y. Rahamim and Y. Shvo, *Organometallics*, 1985, **4**, 1459-1461.
60. B. G. Vaz, C. D. F. Milagre, M. N. Eberlin and H. M. S. Milagre, *Org. Biomol. Chem.*, 2013, **11**, 6695-6698.
61. L. Taghizadeh Ghoochany, C. Kerner, S. Farsadpour, F. Menges, Y. Sun, G. Niedner-Schatteburg and W. R. Thiel, *Eur. J. Inorg. Chem.*, 2013, **2013**, 4305-4317.

62. A. H. L. Machado, H. M. S. Milagre, L. S. Eberlin, A. A. Sabino, C. R. D. Correia and M. N. Eberlin, *Org. Biomol. Chem.*, 2013, **11**, 3277-3281.
63. T. K. Trefz, M. A. Henderson, M. Y. Wang, S. Collins and J. S. McIndoe, *Organometallics*, 2013, **32**, 3149-3152.
64. M. Parera, A. Dachs, M. Solà, A. Pla-Quintana and A. Roglans, *Chemistry – A European Journal*, 2012, **18**, 13097-13107.
65. J. Griffiths, *Anal. Chem.*, 2008, **80**, 5678-5683.
66. A. Dempster, *Philosophical magazine (London, England : 1945)*, 1916, **31**, 438.
67. M. S. B. Munson and F. H. Field, *J. Am. Chem. Soc.*, 1966, **88**, 2621-2630.
68. A. G. Harrison, *Chemical Ionization Mass Spectrometry, Second Edition*, Taylor & Francis, 1992.
69. H. D. Beckey, *International Journal of Mass Spectrometry and Ion Physics*, 1969, **2**, 500-502.
70. H. R. Morris, M. Panico, M. Barber, R. S. Bordoli, R. D. Sedgwick and A. Tyler, *Biochem. Biophys. Res. Commun.*, 1981, **101**, 623-631.
71. M. Barber, R. S. Bordoli, R. D. Sedgwick and A. N. Tyler, *J. Chem. Soc., Chem. Commun.*, 1981, 325-327.
72. D. I. Carroll, I. Dzidic, R. N. Stillwell, K. D. Haegele and E. C. Horning, *Anal. Chem.*, 1975, **47**, 2369-2373.
73. M. Yamashita and J. B. Fenn, *The Journal of Physical Chemistry*, 1984, **88**, 4451-4459.
74. J. B. Fenn, M. Mann, M. Chin-kai, W. Shek-fu and C. M. Whitehouse, *Science*, 1989, **246**, 64.
75. K. Tanaka, H. Waki, Y. Ido, S. Akita, Y. Yoshida, T. Yoshida and T. Matsuo, *Rapid Commun. Mass Spectrom.*, 1988, **2**, 151-153.
76. F. Hillenkamp and M. Karas, *Int. J. Mass Spectrom.*, 2000, **200**, 71-77.
77. L. A. McDonnell and R. M. A. Heeren, *Mass Spectrom. Rev.*, 2007, **26**, 606-643.
78. P. Chaurand, J. L. Norris, D. S. Cornett, J. A. Mobley and R. M. Caprioli, *J. Proteome Res.*, 2006, **5**, 2889-2900.
79. R. M. Caprioli, T. B. Farmer and J. Gile, *Anal. Chem.*, 1997, **69**, 4751-4760.
80. M. D. Eelman, J. M. Blacquiere, M. M. Moriarty and D. E. Fogg, *Angewandte Chemie International Edition*, 2008, **47**, 303-306.
81. M. Dole, L. L. Mack, R. L. Hines, R. C. Mobley, L. D. Ferguson and M. B. Alice, *The Journal of Chemical Physics*, 1968, **49**, 2240-2249.
82. *International Journal of Analytical Chemistry*, 2012, **2012**.
83. R. B. Cole, *J. Mass Spectrom.*, 2000, **35**, 763-772.
84. G. Taylor, *Proceedings of the Royal Society of London. Series A. Mathematical and Physical Sciences*, 1964, **280**, 383-397.
85. D. C. Taflin, T. L. Ward and E. J. Davis, *Langmuir*, 1989, **5**, 376-384.
86. L. Konermann, E. Ahadi, A. D. Rodriguez and S. Vahidi, *Anal. Chem.*, 2012, **85**, 2-9.
87. W. Corporation, *Micromass Q-Tof micro Mass Spectrometer Operator's Guide*, Milford, MA, USA, 2002.
88. A. A. Nazarov, M. Baquié, P. Nowak-Sliwinska, O. Zava, J. R. van Beijnum, M. Groessl, D. M. Chisholm, Z. Ahmadi, J. S. McIndoe, A. W. Griffioen, H. van den Bergh and P. J. Dyson, *Sci. Rep.*, 2013, **3**.
89. K. L. Vikse, M. P. Woods and J. S. McIndoe, *Organometallics*, 2010, **29**, 6615-6618.
90. K. L. Vikse, Z. Ahmadi, J. Luo, N. van der Wal, K. Daze, N. Taylor and J. S. McIndoe, *Int. J. Mass Spectrom.*, 2012, **323-324**, 8-13.
91. S. P. Suter and R. Skalak, *Annual Review of Fluid Mechanics*, 1993, **25**, 1-19.
92. P. S. Academic, Powersim Software AS, Bergen, Norway, 9 edn., 2012.
93. S. Hoops, S. Sahle, R. Gauges, C. Lee, J. Pahle, N. Simus, M. Singhal, L. Xu, P. Mendes and U. Kummer, *Bioinformatics*, 2006, **22**, 3067-3074.

94. R. Hartmann and P. Chen, *Adv. Synth. Catal.*, 2003, **345**, 1353-1359.
95. J. Luo, A. G. Oliver and J. Scott McIndoe, *Dalton Trans.*, 2013, **42**, 11312-11318.
96. Z. Ahmadi and J. S. McIndoe, *Chem. Commun. (Cambridge, U. K.)*, 2013, **49**, 11488-11490.
97. I. U. Khand, G. R. Knox, P. L. Pauson and W. E. Watts, *Journal of the Chemical Society D: Chemical Communications*, 1971, 36a-36a.
98. I. U. Khand, G. R. Knox, P. L. Pauson and W. E. Watts, *Journal of the Chemical Society, Perkin Transactions 1*, 1973, 975-977.
99. P. Magnus, L. M. Principe and M. J. Slater, *The Journal of Organic Chemistry*, 1987, **52**, 1483-1486.
100. J. Blanco-Urgoiti, L. Anorbe, L. Perez-Serrano, G. Dominguez and J. Perez-Castells, *Chem. Soc. Rev.*, 2004, **33**, 32-42.
101. A. J. Fletcher and S. D. R. Christie, *Journal of the Chemical Society, Perkin Transactions 1*, 2000, 1657-1668.
102. O. Geis and H.-G. Schmalz, *Angewandte Chemie International Edition*, 1998, **37**, 911-914.
103. T. Sugihara, M. Yamada, H. Ban, M. Yamaguchi and C. Kaneko, *Angewandte Chemie International Edition in English*, 1997, **36**, 2801-2804.
104. T. Sugihara, M. Yamada, M. Yamaguchi and M. Nishizawa, *Synlett*, 1999, **6**, 771-773.
105. D. C. Billington, I. Malcolm Helps, P. L. Pauson, W. Thomson and D. Willison, *J. Organomet. Chem.*, 1988, **354**, 233-242.
106. T. Sugihara and M. Yamaguchi, *Synlett*, 1998, **1998**, 1384-1386.
107. K. H. Park, I. G. Jung and Y. K. Chung, *Org. Lett.*, 2004, **6**, 1183-1186.
108. N. Jeong, B. K. Sung and Y. K. Choi, *J. Am. Chem. Soc.*, 2000, **122**, 6771-6772.
109. T. Shibata, N. Toshida and K. Takagi, *Org. Lett.*, 2002, **4**, 1619-1621.
110. T. Morimoto, K. Fuji, K. Tsutsumi and K. Kakiuchi, *J. Am. Chem. Soc.*, 2002, **124**, 3806-3807.
111. K. H. Park, S. U. Son and Y. K. Chung, *Chem. Commun. (Cambridge, U. K.)*, 2003, 1898-1899.
112. C. Mukai, M. Uchiyama and M. Hanaoka, *J. Chem. Soc., Chem. Commun.*, 1992, 1014-1015.
113. T. Shibata and K. Takagi, *J. Am. Chem. Soc.*, 2000, **122**, 9852-9853.
114. F. A. Hicks, N. M. Kablaoui and S. L. Buchwald, *J. Am. Chem. Soc.*, 1996, **118**, 9450-9451.
115. F. A. Hicks, N. M. Kablaoui and S. L. Buchwald, *J. Am. Chem. Soc.*, 1999, **121**, 5881-5898.
116. P. Mastrolilli, C. F. Nobile, R. Paolillo and G. P. Suranna, *J. Mol. Catal. A: Chem.*, 2004, **214**, 103-106.
117. P. Magnus, C. Exon and P. Albaugh-Robertson, *Tetrahedron*, 1985, **41**, 5861-5869.
118. V. Rautenstrauch, P. Mégard, J. Conesa and W. Küster, *Angewandte Chemie International Edition in English*, 1990, **29**, 1413-1416.
119. M. Yamanaka and E. Nakamura, *J. Am. Chem. Soc.*, 2001, **123**, 1703-1708.
120. M. A. Bennett and P. B. Donaldson, *Inorg. Chem.*, 1978, **17**, 1995-2000.
121. C. M. Gordon, M. Kiszka, I. R. Dunkin, W. J. Kerr, J. S. Scott and J. Gebicki, *J. Organomet. Chem.*, 1998, **554**, 147-154.
122. E. V. Banide, H. Müller-Bunz, A. R. Manning, P. Evans and M. J. McGlinchey, *Angewandte Chemie International Edition*, 2007, **46**, 2907-2910.
123. M. K. Pallerla, G. P. A. Yap and J. M. Fox, *The Journal of Organic Chemistry*, 2008, **73**, 6137-6141.
124. T. J. M. de Bruin, A. Milet, A. E. Greene and Y. Gimbert, *The Journal of Organic Chemistry*, 2004, **69**, 1075-1080.
125. X. Verdaguer, J. Vázquez, G. Fuster, V. Bernardes-Génisson, A. E. Greene, A. Moyano, M. A. Pericàs and A. Riera, *The Journal of Organic Chemistry*, 1998, **63**, 7037-7052.
126. R. Cabot, A. Lledó, M. Revés, A. Riera and X. Verdaguer, *Organometallics*, 2007, **26**, 1134-1142.
127. D. G. Blackmond, *Angewandte Chemie International Edition*, 2005, **44**, 4302-4320.
128. M. A. Henderson, Ph.D., University of Victoria, 2009.

129. W. Henderson and C. Evans, *Inorg. Chim. Acta*, 1999, **294**, 183-192.
130. C. Decker, W. Henderson and B. K. Nicholson, *Journal of the Chemical Society, Dalton Transactions*, 1999, 3507-3513.
131. N. J. Farrer, R. McDonald and J. S. McIndoe, *Dalton Trans.*, 2006, 4570-4579.
132. N. J. Farrer, R. McDonald, T. Piga and J. S. McIndoe, *Polyhedron*, 2010, **29**, 254-261.
133. W. Henderson and B. K. Nicholson, *J. Chem. Soc., Chem. Commun.*, 1995, 2531-2532.
134. L. S. Santos, G. B. Rosso, R. A. Pilli and M. N. Eberlin, *The Journal of Organic Chemistry*, 2007, **72**, 5809-5812.
135. D. M. Chisholm, A. G. Oliver and J. S. McIndoe, *Dalton Trans.*, 2010, **39**, 364-373.
136. C. Adlhart and P. Chen, *Helv. Chim. Acta*, 2000, **83**, 2192-2196.
137. E. Crawford, T. Lohr, E. M. Leitao, S. Kwok and J. S. McIndoe, *Dalton Trans.*, 2009, 9110-9112.
138. Y. Gimbert, D. Lesage, A. Milet, F. Fournier, A. E. Greene and J.-C. Tabet, *Org. Lett.*, 2003, **5**, 4073-4075.
139. A. D. Allian, M. Tjahjono and M. Garland, *Organometallics*, 2006, **25**, 2182-2188.
140. M. Henderson, S. Kwok and J. S. McIndoe, *J. Am. Soc. Mass Spectrom.*, 2009, **20**, 658-666.
141. V. De Vynck and E. J. Goethals, *Macromol. Rapid Commun.*, 1997, **18**, 149-156.
142. B. R. James, *Homogeneous Hydrogenation*, Wiley, 1973.
143. J. F. Young, J. A. Osborn, F. H. Jardine and G. Wilkinson, *Chemical Communications (London)*, 1965, 131-132.
144. M. A. L. Bennett, P. A., *Chem. Ind. (London)*, 1965, 846.
145. Coffey R.S.; British Patent No.1121642, 1965.
146. J. Halpern, T. Okamoto and A. Zakhariev, *J. Mol. Catal.*, 1977, **2**, 65-68.
147. M. I. Cabrera, P. D. Zgolicz and R. J. Grau, *Applied Catalysis A: General*, 2008, **334**, 291-303.
148. D. J. Nelson, R. Li and C. Brammer, *The Journal of Organic Chemistry*, 2004, **70**, 761-767.
149. M. Bowker, J. Gland, R. Joyner, Y. Li, M. Slin'ko and R. Whyman, *Catal. Lett.*, 1994, **25**, 293-308.
150. N. Koga, C. Daniel, J. Han, X. Y. Fu and K. Morokuma, *J. Am. Chem. Soc.*, 1987, **109**, 3455-3456.
151. D. Wink and P. C. Ford, *J. Am. Chem. Soc.*, 1985, **107**, 1794-1796.
152. D. A. Wink and P. C. Ford, *J. Am. Chem. Soc.*, 1987, **109**, 436-442.
153. S. B. Duckett, C. L. Newell and R. Eisenberg, *J. Am. Chem. Soc.*, 1993, **115**, 1156-1157.
154. S. B. Duckett, C. L. Newell and R. Eisenberg, *J. Am. Chem. Soc.*, 1994, **116**, 10548-10556.
155. I. V. Koptuyug, K. V. Kovtunov, S. R. Burt, M. S. Anwar, C. Hilty, S.-I. Han, A. Pines and R. Z. Sagdeev, *J. Am. Chem. Soc.*, 2007, **129**, 5580-5586.
156. J. Halpern, *Inorg. Chim. Acta*, 1981, **50**, 11-19.
157. D. Chisholm, Ph.D., University of Victoria, 2010.
158. P. J. Dyson, J. S. McIndoe and D. Zhao, *Chem. Commun. (Cambridge, U. K.)*, 2003, 508-509.
159. D. M. Chisholm and J. Scott McIndoe, *Dalton Trans.*, 2008, 3933-3945.
160. T. Müller, A. Badu-Tawiah and R. G. Cooks, *Angewandte Chemie International Edition*, 2012, **51**, 11832-11835.
161. Powersim Software AS, Bergen, Norway, 9 edn., 2012.
162. C. A. Tolman, P. Z. Meakin, D. I. Lindner and J. P. Jesson, *J. Am. Chem. Soc.*, 1974, **96**, 2762-2774.
163. P. Meakin, J. P. Jesson and C. A. Tolman, *J. Am. Chem. Soc.*, 1972, **94**, 3240-3242.
164. M. Armbrüster, M. Behrens, F. Cinquini, K. Föttinger, Y. Grin, A. Haghofer, B. Klötzer, A. Knop-Gericke, H. Lorenz, A. Ota, S. Penner, J. Prinz, C. Rameshan, Z. Révay, D. Rosenthal, G. Rupprechter, P. Sautet, R. Schlögl, L. Shao, L. Szentmiklósi, D. Teschner, D. Torres, R. Wagner, R. Widmer and G. Wowsnick, *ChemCatChem*, 2012, **4**, 1048-1063.
165. M. P. R. Spee, J. Boersma, M. D. Meijer, M. Q. Slagt, G. van Koten and J. W. Geus, *The Journal of Organic Chemistry*, 2001, **66**, 1647-1656.
166. I. N. Michaelides and D. J. Dixon, *Angewandte Chemie International Edition*, 2013, **52**, 806-808.

167. M. Yan, T. Jin, Y. Ishikawa, T. Minato, T. Fujita, L.-Y. Chen, M. Bao, N. Asao, M.-W. Chen and Y. Yamamoto, *J. Am. Chem. Soc.*, 2012, **134**, 17536-17542.
168. K. Urabe, Y. Tanaka and Y. Izumi, *Chem. Lett.*, 1985, **14**, 1595-1596.
169. R. R. Schrock and J. A. Osborn, *J. Am. Chem. Soc.*, 1976, **98**, 2143-2147.
170. L. J. Sewell, G. C. Lloyd-Jones and A. S. Weller, *J. Am. Chem. Soc.*, 2012, **134**, 3598-3610.
171. B. R. James and D. Mahajan, *Can. J. Chem.*, 1979, **57**, 180-187.
172. M. A. Esteruelas, I. González, J. Herrero and L. A. Oro, *J. Organomet. Chem.*, 1998, **551**, 49-53.
173. C. Kohrt, G. Wienhöfer, C. Pribbenow, M. Beller and D. Heller, *ChemCatChem*, 2013, **5**, 2818-2821.
174. B. R. James and D. K. W. Wang, *Can. J. Chem.*, 1980, **58**, 245-250.
175. W. S. Knowles, *Adv. Synth. Catal.*, 2003, **345**, 3-13.
176. J. Cipot, R. McDonald, M. J. Ferguson, G. Schatte and M. Stradiotto, *Organometallics*, 2007, **26**, 594-608.
177. S. Bell, B. Wüstenberg, S. Kaiser, F. Menges, T. Netscher and A. Pfaltz, *Science*, 2006, **311**, 642-644.
178. C. J. Longley, T. J. Goodwin and G. Wilkinson, *Polyhedron*, 1986, **5**, 1625-1628.
179. B. R. James, *Catal. Today*, 1997, **37**, 209-221.
180. S. Kobayashi and H. Ishitani, *Chem. Rev. (Washington, DC, U. S.)*, 1999, **99**, 1069-1094.
181. S. Doran, T. Achard, A. Riera and X. Verdaguer, *J. Organomet. Chem.*, 2012, **717**, 135-140.
182. V. Cadierno, J. Díez, S. E. García-Garrido, J. Gimeno and A. Pizzano, *Polyhedron*, 2010, **29**, 3380-3386.
183. M. Ahlquist, M. Gustafsson, M. Karlsson, M. Thaning, O. Axelsson and O. F. Wendt, *Inorg. Chim. Acta*, 2007, **360**, 1621-1627.
184. M. J. Burk, T. G. P. Harper, J. R. Lee and C. Kalberg, *Tetrahedron Lett.*, 1994, **35**, 4963-4966.
185. W. H. Bernskoetter, E. Lobkovsky and P. J. Chirik, *J. Am. Chem. Soc.*, 2005, **127**, 14051-14061.
186. K. E. Janak and G. Parkin, *J. Am. Chem. Soc.*, 2003, **125**, 13219-13224.
187. J. F. Hooper, R. D. Young, A. S. Weller and M. C. Willis, *Chemistry – A European Journal*, 2013, **19**, 3125-3130.
188. J. B. Lambert and L. G. Greifenstein, *J. Am. Chem. Soc.*, 1974, **96**, 5120-5124.
189. H. Yang, H. Gao and R. J. Angelici, *Organometallics*, 1999, **18**, 2285-2287.
190. J. Blum, A. Rosenfeld, F. Gelman, H. Schumann and D. Avnir, *J. Mol. Catal. A: Chem.*, 1999, **146**, 117-122.
191. M. S. Hill, *ChemInform*, 2011, **42**, no-no.
192. D. J. Harrison, D. R. Edwards, R. McDonald and L. Rosenberg, *Dalton Transactions*, 2008, 3401-3411.
193. R. D. Miller and J. Michl, *Chemical Reviews*, 1989, **89**, 1359-1410.
194. J. F. Harrod and S. S. Yun, *Organometallics*, 1987, **6**, 1381-1387.
195. C. Aitken, J. F. Harrod and E. Samuel, *Journal of Organometallic Chemistry*, 1985, **279**, C11-C13.
196. B.-H. Kim, H.-G. Woo, W. Kim and H. Li, *Journal of Chemical Technology & Biotechnology*, 2006, **81**, 782-788.
197. H. G. Woo, J. F. Walzer and T. D. Tilley, *Journal of the American Chemical Society*, 1992, **114**, 7047-7055.
198. J. J. Chruściel, *Canadian Journal of Chemistry*, 2005, **83**, 508-516.
199. P. Diversi, F. Marchetti, V. Ermini and S. Matteoni, *Journal of Organometallic Chemistry*, 2000, **593-594**, 154-160.
200. M. Itazaki, K. Ueda and H. Nakazawa, *Angewandte Chemie International Edition*, 2009, **48**, 3313-3316.
201. E. E. Smith, G. Du, P. E. Fanwick and M. M. Abu-Omar, *Organometallics*, 2010, **29**, 6527-6533.

202. S. M. Jackson, C. E. Hughes, S. Monfette and L. Rosenberg, *Inorganica Chimica Acta*, 2006, **359**, 2966-2972.
203. S. M. Jackson, University of Victoria Dept of Chemistry University of Victoria, 2007.
204. D. M. Hester, J. Sun, A. W. Harper and G. K. Yang, *Journal of the American Chemical Society*, 1992, **114**, 5234-5240.
205. G. P. Mitchell and T. D. Tilley, *Organometallics*, 1996, **15**, 3477-3479.
206. G. P. Mitchell and T. D. Tilley, *Organometallics*, 1998, **17**, 2912-2916.
207. I. Ojima, S.-I. Inaba, T. Kogure and Y. Nagai, *Journal of Organometallic Chemistry*, 1973, **55**, C7-C8.
208. L. Rosenberg, C. W. Davis and J. Yao, *Journal of the American Chemical Society*, 2001, **123**, 5120-5121.
209. K. Mori, M. Tano, T. Mizugaki, K. Ebitani and K. Kaneda, *New Journal of Chemistry*, 2002, **26**, 1536-1538.
210. <http://www.acmite.com/market-reports/chemicals/world-silicone-market.html>, Accessed March 5, 2014.
211. M. A. Brook, *Silicon in organic, organometallic, and polymer chemistry*, J. Wiley, 2000.
212. N. Asao, Y. Ishikawa, N. Hatakeyama, Menggenbateer, Y. Yamamoto, M. Chen, W. Zhang and A. Inoue, *Angewandte Chemie International Edition*, 2010, **49**, 10093-10095.
213. M. Lee, S. Ko and S. Chang, *J. Am. Chem. Soc.*, 2000, **122**, 12011-12012.
214. S. T. Tan, J. W. Kee and W. Y. Fan, *Organometallics*, 2011, **30**, 4008-4013.
215. T. Y. Lee, L. Dang, Z. Zhou, C. H. Yeung, Z. Lin and C. P. Lau, *Eur. J. Inorg. Chem.*, 2010, **2010**, 5675-5684.
216. B. P. S. Chauhan, A. Sarkar, M. Chauhan and A. Roka, *Appl. Organomet. Chem.*, 2009, **23**, 385-390.
217. T. Mitsudome, S. Arita, H. Mori, T. Mizugaki, K. Jitsukawa and K. Kaneda, *Angewandte Chemie International Edition*, 2008, **47**, 7938-7940.
218. T. Mitsudome, A. Noujima, T. Mizugaki, K. Jitsukawa and K. Kaneda, *Chemical Communications*, 2009, 5302-5304.
219. R. A. Corbin, E. A. Ison and M. M. Abu-Omar, *Dalton Trans.*, 2009, 2850-2855.
220. E. A. Ison, R. A. Corbin and M. M. Abu-Omar, *J. Am. Chem. Soc.*, 2005, **127**, 11938-11939.
221. Y. Lee, D. Seomoon, S. Kim, H. Han, S. Chang and P. H. Lee, *The Journal of Organic Chemistry*, 2004, **69**, 1741-1743.
222. T. Mitsudome, A. Noujima, T. Mizugaki, K. Jitsukawa and K. Kaneda, *Chem. Commun. (Cambridge, U. K.)*, 2009, 5302-5304.
223. R. Aroop K, in *Advances in Organometallic Chemistry*, eds. A. F. H. Robert West and J. F. Mark, Academic Press, 2007, vol. Volume 55, pp. 1-59.
224. S. C. Bart, E. Lobkovsky and P. J. Chirik, *Journal of the American Chemical Society*, 2004, **126**, 13794-13807.
225. J. Stein, L. N. Lewis, Y. Gao and R. A. Scott, *J. Am. Chem. Soc.*, 1999, **121**, 3693-3703.
226. B. Marciniec, in *Hydrosilylation*, ed. B. Marciniec, Springer Netherlands, 2009, vol. 1, ch. 1, pp. 3-51.
227. S. E. Denmark and Z. Wang, *Org. Lett.*, 2001, **3**, 1073-1076.
228. K. Itami, K. Mitsudo, A. Nishino and J.-i. Yoshida, *The Journal of Organic Chemistry*, 2002, **67**, 2645-2652.
229. L. W. Chung, Y.-D. Wu, B. M. Trost and Z. T. Ball, *Journal of the American Chemical Society*, 2003, **125**, 11578-11582.
230. B. M. Trost and Z. T. Ball, *Journal of the American Chemical Society*, 2005, **127**, 17644-17655.

231. B. M. Trost, Z. T. Ball and K. M. Laemmerhold, *Journal of the American Chemical Society*, 2005, **127**, 10028-10038.
232. D. V. Gutsulyak, S. F. Vyboishchikov and G. I. Nikonov, *Journal of the American Chemical Society*, 2010, **132**, 5950-5951.
233. S. V. Maifeld, M. N. Tran and D. Lee, *Tetrahedron Letters*, 2005, **46**, 105-108.
234. N. Sabourault, G. Mignani, A. Wagner and C. Mioskowski, *Organic Letters*, 2002, **4**, 2117-2119.
235. Y. Na and S. Chang, *Organic Letters*, 2000, **2**, 1887-1889.
236. B. M. Trost, M. R. Machacek and Z. T. Ball, *Organic Letters*, 2003, **5**, 1895-1898.
237. M. A. Esteruelas, L. A. Oro and C. Valero, *Organometallics*, 1991, **10**, 462-466.
238. R. Takeuchi and I. Ebata, *Organometallics*, 1997, **16**, 3707-3710.
239. T. A. Betley and J. C. Peters, *Angewandte Chemie International Edition*, 2003, **42**, 2385-2389.
240. R. S. Tanke and R. H. Crabtree, *Journal of the American Chemical Society*, 1990, **112**, 7984-7989.
241. S. Doherty, J. G. Knight, T. H. Scanlan, M. R. J. Elsegood and W. Clegg, *Journal of Organometallic Chemistry*, 2002, **650**, 231-248.
242. A. Tillack, S. Pulst, W. Baumann, H. Baudisch, K. Kortus and U. Rosenthal, *Journal of Organometallic Chemistry*, 1997, **532**, 117-123.
243. R. C. Larock, K. Oertle and G. F. Potter, *Journal of the American Chemical Society*, 1980, **102**, 190-197.
244. G. P. Mitchell and T. D. Tilley, *Journal of the American Chemical Society*, 1998, **120**, 7635-7636.
245. P. B. Glaser and T. D. Tilley, *Journal of the American Chemical Society*, 2003, **125**, 13640-13641.
246. B. Bosnich, *Accounts of Chemical Research*, 1998, **31**, 667-674.
247. P. S. Fier, J. Luo and J. F. Hartwig, *J. Am. Chem. Soc.*, 2013, **135**, 2552-2559.
248. Z. Han, F. Qiu, R. Eisenberg, P. L. Holland and T. D. Krauss, *Science*, 2012, **338**, 1321-1324.
249. C. A. Wheaton and P. G. Hayes, *Chem. Commun. (Cambridge, U. K.)*, 2010, **46**, 8404-8406.
250. A. W. Fraser, J. E. Besaw, L. E. Hull and M. C. Baird, *Organometallics*, 2012, **31**, 2470-2475.
251. T. E. Barder, S. D. Walker, J. R. Martinelli and S. L. Buchwald, *J. Am. Chem. Soc.*, 2005, **127**, 4685-4696.
252. S. Sakamoto, M. Fujita, K. Kim and K. Yamaguchi, *Tetrahedron*, 2000, **56**, 955-964.
253. K. Yamaguchi, *Mass Spectrometry*, 2013, **2**, S0012-S0012.

## Appendix A: Intermediate data for Pauson-Khand reaction

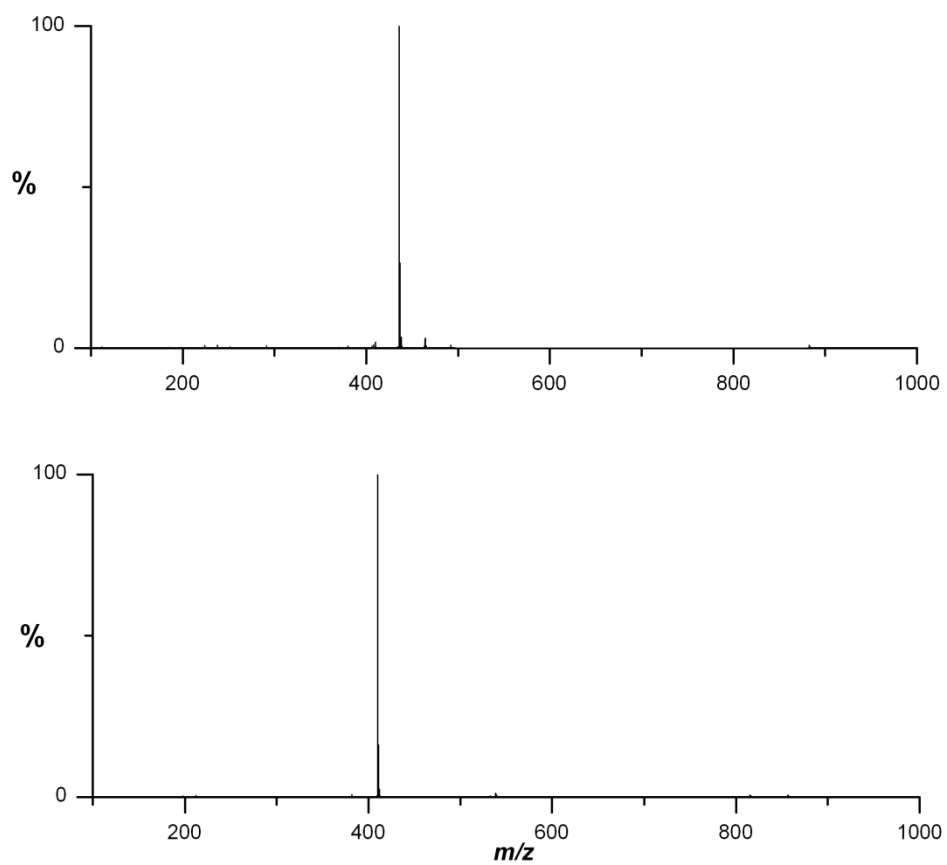


**Figure S11:** Positive-ion ESI-MS in dichloromethane  $[\text{Co}_2(\text{CO})_6(\mathbf{3})][\text{PF}_6]$  (top) and  $[\text{Co}_2(\text{CO})_6(\mathbf{1})][\text{PF}_6]$  (bottom). In both cases, the single peak corresponds to the intact cation.



## Appendix B: Numerical modeling, rate constants and ESI-MS data for hydrogenation reactions

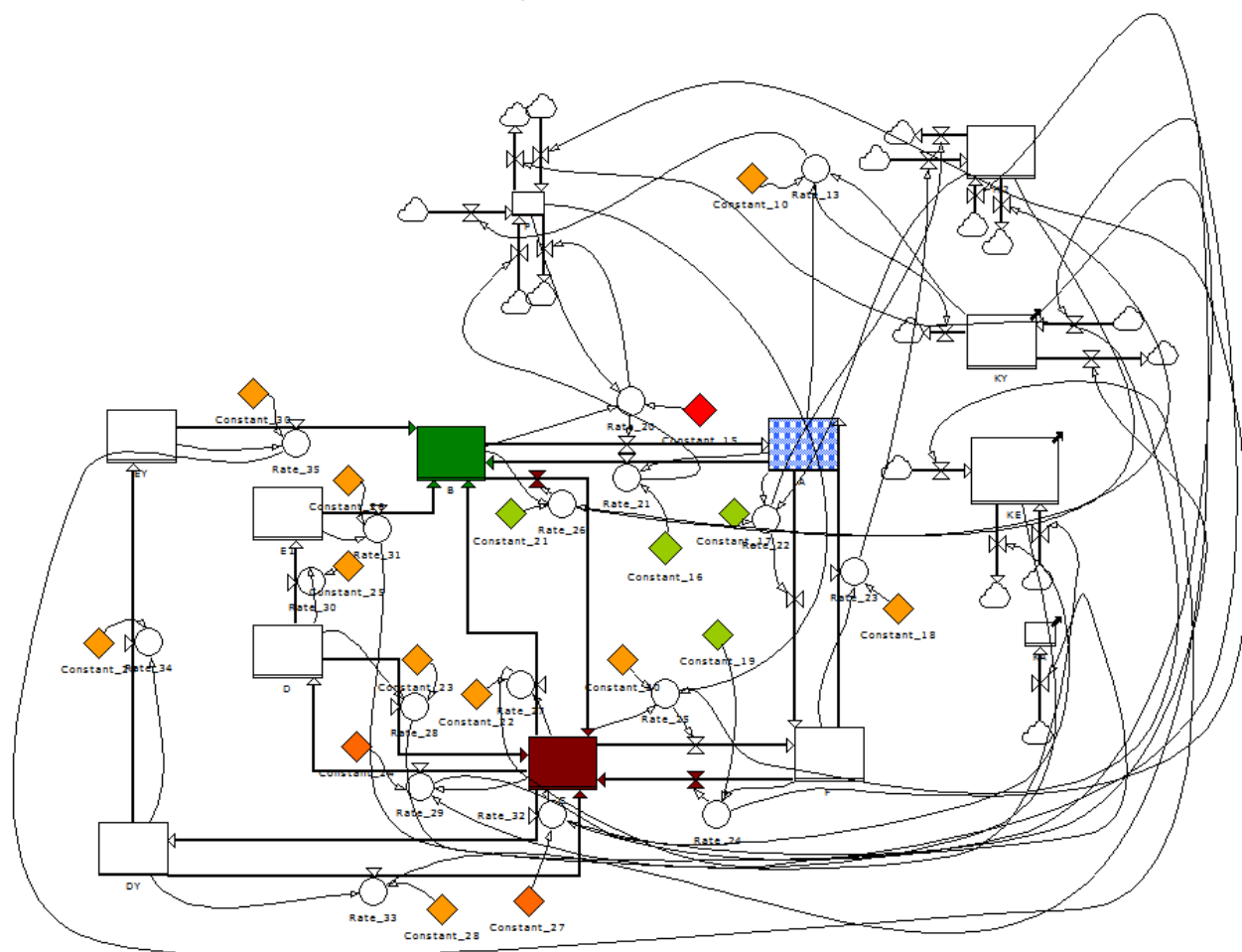


**Figure S1:** Powersim diagram of Wilkinson's hydrogenation mechanism.

Rate constant setting for the reaction at different temperatures

**Table S1.** Rate constants for the reaction at 23°C

| Rate constant, $k$ | Rate constant, $k$ for forward reaction | Rate constant, $k$ for back reaction |
|--------------------|---|--------------------------------------|
| $A \rightarrow B$  | 0.015                                   | 42                                   |
| $A \rightarrow F$  | 4                                       | 0.0001                               |

|                     |        |      |
|---------------------|--------|------|
| $F \rightarrow C$   | 0.0033 | 32   |
| $B \rightarrow C$   | 4000   | 1    |
| $C \rightarrow D$   | 47     | 5000 |
| $C \rightarrow D'$  | 141    | 4000 |
| $D \rightarrow E$   | 10000  | 0    |
| $E \rightarrow B$   | 10000  | 0    |
| $D' \rightarrow E'$ | 10000  | 0    |
| $E' \rightarrow B$  | 10000  | 0    |

**Table S|2.** Rate constants for the reaction at 58°C

| Rate constant, $k$ | Rate constant, $k$ for forward reaction | Rate constant, $k$ for back reaction |
|--------------------|---|--------------------------------------|
| $A \rightarrow B$  | 0.2                                     | 20                                   |
| $A \rightarrow F$  | 4                                       | 0.0001                               |
| $F \rightarrow C$  | 0.155                                   | 15                                   |
| $B \rightarrow C$  | 4000                                    | 1                                    |
| $C \rightarrow D$  | 51                                      | 5000                                 |
| $C \rightarrow D'$ | 153                                     | 4000                                 |
| $D \rightarrow E$  | 10000                                   | 0                                    |
| $E \rightarrow B$  | 10000                                   | 0                                    |

|                     |       |   |
|---------------------|-------|---|
| $D' \rightarrow E'$ | 10000 | 0 |
| $E' \rightarrow B$  | 10000 | 0 |

**Table S|3.** Rate constants for the reaction at 91°C

| Rate constant, $k$  | Rate constant, $k$ for forward reaction | Rate constant, $k$ for back reaction |
|---------------------|---|--------------------------------------|
| $A \rightarrow B$   | 3                                       | 120                                  |
| $A \rightarrow F$   | 6                                       | 0.002                                |
| $F \rightarrow C$   | 2                                       | 100                                  |
| $B \rightarrow C$   | 8000                                    | 1                                    |
| $C \rightarrow D$   | 90                                      | 5000                                 |
| $C \rightarrow D'$  | 250                                     | 4000                                 |
| $D \rightarrow E$   | 10000                                   | 0                                    |
| $E \rightarrow B$   | 10000                                   | 0                                    |
| $D' \rightarrow E'$ | 10000                                   | 0                                    |
| $E' \rightarrow B$  | 10000                                   | 0                                    |

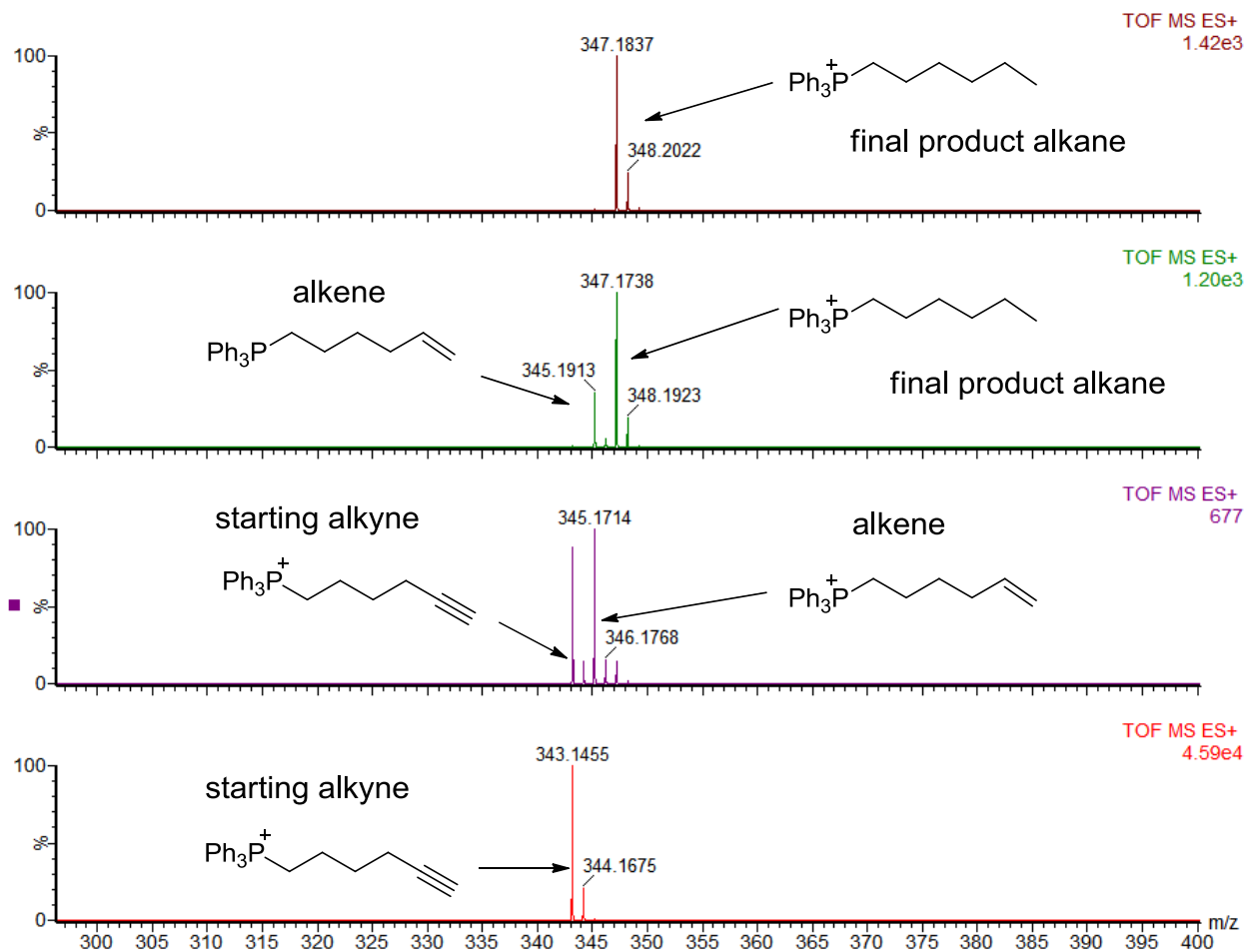


**Figure S|2** Positive-ion ESI-MS in Fluorobenzene,  $[\text{PPh}_3\text{P}(\text{CH}_2)_4\text{CCH}]\text{PF}_6$  (bottom) is the starting material.  $[\text{PPh}_3\text{P}(\text{CH}_2)_5\text{CH}_3]\text{PF}_6$  (top) is the final product.

### Appendix C: Crystal data and structure refinement for PPh<sub>3</sub>P(CH<sub>2</sub>)<sub>4</sub>CCH

|   |   |
|---|---|
| Identification code                     | uvic1304  |
| Empirical formula                       | C <sub>24</sub> H <sub>24</sub> IP  |
| Formula weight                          | 470.30  |
| Temperature                             | 120(2) K  |
| Wavelength                              | 0.71073 Å   |
| Crystal system                          | Monoclinic  |
| Space group                             | P2 <sub>1</sub> /n  |
| Unit cell dimensions                    | $a = 13.0516(10)$ Å $\alpha = 90^\circ$<br>$b = 12.5831(10)$ Å $\beta = 96.207(4)^\circ$<br>$c = 13.2499(10)$ Å $\gamma = 90^\circ$ |
| Volume                                  | 2163.3(3) Å <sup>3</sup>  |
| Z                                       | 4   |
| Density (calculated)                    | 1.444 g.cm <sup>-3</sup>  |
| Absorption coefficient ( $\mu$ )        | 1.559 mm <sup>-1</sup>  |
| F(000)                                  | 944   |
| Crystal color, habit                    | colorless, rod  |
| Crystal size                            | 0.150 × 0.101 × 0.061 mm <sup>3</sup>   |
| $\theta$ range for data collection      | 2.081 to 28.365°  |
| Index ranges                            | -17 ≤ h ≤ 17, -15 ≤ k ≤ 16, -17 ≤ l ≤ 17  |
| Reflections collected                   | 35698   |
| Independent reflections                 | 5405 [ $R_{\text{int}} = 0.0344$ ]  |
| Completeness to $\theta = 25.242^\circ$ | 100.0 %   |
| Absorption correction                   | Numerical   |
| Max. and min. transmission              | 0.9981 and 0.8813   |
| Refinement method                       | Full-matrix least-squares on F <sup>2</sup>   |
| Data / restraints / parameters          | 5405 / 0 / 235  |
| Goodness-of-fit on F <sup>2</sup>       | 1.015   |
| Final R indices [ $I > 2\sigma(I)$ ]    | $R_1 = 0.0236$ , $wR_2 = 0.0521$  |
| R indices (all data)                    | $R_1 = 0.0335$ , $wR_2 = 0.0559$  |

|                             |  |
|-----------------------------|--|
| Extinction coefficient      | n/a  |
| Largest diff. peak and hole | 0.656 and -0.310 e <sup>-</sup> .Å <sup>-3</sup> |

Table 2. Atomic coordinates and equivalent isotropic displacement parameters (Å<sup>2</sup>) for uvic1304\_x. U(eq) is defined as one third of the trace of the orthogonalized U<sub>ij</sub> tensor.

|       | x           | y           | z           | U(eq)    |
|-------|-------------|-------------|-------------|----------|
| P(1)  | 0.59437(4)  | 0.35145(4)  | 0.77633(4)  | 0.015(1) |
| C(1)  | 0.58625(15) | 0.34134(15) | 0.91035(15) | 0.019(1) |
| C(2)  | 0.65005(16) | 0.24609(16) | 0.95519(15) | 0.022(1) |
| C(3)  | 0.64279(18) | 0.23386(18) | 1.06805(16) | 0.028(1) |
| C(4)  | 0.71426(18) | 0.14714(18) | 1.11623(17) | 0.031(1) |
| C(5)  | 0.69245(18) | 0.0405(2)   | 1.07102(18) | 0.035(1) |
| C(6)  | 0.67377(19) | -0.0383(2)  | 1.03465(18) | 0.035(1) |
| C(7)  | 0.72855(14) | 0.35328(14) | 0.75839(14) | 0.016(1) |
| C(8)  | 0.78310(15) | 0.44387(16) | 0.79383(16) | 0.023(1) |
| C(9)  | 0.88741(16) | 0.45062(17) | 0.78475(17) | 0.028(1) |
| C(10) | 0.93784(16) | 0.36803(18) | 0.74190(17) | 0.028(1) |
| C(11) | 0.88443(16) | 0.27791(17) | 0.70810(17) | 0.026(1) |
| C(12) | 0.77930(15) | 0.27011(15) | 0.71609(15) | 0.020(1) |
| C(13) | 0.53804(14) | 0.47189(14) | 0.72400(14) | 0.017(1) |
| C(14) | 0.44746(14) | 0.51100(15) | 0.75743(15) | 0.020(1) |
| C(15) | 0.39882(15) | 0.59753(16) | 0.70789(15) | 0.022(1) |
| C(16) | 0.43910(16) | 0.64432(16) | 0.62686(16) | 0.023(1) |
| C(17) | 0.52931(16) | 0.60550(16) | 0.59386(16) | 0.025(1) |
| C(18) | 0.57886(15) | 0.51915(16) | 0.64136(15) | 0.022(1) |
| C(19) | 0.52645(14) | 0.24431(14) | 0.70879(14) | 0.017(1) |
| C(20) | 0.54421(15) | 0.22521(15) | 0.60839(15) | 0.021(1) |
| C(21) | 0.48296(18) | 0.15309(16) | 0.55023(17) | 0.026(1) |
| C(22) | 0.40499(15) | 0.09917(16) | 0.59120(17) | 0.026(1) |

|       |             |             |             |          |
|-------|-------------|-------------|-------------|----------|
| C(23) | 0.38776(15) | 0.11668(16) | 0.69143(18) | 0.027(1) |
| C(24) | 0.44817(14) | 0.18958(16) | 0.75110(16) | 0.022(1) |
| I(1)  | 0.78749(2)  | 0.13419(2)  | 0.45604(2)  | 0.022(1) |
| H(1A) | 0.6124      | 0.4076      | 0.9442      | 0.023    |
| H(1B) | 0.5133      | 0.3323      | 0.9229      | 0.023    |
| H(2A) | 0.6249      | 0.1803      | 0.9197      | 0.027    |
| H(2B) | 0.7231      | 0.2561      | 0.9436      | 0.027    |
| H(3A) | 0.5708      | 0.2165      | 1.0789      | 0.034    |
| H(3B) | 0.6607      | 0.3024      | 1.1023      | 0.034    |
| H(4A) | 0.7865      | 0.1666      | 1.1084      | 0.037    |
| H(4B) | 0.7072      | 0.1437      | 1.1898      | 0.037    |
| H(6)  | 0.6579      | -0.1053     | 1.0037      | 0.042    |
| H(8)  | 0.7488      | 0.5003      | 0.8239      | 0.027    |
| H(9)  | 0.9247      | 0.5123      | 0.8081      | 0.033    |
| H(10) | 1.0095      | 0.3734      | 0.7357      | 0.034    |
| H(11) | 0.9195      | 0.2212      | 0.6793      | 0.031    |
| H(12) | 0.7424      | 0.2082      | 0.6927      | 0.024    |
| H(14) | 0.4195      | 0.4789      | 0.8133      | 0.024    |
| H(15) | 0.3372      | 0.6247      | 0.7301      | 0.026    |
| H(16) | 0.4050      | 0.7033      | 0.5935      | 0.028    |
| H(17) | 0.5571      | 0.6385      | 0.5383      | 0.030    |
| H(18) | 0.6401      | 0.4920      | 0.6182      | 0.026    |
| H(20) | 0.5981      | 0.2615      | 0.5800      | 0.026    |
| H(21) | 0.4947      | 0.1407      | 0.4817      | 0.032    |
| H(22) | 0.3632      | 0.0501      | 0.5508      | 0.032    |
| H(23) | 0.3346      | 0.0789      | 0.7196      | 0.032    |
| H(24) | 0.4362      | 0.2018      | 0.8196      | 0.027    |

Table 3. Anisotropic displacement parameters ( $\text{\AA}^2$ ) for uvic1304\_x.

The anisotropic displacement factor exponent takes the form:

$$-2\pi^2[h^2a^2U_{11} + \dots + 2hka^*b^*U_{12}]$$

|       | $U_{11}$   | $U_{22}$   | $U_{33}$   | $U_{23}$    | $U_{13}$    | $U_{12}$    |
|-------|------------|------------|------------|-------------|-------------|-------------|
| P(1)  | 0.0150(2)  | 0.0133(2)  | 0.0165(2)  | 0.0010(2)   | 0.0023(2)   | 0.0000(2)   |
| C(1)  | 0.0210(9)  | 0.0210(9)  | 0.0165(9)  | 0.0014(7)   | 0.0043(7)   | 0.0017(7)   |
| C(2)  | 0.0242(10) | 0.0256(10) | 0.0179(10) | 0.0034(8)   | 0.0039(8)   | 0.0046(8)   |
| C(3)  | 0.0340(12) | 0.0317(11) | 0.0191(10) | 0.0019(9)   | 0.0034(9)   | 0.0039(9)   |
| C(4)  | 0.0361(12) | 0.0358(13) | 0.0199(10) | 0.0072(9)   | -0.0042(9)  | 0.0023(10)  |
| C(5)  | 0.0318(12) | 0.0425(14) | 0.0300(12) | 0.0176(11)  | -0.0017(10) | 0.0068(11)  |
| C(6)  | 0.0385(13) | 0.0339(13) | 0.0309(13) | 0.0076(10)  | -0.0079(10) | -0.0082(11) |
| C(7)  | 0.0139(8)  | 0.0172(9)  | 0.0164(9)  | 0.0002(7)   | 0.0011(7)   | -0.0010(7)  |
| C(8)  | 0.0226(10) | 0.0191(9)  | 0.0267(11) | -0.0056(8)  | 0.0018(8)   | -0.0001(8)  |
| C(9)  | 0.0233(10) | 0.0249(10) | 0.0342(12) | -0.0044(9)  | 0.0001(9)   | -0.0084(8)  |
| C(10) | 0.0149(9)  | 0.0399(12) | 0.0301(11) | -0.0018(10) | 0.0037(8)   | -0.0028(9)  |
| C(11) | 0.0217(10) | 0.0266(11) | 0.0290(11) | -0.0045(9)  | 0.0034(8)   | 0.0047(8)   |
| C(12) | 0.0200(9)  | 0.0186(9)  | 0.0217(10) | -0.0034(7)  | 0.0011(8)   | -0.0001(7)  |
| C(13) | 0.0170(9)  | 0.0135(8)  | 0.0189(9)  | -0.0001(7)  | 0.0006(7)   | 0.0002(7)   |
| C(14) | 0.0195(9)  | 0.0199(9)  | 0.0220(10) | 0.0020(8)   | 0.0048(8)   | -0.0005(8)  |
| C(15) | 0.0193(9)  | 0.0225(9)  | 0.0243(10) | -0.0007(8)  | 0.0029(8)   | 0.0036(8)   |
| C(16) | 0.0260(10) | 0.0191(10) | 0.0241(10) | 0.0024(8)   | -0.0013(8)  | 0.0049(8)   |
| C(17) | 0.0302(11) | 0.0227(10) | 0.0224(10) | 0.0054(8)   | 0.0069(8)   | 0.0035(8)   |
| C(18) | 0.0220(10) | 0.0215(10) | 0.0225(10) | 0.0009(8)   | 0.0058(8)   | 0.0031(8)   |
| C(19) | 0.0159(9)  | 0.0137(8)  | 0.0216(10) | 0.0007(7)   | -0.0012(7)  | 0.0002(7)   |
| C(20) | 0.0247(10) | 0.0181(9)  | 0.0202(10) | 0.0029(7)   | -0.0012(8)  | -0.0053(8)  |
| C(21) | 0.0354(12) | 0.0191(10) | 0.0230(11) | 0.0023(8)   | -0.0062(9)  | -0.0023(8)  |
| C(22) | 0.0206(10) | 0.0175(9)  | 0.0381(12) | -0.0006(9)  | -0.0085(9)  | -0.0006(8)  |
| C(23) | 0.0146(9)  | 0.0181(10) | 0.0476(14) | 0.0015(9)   | 0.0053(9)   | -0.0015(7)  |
| C(24) | 0.0166(9)  | 0.0195(10) | 0.0321(11) | -0.0003(8)  | 0.0068(8)   | 0.0016(8)   |



I(1)      0.0215(1)  0.0197(1)  0.0271(1) -0.0048(1)  0.0098(1) -0.0027(1)

Table 4. Bond lengths [ $\text{\AA}$ ] for uvic1304\_x.

| atom-atom   | distance   | atom-atom   | distance   |
|-------------|------------|-------------|------------|
| P(1)-C(13)  | 1.7911(19) | P(1)-C(7)   | 1.7927(19) |
| P(1)-C(1)   | 1.795(2)   | P(1)-C(19)  | 1.7979(19) |
| C(1)-C(2)   | 1.541(3)   | C(2)-C(3)   | 1.516(3)   |
| C(3)-C(4)   | 1.530(3)   | C(4)-C(5)   | 1.484(4)   |
| C(5)-C(6)   | 1.118(3)   | C(7)-C(12)  | 1.389(3)   |
| C(7)-C(8)   | 1.398(3)   | C(8)-C(9)   | 1.382(3)   |
| C(9)-C(10)  | 1.384(3)   | C(10)-C(11) | 1.380(3)   |
| C(11)-C(12) | 1.391(3)   | C(13)-C(14) | 1.396(3)   |
| C(13)-C(18) | 1.401(3)   | C(14)-C(15) | 1.389(3)   |
| C(15)-C(16) | 1.378(3)   | C(16)-C(17) | 1.388(3)   |
| C(17)-C(18) | 1.381(3)   | C(19)-C(20) | 1.396(3)   |
| C(19)-C(24) | 1.399(3)   | C(20)-C(21) | 1.387(3)   |
| C(21)-C(22) | 1.382(3)   | C(22)-C(23) | 1.388(3)   |
| C(23)-C(24) | 1.398(3)   | C(1)-H(1A)  | 0.9900     |
| C(1)-H(1B)  | 0.9900     | C(2)-H(2A)  | 0.9900     |
| C(2)-H(2B)  | 0.9900     | C(3)-H(3A)  | 0.9900     |
| C(3)-H(3B)  | 0.9900     | C(4)-H(4A)  | 0.9900     |
| C(4)-H(4B)  | 0.9900     | C(6)-H(6)   | 0.9500     |
| C(8)-H(8)   | 0.9500     | C(9)-H(9)   | 0.9500     |
| C(10)-H(10) | 0.9500     | C(11)-H(11) | 0.9500     |
| C(12)-H(12) | 0.9500     | C(14)-H(14) | 0.9500     |
| C(15)-H(15) | 0.9500     | C(16)-H(16) | 0.9500     |
| C(17)-H(17) | 0.9500     | C(18)-H(18) | 0.9500     |
| C(20)-H(20) | 0.9500     | C(21)-H(21) | 0.9500     |
| C(22)-H(22) | 0.9500     | C(23)-H(23) | 0.9500     |

C(24)-H(24) 0.9500

Symmetry transformations used to generate equivalent atoms:

Table 5. Bond angles [°] for uvic1304\_x.

| atom-atom-atom    | angle      | atom-atom-atom    | angle      |
|-------------------|------------|-------------------|------------|
| C(13)-P(1)-C(7)   | 107.69(9)  | C(13)-P(1)-C(1)   | 112.16(9)  |
| C(7)-P(1)-C(1)    | 107.16(9)  | C(13)-P(1)-C(19)  | 106.39(9)  |
| C(7)-P(1)-C(19)   | 112.32(9)  | C(1)-P(1)-C(19)   | 111.14(9)  |
| C(2)-C(1)-P(1)    | 110.44(13) | C(3)-C(2)-C(1)    | 111.73(17) |
| C(2)-C(3)-C(4)    | 112.57(18) | C(5)-C(4)-C(3)    | 113.24(19) |
| C(6)-C(5)-C(4)    | 177.7(3)   | C(12)-C(7)-C(8)   | 120.15(17) |
| C(12)-C(7)-P(1)   | 124.00(14) | C(8)-C(7)-P(1)    | 115.80(14) |
| C(9)-C(8)-C(7)    | 119.44(18) | C(8)-C(9)-C(10)   | 120.39(19) |
| C(11)-C(10)-C(9)  | 120.27(19) | C(10)-C(11)-C(12) | 120.07(19) |
| C(7)-C(12)-C(11)  | 119.67(18) | C(14)-C(13)-C(18) | 120.33(17) |
| C(14)-C(13)-P(1)  | 120.11(14) | C(18)-C(13)-P(1)  | 119.13(14) |
| C(15)-C(14)-C(13) | 119.06(18) | C(16)-C(15)-C(14) | 120.66(18) |
| C(15)-C(16)-C(17) | 120.21(18) | C(18)-C(17)-C(16) | 120.31(19) |
| C(17)-C(18)-C(13) | 119.42(18) | C(20)-C(19)-C(24) | 120.07(17) |
| C(20)-C(19)-P(1)  | 118.67(14) | C(24)-C(19)-P(1)  | 120.80(15) |
| C(21)-C(20)-C(19) | 119.81(19) | C(22)-C(21)-C(20) | 120.5(2)   |
| C(21)-C(22)-C(23) | 120.01(19) | C(22)-C(23)-C(24) | 120.36(19) |
| C(23)-C(24)-C(19) | 119.23(19) | C(2)-C(1)-H(1A)   | 109.6      |
| P(1)-C(1)-H(1A)   | 109.6      | C(2)-C(1)-H(1B)   | 109.6      |
| P(1)-C(1)-H(1B)   | 109.6      | H(1A)-C(1)-H(1B)  | 108.1      |
| C(3)-C(2)-H(2A)   | 109.3      | C(1)-C(2)-H(2A)   | 109.3      |
| C(3)-C(2)-H(2B)   | 109.3      | C(1)-C(2)-H(2B)   | 109.3      |
| H(2A)-C(2)-H(2B)  | 107.9      | C(2)-C(3)-H(3A)   | 109.1      |

|                   |       |                   |       |
|-------------------|-------|-------------------|-------|
| C(4)-C(3)-H(3A)   | 109.1 | C(2)-C(3)-H(3B)   | 109.1 |
| C(4)-C(3)-H(3B)   | 109.1 | H(3A)-C(3)-H(3B)  | 107.8 |
| C(5)-C(4)-H(4A)   | 108.9 | C(3)-C(4)-H(4A)   | 108.9 |
| C(5)-C(4)-H(4B)   | 108.9 | C(3)-C(4)-H(4B)   | 108.9 |
| H(4A)-C(4)-H(4B)  | 107.7 | C(5)-C(6)-H(6)    | 180.0 |
| C(9)-C(8)-H(8)    | 120.3 | C(7)-C(8)-H(8)    | 120.3 |
| C(8)-C(9)-H(9)    | 119.8 | C(10)-C(9)-H(9)   | 119.8 |
| C(11)-C(10)-H(10) | 119.9 | C(9)-C(10)-H(10)  | 119.9 |
| C(10)-C(11)-H(11) | 120.0 | C(12)-C(11)-H(11) | 120.0 |
| C(7)-C(12)-H(12)  | 120.2 | C(11)-C(12)-H(12) | 120.2 |
| C(15)-C(14)-H(14) | 120.5 | C(13)-C(14)-H(14) | 120.5 |
| C(16)-C(15)-H(15) | 119.7 | C(14)-C(15)-H(15) | 119.7 |
| C(15)-C(16)-H(16) | 119.9 | C(17)-C(16)-H(16) | 119.9 |
| C(18)-C(17)-H(17) | 119.8 | C(16)-C(17)-H(17) | 119.8 |
| C(17)-C(18)-H(18) | 120.3 | C(13)-C(18)-H(18) | 120.3 |
| C(21)-C(20)-H(20) | 120.1 | C(19)-C(20)-H(20) | 120.1 |
| C(22)-C(21)-H(21) | 119.7 | C(20)-C(21)-H(21) | 119.7 |
| C(21)-C(22)-H(22) | 120.0 | C(23)-C(22)-H(22) | 120.0 |
| C(22)-C(23)-H(23) | 119.8 | C(24)-C(23)-H(23) | 119.8 |
| C(23)-C(24)-H(24) | 120.4 | C(19)-C(24)-H(24) | 120.4 |

Symmetry transformations used to generate equivalent atoms:

Table 6. Torsion angles [ $^{\circ}$ ] for uvic1304\_x.

| atom-atom-atom-atom     | angle       | atom-atom-atom-atom     | angle       |
|-------------------------|-------------|-------------------------|-------------|
| C(13)-P(1)-C(1)-C(2)    | -171.15(13) | C(7)-P(1)-C(1)-C(2)     | -53.16(16)  |
| C(19)-P(1)-C(1)-C(2)    | 69.90(16)   | P(1)-C(1)-C(2)-C(3)     | -178.70(15) |
| C(1)-C(2)-C(3)-C(4)     | -174.04(18) | C(2)-C(3)-C(4)-C(5)     | -59.7(3)    |
| C(13)-P(1)-C(7)-C(12)   | -129.77(17) | C(1)-P(1)-C(7)-C(12)    | 109.37(17)  |
| C(19)-P(1)-C(7)-C(12)   | -13.0(2)    | C(13)-P(1)-C(7)-C(8)    | 52.73(17)   |
| C(1)-P(1)-C(7)-C(8)     | -68.13(17)  | C(19)-P(1)-C(7)-C(8)    | 169.55(15)  |
| C(12)-C(7)-C(8)-C(9)    | 1.1(3)      | P(1)-C(7)-C(8)-C(9)     | 178.72(16)  |
| C(7)-C(8)-C(9)-C(10)    | -0.7(3)     | C(8)-C(9)-C(10)-C(11)   | -0.2(3)     |
| C(9)-C(10)-C(11)-C(12)  | 0.6(3)      | C(8)-C(7)-C(12)-C(11)   | -0.7(3)     |
| P(1)-C(7)-C(12)-C(11)   | -178.12(16) | C(10)-C(11)-C(12)-C(7)  | -0.1(3)     |
| C(7)-P(1)-C(13)-C(14)   | -156.87(15) | C(1)-P(1)-C(13)-C(14)   | -39.20(18)  |
| C(19)-P(1)-C(13)-C(14)  | 82.51(17)   | C(7)-P(1)-C(13)-C(18)   | 30.58(18)   |
| C(1)-P(1)-C(13)-C(18)   | 148.25(15)  | C(19)-P(1)-C(13)-C(18)  | -90.04(17)  |
| C(18)-C(13)-C(14)-C(15) | -0.3(3)     | P(1)-C(13)-C(14)-C(15)  | -172.73(15) |
| C(13)-C(14)-C(15)-C(16) | 0.0(3)      | C(14)-C(15)-C(16)-C(17) | -0.2(3)     |
| C(15)-C(16)-C(17)-C(18) | 0.6(3)      | C(16)-C(17)-C(18)-C(13) | -0.8(3)     |
| C(14)-C(13)-C(18)-C(17) | 0.7(3)      | P(1)-C(13)-C(18)-C(17)  | 173.20(16)  |
| C(13)-P(1)-C(19)-C(20)  | 72.36(17)   | C(7)-P(1)-C(19)-C(20)   | -45.23(18)  |
| C(1)-P(1)-C(19)-C(20)   | -165.27(15) | C(13)-P(1)-C(19)-C(24)  | -99.80(16)  |
| C(7)-P(1)-C(19)-C(24)   | 142.61(15)  | C(1)-P(1)-C(19)-C(24)   | 22.56(18)   |
| C(24)-C(19)-C(20)-C(21) | 1.0(3)      | P(1)-C(19)-C(20)-C(21)  | -171.19(15) |
| C(19)-C(20)-C(21)-C(22) | -0.6(3)     | C(20)-C(21)-C(22)-C(23) | -0.3(3)     |
| C(21)-C(22)-C(23)-C(24) | 0.7(3)      | C(22)-C(23)-C(24)-C(19) | -0.3(3)     |
| C(20)-C(19)-C(24)-C(23) | -0.6(3)     | P(1)-C(19)-C(24)-C(23)  | 171.46(15)  |

Symmetry transformations used to generate equivalent atoms:

**Appendix D: Crystal data and structure refinement for  
PPh<sub>3</sub>P(CH<sub>2</sub>)<sub>5</sub>CH<sub>3</sub>.**

|   |  |
|---|--|
| Identification code                     | uvic1302   |
| Empirical formula                       | C <sub>24</sub> H <sub>28</sub> F <sub>6</sub> P <sub>2</sub>  |
| Formula weight                          | 492.40   |
| Temperature                             | 120(2) K   |
| Wavelength                              | 0.71073 Å  |
| Crystal system                          | Orthorhombic   |
| Space group                             | Pbca   |
| Unit cell dimensions                    | $a = 13.3757(15)$ Å $\alpha = 90^\circ$<br>$b = 17.979(2)$ Å $\beta = 90^\circ$<br>$c = 19.568(2)$ Å $\gamma = 90^\circ$ |
| Volume                                  | 4705.9(9) Å <sup>3</sup>   |
| Z                                       | 8  |
| Density (calculated)                    | 1.390 g.cm <sup>-3</sup>   |
| Absorption coefficient ( $\mu$ )        | 0.242 mm <sup>-1</sup>   |
| F(000)                                  | 2048   |
| Crystal color, habit                    | colorless, tablet  |
| Crystal size                            | 0.230 × 0.180 × 0.070 mm <sup>3</sup>  |
| $\theta$ range for data collection      | 2.081 to 26.481°   |
| Index ranges                            | -16 ≤ h ≤ 16, -22 ≤ k ≤ 22, -24 ≤ l ≤ 24   |
| Reflections collected                   | 55595  |
| Independent reflections                 | 4858 [R <sub>int</sub> = 0.0561]   |
| Completeness to $\theta = 25.242^\circ$ | 100.0 %  |
| Absorption correction                   | Numerical  |
| Max. and min. transmission              | 1.0000 and 0.8375  |
| Refinement method                       | Full-matrix least-squares on F <sup>2</sup>  |
| Data / restraints / parameters          | 4858 / 0 / 306   |
| Goodness-of-fit on F <sup>2</sup>       | 1.044  |
| Final R indices [I > 2σ(I)]             | R <sub>1</sub> = 0.0434, wR <sub>2</sub> = 0.1005  |

|                             |  |
|-----------------------------|--|
| R indices (all data)        | $R_1 = 0.0637$ , $wR_2 = 0.1091$                     |
| Extinction coefficient      | n/a  |
| Largest diff. peak and hole | 0.528 and $-0.451 \text{ e}^- \cdot \text{\AA}^{-3}$ |

Table 2. Atomic coordinates and equivalent isotropic displacement parameters ( $\text{\AA}^2$ ) for *uvc1302\_x*.  $U(\text{eq})$  is defined as one third of the trace of the orthogonalized  $U_{ij}$  tensor.

|       | x           | y           | z           | $U(\text{eq})$ |
|-------|-------------|-------------|-------------|----------------|
| P(1)  | 0.34382(4)  | 0.24259(3)  | 0.34052(3)  | 0.019(1)       |
| C(1)  | 0.33641(15) | 0.26159(12) | 0.25052(11) | 0.025(1)       |
| C(2)  | 0.42290(16) | 0.30731(13) | 0.22289(11) | 0.029(1)       |
| C(3)  | 0.41580(15) | 0.31619(13) | 0.14559(11) | 0.028(1)       |
| C(4)  | 0.50425(16) | 0.35820(13) | 0.11677(11) | 0.029(1)       |
| C(5)  | 0.49729(16) | 0.37350(12) | 0.03995(11) | 0.031(1)       |
| C(6)  | 0.41137(19) | 0.42259(15) | 0.02027(12) | 0.039(1)       |
| C(7)  | 0.24166(14) | 0.18222(11) | 0.36305(10) | 0.023(1)       |
| C(8)  | 0.20236(17) | 0.18428(13) | 0.42860(12) | 0.032(1)       |
| C(9)  | 0.12354(17) | 0.13798(14) | 0.44630(13) | 0.038(1)       |
| C(10) | 0.08302(16) | 0.09057(13) | 0.39891(13) | 0.034(1)       |
| C(11) | 0.12095(19) | 0.08831(15) | 0.33387(13) | 0.042(1)       |
| C(12) | 0.20049(18) | 0.13332(14) | 0.31552(12) | 0.036(1)       |
| C(13) | 0.33259(14) | 0.32456(11) | 0.39177(10) | 0.021(1)       |
| C(14) | 0.27700(15) | 0.38445(12) | 0.36762(11) | 0.026(1)       |
| C(15) | 0.25770(17) | 0.44382(13) | 0.41103(12) | 0.033(1)       |
| C(16) | 0.29278(17) | 0.44357(13) | 0.47731(13) | 0.034(1)       |
| C(17) | 0.34822(15) | 0.38416(13) | 0.50117(12) | 0.031(1)       |
| C(18) | 0.36825(14) | 0.32465(12) | 0.45880(11) | 0.025(1)       |
| C(19) | 0.46246(14) | 0.19939(11) | 0.35605(10) | 0.020(1)       |
| C(20) | 0.47263(15) | 0.12343(12) | 0.34363(11) | 0.025(1)       |
| C(21) | 0.56572(17) | 0.09040(13) | 0.34961(11) | 0.030(1)       |

|       |              |              |             |          |
|-------|--------------|--------------|-------------|----------|
| C(22) | 0.64802(16)  | 0.13271(13)  | 0.36845(11) | 0.031(1) |
| C(23) | 0.63811(15)  | 0.20790(13)  | 0.37994(11) | 0.028(1) |
| C(24) | 0.54581(14)  | 0.24231(12)  | 0.37306(10) | 0.023(1) |
| P(2)  | -0.14461(4)  | -0.03949(3)  | 0.31318(3)  | 0.028(1) |
| F(1)  | -0.15447(10) | -0.12416(7)  | 0.28999(8)  | 0.044(1) |
| F(2)  | -0.13410(11) | 0.04629(9)   | 0.33459(10) | 0.063(1) |
| F(3)  | -0.25964(12) | -0.02943(11) | 0.29599(12) | 0.063(1) |
| F(4)  | -0.03131(13) | -0.05419(11) | 0.33122(15) | 0.070(1) |
| F(5)  | -0.1174(2)   | -0.01839(11) | 0.23812(10) | 0.074(1) |
| F(6)  | -0.1737(2)   | -0.06455(19) | 0.38772(11) | 0.105(1) |
| F(3A) | -0.2397(8)   | -0.0306(6)   | 0.3595(5)   | 0.041(3) |
| F(4A) | -0.0417(7)   | -0.0289(5)   | 0.2722(5)   | 0.034(3) |
| F(5A) | -0.2076(8)   | -0.0069(5)   | 0.2513(5)   | 0.038(3) |
| F(6A) | -0.0841(8)   | -0.0519(5)   | 0.3794(5)   | 0.036(3) |
| H(1A) | 0.3339       | 0.2137       | 0.2255      | 0.030    |
| H(1B) | 0.2732       | 0.2884       | 0.2412      | 0.030    |
| H(2A) | 0.4868       | 0.2826       | 0.2347      | 0.034    |
| H(2B) | 0.4225       | 0.3570       | 0.2446      | 0.034    |
| H(3A) | 0.4124       | 0.2664       | 0.1241      | 0.034    |
| H(3B) | 0.3535       | 0.3431       | 0.1341      | 0.034    |
| H(4A) | 0.5658       | 0.3293       | 0.1258      | 0.035    |
| H(4B) | 0.5104       | 0.4062       | 0.1411      | 0.035    |
| H(5A) | 0.5603       | 0.3971       | 0.0247      | 0.037    |
| H(5B) | 0.4908       | 0.3255       | 0.0156      | 0.037    |
| H(6A) | 0.4113       | 0.4298       | -0.0294     | 0.058    |
| H(6B) | 0.4182       | 0.4709       | 0.0430      | 0.058    |
| H(6C) | 0.3485       | 0.3992       | 0.0343      | 0.058    |
| H(8)  | 0.2295       | 0.2175       | 0.4615      | 0.039    |
| H(9)  | 0.0975       | 0.1391       | 0.4915      | 0.045    |
| H(10) | 0.0287       | 0.0593       | 0.4112      | 0.041    |
| H(11) | 0.0924       | 0.0556       | 0.3011      | 0.051    |

|       |        |        |        |       |
|-------|--------|--------|--------|-------|
| H(12) | 0.2270 | 0.1309 | 0.2705 | 0.044 |
| H(14) | 0.2526 | 0.3847 | 0.3220 | 0.032 |
| H(15) | 0.2200 | 0.4850 | 0.3949 | 0.040 |
| H(16) | 0.2788 | 0.4844 | 0.5066 | 0.041 |
| H(17) | 0.3726 | 0.3843 | 0.5468 | 0.037 |
| H(18) | 0.4063 | 0.2838 | 0.4752 | 0.030 |
| H(20) | 0.4161 | 0.0945 | 0.3311 | 0.030 |
| H(21) | 0.5733 | 0.0387 | 0.3408 | 0.036 |
| H(22) | 0.7115 | 0.1097 | 0.3734 | 0.038 |
| H(23) | 0.6949 | 0.2364 | 0.3927 | 0.034 |
| H(24) | 0.5394 | 0.2944 | 0.3798 | 0.027 |

Table 3. Anisotropic displacement parameters ( $\text{\AA}^2$ ) for *uvic1302\_x*.

The anisotropic displacement factor exponent takes the form:

$$-2\pi^2[h^2a^{*2}U_{11} + \dots + 2hka^*b^*U_{12}]$$

|       | $U_{11}$   | $U_{22}$   | $U_{33}$   | $U_{23}$    | $U_{13}$    | $U_{12}$    |
|-------|------------|------------|------------|-------------|-------------|-------------|
| P(1)  | 0.0166(2)  | 0.0245(3)  | 0.0171(2)  | 0.0001(2)   | -0.0006(2)  | 0.0018(2)   |
| C(1)  | 0.0233(9)  | 0.0309(11) | 0.0210(10) | -0.0005(9)  | -0.0022(8)  | 0.0028(9)   |
| C(2)  | 0.0279(11) | 0.0323(12) | 0.0253(11) | 0.0011(9)   | -0.0033(9)  | -0.0042(9)  |
| C(3)  | 0.0253(10) | 0.0361(12) | 0.0226(11) | 0.0028(9)   | 0.0007(9)   | -0.0031(9)  |
| C(4)  | 0.0269(11) | 0.0334(12) | 0.0272(12) | -0.0013(10) | 0.0001(9)   | -0.0023(9)  |
| C(5)  | 0.0339(12) | 0.0320(12) | 0.0256(11) | -0.0063(10) | 0.0099(10)  | -0.0103(10) |
| C(6)  | 0.0482(15) | 0.0463(15) | 0.0223(12) | 0.0031(11)  | 0.0016(11)  | -0.0029(12) |
| C(7)  | 0.0182(9)  | 0.0251(11) | 0.0240(11) | -0.0003(9)  | -0.0021(8)  | 0.0012(8)   |
| C(8)  | 0.0320(12) | 0.0356(13) | 0.0287(12) | -0.0093(10) | 0.0060(10)  | -0.0066(10) |
| C(9)  | 0.0337(12) | 0.0416(14) | 0.0379(14) | -0.0050(11) | 0.0143(11)  | -0.0062(11) |
| C(10) | 0.0200(10) | 0.0370(13) | 0.0458(15) | 0.0002(11)  | 0.0027(10)  | -0.0064(9)  |
| C(11) | 0.0392(13) | 0.0508(16) | 0.0372(14) | -0.0024(12) | -0.0068(11) | -0.0208(12) |
| C(12) | 0.0383(13) | 0.0473(15) | 0.0232(12) | -0.0029(11) | -0.0007(10) | -0.0143(11) |



|       |            |            |            |             |             |             |
|-------|------------|------------|------------|-------------|-------------|-------------|
| C(13) | 0.0170(9)  | 0.0233(10) | 0.0222(10) | -0.0011(8)  | 0.0010(8)   | -0.0010(8)  |
| C(14) | 0.0229(10) | 0.0284(11) | 0.0281(11) | 0.0036(9)   | -0.0004(9)  | 0.0021(9)   |
| C(15) | 0.0324(12) | 0.0249(11) | 0.0423(14) | 0.0016(10)  | 0.0035(11)  | 0.0059(9)   |
| C(16) | 0.0306(11) | 0.0291(12) | 0.0420(14) | -0.0107(11) | 0.0083(10)  | -0.0020(10) |
| C(17) | 0.0240(10) | 0.0402(13) | 0.0276(12) | -0.0078(10) | 0.0006(9)   | -0.0030(10) |
| C(18) | 0.0192(9)  | 0.0321(12) | 0.0239(11) | -0.0019(9)  | 0.0007(8)   | 0.0028(8)   |
| C(19) | 0.0180(9)  | 0.0274(11) | 0.0154(10) | 0.0045(8)   | 0.0019(8)   | 0.0027(8)   |
| C(20) | 0.0256(10) | 0.0274(11) | 0.0232(11) | 0.0022(9)   | 0.0030(9)   | 0.0008(9)   |
| C(21) | 0.0359(12) | 0.0272(12) | 0.0278(12) | 0.0044(10)  | 0.0065(10)  | 0.0095(9)   |
| C(22) | 0.0243(10) | 0.0470(14) | 0.0224(11) | 0.0061(10)  | 0.0051(9)   | 0.0141(10)  |
| C(23) | 0.0173(10) | 0.0454(14) | 0.0216(11) | 0.0021(10)  | 0.0013(8)   | 0.0004(9)   |
| C(24) | 0.0215(9)  | 0.0280(11) | 0.0186(10) | 0.0021(9)   | 0.0027(8)   | 0.0006(8)   |
| P(2)  | 0.0182(3)  | 0.0371(3)  | 0.0287(3)  | -0.0072(2)  | -0.0003(2)  | 0.0001(2)   |
| F(1)  | 0.0399(8)  | 0.0276(7)  | 0.0643(10) | 0.0051(7)   | -0.0189(7)  | -0.0074(6)  |
| F(2)  | 0.0376(8)  | 0.0538(10) | 0.0987(14) | -0.0471(10) | -0.0153(9)  | 0.0138(7)   |
| F(3)  | 0.0236(9)  | 0.0592(13) | 0.1064(19) | -0.0272(12) | -0.0191(10) | 0.0091(8)   |
| F(4)  | 0.0238(9)  | 0.0459(11) | 0.141(2)   | -0.0357(13) | -0.0284(12) | 0.0053(8)   |
| F(5)  | 0.129(2)   | 0.0443(11) | 0.0480(13) | 0.0083(9)   | 0.0364(14)  | -0.0150(13) |
| F(6)  | 0.111(2)   | 0.178(3)   | 0.0247(11) | 0.0021(14)  | 0.0129(12)  | -0.016(2)   |

Table 4. Bond lengths [ $\text{\AA}$ ] for uvic1302\_x.

| atom-atom   | distance   | atom-atom   | distance   |
|-------------|------------|-------------|------------|
| P(1)-C(13)  | 1.789(2)   | P(1)-C(19)  | 1.793(2)   |
| P(1)-C(1)   | 1.797(2)   | P(1)-C(7)   | 1.800(2)   |
| C(1)-C(2)   | 1.519(3)   | C(2)-C(3)   | 1.524(3)   |
| C(3)-C(4)   | 1.513(3)   | C(4)-C(5)   | 1.531(3)   |
| C(5)-C(6)   | 1.499(3)   | C(7)-C(8)   | 1.387(3)   |
| C(7)-C(12)  | 1.393(3)   | C(8)-C(9)   | 1.387(3)   |
| C(9)-C(10)  | 1.371(3)   | C(10)-C(11) | 1.371(3)   |
| C(11)-C(12) | 1.384(3)   | C(13)-C(14) | 1.391(3)   |
| C(13)-C(18) | 1.396(3)   | C(14)-C(15) | 1.388(3)   |
| C(15)-C(16) | 1.379(3)   | C(16)-C(17) | 1.382(3)   |
| C(17)-C(18) | 1.380(3)   | C(19)-C(20) | 1.394(3)   |
| C(19)-C(24) | 1.396(3)   | C(20)-C(21) | 1.385(3)   |
| C(21)-C(22) | 1.388(3)   | C(22)-C(23) | 1.377(3)   |
| C(23)-C(24) | 1.388(3)   | P(2)-F(6A)  | 1.545(9)   |
| P(2)-F(5)   | 1.560(2)   | P(2)-F(3A)  | 1.569(10)  |
| P(2)-F(6)   | 1.575(2)   | P(2)-F(4)   | 1.5783(17) |
| P(2)-F(3)   | 1.5853(17) | P(2)-F(5A)  | 1.588(9)   |
| P(2)-F(1)   | 1.5939(15) | P(2)-F(2)   | 1.6043(16) |
| P(2)-F(4A)  | 1.605(9)   | C(1)-H(1A)  | 0.9900     |
| C(1)-H(1B)  | 0.9900     | C(2)-H(2A)  | 0.9900     |
| C(2)-H(2B)  | 0.9900     | C(3)-H(3A)  | 0.9900     |
| C(3)-H(3B)  | 0.9900     | C(4)-H(4A)  | 0.9900     |
| C(4)-H(4B)  | 0.9900     | C(5)-H(5A)  | 0.9900     |
| C(5)-H(5B)  | 0.9900     | C(6)-H(6A)  | 0.9800     |
| C(6)-H(6B)  | 0.9800     | C(6)-H(6C)  | 0.9800     |
| C(8)-H(8)   | 0.9500     | C(9)-H(9)   | 0.9500     |
| C(10)-H(10) | 0.9500     | C(11)-H(11) | 0.9500     |

|             |        |             |        |
|-------------|--------|-------------|--------|
| C(12)-H(12) | 0.9500 | C(14)-H(14) | 0.9500 |
| C(15)-H(15) | 0.9500 | C(16)-H(16) | 0.9500 |
| C(17)-H(17) | 0.9500 | C(18)-H(18) | 0.9500 |
| C(20)-H(20) | 0.9500 | C(21)-H(21) | 0.9500 |
| C(22)-H(22) | 0.9500 | C(23)-H(23) | 0.9500 |
| C(24)-H(24) | 0.9500 |             |        |

Symmetry transformations used to generate equivalent atoms:

Table 5. Bond angles [°] for uvic1302\_x.

| atom-atom-atom    | angle      | atom-atom-atom    | angle      |
|-------------------|------------|-------------------|------------|
| C(13)-P(1)-C(19)  | 109.65(9)  | C(13)-P(1)-C(1)   | 112.85(10) |
| C(19)-P(1)-C(1)   | 107.30(9)  | C(13)-P(1)-C(7)   | 107.20(9)  |
| C(19)-P(1)-C(7)   | 111.68(9)  | C(1)-P(1)-C(7)    | 108.23(10) |
| C(2)-C(1)-P(1)    | 114.19(14) | C(1)-C(2)-C(3)    | 111.25(17) |
| C(4)-C(3)-C(2)    | 111.93(18) | C(3)-C(4)-C(5)    | 114.09(18) |
| C(6)-C(5)-C(4)    | 113.86(19) | C(8)-C(7)-C(12)   | 119.0(2)   |
| C(8)-C(7)-P(1)    | 119.89(16) | C(12)-C(7)-P(1)   | 121.13(16) |
| C(7)-C(8)-C(9)    | 120.2(2)   | C(10)-C(9)-C(8)   | 120.3(2)   |
| C(11)-C(10)-C(9)  | 120.0(2)   | C(10)-C(11)-C(12) | 120.5(2)   |
| C(11)-C(12)-C(7)  | 120.0(2)   | C(14)-C(13)-C(18) | 120.06(19) |
| C(14)-C(13)-P(1)  | 119.48(16) | C(18)-C(13)-P(1)  | 119.94(16) |
| C(15)-C(14)-C(13) | 119.1(2)   | C(16)-C(15)-C(14) | 120.6(2)   |
| C(15)-C(16)-C(17) | 120.2(2)   | C(18)-C(17)-C(16) | 120.0(2)   |
| C(17)-C(18)-C(13) | 120.0(2)   | C(20)-C(19)-C(24) | 120.35(18) |
| C(20)-C(19)-P(1)  | 118.77(15) | C(24)-C(19)-P(1)  | 120.52(16) |
| C(21)-C(20)-C(19) | 119.6(2)   | C(20)-C(21)-C(22) | 120.0(2)   |
| C(23)-C(22)-C(21) | 120.3(2)   | C(22)-C(23)-C(24) | 120.5(2)   |
| C(23)-C(24)-C(19) | 119.2(2)   | F(6A)-P(2)-F(3A)  | 87.4(6)    |

|                  |            |                  |            |
|------------------|------------|------------------|------------|
| F(5)-P(2)-F(6)   | 177.28(14) | F(5)-P(2)-F(4)   | 91.56(15)  |
| F(6)-P(2)-F(4)   | 88.99(16)  | F(5)-P(2)-F(3)   | 89.94(14)  |
| F(6)-P(2)-F(3)   | 89.39(15)  | F(4)-P(2)-F(3)   | 176.83(12) |
| F(6A)-P(2)-F(5A) | 166.3(5)   | F(3A)-P(2)-F(5A) | 88.5(6)    |
| F(6A)-P(2)-F(1)  | 98.3(4)    | F(5)-P(2)-F(1)   | 89.05(10)  |
| F(3A)-P(2)-F(1)  | 101.2(4)   | F(6)-P(2)-F(1)   | 88.28(14)  |
| F(4)-P(2)-F(1)   | 89.04(8)   | F(3)-P(2)-F(1)   | 88.18(9)   |
| F(5A)-P(2)-F(1)  | 95.2(3)    | F(6A)-P(2)-F(2)  | 82.7(4)    |
| F(5)-P(2)-F(2)   | 89.51(11)  | F(3A)-P(2)-F(2)  | 79.8(4)    |
| F(6)-P(2)-F(2)   | 93.14(14)  | F(4)-P(2)-F(2)   | 91.05(9)   |
| F(3)-P(2)-F(2)   | 91.76(9)   | F(5A)-P(2)-F(2)  | 83.7(3)    |
| F(1)-P(2)-F(2)   | 178.57(10) | F(6A)-P(2)-F(4A) | 89.2(5)    |
| F(3A)-P(2)-F(4A) | 166.3(5)   | F(5A)-P(2)-F(4A) | 91.7(6)    |
| F(1)-P(2)-F(4A)  | 92.4(3)    | F(2)-P(2)-F(4A)  | 86.6(3)    |
| C(2)-C(1)-H(1A)  | 108.7      | P(1)-C(1)-H(1A)  | 108.7      |
| C(2)-C(1)-H(1B)  | 108.7      | P(1)-C(1)-H(1B)  | 108.7      |
| H(1A)-C(1)-H(1B) | 107.6      | C(1)-C(2)-H(2A)  | 109.4      |
| C(3)-C(2)-H(2A)  | 109.4      | C(1)-C(2)-H(2B)  | 109.4      |
| C(3)-C(2)-H(2B)  | 109.4      | H(2A)-C(2)-H(2B) | 108.0      |
| C(4)-C(3)-H(3A)  | 109.2      | C(2)-C(3)-H(3A)  | 109.2      |
| C(4)-C(3)-H(3B)  | 109.2      | C(2)-C(3)-H(3B)  | 109.2      |
| H(3A)-C(3)-H(3B) | 107.9      | C(3)-C(4)-H(4A)  | 108.7      |
| C(5)-C(4)-H(4A)  | 108.7      | C(3)-C(4)-H(4B)  | 108.7      |
| C(5)-C(4)-H(4B)  | 108.7      | H(4A)-C(4)-H(4B) | 107.6      |
| C(6)-C(5)-H(5A)  | 108.8      | C(4)-C(5)-H(5A)  | 108.8      |
| C(6)-C(5)-H(5B)  | 108.8      | C(4)-C(5)-H(5B)  | 108.8      |
| H(5A)-C(5)-H(5B) | 107.7      | C(5)-C(6)-H(6A)  | 109.5      |
| C(5)-C(6)-H(6B)  | 109.5      | H(6A)-C(6)-H(6B) | 109.5      |
| C(5)-C(6)-H(6C)  | 109.5      | H(6A)-C(6)-H(6C) | 109.5      |
| H(6B)-C(6)-H(6C) | 109.5      | C(7)-C(8)-H(8)   | 119.9      |
| C(9)-C(8)-H(8)   | 119.9      | C(10)-C(9)-H(9)  | 119.8      |

|                   |       |                   |       |
|-------------------|-------|-------------------|-------|
| C(8)-C(9)-H(9)    | 119.8 | C(11)-C(10)-H(10) | 120.0 |
| C(9)-C(10)-H(10)  | 120.0 | C(10)-C(11)-H(11) | 119.7 |
| C(12)-C(11)-H(11) | 119.7 | C(11)-C(12)-H(12) | 120.0 |
| C(7)-C(12)-H(12)  | 120.0 | C(15)-C(14)-H(14) | 120.4 |
| C(13)-C(14)-H(14) | 120.4 | C(16)-C(15)-H(15) | 119.7 |
| C(14)-C(15)-H(15) | 119.7 | C(15)-C(16)-H(16) | 119.9 |
| C(17)-C(16)-H(16) | 119.9 | C(18)-C(17)-H(17) | 120.0 |
| C(16)-C(17)-H(17) | 120.0 | C(17)-C(18)-H(18) | 120.0 |
| C(13)-C(18)-H(18) | 120.0 | C(21)-C(20)-H(20) | 120.2 |
| C(19)-C(20)-H(20) | 120.2 | C(20)-C(21)-H(21) | 120.0 |
| C(22)-C(21)-H(21) | 120.0 | C(23)-C(22)-H(22) | 119.8 |
| C(21)-C(22)-H(22) | 119.8 | C(22)-C(23)-H(23) | 119.7 |
| C(24)-C(23)-H(23) | 119.7 | C(23)-C(24)-H(24) | 120.4 |
| C(19)-C(24)-H(24) | 120.4 |                   |       |

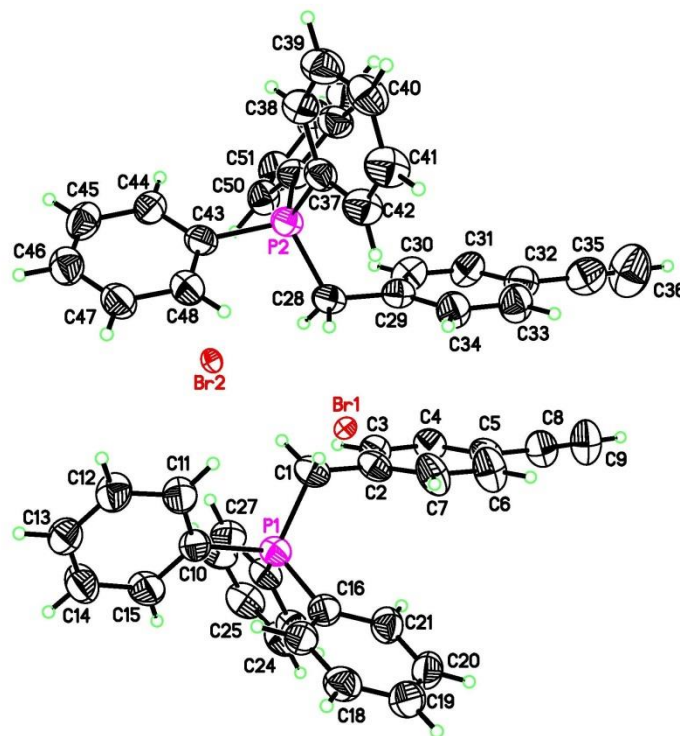
Symmetry transformations used to generate equivalent atoms:

Table 6. Torsion angles [ $^{\circ}$ ] for uvic1302\_x.

| atom-atom-atom-atom     | angle       | atom-atom-atom-atom     | angle       |
|-------------------------|-------------|-------------------------|-------------|
| C(13)-P(1)-C(1)-C(2)    | 66.03(18)   | C(19)-P(1)-C(1)-C(2)    | -54.85(18)  |
| C(7)-P(1)-C(1)-C(2)     | -175.51(15) | P(1)-C(1)-C(2)-C(3)     | 175.67(15)  |
| C(1)-C(2)-C(3)-C(4)     | -177.04(18) | C(2)-C(3)-C(4)-C(5)     | -175.91(19) |
| C(3)-C(4)-C(5)-C(6)     | 63.3(3)     | C(13)-P(1)-C(7)-C(8)    | -29.7(2)    |
| C(19)-P(1)-C(7)-C(8)    | 90.44(19)   | C(1)-P(1)-C(7)-C(8)     | -151.67(17) |
| C(13)-P(1)-C(7)-C(12)   | 149.98(18)  | C(19)-P(1)-C(7)-C(12)   | -89.9(2)    |
| C(1)-P(1)-C(7)-C(12)    | 28.0(2)     | C(12)-C(7)-C(8)-C(9)    | 0.2(3)      |
| P(1)-C(7)-C(8)-C(9)     | 179.92(19)  | C(7)-C(8)-C(9)-C(10)    | -0.9(4)     |
| C(8)-C(9)-C(10)-C(11)   | 0.6(4)      | C(9)-C(10)-C(11)-C(12)  | 0.3(4)      |
| C(10)-C(11)-C(12)-C(7)  | -1.0(4)     | C(8)-C(7)-C(12)-C(11)   | 0.6(4)      |
| P(1)-C(7)-C(12)-C(11)   | -179.0(2)   | C(19)-P(1)-C(13)-C(14)  | 148.69(16)  |
| C(1)-P(1)-C(13)-C(14)   | 29.16(19)   | C(7)-P(1)-C(13)-C(14)   | -89.91(18)  |
| C(19)-P(1)-C(13)-C(18)  | -39.57(18)  | C(1)-P(1)-C(13)-C(18)   | -159.10(15) |
| C(7)-P(1)-C(13)-C(18)   | 81.83(17)   | C(18)-C(13)-C(14)-C(15) | 0.0(3)      |
| P(1)-C(13)-C(14)-C(15)  | 171.68(16)  | C(13)-C(14)-C(15)-C(16) | -0.2(3)     |
| C(14)-C(15)-C(16)-C(17) | 0.4(3)      | C(15)-C(16)-C(17)-C(18) | -0.3(3)     |
| C(16)-C(17)-C(18)-C(13) | 0.1(3)      | C(14)-C(13)-C(18)-C(17) | 0.1(3)      |
| P(1)-C(13)-C(18)-C(17)  | -171.60(16) | C(13)-P(1)-C(19)-C(20)  | 155.52(16)  |
| C(1)-P(1)-C(19)-C(20)   | -81.60(17)  | C(7)-P(1)-C(19)-C(20)   | 36.85(19)   |
| C(13)-P(1)-C(19)-C(24)  | -31.37(19)  | C(1)-P(1)-C(19)-C(24)   | 91.51(17)   |
| C(7)-P(1)-C(19)-C(24)   | -150.04(16) | C(24)-C(19)-C(20)-C(21) | 1.3(3)      |
| P(1)-C(19)-C(20)-C(21)  | 174.41(16)  | C(19)-C(20)-C(21)-C(22) | 0.6(3)      |
| C(20)-C(21)-C(22)-C(23) | -1.3(3)     | C(21)-C(22)-C(23)-C(24) | 0.2(3)      |
| C(22)-C(23)-C(24)-C(19) | 1.7(3)      | C(20)-C(19)-C(24)-C(23) | -2.4(3)     |
| P(1)-C(19)-C(24)-C(23)  | -175.39(15) |                         |             |

Symmetry transformations used to generate equivalent atoms:

## Appendix E: Crystal data and structure refinement for (4-ethynylbenzyl)triphenylphosphonium hexafluorophosphate(V).



|                      |  |
|----------------------|--|
| Identification code  | uvic1217   |
| Empirical formula    | $C_{27}H_{22}BrP$  |
| Formula weight       | 457.33   |
| Temperature          | 120(2) K   |
| Wavelength           | 0.71073 Å  |
| Crystal system       | Triclinic  |
| Space group          | P-1  |
| Unit cell dimensions | $a = 10.8176(15)$ Å $\alpha = 98.278(3)^\circ$<br>$b = 12.4498(18)$ Å $\beta = 94.561(3)^\circ$<br>$c = 18.455(3)$ Å $\gamma = 107.751(3)^\circ$ |
| Volume               | $2322.3(6)$ Å <sup>3</sup>   |

|  |  |
|--|--|
| Z                                      | 4  |
| Density (calculated)                   | 1.308 g.cm <sup>-3</sup>                         |
| Absorption coefficient ( $\mu$ )       | 1.849 mm <sup>-1</sup>                           |
| F(000)                                 | 936  |
| Crystal color, habit                   | light brown, tablet                              |
| Crystal size                           | 0.22 × 0.15 × 0.08 mm <sup>3</sup>               |
| $\theta$ range for data collection     | 1.12 to 26.41°                                   |
| Index ranges                           | -13 ≤ h ≤ 13, -15 ≤ k ≤ 15, -23 ≤ l ≤ 23         |
| Reflections collected                  | 47622  |
| Independent reflections                | 9517 [ $R_{\text{int}} = 0.0384$ ]               |
| Completeness to $\theta = 26.41^\circ$ | 99.7 %   |
| Absorption correction                  | Numerical  |
| Max. and min. transmission             | 0.9390 and 0.7946                                |
| Refinement method                      | Full-matrix least-squares on $F^2$               |
| Data / restraints / parameters         | 9517 / 0 / 523                                   |
| Goodness-of-fit on $F^2$               | 1.066  |
| Final R indices [ $I > 2\sigma(I)$ ]   | $R_1 = 0.0666$ , $wR_2 = 0.2057$                 |
| R indices (all data)                   | $R_1 = 0.0792$ , $wR_2 = 0.2208$                 |
| Largest diff. peak and hole            | 2.125 and -1.731 e <sup>-</sup> .Å <sup>-3</sup> |



Table 2. Atomic coordinates and equivalent isotropic displacement parameters ( $\text{\AA}^2$ ) for uvic1217.  $U(\text{eq})$  is defined as one third of the trace of the orthogonalized  $U_{ij}$  tensor.

|       | x           | y           | z           | $U(\text{eq})$ |
|-------|-------------|-------------|-------------|----------------|
| Br(1) | 0.77064(4)  | -0.00819(4) | 0.13317(2)  | 0.016(1)       |
| Br(2) | 0.54519(5)  | 0.42038(4)  | 0.26878(3)  | 0.027(1)       |
| P(1)  | 0.88338(17) | 0.39375(14) | 0.12470(10) | 0.039(1)       |
| C(1)  | 0.8298(7)   | 0.3242(6)   | 0.2018(4)   | 0.046(2)       |
| C(2)  | 0.9266(7)   | 0.3632(6)   | 0.2713(4)   | 0.044(2)       |
| C(3)  | 0.9253(7)   | 0.4538(6)   | 0.3238(4)   | 0.045(2)       |
| C(4)  | 1.0120(7)   | 0.4873(6)   | 0.3887(4)   | 0.047(2)       |
| C(5)  | 1.1034(8)   | 0.4337(6)   | 0.4019(4)   | 0.049(2)       |
| C(6)  | 1.1048(10)  | 0.3411(8)   | 0.3492(5)   | 0.064(2)       |
| C(7)  | 1.0144(9)   | 0.3062(7)   | 0.2851(4)   | 0.058(2)       |
| C(8)  | 1.1943(8)   | 0.4687(7)   | 0.4686(4)   | 0.056(2)       |
| C(9)  | 1.2666(10)  | 0.4967(8)   | 0.5252(5)   | 0.068(2)       |
| C(10) | 0.7475(7)   | 0.3482(6)   | 0.0529(4)   | 0.042(2)       |
| C(11) | 0.6497(7)   | 0.2417(6)   | 0.0490(4)   | 0.051(2)       |
| C(12) | 0.5472(8)   | 0.2075(6)   | -0.0086(5)  | 0.055(2)       |
| C(13) | 0.5379(8)   | 0.2765(7)   | -0.0588(5)  | 0.056(2)       |
| C(14) | 0.6313(9)   | 0.3817(8)   | -0.0538(5)  | 0.067(2)       |
| C(15) | 0.7377(8)   | 0.4165(7)   | 0.0011(5)   | 0.058(2)       |
| C(16) | 1.0192(7)   | 0.3546(6)   | 0.0933(4)   | 0.045(2)       |
| C(17) | 1.0006(7)   | 0.2812(6)   | 0.0254(4)   | 0.045(2)       |
| C(18) | 1.1030(8)   | 0.2457(7)   | 0.0031(5)   | 0.054(2)       |
| C(19) | 1.2229(9)   | 0.2812(8)   | 0.0484(5)   | 0.060(2)       |
| C(20) | 1.2411(8)   | 0.3524(7)   | 0.1148(5)   | 0.058(2)       |
| C(21) | 1.1389(7)   | 0.3889(7)   | 0.1391(5)   | 0.052(2)       |
| C(22) | 0.9239(7)   | 0.5465(6)   | 0.1508(4)   | 0.043(2)       |
| C(23) | 1.0471(8)   | 0.6234(6)   | 0.1488(4)   | 0.050(2)       |

|       |             |             |             |          |
|-------|-------------|-------------|-------------|----------|
| C(24) | 1.0706(9)   | 0.7392(7)   | 0.1688(5)   | 0.059(2) |
| C(25) | 0.9685(10)  | 0.7797(7)   | 0.1902(5)   | 0.062(2) |
| C(26) | 0.8474(9)   | 0.7047(7)   | 0.1900(5)   | 0.059(2) |
| C(27) | 0.8242(8)   | 0.5876(6)   | 0.1720(4)   | 0.052(2) |
| P(2)  | 0.44593(17) | 0.03327(15) | 0.30060(10) | 0.039(1) |
| C(28) | 0.6126(7)   | 0.1159(6)   | 0.2943(4)   | 0.044(2) |
| C(29) | 0.7112(7)   | 0.1331(6)   | 0.3613(4)   | 0.044(2) |
| C(30) | 0.7149(8)   | 0.2091(6)   | 0.4242(5)   | 0.053(2) |
| C(31) | 0.8016(7)   | 0.2247(7)   | 0.4842(5)   | 0.053(2) |
| C(32) | 0.8917(8)   | 0.1677(8)   | 0.4859(4)   | 0.056(2) |
| C(33) | 0.8924(8)   | 0.0913(8)   | 0.4231(4)   | 0.057(2) |
| C(34) | 0.8039(8)   | 0.0746(7)   | 0.3605(4)   | 0.052(2) |
| C(35) | 0.9886(10)  | 0.1879(8)   | 0.5555(6)   | 0.067(2) |
| C(36) | 1.0546(13)  | 0.2046(12)  | 0.6059(7)   | 0.101(4) |
| C(37) | 0.4248(7)   | -0.1151(6)  | 0.3026(4)   | 0.043(2) |
| C(38) | 0.3085(8)   | -0.1832(7)  | 0.3205(4)   | 0.052(2) |
| C(39) | 0.2852(9)   | -0.2981(7)  | 0.3183(5)   | 0.059(2) |
| C(40) | 0.3786(9)   | -0.3476(7)  | 0.2983(5)   | 0.056(2) |
| C(41) | 0.4940(9)   | -0.2814(7)  | 0.2781(5)   | 0.061(2) |
| C(42) | 0.5186(8)   | -0.1644(7)  | 0.2794(4)   | 0.054(2) |
| C(43) | 0.3452(7)   | 0.0377(6)   | 0.2196(4)   | 0.043(2) |
| C(44) | 0.2301(7)   | 0.0638(6)   | 0.2233(4)   | 0.045(2) |
| C(45) | 0.1523(8)   | 0.0571(7)   | 0.1576(5)   | 0.054(2) |
| C(46) | 0.1874(8)   | 0.0247(6)   | 0.0907(5)   | 0.053(2) |
| C(47) | 0.3040(8)   | -0.0030(7)  | 0.0859(4)   | 0.052(2) |
| C(48) | 0.3841(8)   | 0.0042(7)   | 0.1509(4)   | 0.051(2) |
| C(49) | 0.3985(7)   | 0.0977(6)   | 0.3832(4)   | 0.046(2) |
| C(50) | 0.3903(7)   | 0.2068(7)   | 0.3855(4)   | 0.050(2) |
| C(51) | 0.3763(9)   | 0.2689(8)   | 0.4519(5)   | 0.062(2) |
| C(52) | 0.3646(10)  | 0.2167(10)  | 0.5146(5)   | 0.074(3) |
| C(53) | 0.3733(9)   | 0.1092(9)   | 0.5122(5)   | 0.069(2) |

|        |           |           |           |          |
|--------|-----------|-----------|-----------|----------|
| C(54)  | 0.3895(8) | 0.0473(7) | 0.4457(4) | 0.053(2) |
| H(1A)  | 0.7474    | 0.3378    | 0.2133    | 0.055    |
| H(1B)  | 0.8099    | 0.2406    | 0.1864    | 0.055    |
| H(3)   | 0.8646    | 0.4934    | 0.3154    | 0.054    |
| H(4)   | 1.0082    | 0.5485    | 0.4248    | 0.056    |
| H(6)   | 1.1667    | 0.3024    | 0.3570    | 0.077    |
| H(7)   | 1.0135    | 0.2417    | 0.2503    | 0.069    |
| H(9)   | 1.3242    | 0.5190    | 0.5703    | 0.081    |
| H(11)  | 0.6537    | 0.1946    | 0.0847    | 0.061    |
| H(12)  | 0.4822    | 0.1347    | -0.0132   | 0.066    |
| H(13)  | 0.4665    | 0.2514    | -0.0974   | 0.067    |
| H(14)  | 0.6230    | 0.4304    | -0.0878   | 0.081    |
| H(15)  | 0.8044    | 0.4877    | 0.0032    | 0.070    |
| H(17)  | 0.9185    | 0.2561    | -0.0049   | 0.054    |
| H(18)  | 1.0917    | 0.1971    | -0.0433   | 0.065    |
| H(19)  | 1.2924    | 0.2557    | 0.0330    | 0.072    |
| H(20)  | 1.3237    | 0.3772    | 0.1446    | 0.070    |
| H(21)  | 1.1506    | 0.4363    | 0.1860    | 0.062    |
| H(23)  | 1.1153    | 0.5956    | 0.1336    | 0.060    |
| H(24)  | 1.1552    | 0.7916    | 0.1680    | 0.071    |
| H(25)  | 0.9844    | 0.8596    | 0.2049    | 0.075    |
| H(26)  | 0.7778    | 0.7327    | 0.2024    | 0.071    |
| H(27)  | 0.7401    | 0.5355    | 0.1741    | 0.063    |
| H(28A) | 0.6417    | 0.0777    | 0.2512    | 0.053    |
| H(28B) | 0.6135    | 0.1923    | 0.2845    | 0.053    |
| H(30)  | 0.6550    | 0.2513    | 0.4252    | 0.063    |
| H(31)  | 0.8004    | 0.2769    | 0.5269    | 0.064    |
| H(33)  | 0.9536    | 0.0504    | 0.4230    | 0.068    |
| H(34)  | 0.8059    | 0.0238    | 0.3173    | 0.062    |
| H(36)  | 1.1127    | 0.2193    | 0.6502    | 0.122    |
| H(38)  | 0.2438    | -0.1499   | 0.3344    | 0.062    |

|       |        |         |        |       |
|-------|--------|---------|--------|-------|
| H(39) | 0.2046 | -0.3440 | 0.3305 | 0.071 |
| H(40) | 0.3636 | -0.4268 | 0.2986 | 0.068 |
| H(41) | 0.5571 | -0.3160 | 0.2630 | 0.073 |
| H(42) | 0.5974 | -0.1190 | 0.2650 | 0.064 |
| H(44) | 0.2044 | 0.0859  | 0.2697 | 0.054 |
| H(45) | 0.0735 | 0.0754  | 0.1596 | 0.065 |
| H(46) | 0.1328 | 0.0207  | 0.0468 | 0.064 |
| H(47) | 0.3277 | -0.0263 | 0.0392 | 0.063 |
| H(48) | 0.4636 | -0.0131 | 0.1489 | 0.061 |
| H(50) | 0.3942 | 0.2395  | 0.3419 | 0.060 |
| H(51) | 0.3748 | 0.3453  | 0.4545 | 0.074 |
| H(52) | 0.3505 | 0.2568  | 0.5594 | 0.088 |
| H(53) | 0.3683 | 0.0761  | 0.5556 | 0.082 |
| H(54) | 0.3942 | -0.0280 | 0.4436 | 0.064 |

Table 3. Anisotropic displacement parameters ( $\text{\AA}^2$ ) for uvic1217.

The anisotropic displacement factor exponent takes the form:

$$-2\pi^2[h^2a^{*2}U_{11} + \dots + 2hka^*b^*U_{12}]$$

|       | $U_{11}$  | $U_{22}$  | $U_{33}$  | $U_{23}$   | $U_{13}$  | $U_{12}$  |
|-------|-----------|-----------|-----------|------------|-----------|-----------|
| Br(1) | 0.0158(2) | 0.0150(2) | 0.0170(2) | -0.0009(2) | 0.0019(2) | 0.0043(2) |
| Br(2) | 0.0285(3) | 0.0280(3) | 0.0295(3) | 0.0119(2)  | 0.0028(2) | 0.0120(2) |
| P(1)  | 0.0417(9) | 0.0315(8) | 0.0380(9) | 0.0056(7)  | 0.0037(7) | 0.0058(7) |
| C(1)  | 0.057(4)  | 0.031(3)  | 0.048(4)  | 0.010(3)   | 0.010(3)  | 0.010(3)  |
| C(2)  | 0.058(4)  | 0.032(3)  | 0.039(3)  | 0.008(3)   | 0.007(3)  | 0.010(3)  |
| C(3)  | 0.050(4)  | 0.042(4)  | 0.045(4)  | 0.008(3)   | 0.007(3)  | 0.017(3)  |
| C(4)  | 0.056(4)  | 0.044(4)  | 0.040(4)  | 0.002(3)   | 0.009(3)  | 0.019(3)  |
| C(5)  | 0.066(5)  | 0.046(4)  | 0.041(4)  | 0.009(3)   | 0.011(3)  | 0.023(4)  |
| C(6)  | 0.088(6)  | 0.062(5)  | 0.050(4)  | 0.000(4)   | -0.004(4) | 0.042(5)  |
| C(7)  | 0.088(6)  | 0.051(4)  | 0.041(4)  | 0.004(3)   | -0.001(4) | 0.037(4)  |
| C(8)  | 0.066(5)  | 0.058(5)  | 0.047(4)  | 0.004(4)   | 0.005(4)  | 0.030(4)  |
| C(9)  | 0.080(6)  | 0.072(6)  | 0.055(5)  | -0.008(4)  | -0.010(4) | 0.044(5)  |
| C(10) | 0.042(4)  | 0.042(4)  | 0.041(3)  | 0.006(3)   | 0.005(3)  | 0.013(3)  |
| C(11) | 0.051(4)  | 0.039(4)  | 0.058(4)  | 0.012(3)   | -0.002(3) | 0.006(3)  |
| C(12) | 0.049(4)  | 0.041(4)  | 0.062(5)  | 0.005(3)   | -0.005(4) | 0.003(3)  |
| C(13) | 0.045(4)  | 0.055(5)  | 0.057(5)  | 0.010(4)   | -0.002(3) | 0.004(3)  |
| C(14) | 0.064(5)  | 0.063(5)  | 0.062(5)  | 0.028(4)   | -0.011(4) | 0.000(4)  |
| C(15) | 0.055(5)  | 0.047(4)  | 0.058(5)  | 0.017(4)   | 0.000(4)  | -0.006(3) |
| C(16) | 0.041(4)  | 0.040(4)  | 0.050(4)  | 0.013(3)   | 0.003(3)  | 0.004(3)  |
| C(17) | 0.045(4)  | 0.043(4)  | 0.049(4)  | 0.011(3)   | 0.006(3)  | 0.013(3)  |
| C(18) | 0.061(5)  | 0.053(4)  | 0.056(5)  | 0.019(4)   | 0.016(4)  | 0.023(4)  |
| C(19) | 0.057(5)  | 0.063(5)  | 0.071(6)  | 0.027(4)   | 0.016(4)  | 0.027(4)  |
| C(20) | 0.042(4)  | 0.060(5)  | 0.077(6)  | 0.030(4)   | 0.002(4)  | 0.016(4)  |
| C(21) | 0.048(4)  | 0.050(4)  | 0.054(4)  | 0.010(3)   | -0.002(3) | 0.012(3)  |
| C(22) | 0.056(4)  | 0.032(3)  | 0.037(3)  | 0.005(3)   | 0.004(3)  | 0.009(3)  |

|       |           |           |           |           |           |           |
|-------|-----------|-----------|-----------|-----------|-----------|-----------|
| C(23) | 0.054(4)  | 0.044(4)  | 0.043(4)  | 0.008(3)  | 0.000(3)  | 0.005(3)  |
| C(24) | 0.069(5)  | 0.039(4)  | 0.057(5)  | 0.013(3)  | -0.001(4) | 0.001(4)  |
| C(25) | 0.086(6)  | 0.039(4)  | 0.060(5)  | 0.008(4)  | 0.011(4)  | 0.016(4)  |
| C(26) | 0.078(6)  | 0.040(4)  | 0.061(5)  | 0.012(4)  | 0.016(4)  | 0.018(4)  |
| C(27) | 0.058(4)  | 0.041(4)  | 0.058(4)  | 0.011(3)  | 0.012(4)  | 0.013(3)  |
| P(2)  | 0.0425(9) | 0.0395(9) | 0.0400(9) | 0.0115(7) | 0.0103(7) | 0.0153(7) |
| C(28) | 0.049(4)  | 0.043(4)  | 0.044(4)  | 0.014(3)  | 0.014(3)  | 0.015(3)  |
| C(29) | 0.043(4)  | 0.042(4)  | 0.046(4)  | 0.012(3)  | 0.010(3)  | 0.010(3)  |
| C(30) | 0.048(4)  | 0.044(4)  | 0.062(5)  | -0.001(3) | 0.007(4)  | 0.013(3)  |
| C(31) | 0.043(4)  | 0.060(5)  | 0.052(4)  | -0.001(4) | 0.004(3)  | 0.015(3)  |
| C(32) | 0.048(4)  | 0.065(5)  | 0.049(4)  | 0.011(4)  | 0.002(3)  | 0.009(4)  |
| C(33) | 0.061(5)  | 0.070(5)  | 0.051(4)  | 0.009(4)  | 0.010(4)  | 0.036(4)  |
| C(34) | 0.056(4)  | 0.059(5)  | 0.047(4)  | 0.008(3)  | 0.009(3)  | 0.027(4)  |
| C(35) | 0.065(5)  | 0.068(6)  | 0.065(6)  | 0.003(4)  | 0.012(5)  | 0.019(4)  |
| C(36) | 0.093(8)  | 0.139(12) | 0.064(7)  | -0.014(7) | -0.010(6) | 0.047(8)  |
| C(37) | 0.047(4)  | 0.040(3)  | 0.045(4)  | 0.013(3)  | 0.006(3)  | 0.015(3)  |
| C(38) | 0.051(4)  | 0.049(4)  | 0.056(4)  | 0.017(3)  | 0.008(3)  | 0.014(3)  |
| C(39) | 0.065(5)  | 0.045(4)  | 0.061(5)  | 0.015(4)  | 0.010(4)  | 0.007(4)  |
| C(40) | 0.074(5)  | 0.037(4)  | 0.059(5)  | 0.014(3)  | 0.006(4)  | 0.019(4)  |
| C(41) | 0.075(6)  | 0.046(4)  | 0.069(5)  | 0.013(4)  | 0.022(4)  | 0.027(4)  |
| C(42) | 0.062(5)  | 0.048(4)  | 0.056(4)  | 0.012(3)  | 0.016(4)  | 0.021(4)  |
| C(43) | 0.046(4)  | 0.043(4)  | 0.041(4)  | 0.013(3)  | 0.009(3)  | 0.012(3)  |
| C(44) | 0.041(4)  | 0.043(4)  | 0.051(4)  | 0.009(3)  | 0.005(3)  | 0.013(3)  |
| C(45) | 0.043(4)  | 0.046(4)  | 0.075(6)  | 0.012(4)  | 0.002(4)  | 0.016(3)  |
| C(46) | 0.054(4)  | 0.045(4)  | 0.055(4)  | 0.009(3)  | -0.004(4) | 0.010(3)  |
| C(47) | 0.058(4)  | 0.054(4)  | 0.042(4)  | 0.014(3)  | 0.004(3)  | 0.013(4)  |
| C(48) | 0.053(4)  | 0.059(5)  | 0.044(4)  | 0.015(3)  | 0.007(3)  | 0.020(4)  |
| C(49) | 0.044(4)  | 0.053(4)  | 0.042(4)  | 0.011(3)  | 0.011(3)  | 0.015(3)  |
| C(50) | 0.053(4)  | 0.053(4)  | 0.049(4)  | 0.008(3)  | 0.008(3)  | 0.026(3)  |
| C(51) | 0.071(5)  | 0.068(5)  | 0.055(5)  | 0.004(4)  | 0.009(4)  | 0.036(5)  |
| C(52) | 0.086(7)  | 0.105(8)  | 0.047(5)  | 0.006(5)  | 0.021(4)  | 0.056(6)  |

|       |          |          |          |          |          |          |
|-------|----------|----------|----------|----------|----------|----------|
| C(53) | 0.071(6) | 0.090(7) | 0.052(5) | 0.020(5) | 0.020(4) | 0.031(5) |
| C(54) | 0.058(5) | 0.061(5) | 0.046(4) | 0.016(3) | 0.016(3) | 0.022(4) |

Table 4. Bond lengths [ $\text{\AA}$ ] for uvic1217.

| atom-atom   | distance  | atom-atom   | distance  |
|-------------|-----------|-------------|-----------|
| P(1)-C(10)  | 1.790(7)  | P(1)-C(16)  | 1.795(8)  |
| P(1)-C(22)  | 1.799(7)  | P(1)-C(1)   | 1.814(7)  |
| C(1)-C(2)   | 1.508(10) | C(2)-C(7)   | 1.377(11) |
| C(2)-C(3)   | 1.381(10) | C(3)-C(4)   | 1.389(10) |
| C(4)-C(5)   | 1.375(10) | C(5)-C(6)   | 1.401(11) |
| C(5)-C(8)   | 1.436(11) | C(6)-C(7)   | 1.398(11) |
| C(8)-C(9)   | 1.194(12) | C(10)-C(15) | 1.386(10) |
| C(10)-C(11) | 1.410(10) | C(11)-C(12) | 1.391(10) |
| C(12)-C(13) | 1.368(11) | C(13)-C(14) | 1.375(11) |
| C(14)-C(15) | 1.387(11) | C(16)-C(21) | 1.400(10) |
| C(16)-C(17) | 1.401(10) | C(17)-C(18) | 1.382(10) |
| C(18)-C(19) | 1.396(12) | C(19)-C(20) | 1.366(13) |
| C(20)-C(21) | 1.399(11) | C(22)-C(27) | 1.387(11) |
| C(22)-C(23) | 1.390(10) | C(23)-C(24) | 1.374(11) |
| C(24)-C(25) | 1.409(13) | C(25)-C(26) | 1.357(12) |
| C(26)-C(27) | 1.388(10) | P(2)-C(43)  | 1.796(7)  |
| P(2)-C(37)  | 1.797(7)  | P(2)-C(49)  | 1.803(7)  |
| P(2)-C(28)  | 1.805(7)  | C(28)-C(29) | 1.513(10) |
| C(29)-C(30) | 1.378(10) | C(29)-C(34) | 1.407(10) |
| C(30)-C(31) | 1.344(11) | C(31)-C(32) | 1.371(11) |
| C(32)-C(33) | 1.391(11) | C(32)-C(35) | 1.531(13) |
| C(33)-C(34) | 1.389(11) | C(35)-C(36) | 1.078(14) |
| C(37)-C(38) | 1.381(10) | C(37)-C(42) | 1.401(10) |
| C(38)-C(39) | 1.368(11) | C(39)-C(40) | 1.382(12) |
| C(40)-C(41) | 1.383(12) | C(41)-C(42) | 1.395(11) |
| C(43)-C(44) | 1.384(10) | C(43)-C(48) | 1.414(10) |
| C(44)-C(45) | 1.396(11) | C(45)-C(46) | 1.363(12) |



|              |           |              |           |
|--------------|-----------|--------------|-----------|
| C(46)-C(47)  | 1.411(11) | C(47)-C(48)  | 1.397(10) |
| C(49)-C(50)  | 1.383(10) | C(49)-C(54)  | 1.386(10) |
| C(50)-C(51)  | 1.397(11) | C(51)-C(52)  | 1.403(13) |
| C(52)-C(53)  | 1.365(14) | C(53)-C(54)  | 1.406(12) |
| C(1)-H(1A)   | 0.9900    | C(1)-H(1B)   | 0.9900    |
| C(3)-H(3)    | 0.9500    | C(4)-H(4)    | 0.9500    |
| C(6)-H(6)    | 0.9500    | C(7)-H(7)    | 0.9500    |
| C(9)-H(9)    | 0.9500    | C(11)-H(11)  | 0.9500    |
| C(12)-H(12)  | 0.9500    | C(13)-H(13)  | 0.9500    |
| C(14)-H(14)  | 0.9500    | C(15)-H(15)  | 0.9500    |
| C(17)-H(17)  | 0.9500    | C(18)-H(18)  | 0.9500    |
| C(19)-H(19)  | 0.9500    | C(20)-H(20)  | 0.9500    |
| C(21)-H(21)  | 0.9500    | C(23)-H(23)  | 0.9500    |
| C(24)-H(24)  | 0.9500    | C(25)-H(25)  | 0.9500    |
| C(26)-H(26)  | 0.9500    | C(27)-H(27)  | 0.9500    |
| C(28)-H(28A) | 0.9900    | C(28)-H(28B) | 0.9900    |
| C(30)-H(30)  | 0.9500    | C(31)-H(31)  | 0.9500    |
| C(33)-H(33)  | 0.9500    | C(34)-H(34)  | 0.9500    |
| C(36)-H(36)  | 0.9500    | C(38)-H(38)  | 0.9500    |
| C(39)-H(39)  | 0.9500    | C(40)-H(40)  | 0.9500    |
| C(41)-H(41)  | 0.9500    | C(42)-H(42)  | 0.9500    |
| C(44)-H(44)  | 0.9500    | C(45)-H(45)  | 0.9500    |
| C(46)-H(46)  | 0.9500    | C(47)-H(47)  | 0.9500    |
| C(48)-H(48)  | 0.9500    | C(50)-H(50)  | 0.9500    |
| C(51)-H(51)  | 0.9500    | C(52)-H(52)  | 0.9500    |
| C(53)-H(53)  | 0.9500    | C(54)-H(54)  | 0.9500    |

Symmetry transformations used to generate equivalent atoms:

Table 5. Bond angles [°] for uvic1217.

| atom-atom-atom    | angle    | atom-atom-atom    | angle     |
|-------------------|----------|-------------------|-----------|
| C(10)-P(1)-C(16)  | 110.6(3) | C(10)-P(1)-C(22)  | 106.8(3)  |
| C(16)-P(1)-C(22)  | 111.7(3) | C(10)-P(1)-C(1)   | 107.5(3)  |
| C(16)-P(1)-C(1)   | 110.1(3) | C(22)-P(1)-C(1)   | 110.1(3)  |
| C(2)-C(1)-P(1)    | 115.1(5) | C(7)-C(2)-C(3)    | 118.6(7)  |
| C(7)-C(2)-C(1)    | 120.6(6) | C(3)-C(2)-C(1)    | 120.7(7)  |
| C(2)-C(3)-C(4)    | 120.6(7) | C(5)-C(4)-C(3)    | 121.3(7)  |
| C(4)-C(5)-C(6)    | 118.6(7) | C(4)-C(5)-C(8)    | 121.6(7)  |
| C(6)-C(5)-C(8)    | 119.8(7) | C(7)-C(6)-C(5)    | 119.4(8)  |
| C(2)-C(7)-C(6)    | 121.4(7) | C(9)-C(8)-C(5)    | 178.0(10) |
| C(15)-C(10)-C(11) | 119.8(7) | C(15)-C(10)-P(1)  | 120.6(5)  |
| C(11)-C(10)-P(1)  | 119.6(5) | C(12)-C(11)-C(10) | 118.1(7)  |
| C(13)-C(12)-C(11) | 121.4(7) | C(12)-C(13)-C(14) | 120.4(7)  |
| C(13)-C(14)-C(15) | 119.7(8) | C(10)-C(15)-C(14) | 120.5(7)  |
| C(21)-C(16)-C(17) | 120.4(7) | C(21)-C(16)-P(1)  | 120.2(6)  |
| C(17)-C(16)-P(1)  | 119.2(5) | C(18)-C(17)-C(16) | 119.3(7)  |
| C(17)-C(18)-C(19) | 120.1(8) | C(20)-C(19)-C(18) | 120.6(8)  |
| C(19)-C(20)-C(21) | 120.5(8) | C(20)-C(21)-C(16) | 119.0(8)  |
| C(27)-C(22)-C(23) | 119.6(7) | C(27)-C(22)-P(1)  | 116.9(5)  |
| C(23)-C(22)-P(1)  | 123.5(6) | C(24)-C(23)-C(22) | 120.3(8)  |
| C(23)-C(24)-C(25) | 119.5(8) | C(26)-C(25)-C(24) | 120.1(8)  |
| C(25)-C(26)-C(27) | 120.6(9) | C(22)-C(27)-C(26) | 119.9(7)  |
| C(43)-P(2)-C(37)  | 106.9(3) | C(43)-P(2)-C(49)  | 111.1(3)  |
| C(37)-P(2)-C(49)  | 110.0(3) | C(43)-P(2)-C(28)  | 107.9(3)  |
| C(37)-P(2)-C(28)  | 113.1(3) | C(49)-P(2)-C(28)  | 107.7(3)  |
| C(29)-C(28)-P(2)  | 116.1(5) | C(30)-C(29)-C(34) | 118.2(7)  |
| C(30)-C(29)-C(28) | 120.6(7) | C(34)-C(29)-C(28) | 121.1(7)  |
| C(31)-C(30)-C(29) | 121.2(8) | C(30)-C(31)-C(32) | 122.2(8)  |

|                   |          |                   |           |
|-------------------|----------|-------------------|-----------|
| C(31)-C(32)-C(33) | 118.4(7) | C(31)-C(32)-C(35) | 120.4(8)  |
| C(33)-C(32)-C(35) | 121.2(8) | C(34)-C(33)-C(32) | 120.2(8)  |
| C(33)-C(34)-C(29) | 119.8(7) | C(36)-C(35)-C(32) | 177.4(12) |
| C(38)-C(37)-C(42) | 119.9(7) | C(38)-C(37)-P(2)  | 118.9(6)  |
| C(42)-C(37)-P(2)  | 120.9(6) | C(39)-C(38)-C(37) | 120.8(8)  |
| C(38)-C(39)-C(40) | 120.2(8) | C(39)-C(40)-C(41) | 119.8(7)  |
| C(40)-C(41)-C(42) | 120.6(8) | C(41)-C(42)-C(37) | 118.6(7)  |
| C(44)-C(43)-C(48) | 121.1(7) | C(44)-C(43)-P(2)  | 122.3(5)  |
| C(48)-C(43)-P(2)  | 116.4(6) | C(43)-C(44)-C(45) | 118.8(7)  |
| C(46)-C(45)-C(44) | 121.3(7) | C(45)-C(46)-C(47) | 120.7(7)  |
| C(48)-C(47)-C(46) | 119.1(7) | C(47)-C(48)-C(43) | 119.0(7)  |
| C(50)-C(49)-C(54) | 120.9(7) | C(50)-C(49)-P(2)  | 117.3(5)  |
| C(54)-C(49)-P(2)  | 121.2(6) | C(49)-C(50)-C(51) | 119.9(8)  |
| C(50)-C(51)-C(52) | 118.9(8) | C(53)-C(52)-C(51) | 120.9(8)  |
| C(52)-C(53)-C(54) | 120.2(8) | C(49)-C(54)-C(53) | 119.1(8)  |
| C(2)-C(1)-H(1A)   | 108.5    | P(1)-C(1)-H(1A)   | 108.5     |
| C(2)-C(1)-H(1B)   | 108.5    | P(1)-C(1)-H(1B)   | 108.5     |
| H(1A)-C(1)-H(1B)  | 107.5    | C(2)-C(3)-H(3)    | 119.7     |
| C(4)-C(3)-H(3)    | 119.7    | C(5)-C(4)-H(4)    | 119.4     |
| C(3)-C(4)-H(4)    | 119.4    | C(7)-C(6)-H(6)    | 120.3     |
| C(5)-C(6)-H(6)    | 120.3    | C(2)-C(7)-H(7)    | 119.3     |
| C(6)-C(7)-H(7)    | 119.3    | C(8)-C(9)-H(9)    | 180.0     |
| C(12)-C(11)-H(11) | 120.9    | C(10)-C(11)-H(11) | 120.9     |
| C(13)-C(12)-H(12) | 119.3    | C(11)-C(12)-H(12) | 119.3     |
| C(12)-C(13)-H(13) | 119.8    | C(14)-C(13)-H(13) | 119.8     |
| C(13)-C(14)-H(14) | 120.2    | C(15)-C(14)-H(14) | 120.2     |
| C(10)-C(15)-H(15) | 119.8    | C(14)-C(15)-H(15) | 119.8     |
| C(18)-C(17)-H(17) | 120.3    | C(16)-C(17)-H(17) | 120.3     |
| C(17)-C(18)-H(18) | 119.9    | C(19)-C(18)-H(18) | 119.9     |
| C(20)-C(19)-H(19) | 119.7    | C(18)-C(19)-H(19) | 119.7     |
| C(19)-C(20)-H(20) | 119.8    | C(21)-C(20)-H(20) | 119.8     |

|                     |       |                   |       |
|---------------------|-------|-------------------|-------|
| C(20)-C(21)-H(21)   | 120.5 | C(16)-C(21)-H(21) | 120.5 |
| C(24)-C(23)-H(23)   | 119.8 | C(22)-C(23)-H(23) | 119.8 |
| C(23)-C(24)-H(24)   | 120.3 | C(25)-C(24)-H(24) | 120.3 |
| C(26)-C(25)-H(25)   | 120.0 | C(24)-C(25)-H(25) | 120.0 |
| C(25)-C(26)-H(26)   | 119.7 | C(27)-C(26)-H(26) | 119.7 |
| C(22)-C(27)-H(27)   | 120.0 | C(26)-C(27)-H(27) | 120.0 |
| C(29)-C(28)-H(28A)  | 108.3 | P(2)-C(28)-H(28A) | 108.3 |
| C(29)-C(28)-H(28B)  | 108.3 | P(2)-C(28)-H(28B) | 108.3 |
| H(28A)-C(28)-H(28B) | 107.4 | C(31)-C(30)-H(30) | 119.4 |
| C(29)-C(30)-H(30)   | 119.4 | C(30)-C(31)-H(31) | 118.9 |
| C(32)-C(31)-H(31)   | 118.9 | C(34)-C(33)-H(33) | 119.9 |
| C(32)-C(33)-H(33)   | 119.9 | C(33)-C(34)-H(34) | 120.1 |
| C(29)-C(34)-H(34)   | 120.1 | C(35)-C(36)-H(36) | 180.0 |
| C(39)-C(38)-H(38)   | 119.6 | C(37)-C(38)-H(38) | 119.6 |
| C(38)-C(39)-H(39)   | 119.9 | C(40)-C(39)-H(39) | 119.9 |
| C(39)-C(40)-H(40)   | 120.1 | C(41)-C(40)-H(40) | 120.1 |
| C(40)-C(41)-H(41)   | 119.7 | C(42)-C(41)-H(41) | 119.7 |
| C(41)-C(42)-H(42)   | 120.7 | C(37)-C(42)-H(42) | 120.7 |
| C(43)-C(44)-H(44)   | 120.6 | C(45)-C(44)-H(44) | 120.6 |
| C(46)-C(45)-H(45)   | 119.4 | C(44)-C(45)-H(45) | 119.4 |
| C(45)-C(46)-H(46)   | 119.7 | C(47)-C(46)-H(46) | 119.7 |
| C(48)-C(47)-H(47)   | 120.4 | C(46)-C(47)-H(47) | 120.4 |
| C(47)-C(48)-H(48)   | 120.5 | C(43)-C(48)-H(48) | 120.5 |
| C(49)-C(50)-H(50)   | 120.0 | C(51)-C(50)-H(50) | 120.0 |
| C(50)-C(51)-H(51)   | 120.5 | C(52)-C(51)-H(51) | 120.5 |
| C(53)-C(52)-H(52)   | 119.6 | C(51)-C(52)-H(52) | 119.6 |
| C(52)-C(53)-H(53)   | 119.9 | C(54)-C(53)-H(53) | 119.9 |
| C(49)-C(54)-H(54)   | 120.4 | C(53)-C(54)-H(54) | 120.4 |

Symmetry transformations used to generate equivalent atoms:

Table 6. Torsion angles [°] for uvic1217.

| atom-atom-atom-atom     | angle     | atom-atom-atom-atom     | angle     |
|-------------------------|-----------|-------------------------|-----------|
| C(10)-P(1)-C(1)-C(2)    | -173.0(5) | C(16)-P(1)-C(1)-C(2)    | 66.4(6)   |
| C(22)-P(1)-C(1)-C(2)    | -57.1(6)  | P(1)-C(1)-C(2)-C(7)     | -92.8(8)  |
| P(1)-C(1)-C(2)-C(3)     | 90.0(8)   | C(7)-C(2)-C(3)-C(4)     | 0.8(11)   |
| C(1)-C(2)-C(3)-C(4)     | 178.1(6)  | C(2)-C(3)-C(4)-C(5)     | 1.6(11)   |
| C(3)-C(4)-C(5)-C(6)     | -2.1(12)  | C(3)-C(4)-C(5)-C(8)     | 179.3(7)  |
| C(4)-C(5)-C(6)-C(7)     | 0.2(13)   | C(8)-C(5)-C(6)-C(7)     | 178.8(8)  |
| C(3)-C(2)-C(7)-C(6)     | -2.7(12)  | C(1)-C(2)-C(7)-C(6)     | -180.0(8) |
| C(5)-C(6)-C(7)-C(2)     | 2.2(14)   | C(4)-C(5)-C(8)-C(9)     | 66(25)    |
| C(6)-C(5)-C(8)-C(9)     | -113(25)  | C(16)-P(1)-C(10)-C(15)  | -85.9(7)  |
| C(22)-P(1)-C(10)-C(15)  | 35.8(7)   | C(1)-P(1)-C(10)-C(15)   | 153.9(7)  |
| C(16)-P(1)-C(10)-C(11)  | 94.1(6)   | C(22)-P(1)-C(10)-C(11)  | -144.2(6) |
| C(1)-P(1)-C(10)-C(11)   | -26.1(7)  | C(15)-C(10)-C(11)-C(12) | 1.6(12)   |
| P(1)-C(10)-C(11)-C(12)  | -178.4(6) | C(10)-C(11)-C(12)-C(13) | -2.4(13)  |
| C(11)-C(12)-C(13)-C(14) | 0.6(14)   | C(12)-C(13)-C(14)-C(15) | 2.1(15)   |
| C(11)-C(10)-C(15)-C(14) | 1.0(13)   | P(1)-C(10)-C(15)-C(14)  | -179.0(7) |
| C(13)-C(14)-C(15)-C(10) | -2.9(15)  | C(10)-P(1)-C(16)-C(21)  | 175.6(6)  |
| C(22)-P(1)-C(16)-C(21)  | 56.8(7)   | C(1)-P(1)-C(16)-C(21)   | -65.8(7)  |
| C(10)-P(1)-C(16)-C(17)  | -9.9(7)   | C(22)-P(1)-C(16)-C(17)  | -128.7(6) |
| C(1)-P(1)-C(16)-C(17)   | 108.7(6)  | C(21)-C(16)-C(17)-C(18) | -1.9(11)  |
| P(1)-C(16)-C(17)-C(18)  | -176.4(5) | C(16)-C(17)-C(18)-C(19) | 1.1(11)   |
| C(17)-C(18)-C(19)-C(20) | -0.8(12)  | C(18)-C(19)-C(20)-C(21) | 1.3(12)   |
| C(19)-C(20)-C(21)-C(16) | -2.1(12)  | C(17)-C(16)-C(21)-C(20) | 2.4(11)   |
| P(1)-C(16)-C(21)-C(20)  | 176.8(6)  | C(10)-P(1)-C(22)-C(27)  | 55.3(6)   |
| C(16)-P(1)-C(22)-C(27)  | 176.4(6)  | C(1)-P(1)-C(22)-C(27)   | -61.1(7)  |
| C(10)-P(1)-C(22)-C(23)  | -122.9(6) | C(16)-P(1)-C(22)-C(23)  | -1.9(7)   |
| C(1)-P(1)-C(22)-C(23)   | 120.7(6)  | C(27)-C(22)-C(23)-C(24) | 1.0(11)   |
| P(1)-C(22)-C(23)-C(24)  | 179.2(6)  | C(22)-C(23)-C(24)-C(25) | -0.9(12)  |

|                         |           |                         |           |
|-------------------------|-----------|-------------------------|-----------|
| C(23)-C(24)-C(25)-C(26) | -1.1(13)  | C(24)-C(25)-C(26)-C(27) | 2.9(13)   |
| C(23)-C(22)-C(27)-C(26) | 0.8(11)   | P(1)-C(22)-C(27)-C(26)  | -177.5(6) |
| C(25)-C(26)-C(27)-C(22) | -2.8(13)  | C(43)-P(2)-C(28)-C(29)  | 173.9(5)  |
| C(37)-P(2)-C(28)-C(29)  | -68.0(6)  | C(49)-P(2)-C(28)-C(29)  | 53.8(6)   |
| P(2)-C(28)-C(29)-C(30)  | -74.9(8)  | P(2)-C(28)-C(29)-C(34)  | 107.0(7)  |
| C(34)-C(29)-C(30)-C(31) | -2.1(11)  | C(28)-C(29)-C(30)-C(31) | 179.7(7)  |
| C(29)-C(30)-C(31)-C(32) | 1.0(13)   | C(30)-C(31)-C(32)-C(33) | -0.1(13)  |
| C(30)-C(31)-C(32)-C(35) | -179.9(8) | C(31)-C(32)-C(33)-C(34) | 0.4(13)   |
| C(35)-C(32)-C(33)-C(34) | -179.8(8) | C(32)-C(33)-C(34)-C(29) | -1.6(13)  |
| C(30)-C(29)-C(34)-C(33) | 2.4(11)   | C(28)-C(29)-C(34)-C(33) | -179.4(7) |
| C(31)-C(32)-C(35)-C(36) | 5(30)     | C(33)-C(32)-C(35)-C(36) | -175(29)  |
| C(43)-P(2)-C(37)-C(38)  | -72.8(7)  | C(49)-P(2)-C(37)-C(38)  | 48.0(7)   |
| C(28)-P(2)-C(37)-C(38)  | 168.6(6)  | C(43)-P(2)-C(37)-C(42)  | 100.9(7)  |
| C(49)-P(2)-C(37)-C(42)  | -138.3(6) | C(28)-P(2)-C(37)-C(42)  | -17.7(7)  |
| C(42)-C(37)-C(38)-C(39) | 2.3(12)   | P(2)-C(37)-C(38)-C(39)  | 176.0(6)  |
| C(37)-C(38)-C(39)-C(40) | 0.2(13)   | C(38)-C(39)-C(40)-C(41) | -2.2(13)  |
| C(39)-C(40)-C(41)-C(42) | 1.7(13)   | C(40)-C(41)-C(42)-C(37) | 0.7(13)   |
| C(38)-C(37)-C(42)-C(41) | -2.7(12)  | P(2)-C(37)-C(42)-C(41)  | -176.4(6) |
| C(37)-P(2)-C(43)-C(44)  | 106.8(6)  | C(49)-P(2)-C(43)-C(44)  | -13.3(7)  |
| C(28)-P(2)-C(43)-C(44)  | -131.2(6) | C(37)-P(2)-C(43)-C(48)  | -68.3(6)  |
| C(49)-P(2)-C(43)-C(48)  | 171.6(6)  | C(28)-P(2)-C(43)-C(48)  | 53.7(6)   |
| C(48)-C(43)-C(44)-C(45) | -0.3(11)  | P(2)-C(43)-C(44)-C(45)  | -175.3(6) |
| C(43)-C(44)-C(45)-C(46) | 0.5(11)   | C(44)-C(45)-C(46)-C(47) | -0.1(12)  |
| C(45)-C(46)-C(47)-C(48) | -0.6(12)  | C(46)-C(47)-C(48)-C(43) | 0.8(11)   |
| C(44)-C(43)-C(48)-C(47) | -0.4(11)  | P(2)-C(43)-C(48)-C(47)  | 174.9(6)  |
| C(43)-P(2)-C(49)-C(50)  | -52.4(7)  | C(37)-P(2)-C(49)-C(50)  | -170.6(6) |
| C(28)-P(2)-C(49)-C(50)  | 65.6(7)   | C(43)-P(2)-C(49)-C(54)  | 136.8(6)  |
| C(37)-P(2)-C(49)-C(54)  | 18.6(8)   | C(28)-P(2)-C(49)-C(54)  | -105.1(7) |
| C(54)-C(49)-C(50)-C(51) | 1.8(12)   | P(2)-C(49)-C(50)-C(51)  | -169.0(6) |
| C(49)-C(50)-C(51)-C(52) | -3.0(13)  | C(50)-C(51)-C(52)-C(53) | 3.3(15)   |
| C(51)-C(52)-C(53)-C(54) | -2.3(15)  | C(50)-C(49)-C(54)-C(53) | -0.7(12)  |

P(2)-C(49)-C(54)-C(53)      169.7(7)      C(52)-C(53)-C(54)-C(49)      1.0(14)

Symmetry transformations used to generate equivalent atoms:

## Appendix F: Supporting data for Weller's hydrogenation

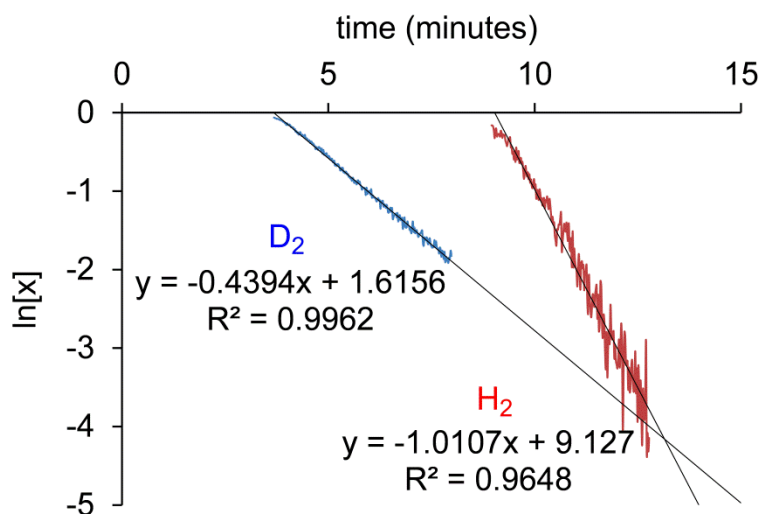


**Figure SI 1.**  $\ln[x]$  vs time plots for alkene hydrogenation by  $H_2$  (red) and  $D_2$  (blue). First order rate constants are  $k_H = 0.9 \pm 0.1 \text{ s}^{-1}$  and  $k_D = 0.44 \pm 0.01 \text{ s}^{-1}$ .

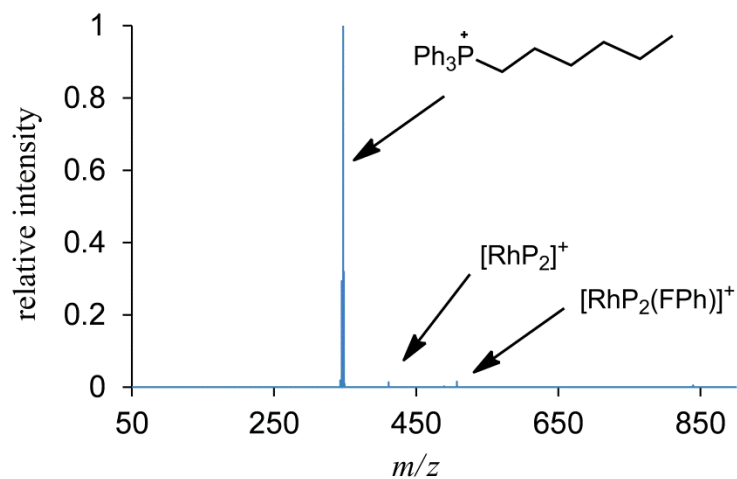


**Figure SI 2** Final product and a mix of  $[RhP_2]^+$  and  $[RhP_2(FPh)]^+$  when hydrogenation is nearly finished.



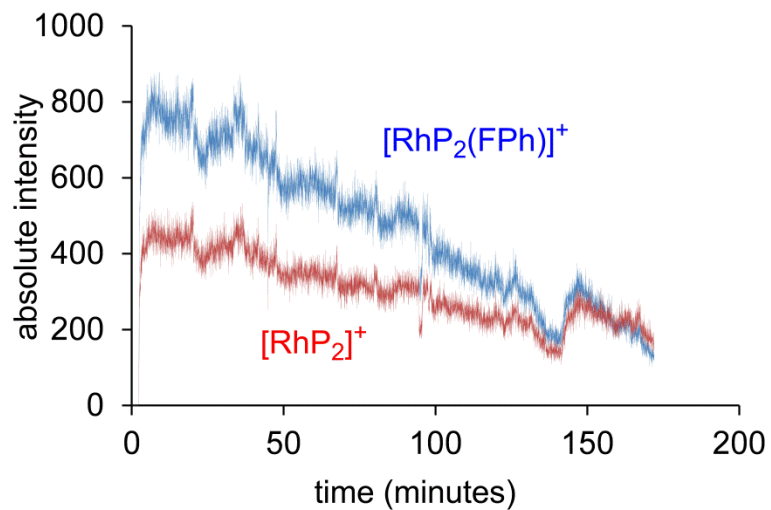


**Figure SI 3**  $[\text{RhP}_2]^+$  and  $[\text{RhP}_2(\text{FPh})]^+$  behavior at 0 °C.

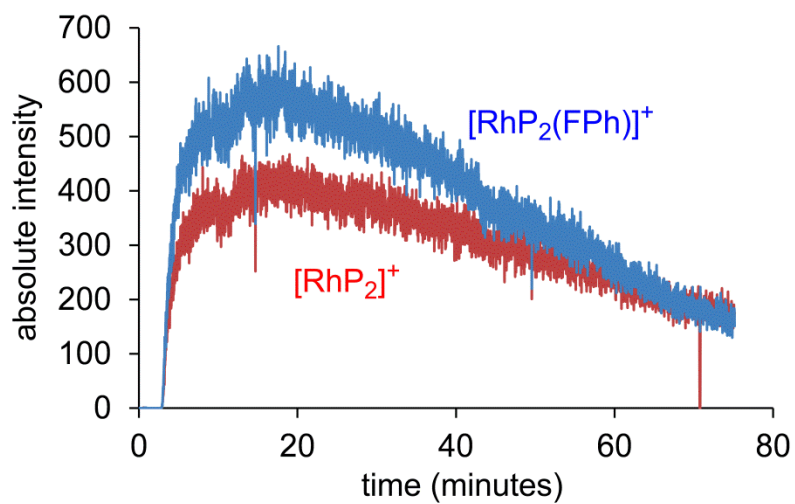


**Figure SI 4.**  $[\text{RhP}_2]^+$  and  $[\text{RhP}_2(\text{FPh})]^+$  behavior at 23 °C.

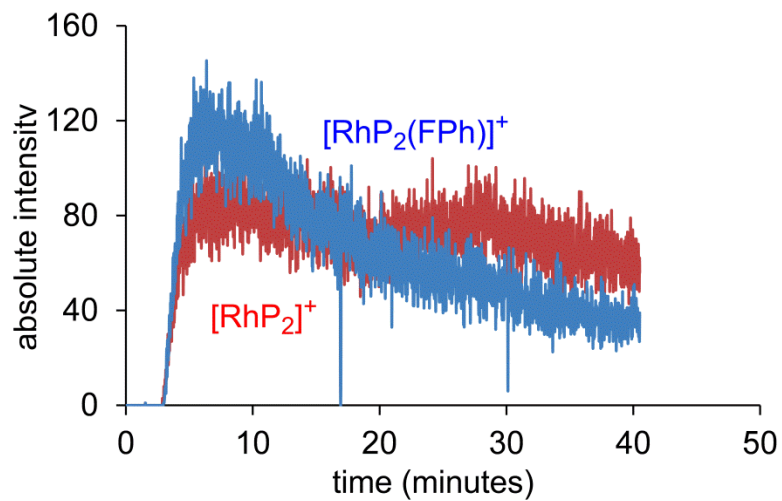


**Figure SI 5.**  $[\text{RhP}_2]^+$  and  $[\text{RhP}_2(\text{FPh})]^+$  behavior at 38 °C.

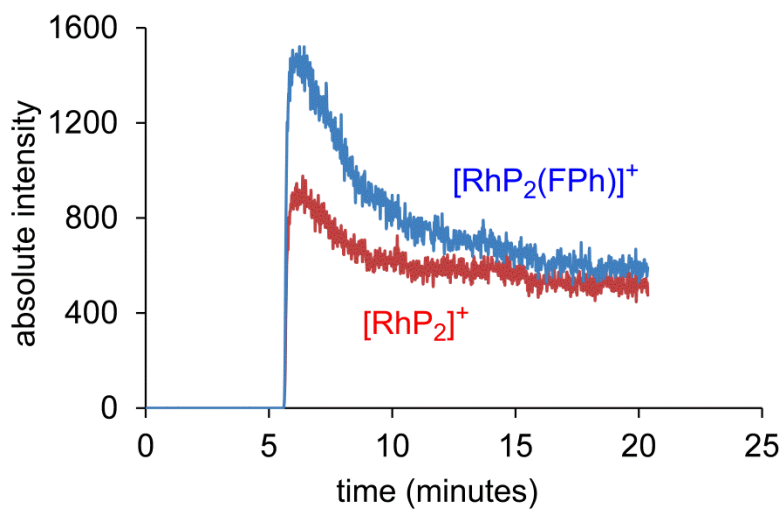


**Figure SI 6.**  $[\text{RhP}_2]^+$  and  $[\text{RhP}_2(\text{FPh})]^+$  behavior at 38 °C.

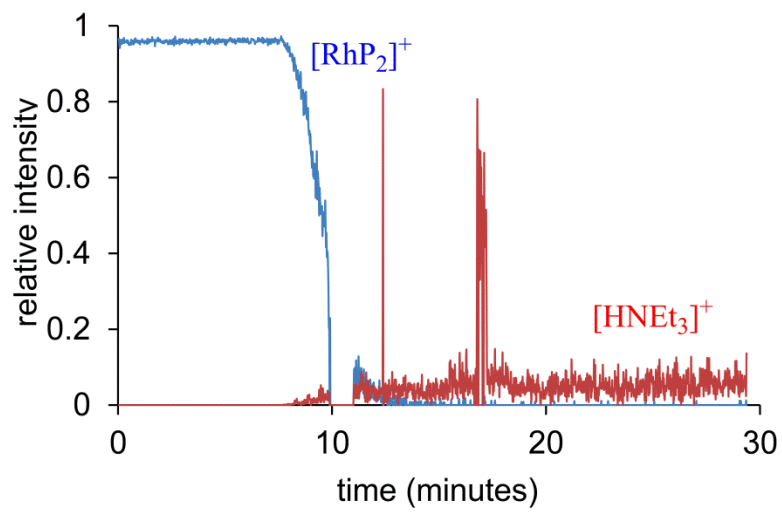


**Figure SI 7** Addition of  $\text{NEt}_3$  leads to the disappearance of  $[\text{RhP}_2]^+$  and the appearance of  $[\text{HNEt}_3]^+$

## Appendix G: Crystal data and structure refinement for PPh<sub>3</sub>P(CH<sub>2</sub>)<sub>5</sub>CH<sub>3</sub>.

|   |  |
|---|--|
| Identification code                     | uvic1302   |
| Empirical formula                       | C <sub>24</sub> H <sub>28</sub> F <sub>6</sub> P <sub>2</sub>  |
| Formula weight                          | 492.40   |
| Temperature                             | 120(2) K   |
| Wavelength                              | 0.71073 Å  |
| Crystal system                          | Orthorhombic   |
| Space group                             | Pbca   |
| Unit cell dimensions                    | $a = 13.3757(15)$ Å $\alpha = 90^\circ$<br>$b = 17.979(2)$ Å $\beta = 90^\circ$<br>$c = 19.568(2)$ Å $\gamma = 90^\circ$ |
| Volume                                  | 4705.9(9) Å <sup>3</sup>   |
| Z                                       | 8  |
| Density (calculated)                    | 1.390 g.cm <sup>-3</sup>   |
| Absorption coefficient ( $\mu$ )        | 0.242 mm <sup>-1</sup>   |
| F(000)                                  | 2048   |
| Crystal color, habit                    | colorless, tablet  |
| Crystal size                            | 0.230 × 0.180 × 0.070 mm <sup>3</sup>  |
| $\theta$ range for data collection      | 2.081 to 26.481°   |
| Index ranges                            | -16 ≤ h ≤ 16, -22 ≤ k ≤ 22, -24 ≤ l ≤ 24   |
| Reflections collected                   | 55595  |
| Independent reflections                 | 4858 [ $R_{\text{int}} = 0.0561$ ]   |
| Completeness to $\theta = 25.242^\circ$ | 100.0 %  |
| Absorption correction                   | Numerical  |
| Max. and min. transmission              | 1.0000 and 0.8375  |
| Refinement method                       | Full-matrix least-squares on F <sup>2</sup>  |
| Data / restraints / parameters          | 4858 / 0 / 306   |
| Goodness-of-fit on F <sup>2</sup>       | 1.044  |
| Final R indices [ $I > 2\sigma(I)$ ]    | $R_1 = 0.0434$ , $wR_2 = 0.1005$   |
| R indices (all data)                    | $R_1 = 0.0637$ , $wR_2 = 0.1091$   |
| Extinction coefficient                  | n/a  |
| Largest diff. peak and hole             | 0.528 and -0.451 e <sup>-</sup> .Å <sup>-3</sup>   |

**Table S 2.** Atomic coordinates and equivalent isotropic displacement parameters ( $\text{\AA}^2$ ) for uvic1302\_x. U(eq) is defined as one third of the trace of the orthogonalized  $U_{ij}$  tensor.

|       | x            | y            | z           | U(eq)    |
|-------|--------------|--------------|-------------|----------|
| P(1)  | 0.34382(4)   | 0.24259(3)   | 0.34052(3)  | 0.019(1) |
| C(1)  | 0.33641(15)  | 0.26159(12)  | 0.25052(11) | 0.025(1) |
| C(2)  | 0.42290(16)  | 0.30731(13)  | 0.22289(11) | 0.029(1) |
| C(3)  | 0.41580(15)  | 0.31619(13)  | 0.14559(11) | 0.028(1) |
| C(4)  | 0.50425(16)  | 0.35820(13)  | 0.11677(11) | 0.029(1) |
| C(5)  | 0.49729(16)  | 0.37350(12)  | 0.03995(11) | 0.031(1) |
| C(6)  | 0.41137(19)  | 0.42259(15)  | 0.02027(12) | 0.039(1) |
| C(7)  | 0.24166(14)  | 0.18222(11)  | 0.36305(10) | 0.023(1) |
| C(8)  | 0.20236(17)  | 0.18428(13)  | 0.42860(12) | 0.032(1) |
| C(9)  | 0.12354(17)  | 0.13798(14)  | 0.44630(13) | 0.038(1) |
| C(10) | 0.08302(16)  | 0.09057(13)  | 0.39891(13) | 0.034(1) |
| C(11) | 0.12095(19)  | 0.08831(15)  | 0.33387(13) | 0.042(1) |
| C(12) | 0.20049(18)  | 0.13332(14)  | 0.31552(12) | 0.036(1) |
| C(13) | 0.33259(14)  | 0.32456(11)  | 0.39177(10) | 0.021(1) |
| C(14) | 0.27700(15)  | 0.38445(12)  | 0.36762(11) | 0.026(1) |
| C(15) | 0.25770(17)  | 0.44382(13)  | 0.41103(12) | 0.033(1) |
| C(16) | 0.29278(17)  | 0.44357(13)  | 0.47731(13) | 0.034(1) |
| C(17) | 0.34822(15)  | 0.38416(13)  | 0.50117(12) | 0.031(1) |
| C(18) | 0.36825(14)  | 0.32465(12)  | 0.45880(11) | 0.025(1) |
| C(19) | 0.46246(14)  | 0.19939(11)  | 0.35605(10) | 0.020(1) |
| C(20) | 0.47263(15)  | 0.12343(12)  | 0.34363(11) | 0.025(1) |
| C(21) | 0.56572(17)  | 0.09040(13)  | 0.34961(11) | 0.030(1) |
| C(22) | 0.64802(16)  | 0.13271(13)  | 0.36845(11) | 0.031(1) |
| C(23) | 0.63811(15)  | 0.20790(13)  | 0.37994(11) | 0.028(1) |
| C(24) | 0.54581(14)  | 0.24231(12)  | 0.37306(10) | 0.023(1) |
| P(2)  | -0.14461(4)  | -0.03949(3)  | 0.31318(3)  | 0.028(1) |
| F(1)  | -0.15447(10) | -0.12416(7)  | 0.28999(8)  | 0.044(1) |
| F(2)  | -0.13410(11) | 0.04629(9)   | 0.33459(10) | 0.063(1) |
| F(3)  | -0.25964(12) | -0.02943(11) | 0.29599(12) | 0.063(1) |
| F(4)  | -0.03131(13) | -0.05419(11) | 0.33122(15) | 0.070(1) |
| F(5)  | -0.1174(2)   | -0.01839(11) | 0.23812(10) | 0.074(1) |
| F(6)  | -0.1737(2)   | -0.06455(19) | 0.38772(11) | 0.105(1) |
| F(3A) | -0.2397(8)   | -0.0306(6)   | 0.3595(5)   | 0.041(3) |
| F(4A) | -0.0417(7)   | -0.0289(5)   | 0.2722(5)   | 0.034(3) |
| F(5A) | -0.2076(8)   | -0.0069(5)   | 0.2513(5)   | 0.038(3) |
| F(6A) | -0.0841(8)   | -0.0519(5)   | 0.3794(5)   | 0.036(3) |
| H(1A) | 0.3339       | 0.2137       | 0.2255      | 0.030    |
| H(1B) | 0.2732       | 0.2884       | 0.2412      | 0.030    |
| H(2A) | 0.4868       | 0.2826       | 0.2347      | 0.034    |
| H(2B) | 0.4225       | 0.3570       | 0.2446      | 0.034    |
| H(3A) | 0.4124       | 0.2664       | 0.1241      | 0.034    |
| H(3B) | 0.3535       | 0.3431       | 0.1341      | 0.034    |

|       |        |        |         |       |
|-------|--------|--------|---------|-------|
| H(4A) | 0.5658 | 0.3293 | 0.1258  | 0.035 |
| H(4B) | 0.5104 | 0.4062 | 0.1411  | 0.035 |
| H(5A) | 0.5603 | 0.3971 | 0.0247  | 0.037 |
| H(5B) | 0.4908 | 0.3255 | 0.0156  | 0.037 |
| H(6A) | 0.4113 | 0.4298 | -0.0294 | 0.058 |
| H(6B) | 0.4182 | 0.4709 | 0.0430  | 0.058 |
| H(6C) | 0.3485 | 0.3992 | 0.0343  | 0.058 |
| H(8)  | 0.2295 | 0.2175 | 0.4615  | 0.039 |
| H(9)  | 0.0975 | 0.1391 | 0.4915  | 0.045 |
| H(10) | 0.0287 | 0.0593 | 0.4112  | 0.041 |
| H(11) | 0.0924 | 0.0556 | 0.3011  | 0.051 |
| H(12) | 0.2270 | 0.1309 | 0.2705  | 0.044 |
| H(14) | 0.2526 | 0.3847 | 0.3220  | 0.032 |
| H(15) | 0.2200 | 0.4850 | 0.3949  | 0.040 |
| H(16) | 0.2788 | 0.4844 | 0.5066  | 0.041 |
| H(17) | 0.3726 | 0.3843 | 0.5468  | 0.037 |
| H(18) | 0.4063 | 0.2838 | 0.4752  | 0.030 |
| H(20) | 0.4161 | 0.0945 | 0.3311  | 0.030 |
| H(21) | 0.5733 | 0.0387 | 0.3408  | 0.036 |
| H(22) | 0.7115 | 0.1097 | 0.3734  | 0.038 |
| H(23) | 0.6949 | 0.2364 | 0.3927  | 0.034 |
| H(24) | 0.5394 | 0.2944 | 0.3798  | 0.027 |

**Table S 3.** Anisotropic displacement parameters ( $\text{\AA}^2$ ) for *uvic1302\_x*.

The anisotropic displacement factor exponent takes the form:

$$-2\pi^2[h^2a^{*2}U_{11} + \dots + 2hka^*b^*U_{12}]$$

|       | $U_{11}$   | $U_{22}$   | $U_{33}$   | $U_{23}$    | $U_{13}$    | $U_{12}$    |
|-------|------------|------------|------------|-------------|-------------|-------------|
| P(1)  | 0.0166(2)  | 0.0245(3)  | 0.0171(2)  | 0.0001(2)   | -0.0006(2)  | 0.0018(2)   |
| C(1)  | 0.0233(9)  | 0.0309(11) | 0.0210(10) | -0.0005(9)  | -0.0022(8)  | 0.0028(9)   |
| C(2)  | 0.0279(11) | 0.0323(12) | 0.0253(11) | 0.0011(9)   | -0.0033(9)  | -0.0042(9)  |
| C(3)  | 0.0253(10) | 0.0361(12) | 0.0226(11) | 0.0028(9)   | 0.0007(9)   | -0.0031(9)  |
| C(4)  | 0.0269(11) | 0.0334(12) | 0.0272(12) | -0.0013(10) | 0.0001(9)   | -0.0023(9)  |
| C(5)  | 0.0339(12) | 0.0320(12) | 0.0256(11) | -0.0063(10) | 0.0099(10)  | -0.0103(10) |
| C(6)  | 0.0482(15) | 0.0463(15) | 0.0223(12) | 0.0031(11)  | 0.0016(11)  | -0.0029(12) |
| C(7)  | 0.0182(9)  | 0.0251(11) | 0.0240(11) | -0.0003(9)  | -0.0021(8)  | 0.0012(8)   |
| C(8)  | 0.0320(12) | 0.0356(13) | 0.0287(12) | -0.0093(10) | 0.0060(10)  | -0.0066(10) |
| C(9)  | 0.0337(12) | 0.0416(14) | 0.0379(14) | -0.0050(11) | 0.0143(11)  | -0.0062(11) |
| C(10) | 0.0200(10) | 0.0370(13) | 0.0458(15) | 0.0002(11)  | 0.0027(10)  | -0.0064(9)  |
| C(11) | 0.0392(13) | 0.0508(16) | 0.0372(14) | -0.0024(12) | -0.0068(11) | -0.0208(12) |
| C(12) | 0.0383(13) | 0.0473(15) | 0.0232(12) | -0.0029(11) | -0.0007(10) | -0.0143(11) |
| C(13) | 0.0170(9)  | 0.0233(10) | 0.0222(10) | -0.0011(8)  | 0.0010(8)   | -0.0010(8)  |
| C(14) | 0.0229(10) | 0.0284(11) | 0.0281(11) | 0.0036(9)   | -0.0004(9)  | 0.0021(9)   |
| C(15) | 0.0324(12) | 0.0249(11) | 0.0423(14) | 0.0016(10)  | 0.0035(11)  | 0.0059(9)   |
| C(16) | 0.0306(11) | 0.0291(12) | 0.0420(14) | -0.0107(11) | 0.0083(10)  | -0.0020(10) |
| C(17) | 0.0240(10) | 0.0402(13) | 0.0276(12) | -0.0078(10) | 0.0006(9)   | -0.0030(10) |
| C(18) | 0.0192(9)  | 0.0321(12) | 0.0239(11) | -0.0019(9)  | 0.0007(8)   | 0.0028(8)   |
| C(19) | 0.0180(9)  | 0.0274(11) | 0.0154(10) | 0.0045(8)   | 0.0019(8)   | 0.0027(8)   |
| C(20) | 0.0256(10) | 0.0274(11) | 0.0232(11) | 0.0022(9)   | 0.0030(9)   | 0.0008(9)   |
| C(21) | 0.0359(12) | 0.0272(12) | 0.0278(12) | 0.0044(10)  | 0.0065(10)  | 0.0095(9)   |
| C(22) | 0.0243(10) | 0.0470(14) | 0.0224(11) | 0.0061(10)  | 0.0051(9)   | 0.0141(10)  |
| C(23) | 0.0173(10) | 0.0454(14) | 0.0216(11) | 0.0021(10)  | 0.0013(8)   | 0.0004(9)   |
| C(24) | 0.0215(9)  | 0.0280(11) | 0.0186(10) | 0.0021(9)   | 0.0027(8)   | 0.0006(8)   |
| P(2)  | 0.0182(3)  | 0.0371(3)  | 0.0287(3)  | -0.0072(2)  | -0.0003(2)  | 0.0001(2)   |
| F(1)  | 0.0399(8)  | 0.0276(7)  | 0.0643(10) | 0.0051(7)   | -0.0189(7)  | -0.0074(6)  |
| F(2)  | 0.0376(8)  | 0.0538(10) | 0.0987(14) | -0.0471(10) | -0.0153(9)  | 0.0138(7)   |
| F(3)  | 0.0236(9)  | 0.0592(13) | 0.1064(19) | -0.0272(12) | -0.0191(10) | 0.0091(8)   |
| F(4)  | 0.0238(9)  | 0.0459(11) | 0.141(2)   | -0.0357(13) | -0.0284(12) | 0.0053(8)   |
| F(5)  | 0.129(2)   | 0.0443(11) | 0.0480(13) | 0.0083(9)   | 0.0364(14)  | -0.0150(13) |
| F(6)  | 0.111(2)   | 0.178(3)   | 0.0247(11) | 0.0021(14)  | 0.0129(12)  | -0.016(2)   |

**Table S 4.** Bond lengths [Å] for uvic1302\_x.

| atom-atom   | distance   | atom-atom   | distance   |
|-------------|------------|-------------|------------|
| P(1)-C(13)  | 1.789(2)   | P(1)-C(19)  | 1.793(2)   |
| P(1)-C(1)   | 1.797(2)   | P(1)-C(7)   | 1.800(2)   |
| C(1)-C(2)   | 1.519(3)   | C(2)-C(3)   | 1.524(3)   |
| C(3)-C(4)   | 1.513(3)   | C(4)-C(5)   | 1.531(3)   |
| C(5)-C(6)   | 1.499(3)   | C(7)-C(8)   | 1.387(3)   |
| C(7)-C(12)  | 1.393(3)   | C(8)-C(9)   | 1.387(3)   |
| C(9)-C(10)  | 1.371(3)   | C(10)-C(11) | 1.371(3)   |
| C(11)-C(12) | 1.384(3)   | C(13)-C(14) | 1.391(3)   |
| C(13)-C(18) | 1.396(3)   | C(14)-C(15) | 1.388(3)   |
| C(15)-C(16) | 1.379(3)   | C(16)-C(17) | 1.382(3)   |
| C(17)-C(18) | 1.380(3)   | C(19)-C(20) | 1.394(3)   |
| C(19)-C(24) | 1.396(3)   | C(20)-C(21) | 1.385(3)   |
| C(21)-C(22) | 1.388(3)   | C(22)-C(23) | 1.377(3)   |
| C(23)-C(24) | 1.388(3)   | P(2)-F(6A)  | 1.545(9)   |
| P(2)-F(5)   | 1.560(2)   | P(2)-F(3A)  | 1.569(10)  |
| P(2)-F(6)   | 1.575(2)   | P(2)-F(4)   | 1.5783(17) |
| P(2)-F(3)   | 1.5853(17) | P(2)-F(5A)  | 1.588(9)   |
| P(2)-F(1)   | 1.5939(15) | P(2)-F(2)   | 1.6043(16) |
| P(2)-F(4A)  | 1.605(9)   | C(1)-H(1A)  | 0.9900     |
| C(1)-H(1B)  | 0.9900     | C(2)-H(2A)  | 0.9900     |
| C(2)-H(2B)  | 0.9900     | C(3)-H(3A)  | 0.9900     |
| C(3)-H(3B)  | 0.9900     | C(4)-H(4A)  | 0.9900     |
| C(4)-H(4B)  | 0.9900     | C(5)-H(5A)  | 0.9900     |
| C(5)-H(5B)  | 0.9900     | C(6)-H(6A)  | 0.9800     |
| C(6)-H(6B)  | 0.9800     | C(6)-H(6C)  | 0.9800     |
| C(8)-H(8)   | 0.9500     | C(9)-H(9)   | 0.9500     |
| C(10)-H(10) | 0.9500     | C(11)-H(11) | 0.9500     |
| C(12)-H(12) | 0.9500     | C(14)-H(14) | 0.9500     |
| C(15)-H(15) | 0.9500     | C(16)-H(16) | 0.9500     |
| C(17)-H(17) | 0.9500     | C(18)-H(18) | 0.9500     |
| C(20)-H(20) | 0.9500     | C(21)-H(21) | 0.9500     |
| C(22)-H(22) | 0.9500     | C(23)-H(23) | 0.9500     |
| C(24)-H(24) | 0.9500     |             |            |

Symmetry transformations used to generate equivalent atoms:

**Table S 5.** Bond angles [°] for uvic1302\_x.

| atom-atom-atom   | angle      | atom-atom-atom  | angle      |
|------------------|------------|-----------------|------------|
| C(13)-P(1)-C(19) | 109.65(9)  | C(13)-P(1)-C(1) | 112.85(10) |
| C(19)-P(1)-C(1)  | 107.30(9)  | C(13)-P(1)-C(7) | 107.20(9)  |
| C(19)-P(1)-C(7)  | 111.68(9)  | C(1)-P(1)-C(7)  | 108.23(10) |
| C(2)-C(1)-P(1)   | 114.19(14) | C(1)-C(2)-C(3)  | 111.25(17) |
| C(4)-C(3)-C(2)   | 111.93(18) | C(3)-C(4)-C(5)  | 114.09(18) |



|                   |            |                   |            |
|-------------------|------------|-------------------|------------|
| C(6)-C(5)-C(4)    | 113.86(19) | C(8)-C(7)-C(12)   | 119.0(2)   |
| C(8)-C(7)-P(1)    | 119.89(16) | C(12)-C(7)-P(1)   | 121.13(16) |
| C(7)-C(8)-C(9)    | 120.2(2)   | C(10)-C(9)-C(8)   | 120.3(2)   |
| C(11)-C(10)-C(9)  | 120.0(2)   | C(10)-C(11)-C(12) | 120.5(2)   |
| C(11)-C(12)-C(7)  | 120.0(2)   | C(14)-C(13)-C(18) | 120.06(19) |
| C(14)-C(13)-P(1)  | 119.48(16) | C(18)-C(13)-P(1)  | 119.94(16) |
| C(15)-C(14)-C(13) | 119.1(2)   | C(16)-C(15)-C(14) | 120.6(2)   |
| C(15)-C(16)-C(17) | 120.2(2)   | C(18)-C(17)-C(16) | 120.0(2)   |
| C(17)-C(18)-C(13) | 120.0(2)   | C(20)-C(19)-C(24) | 120.35(18) |
| C(20)-C(19)-P(1)  | 118.77(15) | C(24)-C(19)-P(1)  | 120.52(16) |
| C(21)-C(20)-C(19) | 119.6(2)   | C(20)-C(21)-C(22) | 120.0(2)   |
| C(23)-C(22)-C(21) | 120.3(2)   | C(22)-C(23)-C(24) | 120.5(2)   |
| C(23)-C(24)-C(19) | 119.2(2)   | F(6A)-P(2)-F(3A)  | 87.4(6)    |
| F(5)-P(2)-F(6)    | 177.28(14) | F(5)-P(2)-F(4)    | 91.56(15)  |
| F(6)-P(2)-F(4)    | 88.99(16)  | F(5)-P(2)-F(3)    | 89.94(14)  |
| F(6)-P(2)-F(3)    | 89.39(15)  | F(4)-P(2)-F(3)    | 176.83(12) |
| F(6A)-P(2)-F(5A)  | 166.3(5)   | F(3A)-P(2)-F(5A)  | 88.5(6)    |
| F(6A)-P(2)-F(1)   | 98.3(4)    | F(5)-P(2)-F(1)    | 89.05(10)  |
| F(3A)-P(2)-F(1)   | 101.2(4)   | F(6)-P(2)-F(1)    | 88.28(14)  |
| F(4)-P(2)-F(1)    | 89.04(8)   | F(3)-P(2)-F(1)    | 88.18(9)   |
| F(5A)-P(2)-F(1)   | 95.2(3)    | F(6A)-P(2)-F(2)   | 82.7(4)    |
| F(5)-P(2)-F(2)    | 89.51(11)  | F(3A)-P(2)-F(2)   | 79.8(4)    |
| F(6)-P(2)-F(2)    | 93.14(14)  | F(4)-P(2)-F(2)    | 91.05(9)   |
| F(3)-P(2)-F(2)    | 91.76(9)   | F(5A)-P(2)-F(2)   | 83.7(3)    |
| F(1)-P(2)-F(2)    | 178.57(10) | F(6A)-P(2)-F(4A)  | 89.2(5)    |
| F(3A)-P(2)-F(4A)  | 166.3(5)   | F(5A)-P(2)-F(4A)  | 91.7(6)    |
| F(1)-P(2)-F(4A)   | 92.4(3)    | F(2)-P(2)-F(4A)   | 86.6(3)    |
| C(2)-C(1)-H(1A)   | 108.7      | P(1)-C(1)-H(1A)   | 108.7      |
| C(2)-C(1)-H(1B)   | 108.7      | P(1)-C(1)-H(1B)   | 108.7      |
| H(1A)-C(1)-H(1B)  | 107.6      | C(1)-C(2)-H(2A)   | 109.4      |
| C(3)-C(2)-H(2A)   | 109.4      | C(1)-C(2)-H(2B)   | 109.4      |
| C(3)-C(2)-H(2B)   | 109.4      | H(2A)-C(2)-H(2B)  | 108.0      |
| C(4)-C(3)-H(3A)   | 109.2      | C(2)-C(3)-H(3A)   | 109.2      |
| C(4)-C(3)-H(3B)   | 109.2      | C(2)-C(3)-H(3B)   | 109.2      |
| H(3A)-C(3)-H(3B)  | 107.9      | C(3)-C(4)-H(4A)   | 108.7      |
| C(5)-C(4)-H(4A)   | 108.7      | C(3)-C(4)-H(4B)   | 108.7      |
| C(5)-C(4)-H(4B)   | 108.7      | H(4A)-C(4)-H(4B)  | 107.6      |
| C(6)-C(5)-H(5A)   | 108.8      | C(4)-C(5)-H(5A)   | 108.8      |
| C(6)-C(5)-H(5B)   | 108.8      | C(4)-C(5)-H(5B)   | 108.8      |
| H(5A)-C(5)-H(5B)  | 107.7      | C(5)-C(6)-H(6A)   | 109.5      |
| C(5)-C(6)-H(6B)   | 109.5      | H(6A)-C(6)-H(6B)  | 109.5      |
| C(5)-C(6)-H(6C)   | 109.5      | H(6A)-C(6)-H(6C)  | 109.5      |
| H(6B)-C(6)-H(6C)  | 109.5      | C(7)-C(8)-H(8)    | 119.9      |
| C(9)-C(8)-H(8)    | 119.9      | C(10)-C(9)-H(9)   | 119.8      |
| C(8)-C(9)-H(9)    | 119.8      | C(11)-C(10)-H(10) | 120.0      |
| C(9)-C(10)-H(10)  | 120.0      | C(10)-C(11)-H(11) | 119.7      |

|                   |       |                   |       |
|-------------------|-------|-------------------|-------|
| C(12)-C(11)-H(11) | 119.7 | C(11)-C(12)-H(12) | 120.0 |
| C(7)-C(12)-H(12)  | 120.0 | C(15)-C(14)-H(14) | 120.4 |
| C(13)-C(14)-H(14) | 120.4 | C(16)-C(15)-H(15) | 119.7 |
| C(14)-C(15)-H(15) | 119.7 | C(15)-C(16)-H(16) | 119.9 |
| C(17)-C(16)-H(16) | 119.9 | C(18)-C(17)-H(17) | 120.0 |
| C(16)-C(17)-H(17) | 120.0 | C(17)-C(18)-H(18) | 120.0 |
| C(13)-C(18)-H(18) | 120.0 | C(21)-C(20)-H(20) | 120.2 |
| C(19)-C(20)-H(20) | 120.2 | C(20)-C(21)-H(21) | 120.0 |
| C(22)-C(21)-H(21) | 120.0 | C(23)-C(22)-H(22) | 119.8 |
| C(21)-C(22)-H(22) | 119.8 | C(22)-C(23)-H(23) | 119.7 |
| C(24)-C(23)-H(23) | 119.7 | C(23)-C(24)-H(24) | 120.4 |
| C(19)-C(24)-H(24) | 120.4 |                   |       |

Symmetry transformations used to generate equivalent atoms:

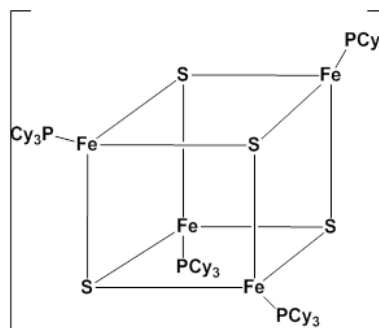
**Table S 6.** Torsion angles [°] for *uvic1302\_x*.

| atom-atom-atom-atom     | angle       | atom-atom-atom-atom     | angle       |
|-------------------------|-------------|-------------------------|-------------|
| C(13)-P(1)-C(1)-C(2)    | 66.03(18)   | C(19)-P(1)-C(1)-C(2)    | -54.85(18)  |
| C(7)-P(1)-C(1)-C(2)     | -175.51(15) | P(1)-C(1)-C(2)-C(3)     | 175.67(15)  |
| C(1)-C(2)-C(3)-C(4)     | -177.04(18) | C(2)-C(3)-C(4)-C(5)     | -175.91(19) |
| C(3)-C(4)-C(5)-C(6)     | 63.3(3)     | C(13)-P(1)-C(7)-C(8)    | -29.7(2)    |
| C(19)-P(1)-C(7)-C(8)    | 90.44(19)   | C(1)-P(1)-C(7)-C(8)     | -151.67(17) |
| C(13)-P(1)-C(7)-C(12)   | 149.98(18)  | C(19)-P(1)-C(7)-C(12)   | -89.9(2)    |
| C(1)-P(1)-C(7)-C(12)    | 28.0(2)     | C(12)-C(7)-C(8)-C(9)    | 0.2(3)      |
| P(1)-C(7)-C(8)-C(9)     | 179.92(19)  | C(7)-C(8)-C(9)-C(10)    | -0.9(4)     |
| C(8)-C(9)-C(10)-C(11)   | 0.6(4)      | C(9)-C(10)-C(11)-C(12)  | 0.3(4)      |
| C(10)-C(11)-C(12)-C(7)  | -1.0(4)     | C(8)-C(7)-C(12)-C(11)   | 0.6(4)      |
| P(1)-C(7)-C(12)-C(11)   | -179.0(2)   | C(19)-P(1)-C(13)-C(14)  | 148.69(16)  |
| C(1)-P(1)-C(13)-C(14)   | 29.16(19)   | C(7)-P(1)-C(13)-C(14)   | -89.91(18)  |
| C(19)-P(1)-C(13)-C(18)  | -39.57(18)  | C(1)-P(1)-C(13)-C(18)   | -159.10(15) |
| C(7)-P(1)-C(13)-C(18)   | 81.83(17)   | C(18)-C(13)-C(14)-C(15) | 0.0(3)      |
| P(1)-C(13)-C(14)-C(15)  | 171.68(16)  | C(13)-C(14)-C(15)-C(16) | -0.2(3)     |
| C(14)-C(15)-C(16)-C(17) | 0.4(3)      | C(15)-C(16)-C(17)-C(18) | -0.3(3)     |
| C(16)-C(17)-C(18)-C(13) | 0.1(3)      | C(14)-C(13)-C(18)-C(17) | 0.1(3)      |
| P(1)-C(13)-C(18)-C(17)  | -171.60(16) | C(13)-P(1)-C(19)-C(20)  | 155.52(16)  |
| C(1)-P(1)-C(19)-C(20)   | -81.60(17)  | C(7)-P(1)-C(19)-C(20)   | 36.85(19)   |
| C(13)-P(1)-C(19)-C(24)  | -31.37(19)  | C(1)-P(1)-C(19)-C(24)   | 91.51(17)   |
| C(7)-P(1)-C(19)-C(24)   | -150.04(16) | C(24)-C(19)-C(20)-C(21) | 1.3(3)      |
| P(1)-C(19)-C(20)-C(21)  | 174.41(16)  | C(19)-C(20)-C(21)-C(22) | 0.6(3)      |
| C(20)-C(21)-C(22)-C(23) | -1.3(3)     | C(21)-C(22)-C(23)-C(24) | 0.2(3)      |
| C(22)-C(23)-C(24)-C(19) | 1.7(3)      | C(20)-C(19)-C(24)-C(23) | -2.4(3)     |
| P(1)-C(19)-C(24)-C(23)  | -175.39(15) |                         |             |

Symmetry transformations used to generate equivalent atoms:

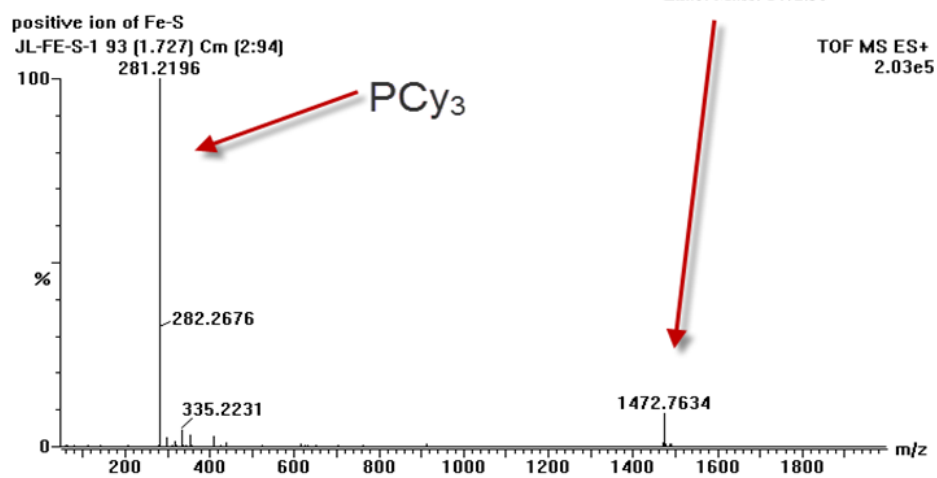
## Appendix H: Data for collaboration projects

MS

 $\text{BPh}_4^-$ 

Chemical Formula:  $\text{C}_{72}\text{H}_{132}\text{Fe}_4\text{P}_4\text{S}_4$   
 Exact Mass: 1472.56

Chemical Formula:  $\text{C}_{24}\text{H}_{20}\text{B}^-$   
 Exact Mass: 319.17



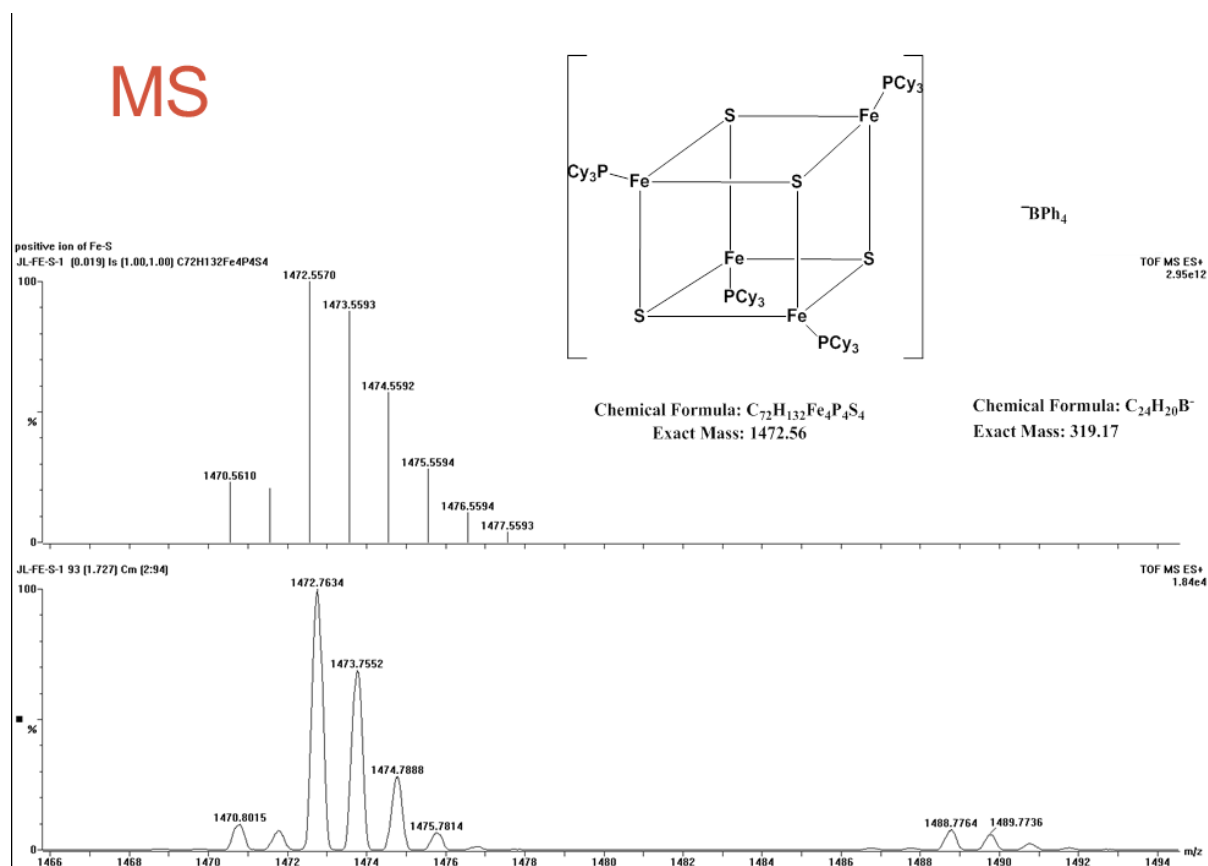


Figure SI 8 MS of FeS cluster 1

## MS/MS

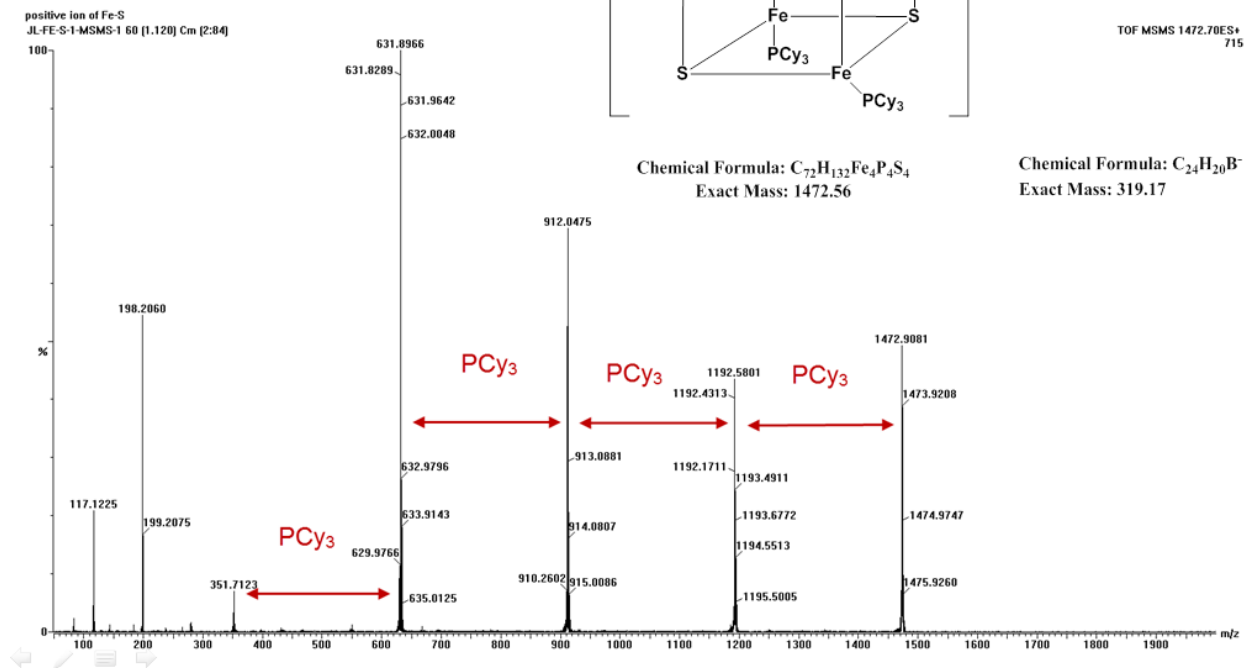


Figure SI 9 MS/MS of FeS cluster 1

MS

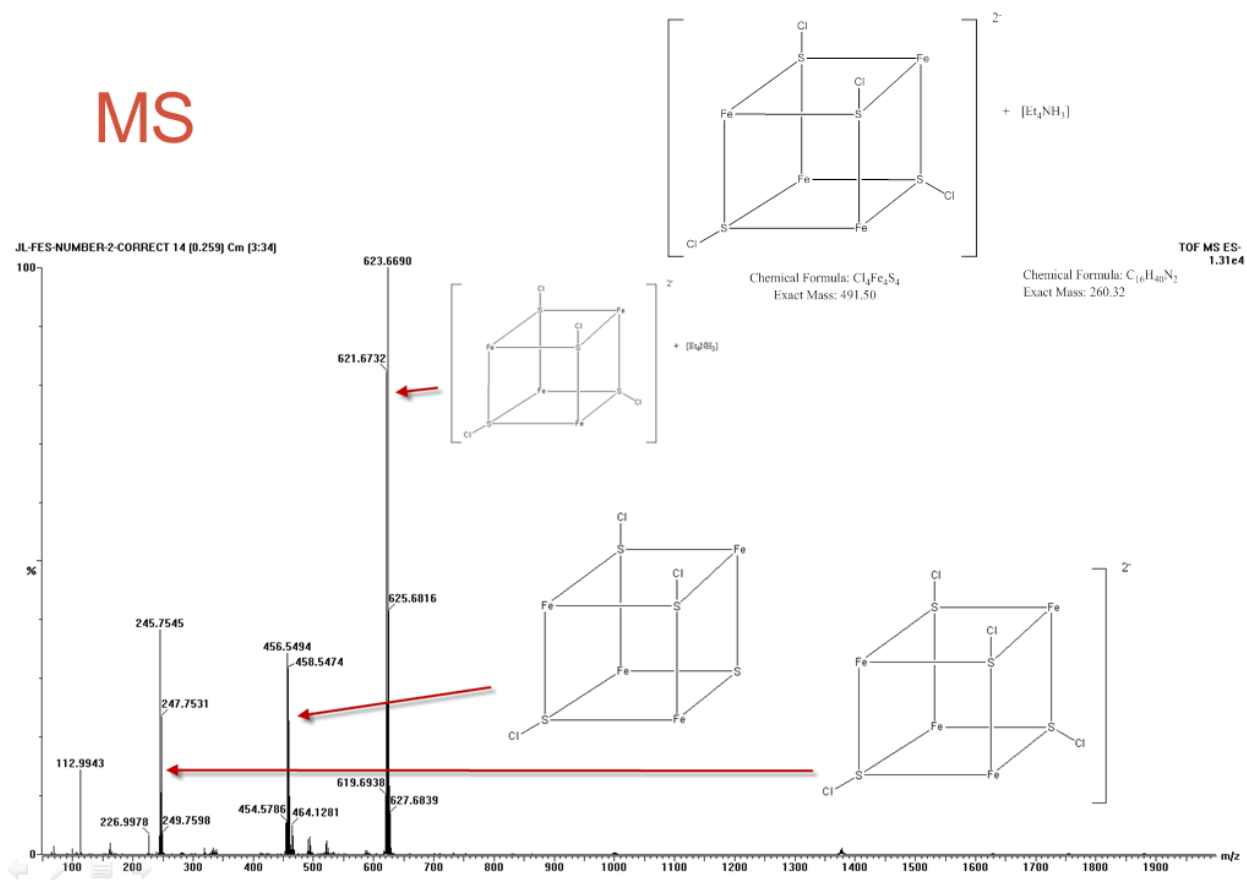


Figure SI 10 MS of FeS cluster 2

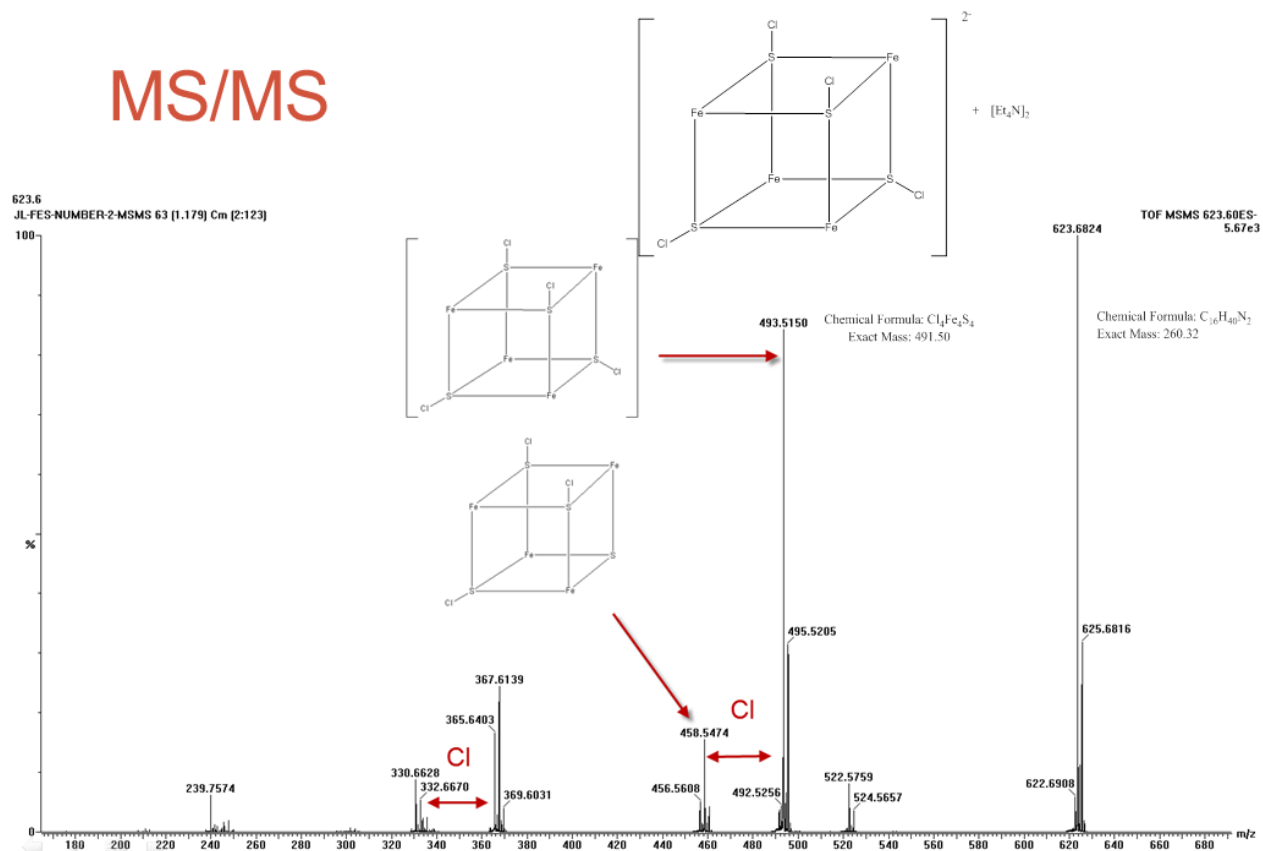


Figure SI 11 MS/MS of FeS cluster 2



## MS

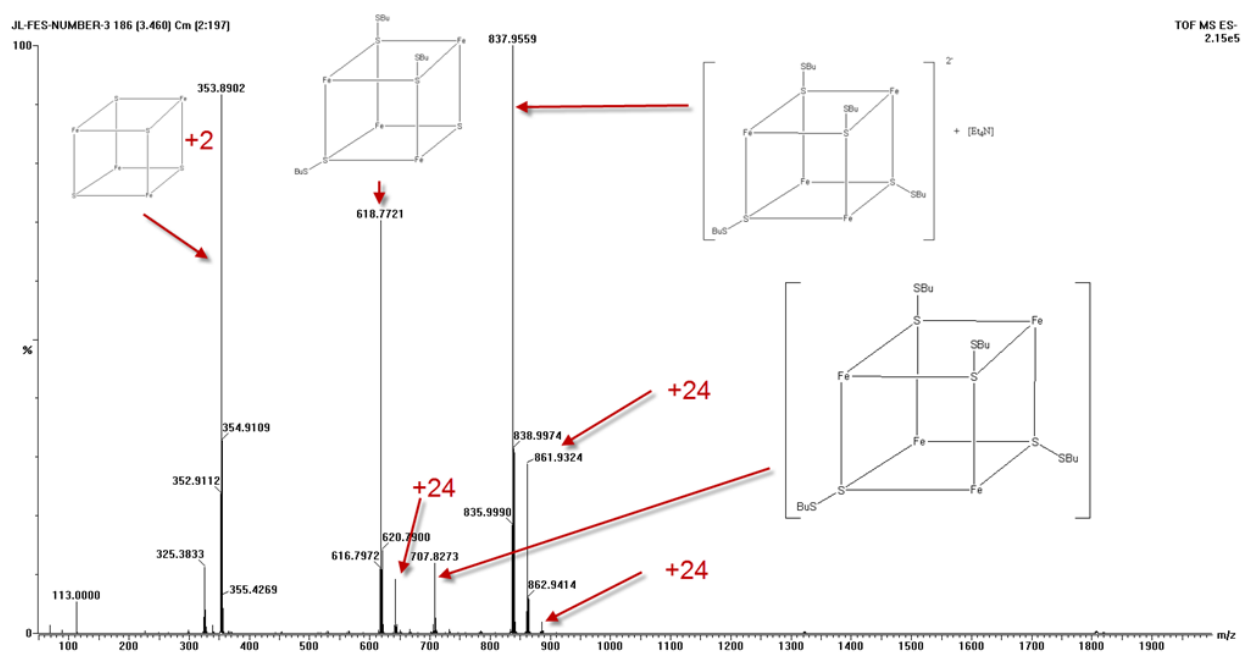


Figure SI 12 MS of FeS cluster 3

## MS/MS

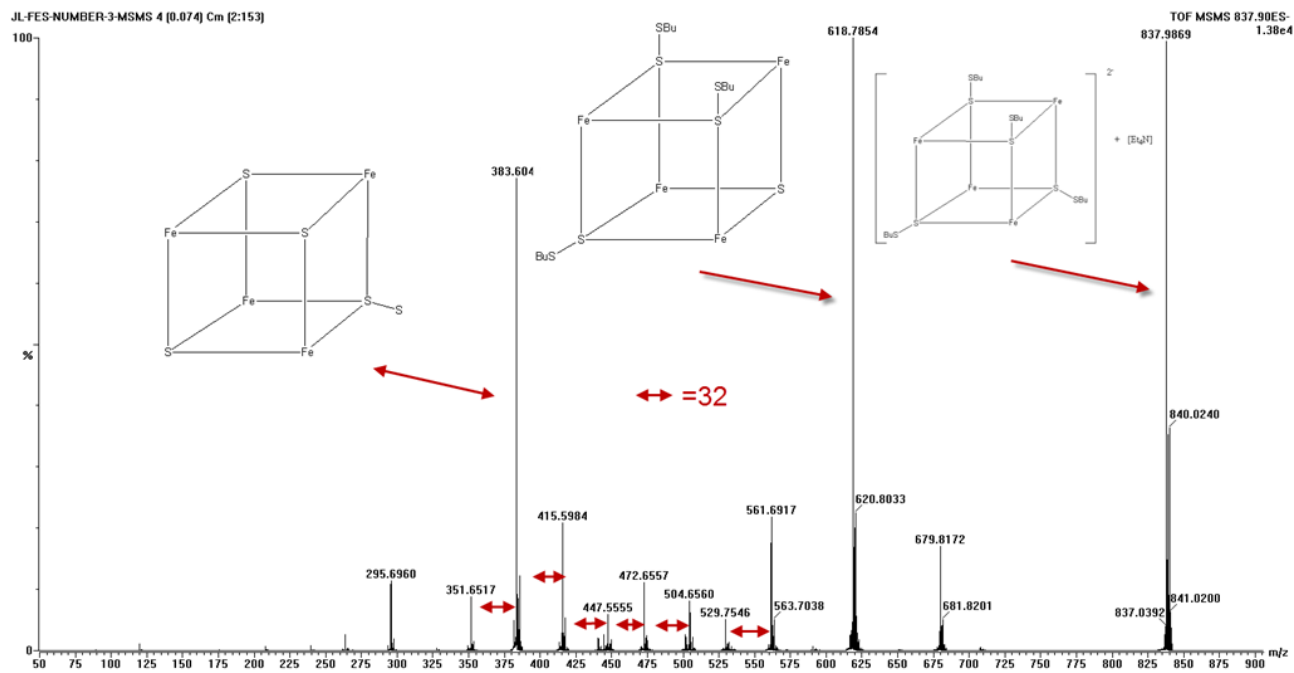


Figure SI 13 MS/MS of FeS cluster 3

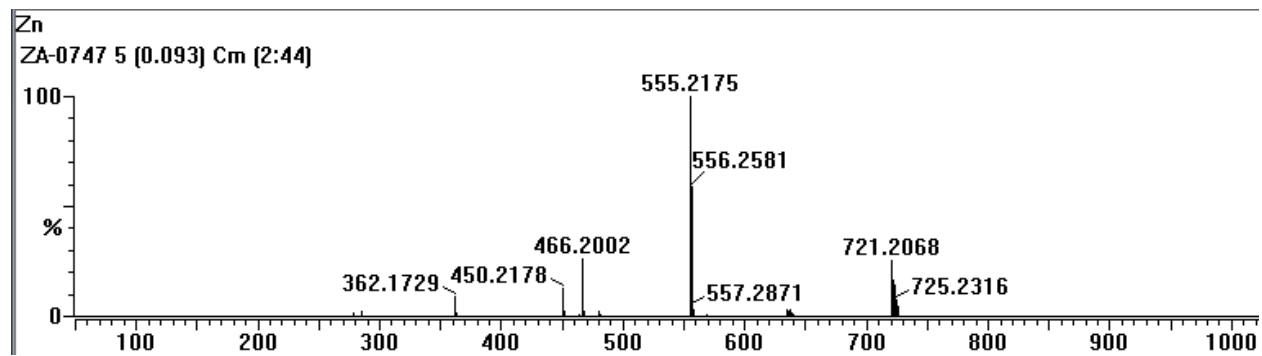


Figure SI 14 Initial MS of catalyst only for Zn polymerization project

Table 8 Assignment of peaks in the spectrum

|                    |            |  |                                       |
|--------------------|------------|--|---------------------------------------|
| C23H25NOP          | 362.1<br>7 |  | catalyst loss one arm                 |
| C27H34NOP2         | 450.2<br>1 |  | catalyst loss N-Bn                    |
| C27H34NO2P2        | 466.2<br>1 |  | not very sure of the structure,       |
| C34H41N2OP2        | 555.2<br>7 |  | this is the ligand drop from catalyst |
| C38H47N2O4P2<br>Zn | 721.2<br>3 |  | this is the catalyst charge is on Zn  |

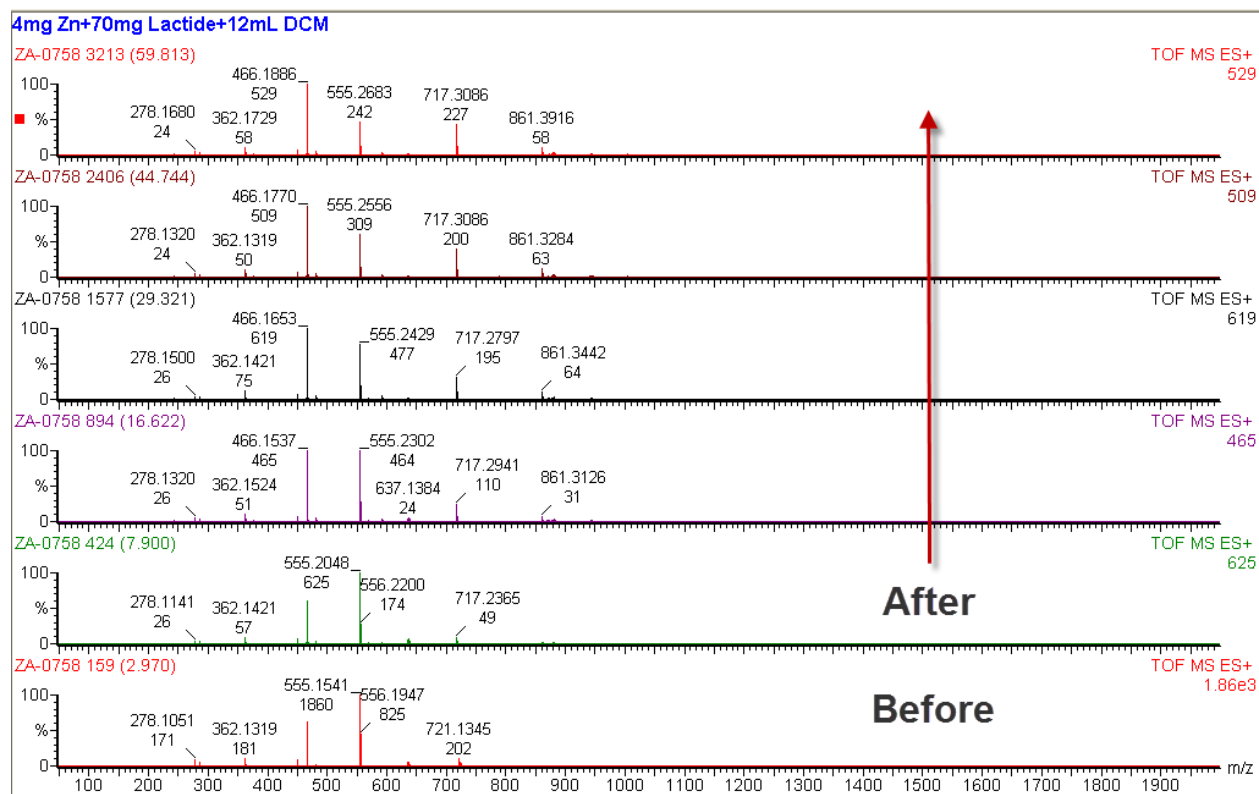


Figure SI 15 MS after addition of lactide, showing disappearance of catalyst and assignment of any new peaks.

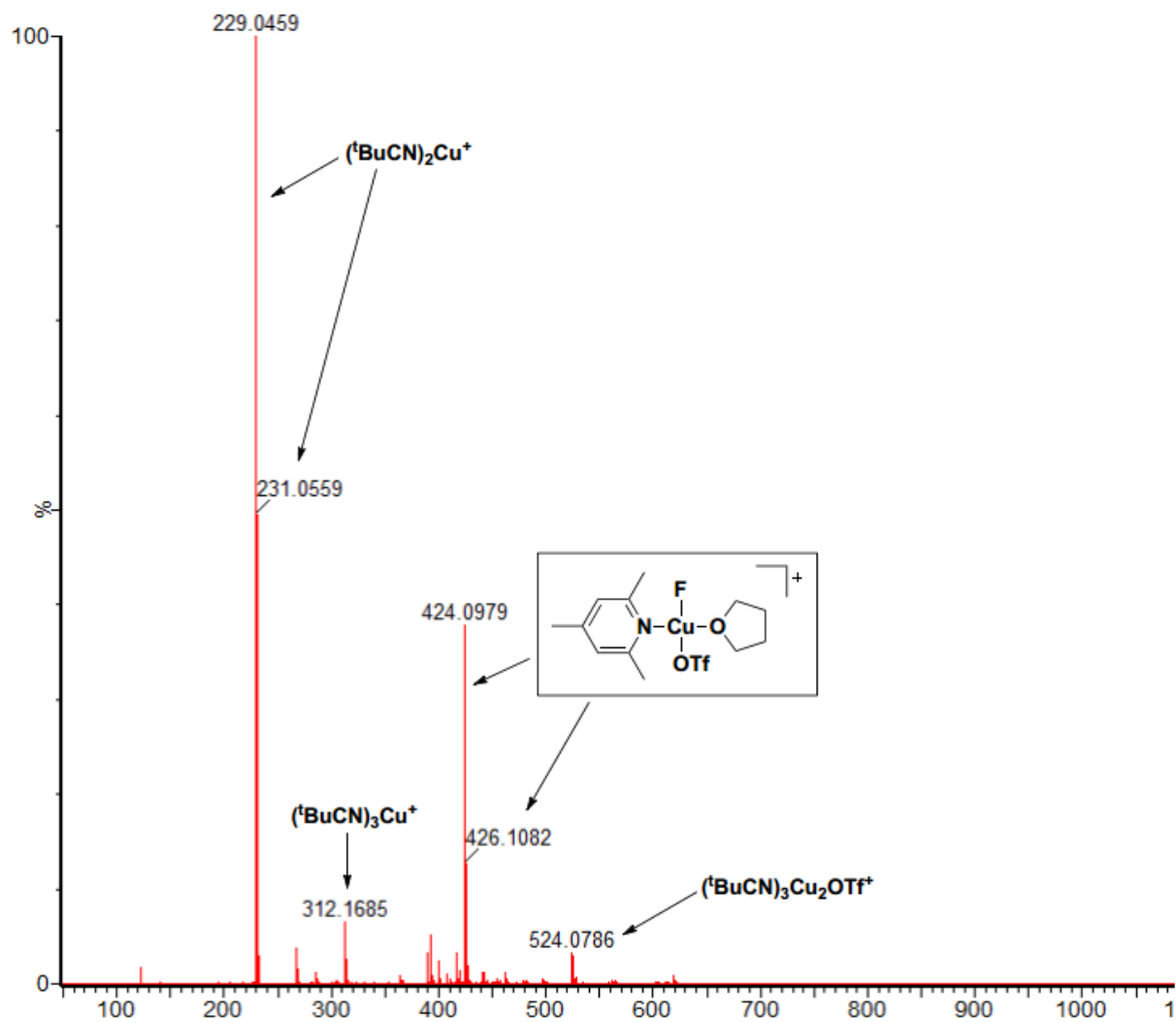
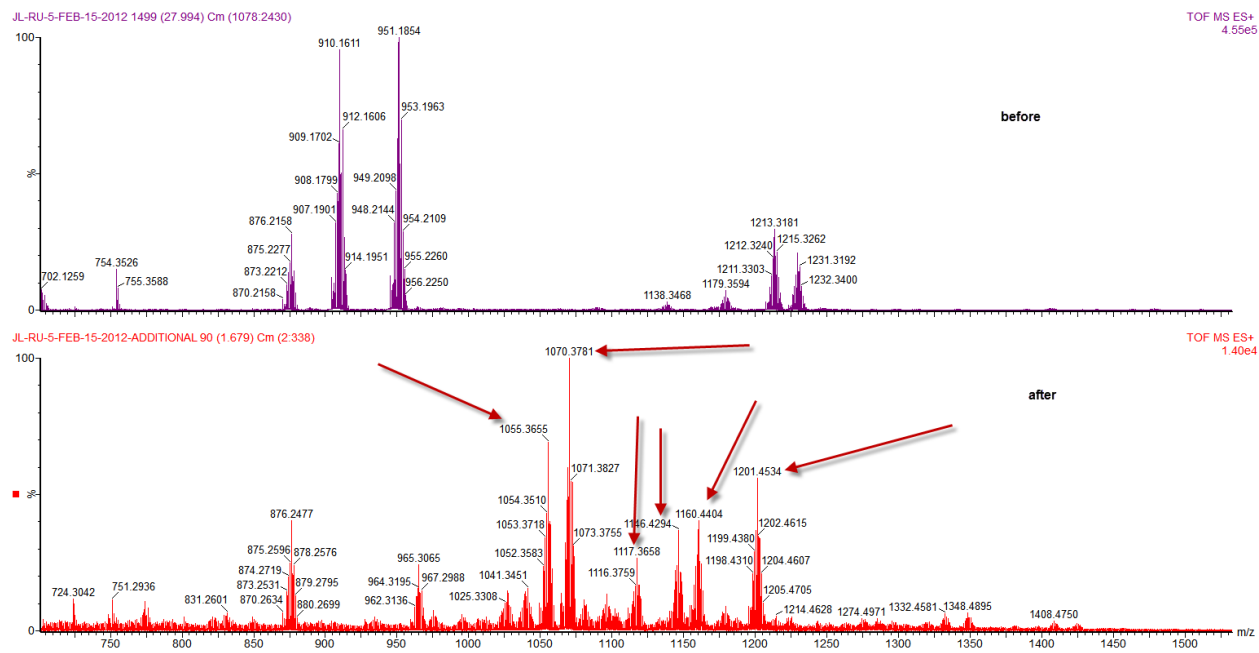


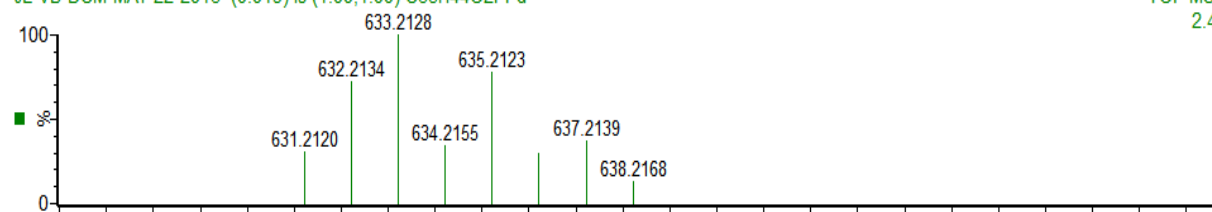
Figure SI 16 MS of intermediate of Copper-Mediated Fluorination



vb 3mg neutral ligand 8mg MeCN cant disolve sphos, DCM can, 6ml RT

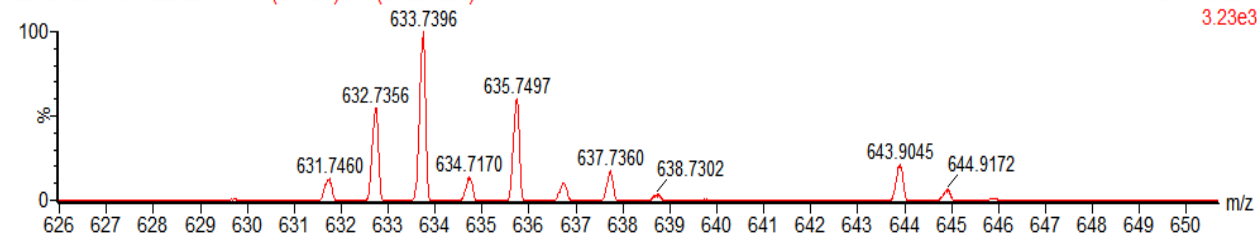
JL-VB-DCM-MAY-22-2013 (0.019) Is (1.00,1.00) C<sub>35</sub>H<sub>44</sub>O<sub>2</sub>PPd

TOF MS ES+  
2.49e12



JL-VB-DCM-MAY-22-2013 3617 (67.451) Cm (3462:3693)

TOF MS ES+  
3.23e3



vb 3mg neutral ligand 8mg MeCN cant disolve sphos, DCM can, 6ml RTmsms633.7

JL-VB-DCM-MAY-22-2013-MSMS633 38 (0.709) Cm (1:243)

TOF MSMS 633.70ES+  
1.03e3

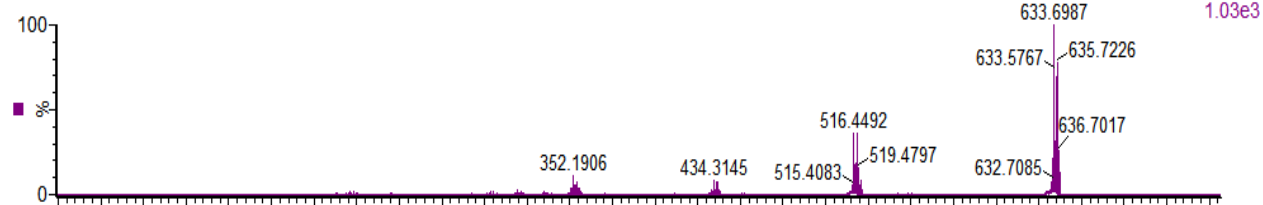


Figure SI 18 Potential activated version of Pd( $\eta^3$ -1-PhC<sub>3</sub>H<sub>4</sub>)( $\eta^5$ -C<sub>5</sub>H<sub>5</sub>).